In situ Plasticization of Starch and Co-blending with Bio-based Polyesters:

An Investigation into The Process Parameters for Continuous Thermoplastic Starch Co-Polyester Manufacturing

by

Bryon Wolff

A thesis
presented to the University of Waterloo
in fulfillment of the
thesis requirement for the degree of
Master of Applied Science
in
Chemical Engineering

Waterloo, Ontario, Canada, 2019

AUTHOR'S DECLARATION

I hereby declare that I am the sole author of this thesis. This is a true copy of the thesis, including any required final revisions, as accepted by my examiners.

I understand that my thesis may be made electronically available to the public.

Abstract

As companies search for sustainable solutions, the need has arisen to develop alternative polymer platforms comprising a portion, or 100%, of bio-based materials. The ultimate goal would be to produce bio-based polymers which offer ease of processing, excellent stability, as well as mechanical and physical properties similar to those currently found in olefinic polymers. Starch-resin copolymers, produced in patent WO 2013116945A1 (Wolff 2013), offer several properties similar to olefinic polymers. However, due to the nature of batch reactor processes, the ability to economically scale the process is not favourable.

Chemical modification of starch through reactive extrusion (REX) (Moad 2011) suggests that similar starch copolymer characteristics, as found in the patented batch process, would be available. However, dry state synthesis of maleic grafted starch, described in the patent, could not be supported with REX process (Zuo 2013). As such, alternative sequencing of materials may be required to address this limitation.

The object of the investigation is to determine the parameters at which specific starches could be destructured (plasticized), chemically modified, and transesterified to produce starch copolyester resins.

Examinations were performed with a three piece, CW Brabender (CWB) 60 cc internal mixer with intermeshing Banbury blades, connected to a CWB Intelli-Torque Plasticorder Torque Rheometer, and supported with CWB WinMix Data Software. The WinMix Software captured stock (material) temperatures, torque, and specific energy, in real time. As such, gelatinization, half-esterification and transesterification kinetics were studied for starch mixtures of various levels of plasticizers / dicarboxylic acid anhydride / polyester, under different temperatures and blade speeds.

The evaluations indicated the fastest rate of gelatinization occurred with the addition of 10% water. However, the kinetics of the half-esterification and transesterification processes favoured high temperatures. In particular, the transesterification reaction was faster at temperatures exceeding 150°C. Those high temperatures are not favourable for the use of water as a plasticizer. At these temperatures, the water of plasticization boils off. As such, blends of water and glycerol were considered to rapidly plasticize the starch and keep it plasticized at elevated temperatures.

With the understanding of processing parameters, the next steps are to conduct NMR analysis of the starch copolyester polymers generated using this technique in order to understand the polymers' structure, then adjust the parameters to optimize the physical and mechanical properties.

Acknowledgements

I would like to express my sincere gratitude to my supervisor, Dr. Leonardo Simon, for this opportunity and supporting me, along the way, with his assistance and guidance.

Special thanks to Charles Dal Castel and Ryan Park for their assistance and constructive discussions.

Thanks goes to Ingredion Incorporated of Bedford Park IL for supporting the research through the supply of commercial grade starch samples.

I would like to thank all my family and friends for their patience and support over the last several years as I worked towards completing this degree.

Finally, I am extremely grateful and blessed with the encouragement and support that I received from my wife. She was there, with me, in the late hours of final report writing, assisting me in proof reading those last few pages. It was with her help that those last few typos were caught. I appreciated everything that she has done. Thank you very much.

Dedication

To my loving wife, Rosemary

Table of Contents

List of Figures

List of Tables

List of Appendix

List of Abbreviations

Label "0.1%"	Label for 30050 starch compounded with 0.1% free radical initiator dibenzoyl peroxide
Label "0.3%"	Label for 30050 starch compounded with 0.3% free radical initiator dibenzoyl peroxide
101	Trigonox 101 peroxide
%	Percentage
<	Less than
>	Greater than
$\geq$	Greater than or equal to
μm	micrometers
30050-0.7%	Label for 30050 dried to 0.7% moisture and compounded
30050-101	Label for 30050 starch compounded with free radical initiator Trigonox 101
30050-3%	Label for 30050 dried to 3% moisture and compounded
30050-8%	Label for 30050 dried to 8% moisture and compounded
30050-Ben	Label for 30050 starch compounded with free radical initiator dibenzoyl peroxide
30050-Lau	Label for 30050 starch compounded with free radical initiator dilauroyl peroxide
55310-0.7%	Label for 55310 dried to 0.7% moisture and compounded
55310-101	Label for 55310 starch compounded with free radical initiator Trigonox 101

55310-Ben	Label for 55310 starch compounded with free radical initiator dibenzoyl peroxide
55310-Lau	Label for 55310 starch compounded with free radical initiator dilauroyl peroxide
A	A constant in the Arrhenius equation
ASTM	American Society for Testing and Materials
ATR	Attenuated total reflectance
Ben	Dibenzoyl peroxide
-C=C-	Carbon to carbon double bond
C=O	Ester bond formation
C_1	Carbon number 1 in the glucose molecule unit of starch
C_2	Carbon number 2 in the glucose molecule unit of starch
C_2-OH	Hydroxyl group on carbon 2 in the glucose molecule unit of starch
C_3	Carbon number 3 in the glucose molecule unit of starch
C_3-OH	Hydroxyl group on carbon 3 in the glucose molecule unit of starch
C_6	Carbon number 6 in the glucose molecule unit of starch
C_6-OH	Hydroxyl group on carbon 6 in the glucose molecule unit of starch
-CH	Hydrogen to carbon bond
-CH2	Two hydrogens bonded to single carbon
-CH3	Three hydrogens bonded to single carbon

cm^{-1}	Centimeters inverse wavelength measurement
C-O	Oxygen to carbon bond
CWB	CW Brabender
DM-120	Label for Dent Maize compounded with CWB body temperature at 150°C and at 120 RPM
DM-150C	Label for Dent Maize compounded with CWB body temperature at 150°C
DM-160C	Label for Dent Maize compounded with CWB body temperature at 160°C
DM-170C	Label for Dent Maize compounded with CWB body temperature at 170°C
DM-180C	Label for Dent Maize compounded with CWB body temperature at 180°C
DM-45-150	Label for Dent Maize compounded with CWB body temperature at 150°C and at 45 RPM
DM-45-90	Label for Dent Maize compounded with CWB body temperature at 90°C and at 45 RPM
DM-60	Label for Dent Maize compounded with CWB body temperature at 150°C and at 60 RPM
DM-90C	Label for Dent Maize compounded with CWB body temperature at 90°C
DM-G20	Label for Dent Maize with 20 % glycerol added
DM-W0	Label for Dent Maize with zero water added
DM-W1:G1	Label for Dent Maize with water:glycerol ratio addition of 1:1

DM-W1:G3	Label for Dent Maize with water:glycerol ratio addition of 1:3
DM-W1:G4	Label for Dent Maize with water:glycerol ratio addition of 1:4
DM-W10	Label for Dent Maize with ten % water added
DM-W20	Label for Dent Maize with 20 % water added
DM-W3:G1	Label for Dent Maize with water:glycerol ratio addition of 3:1
DM-W5	Label for Dent Maize with five % water added
DP	Degree of polymerization
DS	Degree of substitution
DSC	Differential Scanning Calorimetry
E_a	Activation energy
FTIR	Fourier Transform Infrared Spectroscopy
g	gram
H_2O	Water
Hylon-0.7%	Label for Hylon dried to 0.7% moisture and compounded
Hylon-1.6%	Label for Hylon dried to 1.6% moisture and compounded
Hylon-101	Label for Hylon VII starch compounded with free radical initiator Trigonox 101
Hylon-7%	Label for Hylon dried to 7% moisture and compounded
Hylon-Ben	Label for Hylon VII starch compounded with free radical initiator dibenzoyl peroxide

Hylon-Lau	Label for Hylon VII starch compounded with free radical initiator dilauroyl peroxide
I	Concentration
I_o	Initial concentration
J	Joule
J/g	Joules / gram
k_d	Reaction rate of the decomposition
L/D	Length / Diameter
Lau	Dilauroyl peroxide
lb	Pound
MAH	Maleic Anhydride
MAH-1X	Label for 30050 starch compounded with 1% MAH and 0.1% free radical initiator dibenzoyl peroxide
MAH-2X	Label for 30050 starch compounded with 2% MAH and 0.1% free radical initiator dibenzoyl peroxide
MAH-3X	Label for 30050 starch compounded with 3% MAH and 0.1% free radical initiator dibenzoyl peroxide
mg	milligram
nm	nanometers
ºC	degrees Celsius
-OH	Hydroxyl functional group
PBAT	Poly(butylene adipate-co-terephthalate) resin

PBAT-Lau	Label for Hylon VII starch compounded with free radical initiator dilauroyl peroxide and PBAT resin
PBS	Polybutylene Succinate resin
pH	Indicates the degree of acid or basicity of a solution
PHA	Polyhydroxylalkanotes
PLA	Poly(lactic acid) resin / Polylactic acid
PLA-Lau	Label for Hylon VII starch compounded with free radical initiator dilauroyl peroxide and PLA resin
POM	Polarized optical microscope
R	Universal gas constant
REX	Reaction extrusion
RPM	Revolutions per minute
sec	seconds
SEM	Scanning electron microscopy
t	Time
T	Temperature
t=0	Label for 55310 starch dried to 0.7% moisture, blended with other ingredients and allow to sit for zero hours before compounding
t=2	Label for 55310 starch dried to 0.7% moisture, blended with other ingredients and allow to sit for two hours before compounding

t=24	Label for 55310 starch dried to 0.7% moisture, blended with other ingredients and allow to sit for 24 hours before compounding
t=5	Label for 55310 starch dried to 0.7% moisture, blended with other ingredients and allow to sit for five hours before compounding
T_g	Glass transition temperature
TGA	Thermal Gravimetric Analysis
T_{gel}	gelatinization temperature
TPS	Thermoplastic starch
wt-%	Weight Percent
XRD	X-ray diffraction
α	alpha
β	Beta
δ	Bending of the bond seen in the FTIR spectra
ΔH_c	Enthalpy (heat) of fusions
ΔH_m	Enthalpy (heat) of crystallization
ΔH_{m0}	Enthalpy (heat) of crystallization at 100% crystalline state
ν	Stretching of the bond seen in the FTIR spectra
χ_c	Degree of crystallinity
Zn/Se	Zinc Selenide crystal for the ATR

Chapter 1
Introduction

1.1 Motivation and Objectives

There is increased demand by consumers to improve the sustainability of consumers goods. As companies search for sustainable solutions, the need has risen to develop alternative polymer platforms comprising a portion, or 100%, of bio-based materials. The ultimate goal would be to produce bio-based polymers which have the ease of processing, excellent stability, and offer the mechanical and physical properties similar to those currently found in olefinic polymers. Starch-resin copolymers, produced in patent WO 2013116945A1 Wolff (Wolff, 2013), offer several properties similar to olefinic polymers. However, due to the nature of batch reactor processes, the ability to economically scale the process is not favourable.

Chemical modification of starch through reactive extrusion (REX) (Moad, 2011) suggests that similar starch copolymer characteristics, as found in the patented batch process, would be available. However, the dry state synthesis of maleic grafted starch, described in the patent, could not be supported with REX process (Zuo 2013). As such, alternative sequencing of materials may be required to address this and other limitations.

The objective of this research investigation is to determine the parameters under which specific starches could be destructured (plasticized), chemically modified, and transesterified in the presence of polyester resins to produce stable starch copolyester polymers. The goal is to provide insight about the variables controlling the process as well as developing a technology to enable sustainable thermoplastics.

1.2 Thesis Layout

This thesis is organized in six Chapters:

Chapter 1 establishes the motivation and objectives of the thesis. It defines the overall structure of the studies and the experimental design.

Chapter 2 reviews and discusses the relevant background required for this document. It looks at the relevant existing literature and outlines the fundamental aspects pertinent to the subsequent chapters.

Chapter 3 presents the considerations and specific choices of materials and methods as they pertain to: raw material selection; compounding techniques employed; the systematic development of compounds; and the methods of analysis as applied in characterizing the compounds.

Chapter 4 reports the results and contains te discussion about the influences of plasticizers consisting of water and other plasticizers; temperature and revolutions per minute (RPM), shear on the destructuring of a variety of other starches with varying levels of amylose, viscosities and chemical modification.

Chapter 5 reports the results and contains the discussion on the influences of free radical initiators; maleic anhydride (MAH) grafting agent; and various polyesters on polymer development of the various starch co-polyester polymers synthesized.

Chapter 6 presents the general conclusions regarding the work carried out in this thesis and offers recommendations for future research on this topic.

1.3 Experimental Design

The objective of this research is to establish the parameters for the synthesis of starch copolyester. This process starts with understanding starch and the conditions which are required for its physical and chemical modification. It examines the influence of different type of starches, while taking into consideration the various sources and ratios of amylose/amylopectin. As well, it looks at starches which do and do not contain chemical modifications. The initial focus will be on the gelatinization of the starch granule and then progress to an understanding of the influences that grafting agents, free radical initiators and polyester resins have on the synthesized polymer.

These examinations are to be performed with a three piece, CW Brabender (CWB) 60 cc internal mixer with intermeshing Banbury blades, connected to a CWB Intelli-Torque Plasticorder Torque Rheometer and supported with CWB WinMix Data Software. The WinMix Software will capture the stock (material) temperatures, torque, and specific energy, in real time. As such, gelatinization, half-esterification and transesterification kinetics can be studied for starch mixtures of various levels of plasticizers / dicarboxylic acid anhydride / free radical initiators and polyester resins, under different temperatures and blade speeds.

The materials synthesized will be characterized, via the various techniques discussed in chapter three, for their physical-chemical properties. The findings from the investigation will be examined in subsequent chapters. From their review, conclusions will be drawn and commented on at the end of this thesis.

Chapter 2
Literature Review

2.1 Introduction

As companies search for sustainable solutions, the need has risen to develop alternative polymer platforms comprising a portion, or 100%, of bio-based materials. The objective is to achieve bio-based polymers which offer ease of processing, excellent stability, and mechanical and physical properties found in olefinic polymers at a reasonable cost.

Olefinic polymers are built from ethylene and propylene monomers. Both originate from petrochemical production and have a low cost. According to ICIS Houston in the period of May - July 2018, pricing on polymer monomer grade ethylene was between US$0.13 and US$0.14 per pound and propylene was between US$0.575 and US$0.58 per pound. (Figure 2-1 & 2-2) As such, while considering raw materials for bio-based polymers, attention must be paid to their cost, availability, and the chemical and physical properties that they offer the final polymer. Over the last couple of decades, significant research and development has advanced bio-based polymers. This thesis plans to investigate the parameters required for the synthesis of starch copolyester and the influences that these raw materials groups, listed below, have on those parameters.

- Starches
- Plasticizer
- MAH
- Free radical initiator
- Polyester

This chapter goes into the relevant literature review on the background of these raw materials and sets forth the foundation from which the work in this thesis expands upon. As well, it looks

at some of the potential proposed mechanisms for esterification and transesterification which may be possible when these raw materials come together.

Figure 2-1 ICIS marketing research of ethylene contract pricing for the period April to May 2018 (ICIS Marketing Research 2018)

Figure 2-2 ICIS marketing research of propylene contract pricing for the period April to May 2018 (ICIS Marketing Research 2018)

2.2 Starches

Starches are a viable, renewable and biodegradable raw material, which makes them ideal for consideration in building biopolymers. (French 2009) They are a major component of cereal grains and isolates from cereal kernels, vegetables tubers, or roots which are recovered through their wet milling and other various subsequent processes. (Kalambur 2012) Corn and wheat crops are the major source of starch in North America. (Kalambur 2012) Starches are commercially available in many native (none chemical modified) and chemically modified varieties. As a raw material, starch lend its themself to modification which can enhance its chemical and physical properties and enrich those of biobased polymers. (Kalambur 2012)

2.2.1 Molecular Structure of Starch

Starch's polymer chains are protected inside the structure called granules. These structures are designed to provide a stable storage environment for carbohydrates until time of need. In their native forms, they are stable in water at ambient temperatures. However, they are created to be rapidly metabolized on demand to support the plant's requirement for fast energy in the vent of ripening fruit, germination of seeds, and/or the sprouting of roots and/or tubers. (Bemiller 2009)

Starch granules are typically between 1-100μm in size (Bemiller 2009). Their size and shape depend on the species and location within the plant from which the starch is extracted (Bemiller 2009). Jenkin proposed a schematic for a multilayer native starch structure seen in Figure 2-3. In Figure 2-4, this photo depicts the layers which he describes in Figure 2-3. Jenkin suggested that these layers reveal alternating amorphous and semi-crystalline shells (growth rings) of about 100 – 400 nm in size. Within these regions, crystalline lamella exists in section of 9-10 nm consisting of alternating amorphous regions of smaller dimension as demonstrated in Figure 2-3. (Jenkins 1995).

There are two types of polysaccharide macromolecule polymers existing within the starch granule, amylose and amylopectin. Amylose is a sparsely branched linear polymer mainly based on polymerized α -1,4- D glucopyranosyl units with molecular weights in the range of 10^5 to 10^6 g/mol and degree of polymerization (DP) in the range $1x10^2$- $4x10^5$ (Figure 2-7 & 2-14). (Xie,2009) Amylose, within the granule, presents spiral-shaped single or double-helices with a rotation on the α-(1–4) link and with six units of glucoses per rotation. (Xie,2009) This structure proposed by Xie, has the hydroxyl groups of the glucose units mainly orientated towards the exterior of the helices and offers the ability for hydrogen bonding between helices. As such, the higher hydrogen bond density exists between the amylose helices within the granule. This configuration results in significantly more energy being required to dissociate these bonds during the melting or gelatinization process. As such, as the amylose content increases in the starch granule so does the melting point, due to this phenomenon. (Jenkins 1995)
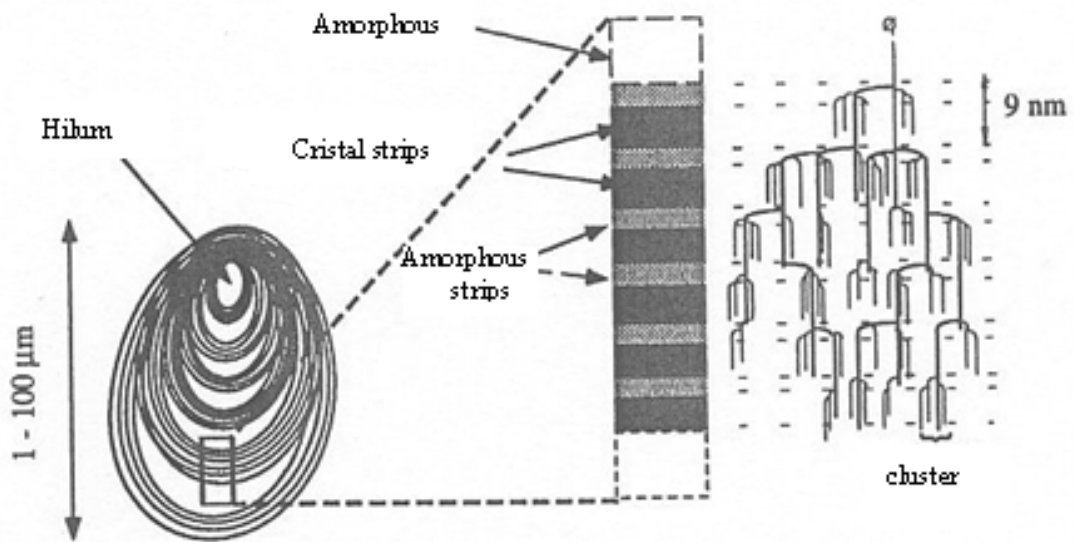
Figure 2-3 Schematic diagram of starch granule structure (amorphous and crystalline regions). (Jenkins 1995)
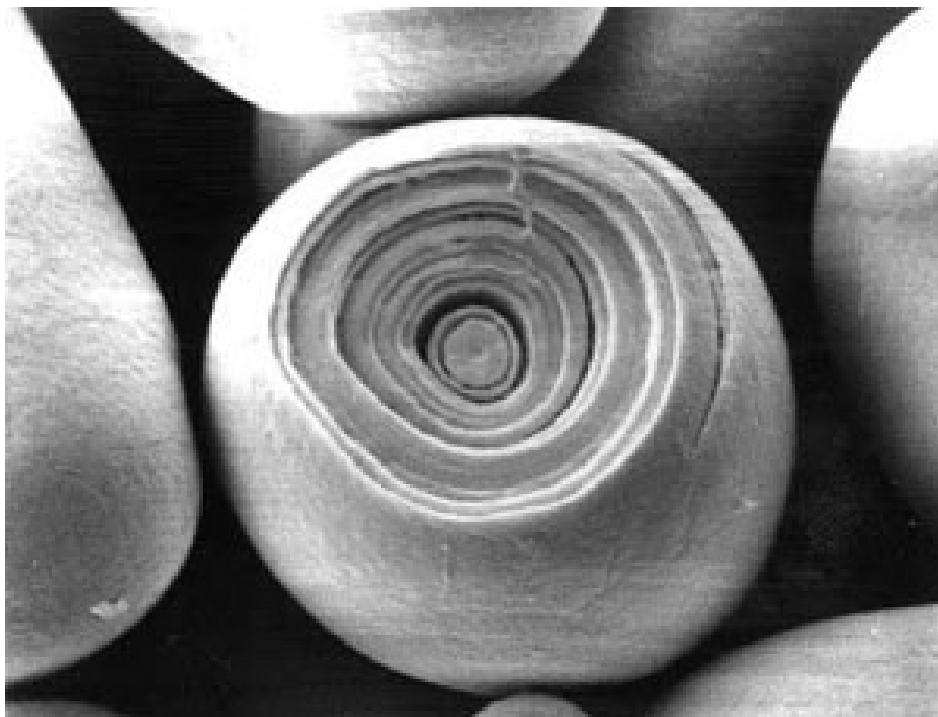
Figure 2-4 Starch Kernel (Bemiller 2009)
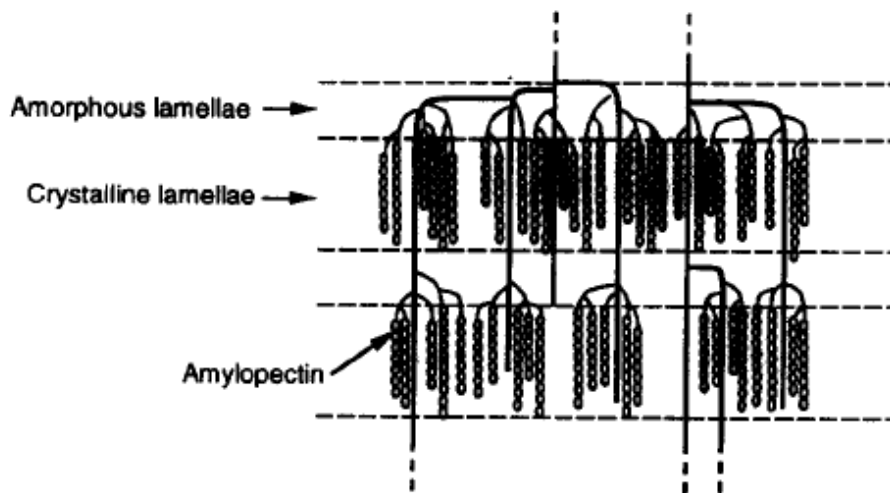
Figure 2-5 Proposed structure of amylopectin structure with no amylose (Jenkins 1995) [waxy starch]
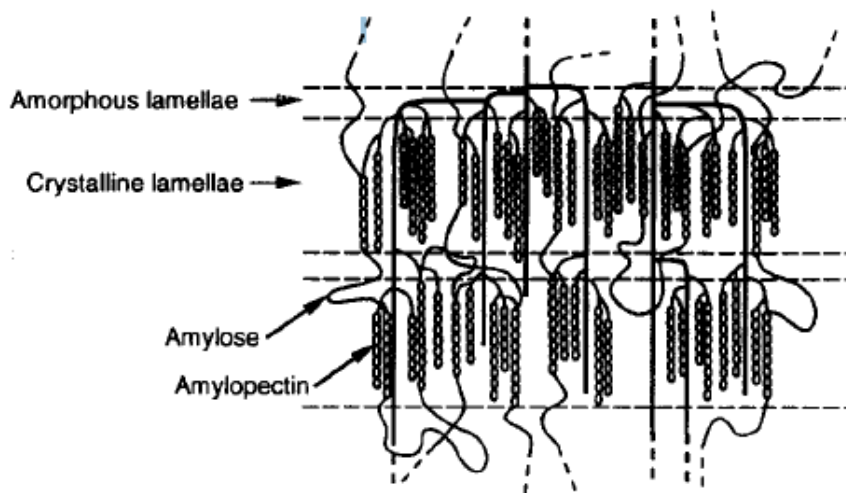
Figure 2-6 Proposed structure of amylopectin and amylose in a co-crystallinity matrix

(Jenkins 1995) [maize]
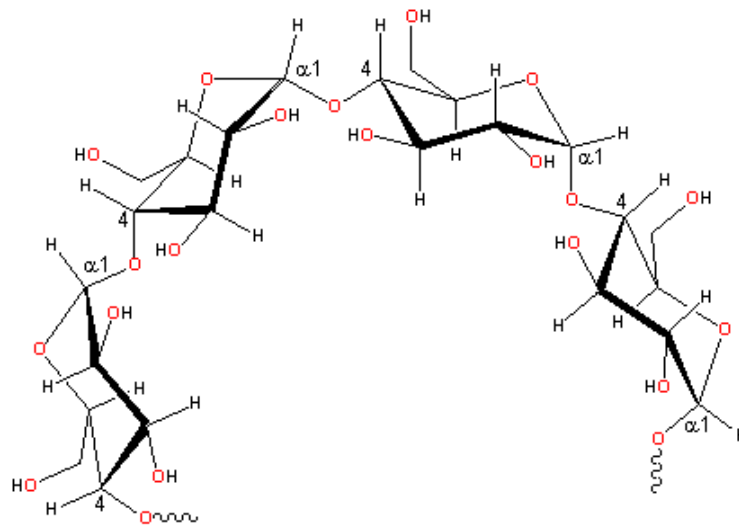
Figure 2-7 Amylose Structure (Bemiller 2009)
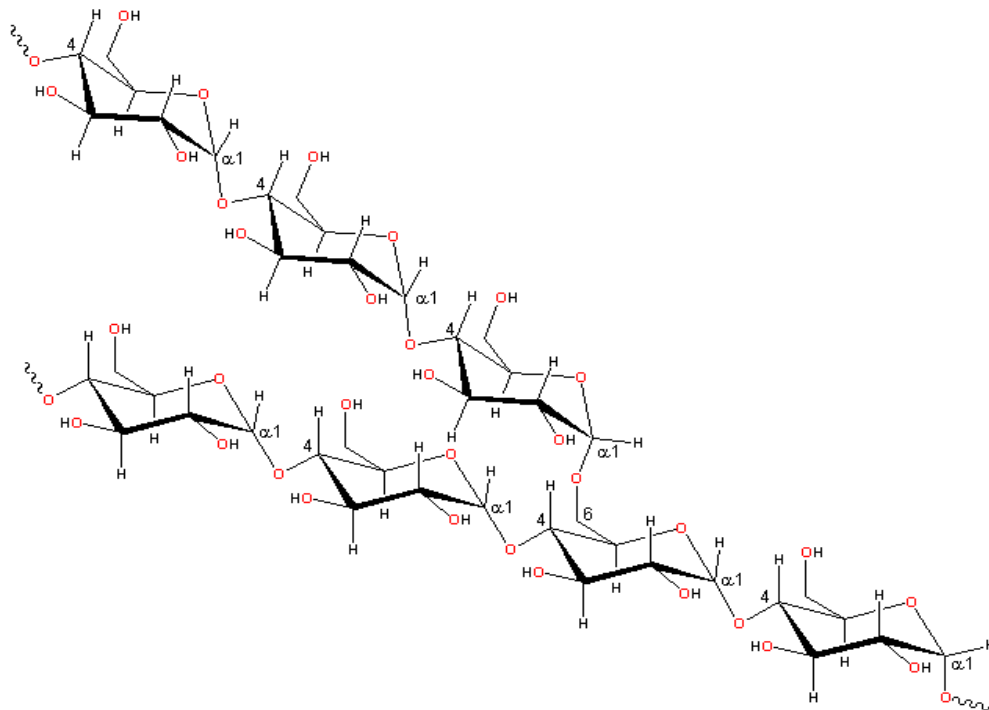
Figure 2-8 Amylopectin structure (Bemiller 2009)

Amylopectin, on the other hand, is a highly multiple-branched polymer with high molecular weight ranging from $1x10^7$ to $4x10^9$ (Figure 2-8 & 2-15). Amylopectin is based on a complex structure consisting of about 95% α 1,4- D glucopyranosyl units and the balance, about 5%, of branches taking place at α-(1–6). (Xie 2009) These branching points occur about every 22–70 glucose units and generate branches of approximately 15 DP in length. (Xie 2009) These short chain amylopectin branches tend to form double helical structures, generating a grape-branch like assembly while associating themselves into close quarters with each other. (Bemiller 2009) It is within this arrangement that the double helical structures align themselves together, parallel to the axis of the large helix, forming regions of crystallinity within the starch granule. (Yu & Christie 2005) This crystallinity can be identified through the presence of birefringence maltase cross as detected under a microscope with polarized light. (Bemiller 2009)

2.2.2 Morphology

 The Morphology of starch polymers is controlled through two properties, those being the polymer's molecular weight and the frequency of branches (amylose / amylopectin ratio) (Moad 2011)

High amylose starch is composed predominantly of linear chains with molecular weights in the range 10^5–10^6 DP, having relatively few α-1,6 linkages or branch points. While, amylopectin starch is highly branched with many α-1,6-linkages and significantly higher molecular weight than that of amylose. (Xie 2009) The proportion of amylose chains in native starches are genetically established and generally consistent within given plant species (Bemiller 2009). Amylose fractions typically range from about 20–30% to about 70–80% in genetically modified organisms and essentially zero amylose content in waxy starch type species (Jenkins 1995).

The starches with different crystalline starches perform substantially differently in their rheological behavior, their processing characteristics, and affect the mechanical properties of

the final bio-polymer. Of note are starches with high amylose content. In the context of reactive extrusion (REX), starches with higher levels of amylose require significantly higher temperatures for gelatinization. While they are less prone to thermal and shear degradation during extrusion, high amylose starches are more disposed to retrogradation and syneresis (Moad 2011).

2.2.3 Physicochemical Changes in Starch during Processing

Native starches behave differently during processing than chemically modified versions and as such require different process conditions and formulations. In processing native starches, the first step is to open the starch granule and expose the polymeric chains. Typical processes considered to achieve the starch granule opening are the application of heat, shear, and /or plasticization.

> "*The melting point of native starch granules is around 170ºC-190ºC. Applying that amount of heat to starch granules will result in decomposition of the starch before melting can be achieved. Since mechanical properties are proportional to molecular weight, attempts to melt the starch is not desirable*". (Kalambur, 2012)

> The application of shear on native starch granules, through the process of extrusion, can result in size reduction from shearing the granule and the exposure of the polymer chains. Like melt processing, this process reduces the molecular weight and is not desirable. (Kalambur, 2012)

> The plasticization of the starch granule in a suitable solvent, like water or a blend thereof, results in the swelling of the starch granule. Then, upon the application of shear, the swollen granule breaks open and releases the polymeric chains. Unlike melting and shear, the implementation of plasticization first helps maintain

the overall molecular weights of the polymeric chains in the starch granule. (Kalambur, 2012)

2.2.4 Gelatinization

Starch, by nature's design, is a highly organized structure of macromolecules shrouded in a hard-outer wall forming the granule (Figure 2-4). When heated in water, it undergoes a transformation which breaks down the granule and the crystalline structure between the macromolecules to create a mixture of polymers in solution.(Bemiller 2009) Ratnayake refers to this process as gelatinization. (Ratnayake 2008) In Ratnayake and Jackson's review on Starch Gelation in Advances in Food and Nutrition Research, they commented that gelatinization of starch is a very complex process.

As the point of reference, the graphic interpretation of microstructure and phase transition of starch as a result of gelatinization, offered by Yu & Christie (2005) and depicted in Figure 2-11, has been considered for this thesis. They highlight that the amylose and amylopectin are partly separated during gelatinization due to, what is believed to be, incompatibility (Yu & Christie 2005).   In thermoplastic starch systems, which are developed in lower levels of solvent, they surmise that higher heats and shear from extrusion / processing are required in order to achieve gelatinization. In their model, the gelatinized segments of amylopectin forms gel balls as noted with the swelling of the starch granule and the formation of viscosity paste. In the presence of the solvent, like water, the amylopectin molecules and branches are in an amorphous state. Even on cycling the starch polymer in solutions over a broad temperature range, the amorphous amylopectin is seen as going through little or no morphological change (Yu & Christie 2005)(Figure 2-11).

This cannot be said for the amylose segment of the starch in solution. On cycling the starch polymer in solutions over a broad temperature range, the amylose polymer fraction goes through significant morphological change. Upon cooling, the amorphous amylose chains

reorganize themselves back into their crystalline structure. Then on heating, they revert to their amorphous orientation (Yu & Christie 2005). Yu & Christie describe this event as a certain type of "memory" within the starch polymer.

Native starch cannot be melt processed directly in the absence of water or plasticizer. Starch gelatinization / destructuring is necessary to render the starch thermoplastic prior to melt compounding. As the melting temperature of native starches are higher than the thermal decomposition temperature, gelatinization is used to avoid shear and /or thermal decomposition (Zhang 2007).

As discussed by Jenkins 1995, high amylose starches form single or double helices structures rotating in on itself and forming hydrogen bonding. As such, gelatinization of high amylose starches requires higher process temperatures than that for low amylose starch. Typical process temperatures for low amylose starch is 70–80ºC, while gelatinization temperature for high (>50%) amylose starch can range 120–140ºC (Yu & Chirstie 2005). This high temperature, required for amylose rich starches, imposes challenges with extrusion processing conditions. The higher gelatinization temperature for amylose rich starches exceeds the boiling point of water. As such, water will evaporate from the starch paste matrix and the advantages of the gelatinized starch are gone. Alternative plasticizers or blends, which are stable at these process temperatures, need be considered (Kalambur 2012).

The gelatinization temperature can be determined by slowly heating starch in a mixture with water, or a glycerol and water blend under a Polarized Optical Microscope (POM). The starch granules will show birefringence maltase cross clearly at 20ºC (Figure 2-10). As the birefringence cross begins to blur, the gelatinization temperature (T_{gel}) is determined. With high levels of amylose starches, T_{gel} could exceed 120ºC as the hydrogen bonds are broken, while regular starches of higher level amylopectin, would be around 70-80ºC (Zhang 2007).
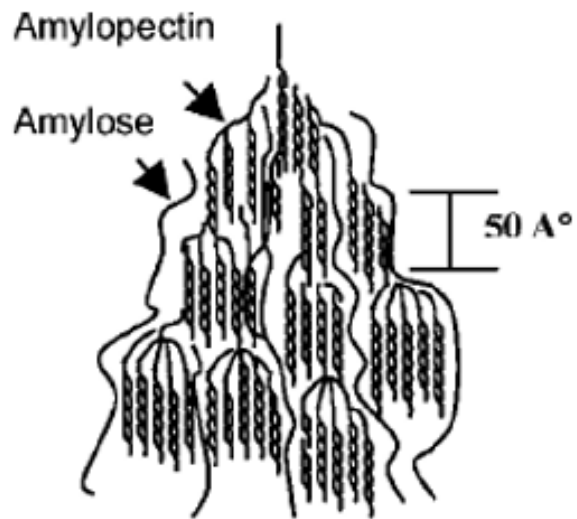
Figure 2-9 Schematic representation of the high-density amylopectin helices structures in ungelatinized starch (Yu & Chirstie 2005)
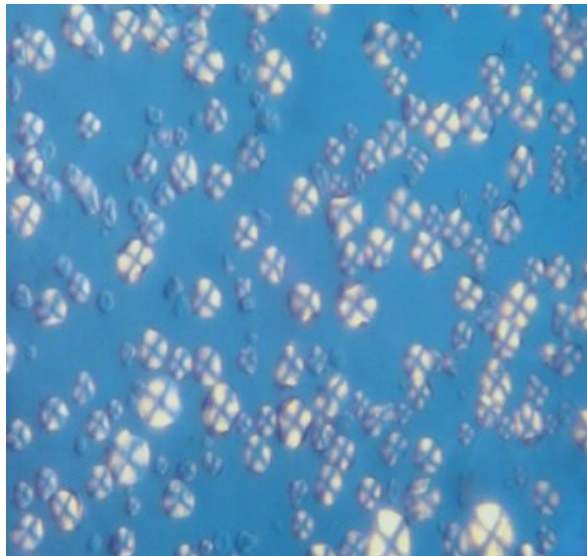
Figure 2-10 Birefringence maltase cross displayed under polarized optical microscope (Bemiller 2009)
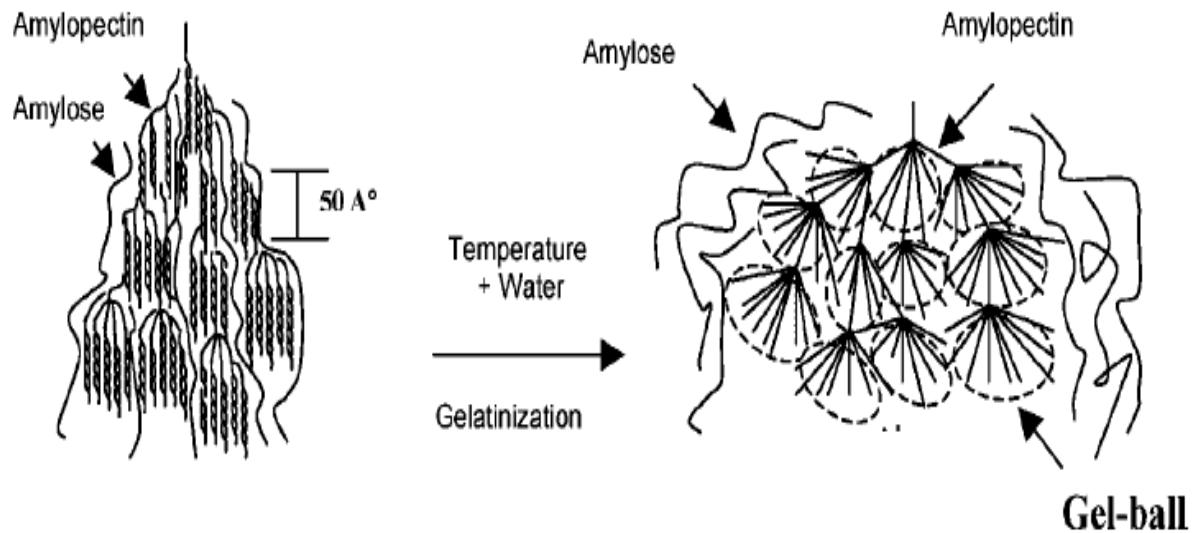
Figure 2-11 Schematic representation of microstructure and phase transition of starch as a result of gelatinization (Yu & Christie 2005) retrogradation & syneresis

2.2.5 Retrogradation and Syneresis

Retrogradation is the process associated with aged gelatinized starch. The crystalline nature from the helical structure of the amylopectin and amylose in the pre-gelatinized starch is part of the memory of the molecule. As the gelatinized starch ages, the starch chains begin to expel water from between the branches and re-associate themselves. The amylopectin and amylose re-crystallize and form themselves into helical structures and crystallites. The process whereby water is expelled from the polymer network of gelatinized starch is referred to as syneresis. (Ottenhof 2004) Yu & Christie 2005 proposed the model outlined below which describes the transformation from starch granule through gelatinization to retrogradation (Figure 2-12).
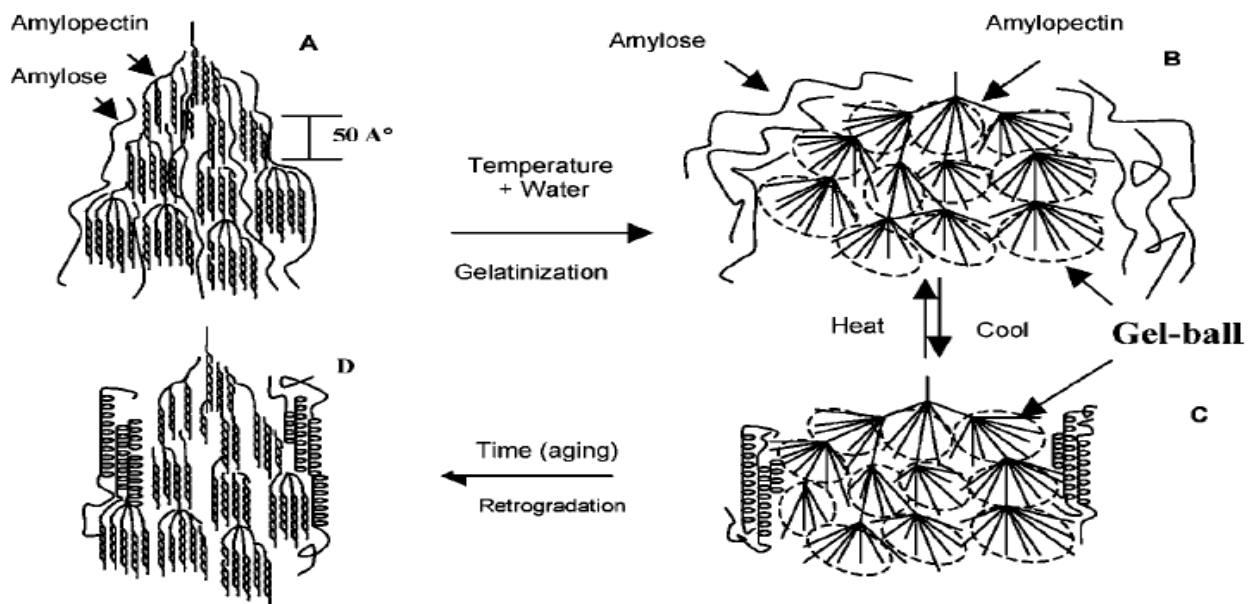
Figure 2-12 Schematic representation of microstructure and phase transition of starch during gelatinization and retrogradation (Yu & Christie 2005)

2.2.6 Rheology

The rheological properties of the starch depend on: the type of starch under consideration; the amylose / amylopectin ratio; the amount of moisture; the temperature and the presence of modification or not. (Xie F 2009)

Xie, in his research, noted the effects on viscosity and shear stress as it relates to the variables of amylose / amylopectin ratio, the amount of moisture and the temperature. First, Xie looked at the amylose / amylopectin ratio, by examining the effect on viscosity and shear stress over a series of samples at steady temperature (130°C) and moisture level (23%).   It was found that as shear rate is increased, the viscosity dropped, and shear stress decreased. However, as the

amylose content in the starch was increased, at any given shear rate, a higher viscosity and shear stress was noted. (Xie F 2009)

When evaluating high amylose starches with 23% moisture content over temperatures ranging from 110°C to 140°C, as shear rates were increased, the viscosity dropped, and shear stress increased. However, with higher temperatures, lower viscosity and lower shear stress were found. (Xie F 2009)

As moisture content over a range from 19% to 27% was evaluated with high amylose starch, and temperature steady at 130°C, it was reported that as the shear rate was increased, the viscosity dropped, and shear stress increased. However, with higher moisture levels, lower viscosities and shear stress were seen. (Xie F 2009)

2.3 Chemical Modification

Starch modifications were developed to offer specific traits and benefits for a wide range of applications. Certain modifications help starch reduce the degree of retrogradation and gelling tendencies of the amylose fractions. Other modifications allow starch the ability to increase the water-holding capability at low temperature, while alternative chemical modification provides for enhanced hydrophilic or hydrophobic characteristics. (Bemiller 2009) The ability to hold water is a manner to prevent syneresis and retrogradation.

In Moad's analysis of the starch granule, the potential areas for chemical reactions were identified as occurring at the non-reducing and reducing chain end, the hemiacetal chain end, or at the hydroxyl groups located at C_6, C_2 and C_3 (Figure 2-13, 2-14 & 2-15). (Moad 2011) The primary C_6 and secondary C_2, C_3 hydroxyl groups of starch have been recognized as reactive when catalyzed by acid or base. Base catalyzation is employed in grafting of anhydrides, and the base is often used in stoichiometric with respect to reagent. (Moad 2011) However, reaction

17

with starches in highly alkaline media are prone to change of color of starch from white to pale yellow. While acid-catalysis reactions will hydrolytically degrade the starch, balancing the level of catalysis is critical to achieving the desired product. (Moad 2011)
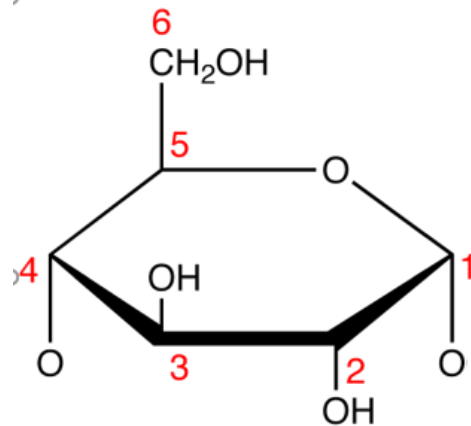
Figure 2-13 Structure of the glucose molecule (Moad 2011)
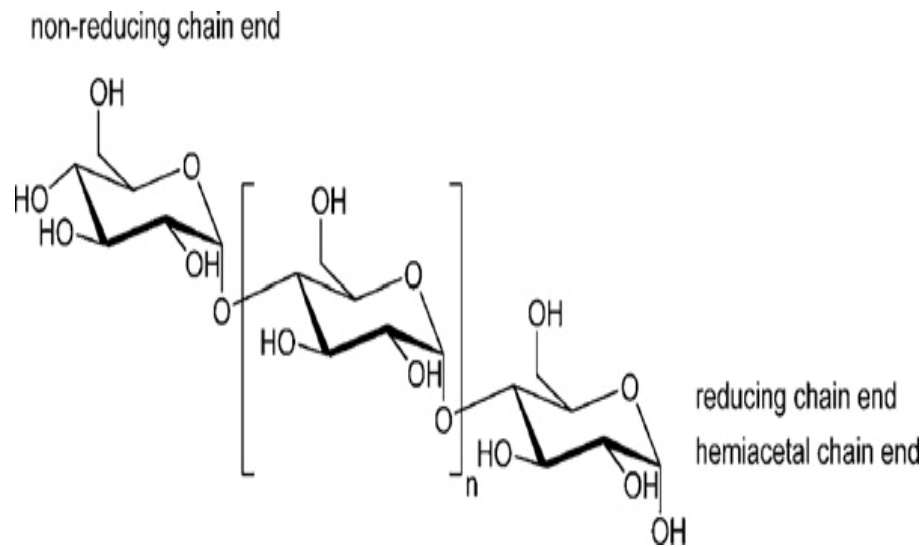
Figure 2-14 Amylose – Chain Ends (Moad 2011)
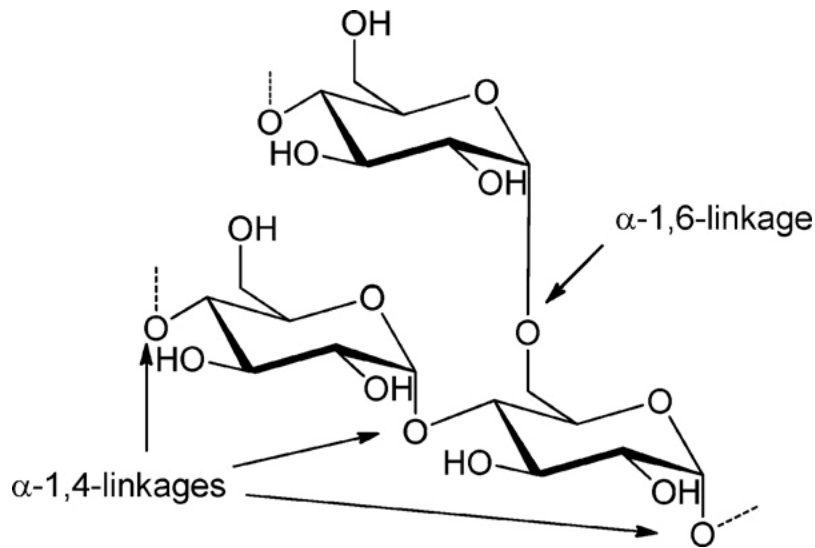
Figure 2-15 Amylopectin – Identification of Branching (Moad 2011)

In Morton's review of the chemical process for starch modification, he summarized chemical modification as occurring in one of the following three states: (Bemiller 2009)

- In suspension, where the starch is dispersed in water, the chemical reaction occurs, the modified starch is precipitated, rinsed and dried.

- In a paste, where the starch is gelatinized with chemicals in a small amount of water, the paste is stirred and when the reaction is complete, the starch is air dried.

- In the solid state, dry starch is treated with chemicals in a water solution, air dried, and finally reacted at high temperature ($\geq 100^{\circ}$C).

Twin-screw extruders are commonly used to produce modified starches in a continuous process with a more consistent product quality. The extruder has the advantage of being an excellent mixing device and is particularly suitable for processing highly viscous fluids, such as gelatinized starch. (Moad 2011) Thus, with the use of reaction extrusion (REX), starch modification can be performed in an homogeneous medium. The extruder also displays good heat transfer and plug flow characteristics. (Moad 2011) Variations in twin screw designs offer

good control over residence times, dispersion and distributions, thereby providing opportunities for the addition (or removal) of reagents and additives during the process, such as processing aids and stabilizers. (Moad 2011)

When describing a starch modification /derivative, several factors are considered: (Bemiller 2009)

- The plant source (Corn, Waxy Maize, Potato, Cassava, Pea etc.)

- Any prior treatment that the starch may have seen before chemical modification, for example if the starch is oxidized, acid-catalyzed or dextrinization

- The amylose / amylopectin ratio / content

- Some idea, or measurement, of molecular weight distribution

- The degree of polymerization (DP) in terms of the number α-D glucopyranose units

- The type of derivation imposed on the starch—whether it is esterification, etherification or oxidation of the starch granule

- The nature of the substituent group, if the starch reacted with acetates, hydroxypropyl or other functional groups

- The degree of substitution (DS) or the molar substitution of the available hydroxyl groups of the α-D glucopyranose units by the substituent group. There are three hydroxyl groups on each α-D glucopyranose unit, as such, the maximum value for DS is 3. When chemical modification occurs, the value for DS is expressed as an average substitution of the three hydroxyl groups on the α-D glucopyranose unit. The hydroxyl groups are located on carbon C_2, C_3 & C_6 of the α-D glucopyranose units (anhydrous AGS) with C_6 generally being the point of greatest substitution.

- The physical form, whether it be granular or pregelatinized

- The presence of associated components (proteins, fatty acids, fats, phosphorous compounds etc.) or native substituents

20

Morton pointed out that in some applications more than one chemical modification / treatment may be applied in order to obtain the desired properties of the starch. (Bemiller 2009) The following are but a few of those chemical modifications / treatments which are regularly preformed on starches.

2.3.1 Oxidation

Oxidation of starches helps address the shortfalls of native starches in paper applications due to the thermal degradation as a result of continuous cooking of the starches for sizing and coatings applications. Starch oxidation lowers the viscosities of high-solid dispersions while reducing the potential of increasing viscosity through continuous cooking (gelatinization). Oxidation depolymerizes the starch in a controlled chemical modification, resulting in reduced viscosity through limited cleavage of the α-1,6 linkage within amylopectin, and the minor introduction of carbonyl and carboxyl group at C_2 C_3. The presence of these additional functional groups minimizes the retrogradation of the amylose and offers viscosity stability. (Bemiller 2009)

Sodium hypochlorite is one of the main reagents which is employed for the oxidation of starch. In the process, polymer chains are cleaved and oxidation of the hydroxyl groups to carbonyl and carboxyl groups is achieved. Oxidation occurs randomly at primary hydroxyl (C_6), secondary hydroxyl (C_2 and C_3), aldehydic reducing end groups, and minor cleavage of C_2-C_3 bonds. (Xie 2011)

The scission of the glucosidic linkages results in depolymerization of amylose and amylopectin, hence decreasing the swelling. The formation of carbonyl and carboxyl groups reduces gelatinization temperature, increases solubility and decreases gelatinization. The carbonyl and carboxyl groups also reduce the thermal stability of the oxidized starch resulting in browning. As well, the bulkiness of the carboxyl and carbonyls sterically interferes with the tendency of amylose to associate and retrograde. (Xie 2011, Moad 2011, Bemiller 2009) In Figure 2-16,

21

Moad proposes a mechanism for base catalyzed, oxidation of starch generating carbonyl and carboxyl groups.
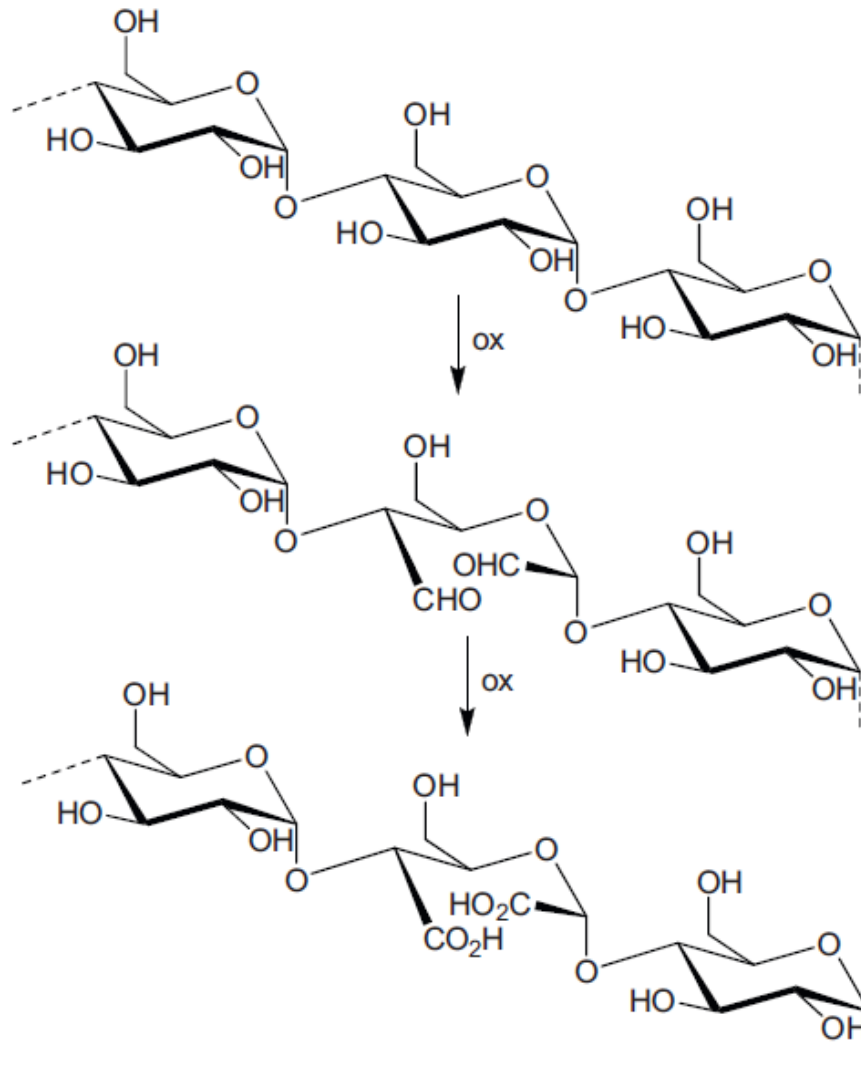
Figure 2-16 Oxidation mechanism of Starch (Moad 2011)

Oxidized starch was developed for the coating and sizing of corrugated, box board and paper. The goal was to achieve higher filler or fiber retention and smoother/ finer surfaces on the paper (sizing and sealing the pores). (Bemiller 2009) As the paper mills were continuously cooking the starches, modification was required to address the need for lower viscosities for uniform coating and prevention of retrodegradation. (Bemiller 2009)

2.3.2 Esterification

Esterification of starch was found to create a stable thickening agent which would work over larger temperature ranges (including refrigeration), high shear rates and low pHs, without syneresis (weeping resistance) or retrogradation. (Bemiller 2009) Many of these properties would be ideal to incorporate into a biopolymer.

Starch esters are prepared by reacting starch with acid chlorides and anhydrides (acetic anhydride, higher anhydrides, maleic anhydride, alkyl/alkenyl succinic anhydrides). Starch esterification with an anhydride may be achieved through catalyzation by acid or base or free radical initiator. When base-catalysis is employed the amount of base used is typically stoichiometric. In Figure 2-18, Moad proposes a reaction mechanism for base-catalyzed succinic anhydride esterification and in Figure 2-17 to 2-21, he offers a reaction mechanism for esterification starch with maleic anhydride. (Bemiller 2009, Moad 2011)

2.3.3 Transesterification and Cross-linking

Starch contains two types of hydroxyls, primary (C_6-OH) and secondary (C_2-OH and C_3-OH). These hydroxyls are able to react with multifunctional reagents resulting in starch cross-linking. Cross-linking is used to restrict swelling of the starch granule or to prevent gelatinization of the starch. (Bemiller 2009)
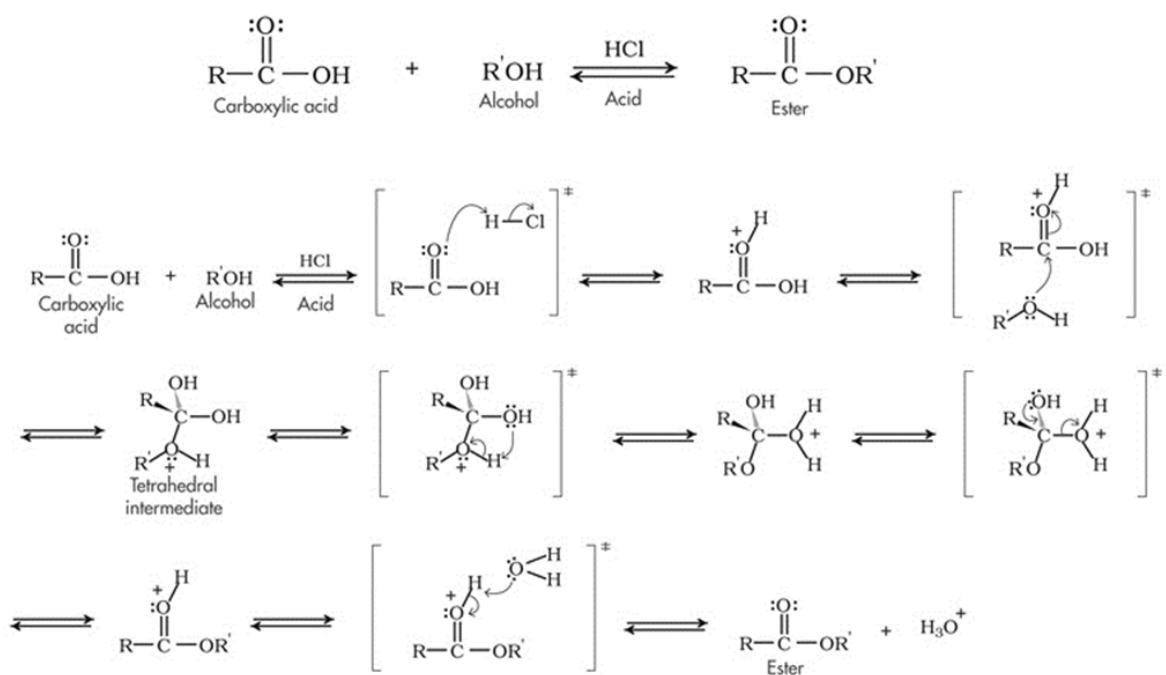
Figure 2-17 Starch Acetate Esterification (Moad 2011)
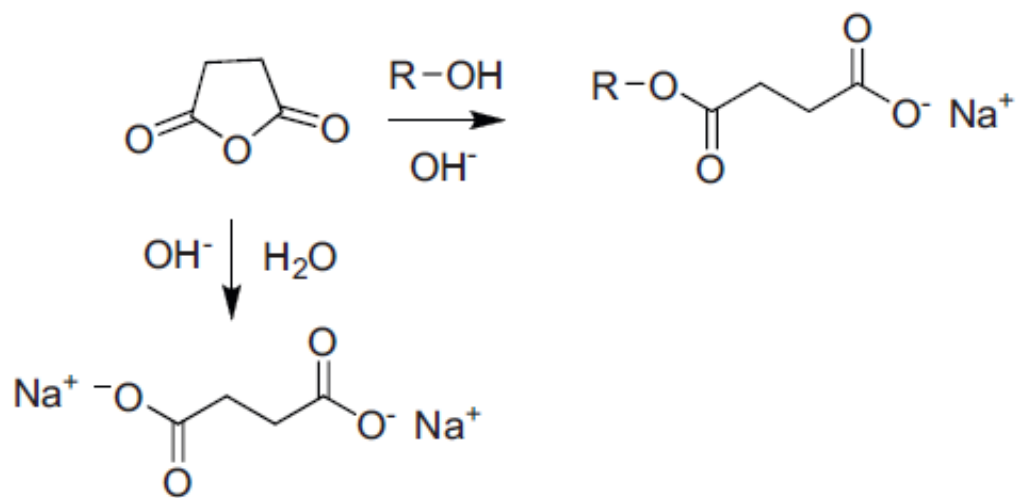
Figure 2-18 Succinic Anhydride Esterification (Moad 2011)
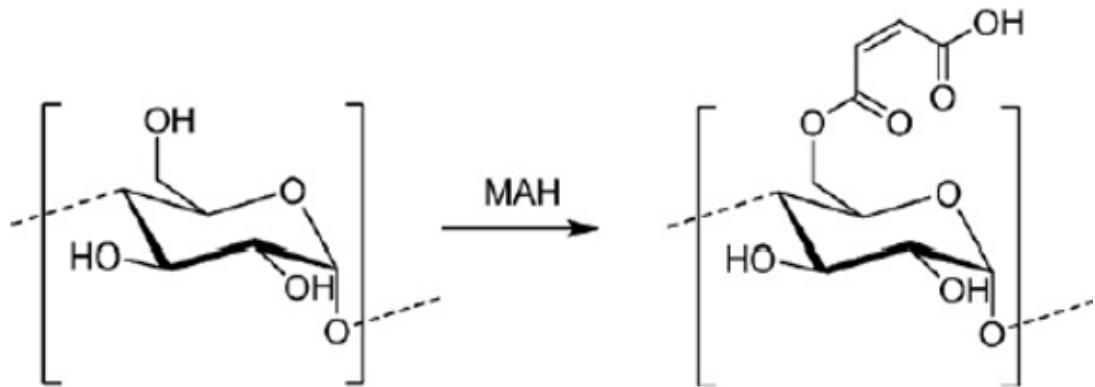
Figure 2-19 Maleic Anhydride Esterification (Moad 2011)
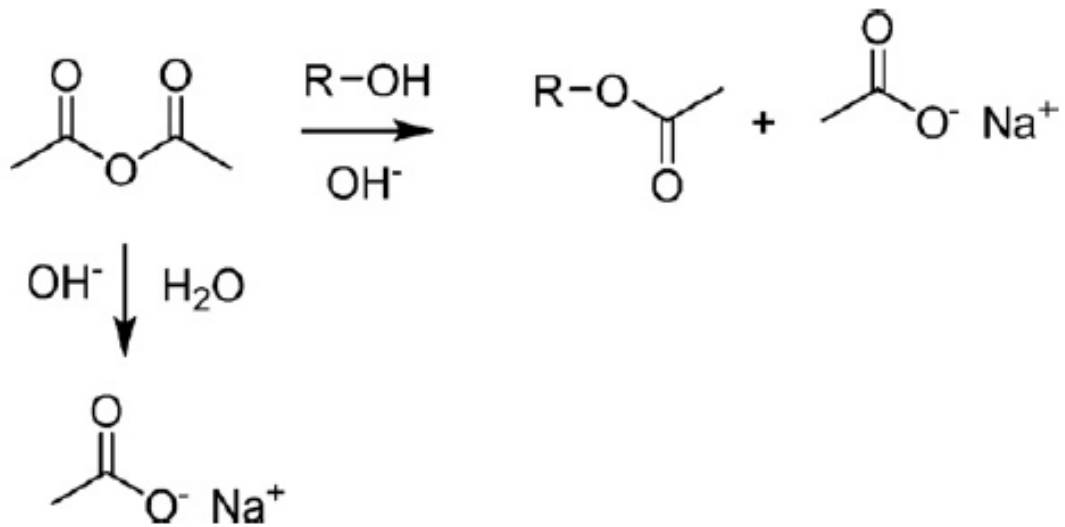
Figure 2-20 Acetic Anhydride Esterification (Moad 2011)
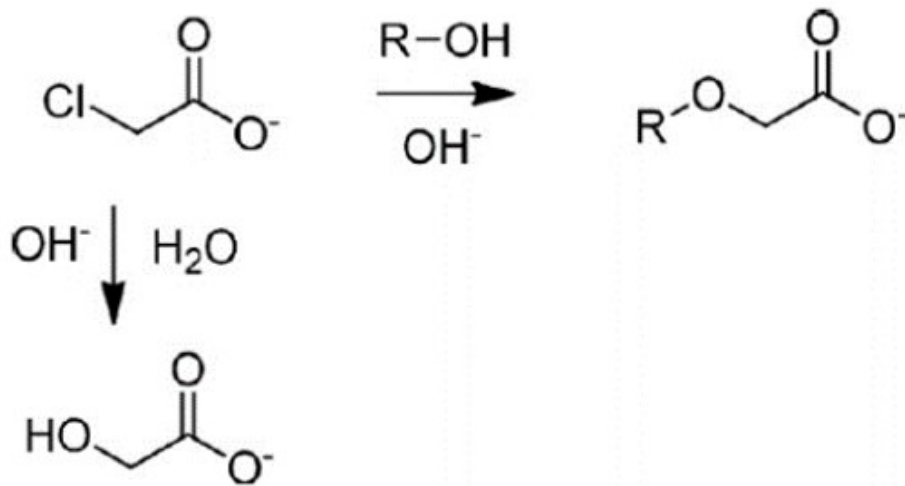
Figure 2-21 Alkyl Esterification (Moad 2011)

Starches with low levels of cross-linking show a higher peak viscosity than that of native starches with reduced viscosity. The chemical bonding can maintain the granule's integrity in a swollen state, prevents loss of viscosity, and provides resistance to mechanical shear while increasing levels of cross-linking will reduce granule swelling and decrease viscosity. At high levels of cross-linking, granules will not swell, and the starch will not gelatinize in boiling water under autoclave conditions. Morton commented that the employment of dicarboxylic acids or anhydrides offers the ability of transesterification to occur, thereby cross-linking starch chains. These cross-links create a more shear and viscosity stable gelatinized starch over a wider range of temperatures. (Bemiller 2009). This ability to stabilize starches against shear and temperature offers several benefits in the design of bio-based thermoplastic.

2.4 Thermoplastic Starch Production

Overview
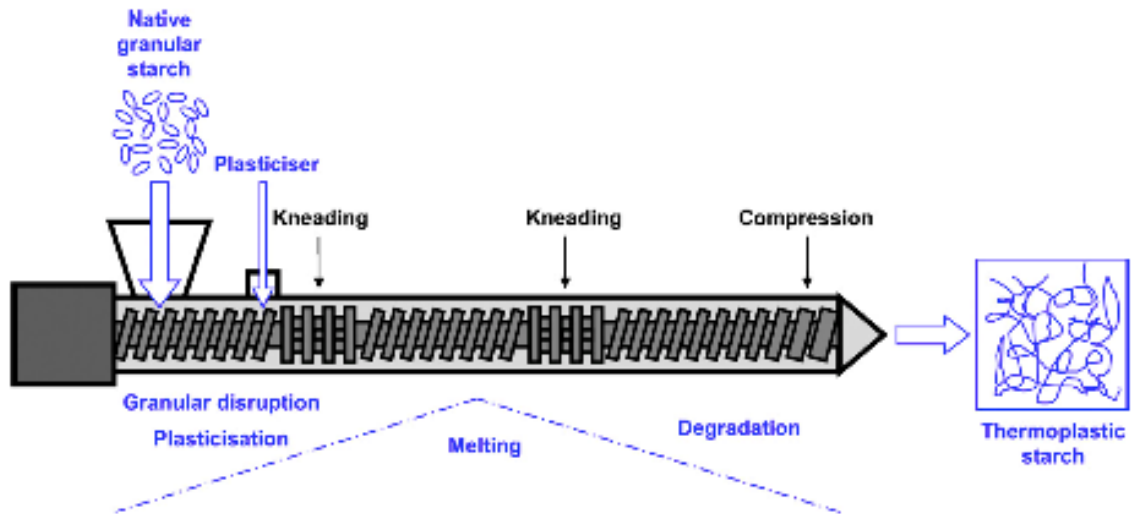
Figure 2-22 Schematic Representation of Starch Processing by Extrusion (Xie F. 2007)

Starch is a renewable, low cost, biodegradable polymeric material. As such, it poses an attractive substitute for petroleum-based plastics (Chaudhary 2008) It is highly desirable to use extrusion equipment when processing starch because it is commonly available in the plastics industry.

The construction of starch-based polymers is comprised of several steps which encompass chemical and physical processes. Such aspects covered are: the diffusion of water into the granule; granule expansion; gelatinization; shear and / or thermal decomposition; melting and crystallization. (Liu 2009 & Xie F. 2007) Figure 2-22 shows a typical representation of an extruder used for processing starch and the role of the respective regions in the extruder.

Gelatinization is particularly important as it relates to other processes. It is the basis of the conversion of the starch granules to a thermoplastic. (Zhang 2007) Different extrusion processing conditions alter the transformation of the starch during gelatinization. Modification of these conditions are required to address the type of starch and extruder screw speed. For example, higher amylose starches may require an increase in extruder screw speed to address the higher crystallinity due to the hydrogen bonding of the amylose helix. (Chaudhary 2008)

Thermoplastic starch resins may include the addition of processing aids and plasticizers to aid gelatinization during processing, thus producing suitable mechanical properties in the finished product. Extruder screw speed is a particularly useful processing variable since it is readily available for change during extrusion operation, controls the amount of work done on the material during processing, affects the extent of degradation of starch, and alters the rheology of starch melts. (Chaudhary 2008) The differences in melt viscosity can be achieved through the selection of starches with various levels of amylose content. Higher amylose content equates to a higher melt viscosity, thus affecting the die pressure for a set of extruder conditions. However, through chemical modification of high amylose starches, lower viscosity can be achieved resulting in a lower die pressure. (Thuwall 2006)

2.4.1 Plasticizers

Starches have a "memory" and naturally form helical structures of the amylopectin and amylose. As such, in their native form, starches will degrade before their melt point is obtained. (Yu & Christie 2005) To avoid degradation of the starch through either heat or shear, the hydrogen bonds of the hydroxyl groups within the helical structures need to be dissociated. This can be achieved through the gelatinization of the starch with a suitable plasticizer. (Kaseem 2011)

The most effective plasticizer for the gelatinization of starch is water. Willett studied the relationship between viscosity and shear rate as it pertains to various levels of moisture content and temperature. In general terms, Willett's results showed temperature had a greater impact on viscosity to shear rate than did moisture content. In rough terms, as both temperature and moisture contents were increased, a subsequent drop in viscosity was noted. (Willett 1995) Thunwall observed a similar relationship when investigating the correlation between viscosity and shear rate as it pertains to oxidized and non-potato starches at various levels of glycerol and temperature. (Thunwall 2006)

Although water is more effective as a plasticizer than glycerol, glycerol is better suited for extrusion and other thermo-processing. This is due to glycerol's higher boiling point, availability and low cost. Figure 2-23 depicts the common plasticizers documented for starches and the relative frequency of their use. (Kaseem 2011)
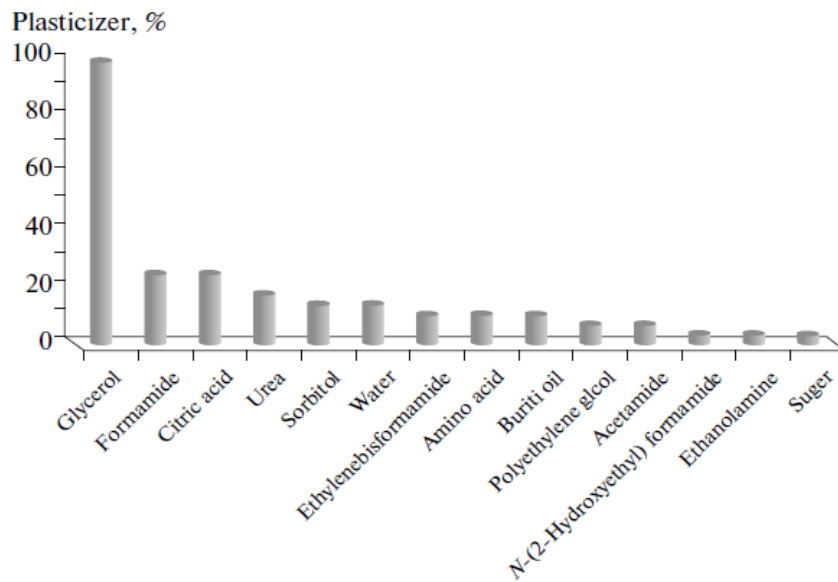
Figure 2-23 Familiar starch plasticizers as a percentage for glycerol (100% glycerol) (Kaseem 2011)

2.4.2 Free Radical Initiators

Free radical initiators are applied in polymerization to start the reactions. In free radical polymerization there exists three fundamental stages which are defined by the mechanism of reaction: initiation, propagation and termination. It is in the initiation stage that the free radical initiator plays an essential role. (Odian 2004)

In the initiation stage, peroxide thermal homolytically dissociates creating the active intermediates which advance the chemical reaction.

Initiation

$$I \longrightarrow 2R^*_0 \quad \textbf{Equation 2-1}$$

$$2R^*_0 + M \longrightarrow R^*_1 \quad \textbf{Equation 2-2}$$

As such, the decomposition rate for peroxide can be expressed as

$$\frac{-\partial[I]}{\partial t} = k_d[I] \quad \textbf{Equation 2-3}$$

whereby k_d is the reaction rate of the decomposition at a temperature and $[I_o]$ in the concentration of the initiator at time equals zero. On the integration of the reaction rate, a function as an expression of time taken for peroxide to dissociate is obtained. (Odian 2004)

$$[I] = [I_0]e^{-k_d t} \quad \textbf{Equation 2-4} \qquad \text{or} \qquad ln\frac{[I_0]}{[I]} = k_d t \quad \textbf{Equation 2-5}$$

Free radical initiator chemistry has adopted the convention of describing their reactivity through the expression of their half-life time at a particular temperature. Half-life is the time at which the concentration of the initiator $[I]$ decreases to one half of its original value. (Odian 2004) As such, when substituting ln 2 = 0.693 into the equation, it can be simplified.

$$t_{1/2} = \frac{0.693}{k_d} \qquad \textbf{Equation 2-6}$$

Peroxide free radical initiator dissociation reactions follow the Arrhenius equation and allow for the calculation of reaction rate as a function of temperature. It goes without saying, that as processing temperatures increase so will the reaction rate. (Odian 2004)

$$k_d = Ae^{-E_a/RT} \qquad \textbf{Equation 2-7} \qquad \text{or} \qquad ln\ k_d = \frac{ln\ A - E_a}{RT} \qquad \textbf{Equation 2-8}$$

From Equation 2-8, on the graphing of the values of ln k_d against 1/T (K) a straight line is obtained. From the equation of that line, ln A is obtained from the y intercept and E_a/R from the line's slope. Given that information, subsequently half-life times can be calculated for any other particular processing temperature.

Table 2-1 Table of Properties for Trigonox 101

Trigonox 101	T(°C) – 1h	T(°C) – 10 h	T(°C) – 15 second
Half-life temperatures	147 °C	124 °C	214 °C
Reaction rate k_d	1.925×10^{-4}	1.925×10^{-5}	0.0462

Displayed in Table 2-1 are the half-life temperatures for 1 and 10 hours for Trigonox 101. From that information, the reaction rates for each temperature are calculated with Equation 2-8. When the equations outlined above are applied to the data in Table 2-1, the graph for Trigonox 101 Activation Energy is generated (Figure 2-24). With that information, there is the ability to calculate the reaction temperature for the peroxide dissociation for any half-life time. In Table 2-1, the temperature of 214°C was calculated to achieve half-life of 15 seconds.
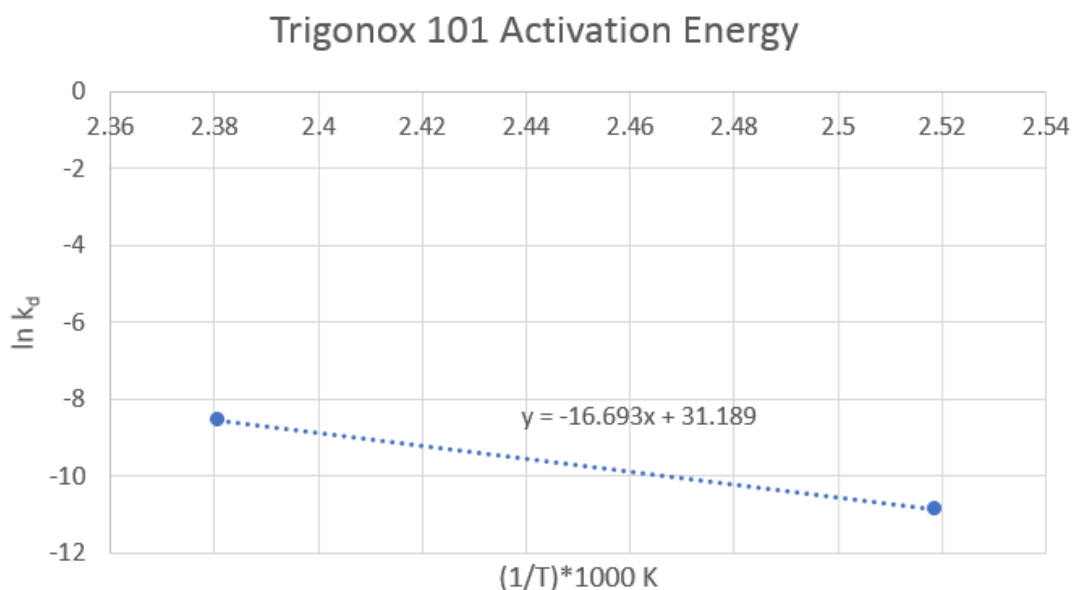
Figure 2-24 Trigonox Activation Energy - Graph of ln k_d versus T^{-1} K

Understanding the concept of reaction rate and kinetic calculations are important in migrating from the original work conducted in the Wolff's patent (2013)to potentially a twin-screw extruder. As outlined, Trigonox 101 was chosen for discussion for review here because it is a free radical initiator for the chemical modification in the batch reactor and subsequent steps. In the batch reactor described in Wolff's patent (2013), thermoplastic starch (TPS) was generated in the presence of peroxide. The mixture was exposed to 82º-96ºC for a minimum of 6 hours under vacuum before being discharged. In the subsequent stages, the thermoplastic starch was melt fluxed with the polyester at 160ºC in a Banbury internal mixer for 20 minutes before the starch copolyester polymer was transferred to a single screw extruder for pelletization. One of the advantages of this batch process is the easy of control of the residence time.

In a twin-screw extruder, the time is limited to how long the raw materials remain within it. As such, complete polymerization is constrained to this time frame and limited to shorter residence times as compared to batch processes like the Banbury internal mixer. An extruder with a 52:1 L/D, 53 mm twin screw extruder operating at 100 RPM, this time ranges from 80 – 120 seconds

depending on the twin screw extruder's element configuration. This time frame is referred to as the residence time. Therefore, the residence time in an extruder (about 2 minutes) is significant smaller than the residence time on an internal mixer (about 20 minutes).

In conclusion, the kinetics of the free radical initiator and the half-life time for the free radical initiator needs to be adjusted according to the time of processing equipment. If the half-life time of the free radical initiator is much longer than the residence time experience by the equipment, than the contribution of the free radical initiator is of limited or not benefit to the overall process requiring chemical reactions to the polymer. As such, high temperatures and the nature of the free radical initiators (peroxides) with fast reaction rates should be considered when migrating from a batch process with long residence time to a continuous process with short residence time.

2.5 Addition of other Biopolymers

Over the past several years, thermoplastic starches have been compounded with other biopolymers in order to enhance the properties of the thermoplastic starch (TPS). Compounds of TPS have been made with the following biopolymers: Polylactic Acid (PLA) has similar mechanical properties to traditional polymer, however much lower thermal properties due to its low T_g at 60°C; Polyhrdroxyalkanoates (PHA) produced by bacterial fermentation with potential to replace conventional hydrocarbons with Tg from -40°C to 5°C and melting temperatures in the range from 50°C to 180°C; Polybutylene Succinate (PBS), a semi-crystalline polyester with melt point higher than that of PLA and similar mechanical properties to those of polyethylene; and Poly(butylene adipate-co-terephthalate)(PBAT) has similar mechanical and thermal properties to conventional polymer. *(Phua 2013)*

2.6 Reaction Mechanisms

Numerous papers have been written which cover the topics of potential mechanism for maleation, etherification, esterification and transesterification of starches and various polyesters. Some of the more prominent articles published were by Stagner 2011, Raquez 2006 / 2008, Narayan 2009, Moad 2011, Hablot 2012, Kalambur 2012 and Nabar 2005.

In sample preparation, all the raw materials are comingled before introduction to the CWB Intelli-Torque Plasti-Corder® Rheometer 3-piece mixer/measuring head with Banbury Blades. As such, several potential reaction mechanisms could be possible. These are but a few of the potential mechanisms which could be considered:

- Maleated Poly(butylene adipate-co-terephthalate) PBAT in the presence of peroxide

- Maleated Polylactic Acid (PLA) in the presence of peroxide

- Maleated Starch

- Starch hydrolysis followed by its subsequent maleation

- Starch ether formation with glycerol

- Various combinations of each one of them.

2.6.1 Maleation of Poly(butylene adipate-co-terephthalate) (PBAT)

Nabar studied the effects of maleated poly(butylene adipate-co-terephthalate) as a compatibilizer. In Nabar's mechanism scheme, it is proposed that the PBAT reacts with the free radical initiator creating a radical which subsequently reacts with the maleic anhydride. That structure goes through β-scission and maleates a portion of the PBAT molecule. (Nabar 2005) (Figure 2-25)
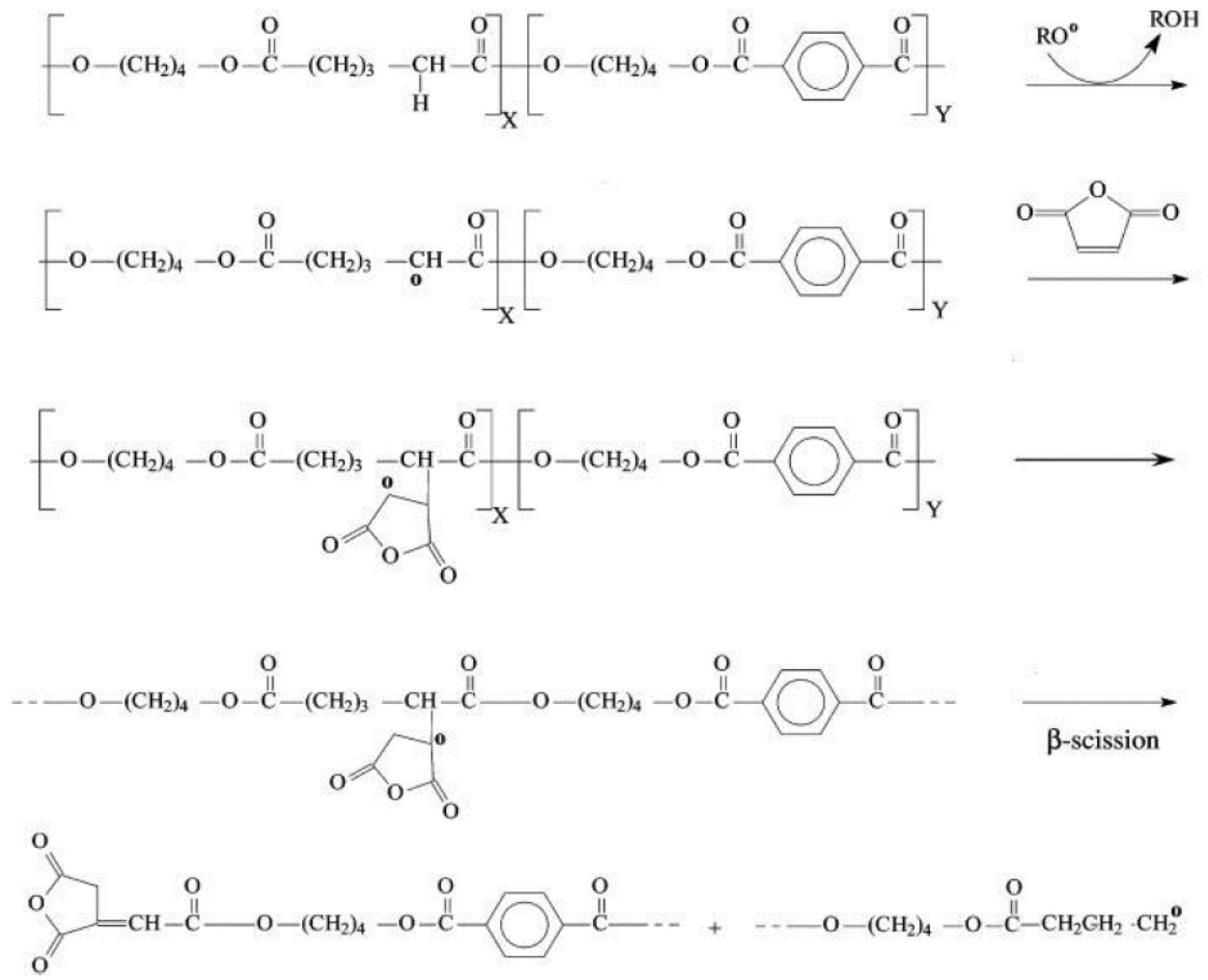
Figure 2-25 Proposed free radical initiated maleation mechanism followed by β-scission of PBAT (Nabar 2005)

2.6.2   Maleation of Polylactic Acid (PLA)

Kalambur 2012, in his studies, looked at the reaction of maleic anhydride with polylactic acid (PLA). From there, the authors proposed the free radical initiated maleation mechanism of polylactic acid (PLA). (Figure 2-26)

PLA   Maleic anhydride   Maleated PLA
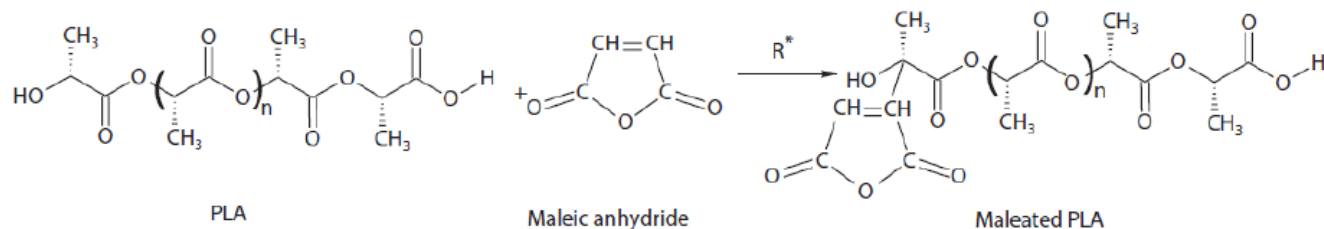
Figure 2-26 Proposed free radical initiated maleation mechanism of PLA (Kalambur 2012)

2.6.3 Raquez's Maleation of Starch

Raquez, in her papers and PhD thesis, proposed three different mechanisms on the reactions between glycerol, water, maleic anhydride, a free radical initiator and starch in a twin-screw extruder. (Raquez 2008) Her work covered: the maleation of starch; the hydrolysis of starch; and starch glycerylate formation.

The first mechanism looked at the reaction between maleic anhydride and starch. In it, Raquez suggests that the maleic anhydride forms an ester with hydroxyl group of C_6 of the glucose unit as offered in Figure 2-27.

In the second mechanism, Raquez proposed that starch, in the presence of a free radical initiator and an excess of water, would hydrolyze, resulting in a reduction of the starch's molecular weight. Figure 2-28

In the third and final mechanism, she proposed that starch, in the presence of a free radical initiator and an excess of glycerol, would result in hydrolysis of the starch followed by formation a starch glycerylate. Figure 2-29
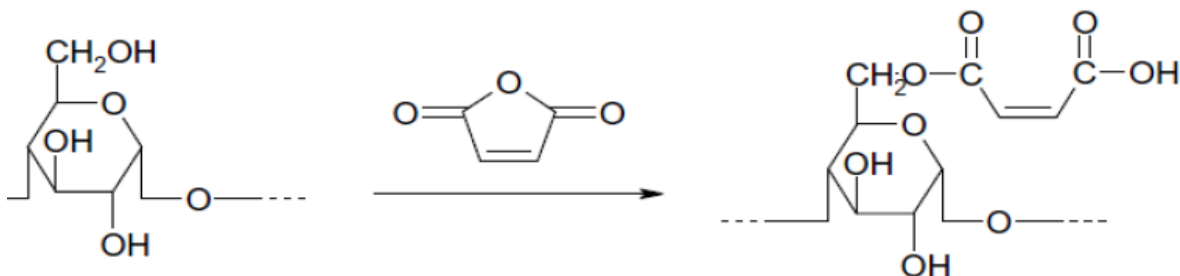
Figure 2-27 Esterification reaction of starch with maleic anhydride occurring at the C$_6$ hydroxyl position on starch – (Raquez 2008)
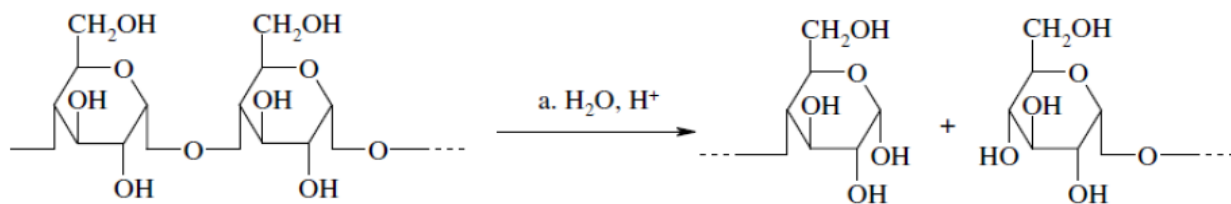
Figure 2-28 Hydrolysis and glucosidation of starch in the presence of water and proton donator (Raquez 2008)
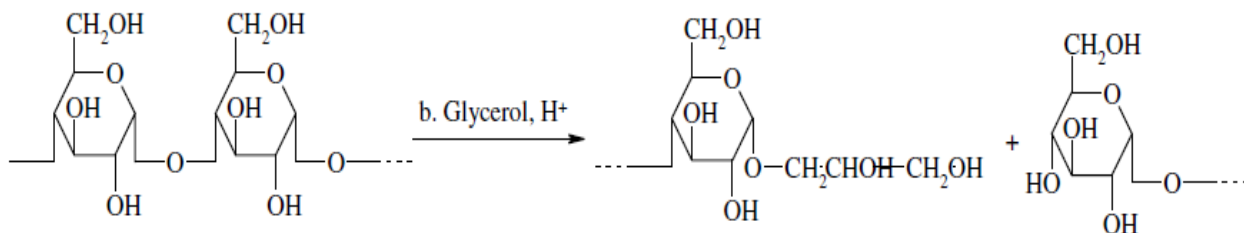
Figure 2-29 Hydrolysis and starch ether formation with glycerol glycerylated starch (Raquez 2008)

2.6.4 Glycerylated Starch and Starch Polyesters Graft Copolymers

Hablot's paper "Reactive extrusion of glycerylated starch and starch polyesters graft copolymers" offers two groups of reaction schemes from his investigation. The first was regarding reactions between starch, maleic anhydride, glycerol, and water (Figure 2.30). The second was on the concept of transesterification of starch with a polyester like PBAT. (Figure 2-31) (Hablot 2012)

In the reactions with starches, Hablot offers a mechanism which suggests the generation of ethers between the starch, maleic anhydride and glycerol, where various species of starch glycerylate are formed. Hablot's first group of mechanisms were a similar concept to what Raquez 2008 had proposed. However, Hablot suggests the potential of an equilibrium that exists between certain starch glycerylate species. (Hablot 2012) (Figure 2-30)

In the second group of mechanisms, Hablot suggests the potential for three separate mechanisms for transesterification between starch glycerylate and a polyester through reactions with maleic anhydride (Hablot 2012) (Figure 2-31, 2-32, 2-33, & 2-34). In each one the mechanisms proposed by Nabar, Kalambur, Raquez and Hablot, they were able to support their proposals through the analysis of their FTIR curves.
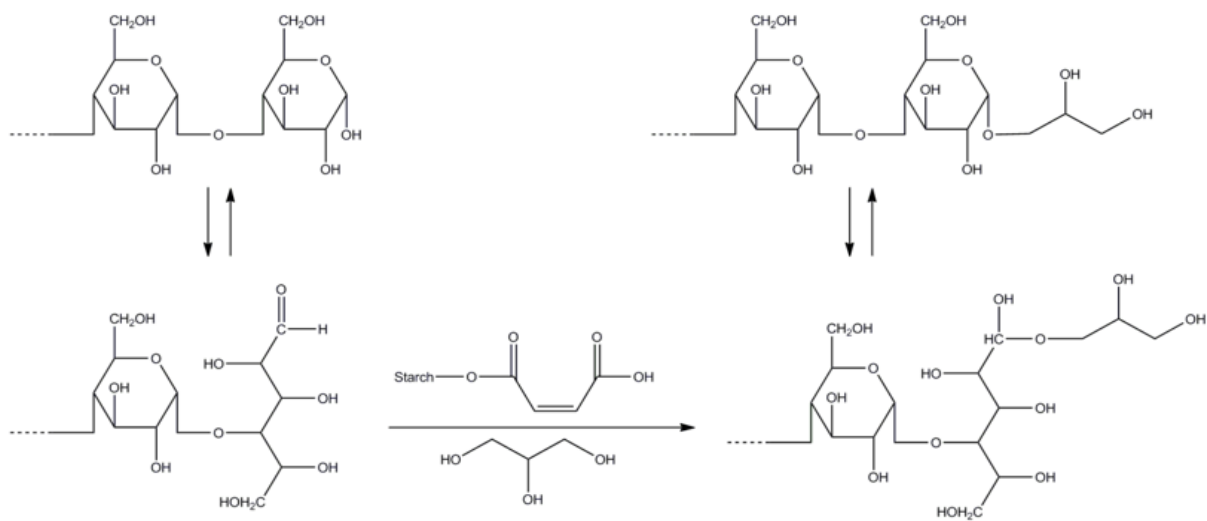
Figure 2-30 Ether formation in the presence of maleated starch in excess glycerol (Hablot 2012)
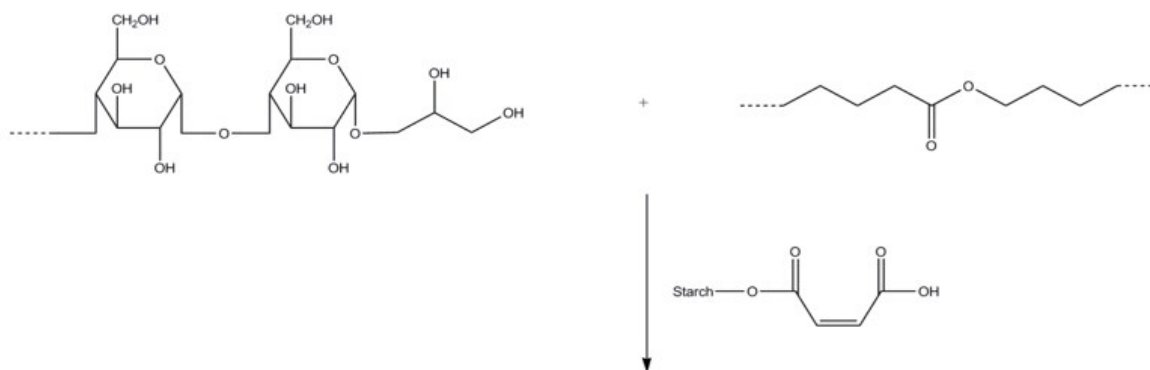
Figure 2-31 The second propose mechanisms of transesterification reactions between starch and PBAT in the presence of maleic anhydride, glycerol and water (Hablot 2012)
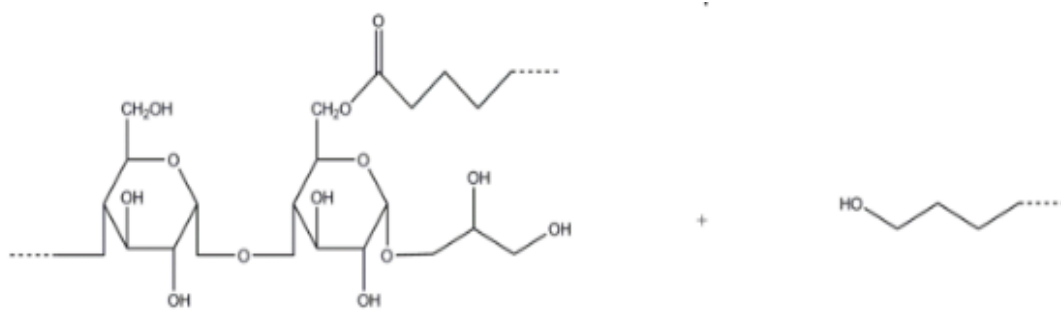
Figure 2-32 Transesterification at C_6 (Hablot 2012)

Figure 2-33 [and / or] Transesterification at C_1 (Hablot 2012)
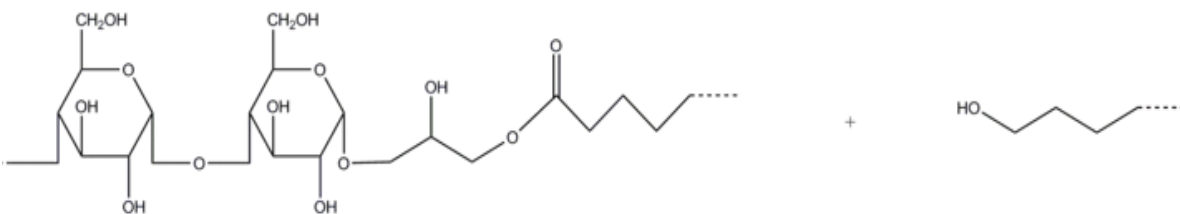
Figure 2-34 [and / or] Starch grafted glycerol transesterification (Hablot 2012)

2.7 Polymer Characterization.

Chemical characterization of the materials synthesized were conducted through the implementation of the standard testing methods established by America Society for Testing and Materials (ASTM). This section covers the methodologies of,

- Fourier Transform Infrared Spectroscopy (FTIR) ASTM E1252

- Differential Scanning Calorimetry (DSC) ASTM D3418

- Thermogravimetric Analysis (TGA) ASTM E1131

2.7.1 Fourier Transform Infrared Spectroscopy

Fourier Transform Infrared Spectroscopy (FTIR) is a valuable tool in understanding the molecular structure for polymers. With polymer synthesis, FTIR can qualitatively and quantitatively determine the formation of certain bond structures, such as ether, esters, carbonyl and carboxyl groups. (Griffiths 2007) FTIR can detect the characteristic signature associated with each configuration of organic atoms. Then, by referring to existing spectral tables of function groups, their presence can be determined. Quantitative determination of the functional group concentrations of an organic species can be determined with the application of Beer's Law. (Griffiths 2007) Figure 2-35 offers an FTIR spectrum in absorption mode and depicts the unique spectral signatures that are available for the specific functional groups. (Griffiths 2007) Beside each peak, the functional group is noted.
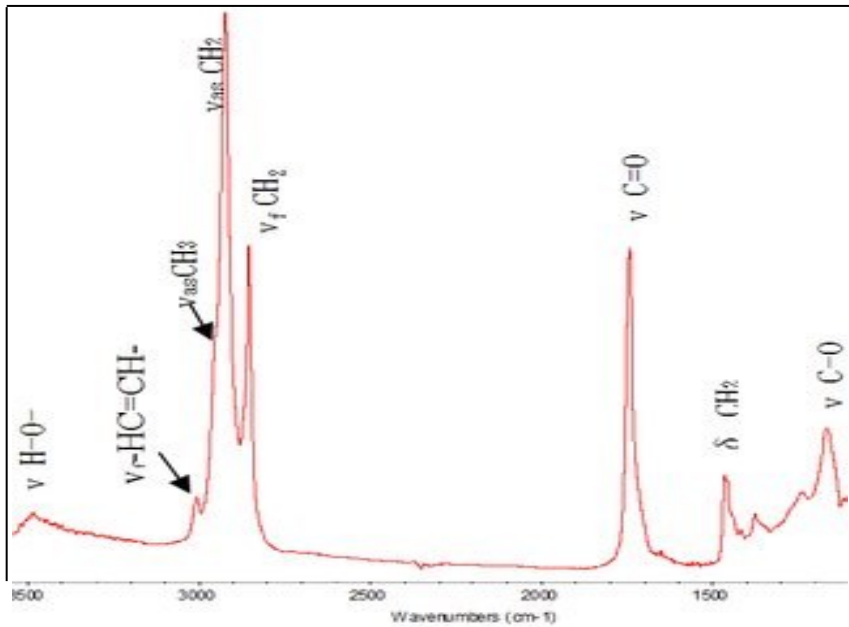
Figure 2-35 FTIR spectrum of thermal plastic starch with PBAT (Griffiths 2007)

2.7.1 Differential Scanning Calorimetry (DSC)

ASTM D3418 defines the standard test method for measurement of transition temperatures, and enthalpies of fusion and crystallization of polymers, by Differential Scanning Calorimetry (DSC).

DSC provides a rapid thermal analysis through the measurement of energy given off, or absorbed, by the material during phase transitions as a result of morphological or chemical changes as a polymer is heated/cooled over specified temperature ranges. Specific values for heat capacity, heat flow and phase transitions temperatures can be obtained from the DSC. Differential scanning calorimetry can be used to identifying specific polymers, polymer alloys, and certain polymer additives, through thermal transitions as outline the ASTM method ASTM D3418.

Table 2-2 Characteristic FTIR bands of starch and associated polymers (Aldrich)

Wavelength	Assignment
3300-3900	O-H Stretching from moisture
3200-3400 cm^{-1}	O-H stretching from glycerol
2940 cm^{-1}	ν CH=CH Alkene
2920 cm^{-1}	ν CH3 C-H stretching
2890 cm^{-1}	ν CH2 C-H stretching
1850 cm^{-1}	ν C-O-C maleic anhydride
1728 cm^{-1}	ν C=O carbonyl
1710 -1715 cm^{-1}	ν C=O esters
1640 – 1690 cm^{-1}	ν C=C stretching
1462 cm^{-1}	δ CH2 alkane
1325-1440 cm^{-1}	δ C-H alkane bending
1243 cm^{-1}	δ O-H bending
900-1250 cm^{-1}	ν C-O stretching
1160 cm^{-1}	ν C-O stretching aliphatic ether
770 cm^{-1}	δ C-H bending

The DSC can provide an examination of the crystallinity of a material and look at its change in morphology following chemical modification. The enthalpy (heat) of melt (fusion) (ΔH_m) is the measurement of heat absorbed during the phase transformation from solid to liquid. The enthalpy (heat) of crystallizations (ΔH_c) is the measurement of the heat given off during the phase transition from liquid to solid. The determination of ΔH_m and ΔH_c is through the integration of the areas under the peaks of a normalized DSC curve. The units of measurement for ΔH_m and ΔH_c are recorded in Joules / gram (J/g) (Widmann 2001).

The degree of crystallinity (χ_c) in a material is a function of the enthalpy of melt for the material in its current state, divided by its enthalpy of melt at 100% crystalline state (ΔH_{m0}) as outlined in Equation 2-9. (Sichina 2000) The values for ΔH_{m0} are found in literature.

$$Degree\ of\ crystallinity\ (\chi) = \frac{[\Delta Hm - \Delta Hc]}{\Delta Hm0}\ x\ 100\% \qquad \textbf{Equation 2-9 Degree of crystallinity}$$

2.7.2 Thermogravimetric Analysis (TGA)

Thermogravimetric analysis (TGA) determines endotherms, exotherms, and weight loss on heating /cooling used in identifying specific polymers. ASTM E1131 is the standard test method for compositional analysis by thermogravimetry. This test method provides a general technique incorporating thermogravimetry to determine the amount of highly volatile matter, medium volatile matter, combustible material, and ash content of compounds. This test method will be useful in performing a compositional analysis in cases where agreed upon by interested parties. (ASTM E1131) TGA analysis is beneficial in determining if the product evaluated is obtained from melt mixture of independent ingredients, a material exhibiting covalent bonding or intramolecular interactions, between the various raw materials. The shifts in the peaks from the raw materials suggest the potential of some bond interaction between the raw materials and is reflected in thermal stability changes of the material being evaluated.

In situations of potential covalent bonds occurring, TGA can be used to investigate chemical reactions where there is the potential for changes in weight. With stoichiometric reaction, the molar mass of the eliminated molecule can be determined and, as such, indicates how complete the chemical reaction achieved. (Widmann 2001)

Chapter 3
Materials and Methods

3.1 Introduction:

The foundation of this work was built on the selection of specific materials and methods which were employed, followed by the subsequent examination and analysis of the data gathered.

In this chapter, the considerations and specific choices of materials and methods are discussed as they relate to these topics:

- Raw material selection

- Sample Preparation

- Systematic development of compounds for analysis

- Characterization methods of analysis as applied to products developed in compounding

3.2 Raw Materials

3.2.1 Starches

Consideration was given to the materials selected based on their contrasting properties and commercial availability. In the example of starch selection, one of the questions considered dealt with which type of starch would destructure the fastest under given conditions.

The starch samples were obtained from Ingredion Incorporated of Bedford Park IL USA. A generic food grade maize dent starch was selected as a reference material for a base line comparison. The other samples were chosen from Ingredion's product portfolio based on the various properties which they offer. The properties taken into consideration were:

- **Type of starch**: Corn (Maize) or Potato

- **Morphology** based on amylose content: Ranging from 1% through 70 % amylose (1% / 25% / 70%). Starches with higher levels of amylose contain larger areas of crystallinity

- **Viscosity:** Ranging from high viscosity of conventional dent starch through to the lower viscosity of modified versions

- **Chemical Modification**: Oxidized starches displaying various levels of carbonyl and carboxyl group formation between C2-C3 in the glucose unit structure (ranging 0.1% through 3%)

3.2.2 Plasticizers

As discussed in the literature reviews, both water and glycerol are efficient at destructuring and plasticizing starch. These materials were sourced from:

- Honeywell High Purity Water Lot # DA 150

- Brenntag Glycerol ≥98 % pure Lot# 1306030035

3.2.3 Polyester Resins

Consideration was taken to evaluate the dominant commercial and biodegradable resins. Aliphatic polyester resin, polylactic acid (PLA) and aromatic / aliphatic copolyester resin, polybutylene adipate terephthalate (PBAT) polyester resins were identified as the resins of choice. It is to be noted that both polyesters are hydroscopic in natural and will hydrolysis in the presence of heat, shear and water to form lower molecular weight polymers. Samples were acquired from BASF and NatureWorks.

- PBAT - BASF Ecoflex F Blend C1200 Lot 15197068E0 item# 50167513

- PLA - NatureWorks Ingeo 4043D Lot # C10428B111

Table 3-1 summarizes the starches evaluated in this study.

Table 3-1 Ingredion Incorporate starch samples selected for evaluation

Name	Description	Lot Number	Amylose: Amylopectin ratio	Moisture level %
Hylon VII	GMO Hi-Amylose Corn	KCK5510	70:30	7.83
30050	Paper coating - Chemically modified between C_2 and C_3 with 0.1-0.3% of carbonyl and carboxyl group formation.	1246150100	25:75	8.02
55310	Modified - Reduced Viscosity Oxidized	7280100001	25:75	6.60
Novation 1600	Potato	6/28/2017	25:75	10.58
055720	Modified - Reduced Viscosity Oxidized	7281129102	25:75	6.73
Stablebond 055110	Modified Reduced Viscosity	7284212104	25:75	4.25
Amioca	Waxy Maize Starch – predominately amylopectin	ED8646	1:99	5.89
Dent starch	Food Grade Maize Starch (conventional)	SA18D00312	25:75	10.21

3.2.4 Peroxides

The challenge in working with organic peroxides is the danger associated with their rapid decay and the release of hydrogen, if handled incorrectly. As such, the organic peroxides were chosen with respect to safety and the properties offered. Selection of the organic peroxides was based on the criteria of:

- Stability at room temperature

- Free radical initiator half-life at compounding temperatures

Three organic peroxides were identified, and they were acquired from:

- AkzoNobel Trigonox 101 (2-5 Dimethyl, 2-5-di(tert-butylperoxyl) hexane)

  Lot # PAE 12051D1201

- Alfa Aesar Dilauroyl Peroxide 97% pure (item#L14310-100g), lot#10185597

- Alfa Aesar Dibenzoyl Peroxide 97% pure (dry weight basis) with 25% water (item#L13174-50g), Lot# 10186486

Table 3-2 Peroxides and their half-life (Aldrich)

	T(^{o}C) – 1h	T(^{o}C) – 10 h	T(^{o}C) – > 15 second
Trigonox 101	147	124	**214**
Dibenzoyl Peroxide 97% pure	91	72	**<150**
Dilauroyl Peroxide 97% pure	79	61	**<130**

Note: the half-life of each material and the temperature to achieve less than 15 seconds

3.2.5 Grafting Agent

Maleic Anhydride (MAH) is a well-known building block in polymerization. Its bifunctional nature allows for covalent bonding between polymers, starches and other materials. High purity (99.0%+) maleic anhydride pastels (item # 63200-500G-F) Lot # BCBP1063V

were acquired from Fluka Analytical.

3.3 Sample Preparations

3.3.1 Formulation sheets

Formulations sheets (Figure 3-3) were developed to calculate the specific weights of each ingredient for compounding in a CWB Mixer-Measuring Head for an open volume of 60cc. The example below is for thermoplastic starch compound formulation. A mixture of starch and a plasticizer blend of glycerol and water were compounded in Mixer-Measuring Head with Banbury blades rotating at 45 RPM and initial mixer body preheated temperature of 150°C.

Table 3-3 Compounding Formulation Sheet

Blade Type:	Banbury Blades						Temp:	150ºC	
Ingredients	Addition	phr	spec. gravity kg/ltr	volume phr/sg	batch weight	US$/#	ml of liquid	gram weight
Starch	a	31.10	1.20 0	25.9167	0.11242	$0.45		50.99
PBAT	b	0.00	1.26	0.0000	0.00000	$1.95		0.00
MAH (powder)	b	0.00	1.310	0.0000	0.00000	$1.55		0.00
Glycerin	a	7.78	1.129	6.8911	0.02812	$0.59	11.30	12.76
Peroxide	b	0.00	0.877	0.0000	0.00000	$4.10	0.00	0.00
Water (demineralized)	a	1.50	1.000	1.5000	0.00542	$0.01	2.46	2.46
Totals		40.4		34.3	0.1	$0.46		66.2
		phr		ltr/kg	lbs	lbs		grams

3.3.2 Compounding Techniques

Formulations were developed to explore starch's behaviour in various compounding situations. This technique was developed to manufacture the samples for evaluation which offer some form of consistency and reproducibility. Dry raw materials were weighed out on Sartorius Signum 1 scale and placed into a stainless-steel bowl where they were whisked together. Liquids were premeasured and uniformly blended. Using a 5 ml syringe, the required volume of blended liquids was drawn and introduced slowly into the dry mix while under continuous whisking. C W Brabender (CWB) 3-piece Mixer-Measuring Head with Banbury style blades (Figure 3-1 and 3-3) were mounted on CWB Intelli-Torque Plasti-Corder® Torque Rheometer (Figure 3-2). The predetermined amount of mixture was introduced into CWB quick load chute with piston and 5 kilo weight. The chute was placed on the Mixer-Measuring Head once the Intelli-Torque Plasti-Corder® Torque Rheometer had reached the established conditions and completed calibration. The quick load chute with piston and 5 kilo weight were employed to quickly, efficiently and uniformly introduce the formulation into the torque rheometer mixer in an effort to create reproducible data and process so that information collected could be compared.

Figure 3-1 View of thermoplastic starch on rotor of the CWB mixer on opening

3.3.3 CWB Intelli-Torque Plasti-Corder® Rheometer Compounding

CWB Intelli-Torque Plasti-Corder® Rheometer with 3-piece mixer/measuring head with Banbury Blades was employed to generate the compounds. Banbury blades were chosen as they duplicate the mixing action of a commercial Banbury Mixer which offers medium shear-rate mixing action ideal for compounding studies. The Intelli-Torque Plasti-Corder® with WINMIX® software program captures the mix blade speed, torque rheometry, and body and material temperatures in real time during the compounding process, then offers the data in graphic or excel format for further analysis in OriginLab's Origin® or other analytical softwares.

Figure 3-2 C.W. Brabender Plasticorder

Figure 3-3 Thermoplastic starch covered Banbury rotors

3.4 The systematic development of compounds for analysis

The experimental design identified that several formulations /compounds were required so that the following concepts could be explored:

  i.   The destructuring and plasticization of food grade maize dent starch

 ii.   The destructuring and plasticization of various starches

iii.   The effect of free radical initiators on chemically modifying starch

 iv.   The effects of MAH on chemically modifying starch

v.   The effects of pre-drying starch before compounding

vi.   The investigation of compounds made with PBAT and PLA

3.4.1 Destructuring and plasticization of regular dent starch

Multiple trials were designed to explore the relationship between several variables and their influence on the rate at which dent maize starch would destructure and plasticize during compounding. These studies cover the concepts outlined, while examining their impact on the gelatinization of regular dent starch,

- at various levels of water addition in compounding

- over various ratios of water and glycerol in compounding

- over various shear in compounding

- over various temperature employed in compounding

Data was collected on torque and temperature as a function of time from the CWB and compared to establish relationships of these variable on destructuring and plasticizing dent maize starch.

3.4.2 Destructuring and plasticization of various starches

In the previous section, the relationship between several variables and their influence on the rate at which dent starch destructures during compounding were explored. Subsequently, an assessment of a variety of starches and their rate of gelatinization was undertaken with a standardized group of conditions. The data was collected for analysis.

3.4.3 The effect of free radical initiators

Three of the starches were selected from the previous group of starches based on their ability to quickly and efficiently destructure and plasticize under the conditions considered.

These starches were compounded with the three organic peroxides and the properties examined. In each formulation, one of the chosen starches was compounded with the other materials outlined. Note that these starches were conditioned before compounding for this evaluation.

3.4.4 The effect of increasing free radical initiator

The experimental design examines the impact of increasing the amount of the fastest free radical initiator. In this scenario, the amount of organic peroxide was increased by three times the initial amount added, then compared to the baseline compound.

3.4.5 The effects of MAH on chemically modifying starch

Maleic Anhydride (MAH) is a well-known building block in polymerization. Its bifunctional nature allows for covalent bonds to be formed. This experimental design examines the starch polyester compound and the impact of increasing the amount of MAH added during compounding. The quantity of MAH added increased by two and three times over the initial amount.

3.4.6 The effect of pre-drying the starch before compounding

Starch samples were dried in a Cascade TEK 5 cubic foot vacuum oven at 104°C and under 4.40 Torr vacuum (Figure 3-3). At timed intervals of three and five hours, samples were pulled

and moisture content determined with Ohaus MB 45 moisture balance. Following this, the dried samples were compounded according to the design outlined in section 5.

Vacuum level

Temperature in the oven

Ohaus MB45 Moisture Balance
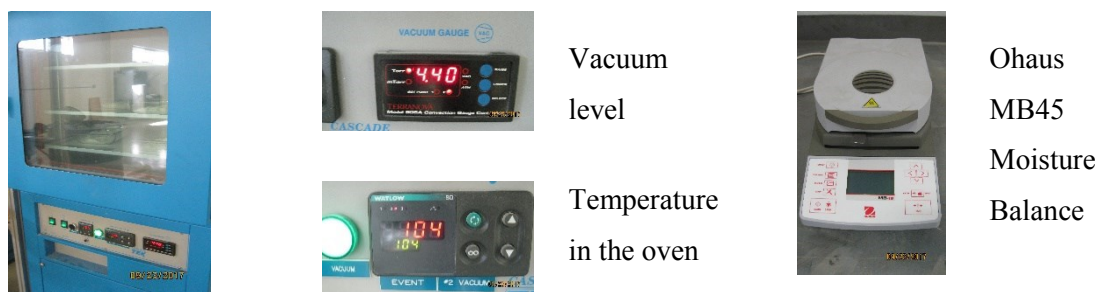
Figure 3-4 Photos of the Cascade TEK Vacuum Oven and Process Conditions.

3.4.7 Pre-drying starch and master batching

This study assumed that drying the starch imparted some value to the process. Accepting that premise, the concept of pre-dying the starch offline may be required. Given the time required for drying, the hypothesis was raised "if the starch is dried offline and blended with the other ingredients, would there be a shelf life to the mixture" To explore that notion, and to understand the impact of allowing a master batched formulation of dry starch to sit for a period of time, one starch sample was dried for five hours and analyzed for moisture content. Four samples, large enough for compounding, were drawn and mixed together with all the other ingredients. Each mixture was placed in a labeled zip lock bag. These mixtures were left standing for a predetermined time before compounding. At time zero (0 seconds) bag 1 was immediately compounded. Then at two hours, five hours and 24 hours, the other corresponding labeled materials were compounded.

3.4.8 Investigation of compounds with PBAT and PLA

The experimental design to this point focused on compounding PBAT polyester with starches. As such, an investigation of PLA-starch compounds was conducted, and its properties compared with PBAT – starch compounds.

3.5 Characterization methods of analysis

3.5.1 Fourier Transform Infrared Spectroscopy (FTIR)

Chemical analysis of the compounded samples was conducted on a Perkin Elmer Spectrum 400 MIR FITR equipped with an Universal ATR. Each sample was scanned four times with a single bounce through a Diamond/ZnSe crystal with a resolution of 4 cm^{-1}. The total scan covered the spectrum from 4,000 – 650 cm^{-1}. Perkin Elmer Spectrum 400 MIR FITR calibration was verified with polystyrene film calibration standard and an atmospheric correction was captured before ATR FTIR spectrum of the samples were taken in accordance to ASTM E1252

3.5.2 Differential Scanning Calorimetry (DSC)

Differential Scanning Calorimetry (DSC) analysis of the samples were conducted on a Perkin Elmer DSC 8500 with Pyris software in accordance to ASTM D3418. The DSC was calibrated with Indium and Zinc and the verification of the calibrate was conducted with Indium standard. DSC was conducted in an inert nitrogen atmosphere with a flow rate of 30 ml min^{-1}. All temperature transitions occurred with a uniform temperature rate change of 10°C min^{-1}. Samples weighing between 3-12 mg were hermetically sealed in 50ml aluminum pans. The samples were subjected to two cycles of heating and cooling as per the following program: (i) samples were held at 40°C for five minutes, (ii) ramped from 40 ^{o}C to 190°C, (iii) held for five minutes at 190 ^{o}C, (iv) cooled from 190°C to 40°C, (v) held for five minutes at 40°C, (vi) ramped from 40°C to 190°C, (vii) held for five minutes at 190°C, (vii) cooled from 190°C to 40°C, (ix) held for five

minutes at 40°C. Following this process, the curve from the second heating pass was analyzed for temperatures of melt onset, melt end, and peak temperature and heat of fusion with the Pyris software. The second cooling curve was also analyzed for crystallization, looking for the temperatures for the onset, end point, and peak temperature and heat of crystallization.

3.5.3 Thermal Gravimetric Analysis (TGA)

Thermal Gravimetric Analysis (TGA) were conducted on the samples with a Perkin Elmer Pyris 1 TGA instrument in conjunction with Pyris software in accordance to ASTM E1131. The TGA's temperature calibration was established with reference samples of Nickel, Perkalloy, Zinc and Iron. The weight calibration was established with certified Troemner 100 mg standard weight. TGA was conducted in an inert nitrogen atmosphere with a flow rate of 30 ml min^{-1}. All temperature transitions occurred with a uniform temperature rate change of 10°C min^{-1}. Samples weighing between 5-10 mg were placed in ceramic pans. The samples were subjected to the following program: (i) samples were held at 50°C for five minutes, (ii) ramped from 50°C to 600°C, (iii) held for five minutes at 600°C, (iv) cooled from 600°C to 50°C. Following this, the samples were analyzed for composition as outlined in the ASTM standard.

Chapter 4

Results and Discussions: Destructuring and Plasticization of Starch

4.1 Introduction

When looking to migrate the process outlined in Wolff's patent (2013) to a twin screw extruder, there is the need to define the challenges in the process which will have to be addressed up front. Understanding these limitations helps make the experimental results more meaningful and aids in the success of process migration to a twin screw extruder.

Reaction extrusion involves several processes within the confines of the extruder's length and limited time. These processes may be broken down into stages, however it is probable that some could overlap others and occur simultaneously. For the purpose of this thesis it is assumed that these stages occur one after the other. (Xie F. 2007)

Stage 1. Destructuring and plasticization of starch

Stage 2. Chemical modification of starch with maleic anhydride

Stage 3. Introduction of polyesters

Stage 4. Chemical reactions

Stage 5. Venting of gases

Stage 6. Mixing

Stage 7. Venting of gases

Stage 8. Meter of the material to die

As there are several stages / processes that need to be performed within the confines of the extruder within a limited time, the goal is to identify the most time efficient parameters that will allow for the desired results to be achieved.

One significant challenge in the formation of starch copolymers with polyesters is with the chemical modification of starch. To achieve effective modification, the starch granule must open first and form the gel ball as describe by Yu & Christie, 2005. This process is the destructuring and plasticization of the starch.

In this chapter, multiple trials were designed to explore the relationship between several variables and their influence on the rate at which dent maize starch would destructure and plasticize during compounding. These studies cover the concepts outlined, while examining their impact on the gelatinization of regular dent starch:

- at various levels of water addition in compounding
- over various ratios of water and glycerol in compounding
- over various shear rates in compounding
- over various temperature employed in compounding.

Time is money when performing reaction extrusion with a twin screw extruder. The limitation of resident time, the time that the materials remain in the extruder, dictates the total time frame available to perform every step in the desired process(es) or reactive extrusion polymerization. These studies were carried out in a laboratory scale internal mixer instead of an extruder because of the flexibility offered by the internal mixer with respect to running experiments in different times.

As a point of reference, residence time on a 42 mm with 52:1 L/D Leistritz twin screw extruder, configured for reaction extrusion with starch, maleic anhydride, glycol, and polyester, was

determined to be one minute and thirty seconds. This residence time frame was established on a 42 mm with 52:1 L/D lab line located at company Leistritz Extrusion Ltd. in Sommerville NJ.

As such, the limitation of one minute and thirty seconds was accepted as the window of evaluation when looking at these properties being assessed.

4.2 The influence of water on the destructuring of dent starch

Common dent starch was chosen to create a baseline for studying the influences of various parameters on the process of destructuring starch. The dent starch sample utilized in these evaluations contained 10.2% moisture as determined with Ohaus MB45 moisture balance. Blends of starch with various amounts of water, as outlined in Table 4-1, were evaluated for torque and temperature over time with CWB Intelli-Torque Plasti-Corder® Rheometer with 3-piece mixer/measuring head and Banbury Blades with body temperature at 90°C. The temperature of 90°C was recognised by Yu & Christie (2005) as being high enough for the gelatinization of dent starch, while being below the boiling point of water. Employing this temperature mitigates the potential for moisture loss due to evaporation, thereby identifying the amount of water required to effectively destructure the starch granule and within what timeframe.

Table 4-1 Formulations evaluated in an effort to interrupt the influence of water on the destructuring starch

Label	Starch	Water Wt-%	Glycerol Wt-%	Screw Speed RPM	Temperature °C
DM-W0	Dent Maize	0	--	45	90
DM-W5	Dent Maize	5	--	45	90
DM-W10	Dent Maize	10	--	45	90
DM-W20	Dent Maize	20	--	45	90

In Figure 4-1 the initial slope of the curve represents the rate at which the dent starch is being destructured. The increase in torque reflects the opening of the amylopectin and amylose molecules from their granule structure thereby increasing the viscosity of the mix. The height of the curve denotes the amount of energy required to complete the destructure of the starch granule. In fact, the height of the curve or the area under the curve are indicative of the work required during this process. The decline of the torque curve following the maximum height illustrates the plasticization of the amylopectin and amylose molecules and indicates the effectiveness of that specific amount of water to reduce the viscosity of the mixture.
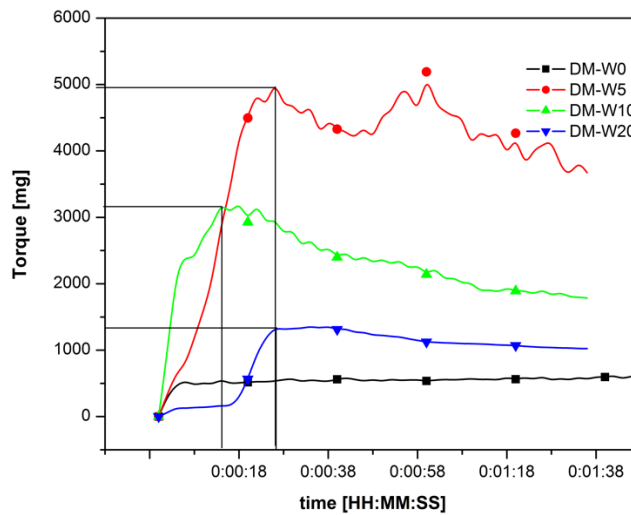
Figure 4-1 Displays of the torque measurements as a function of time for the blends of starch and water outlined in Table 4-1

Table 4-2 Summary of the energy (torque) and time required to destructure starch compounds outlined in Table 4-1

Property	DM-W0	DM-W5	DM-W10	DM-W20
Total moisture Wt-%	10.21%	15.21%	20.21%	30.21%
Onset Torque [mg]	650	985	0	214
Max Torque [mg]	>10,000	5093	3235	1334
Delta Torque [mg]	>10,000	4108	3235	1120
Time [sec] at onset	360	7	0	17
Time to max torque [sec]	366	26	14	26
Initial Temp [°C] at onset	87	70.1	72.4	74.9
Final[°C]	103	78.4	73.7	71.9
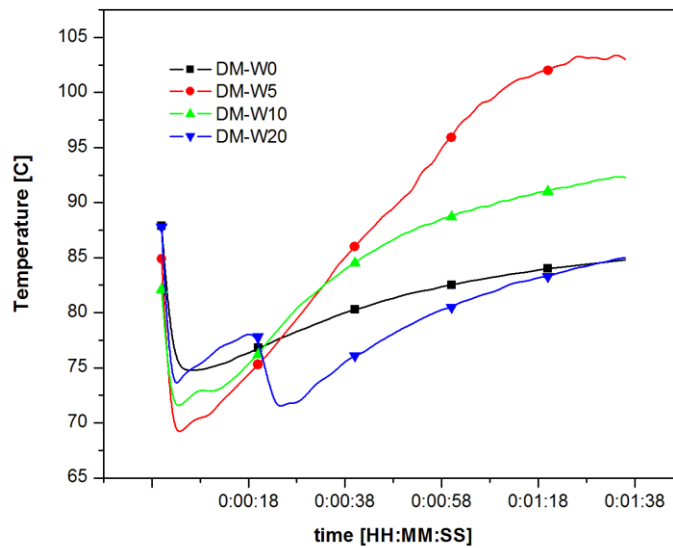
Figure 4-2 Displays of the temperatures of the mixes measured as a function of time for the blends of starch and water outlined in Table 4-1
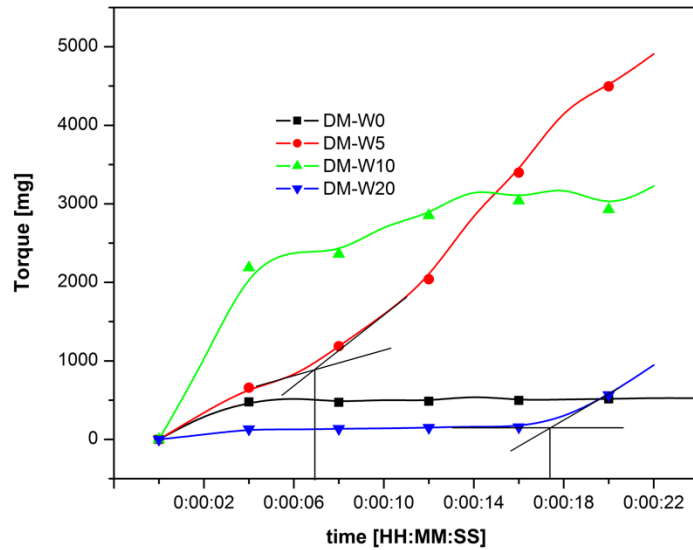
Figure 4-3 Displays of the torque measurements as a function of time for the mixes of starch and water outlined in Table 4-1 during the first 22 seconds.
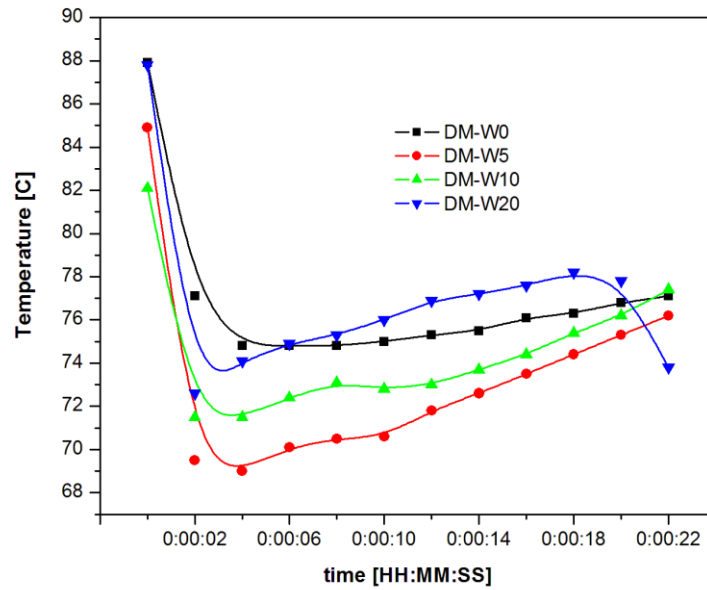
Figure 4-4 Displays of the temperatures of the mixes measured as a function of time for the blend of starch and water outlined in Table 4-1 during the first 22 seconds.

62

The addition of 5% moisture seems to offer the ability to quickly destructure the starch (DMW5). However, when the temperature parameter is taken into consideration, a dramatic increase is noted. This temperature increase is believed to be a result of a lack of plasticizer. The energy transferred into the mixture by the rotating Banbury Blades is not sufficiently compensated and allow for free movement of the amylopectin and amylose molecules due to lack of plasticizer. As a result, higher torque values are recorded, reflecting higher viscosities of the mixture. With the continuous addition of energy into the mixture, higher shear occurs between the molecules which translates into additional heat being captured within the mix. The net result is an increase in temperature which exceeds the boiling point of water, thus resulting in the evaporation of the plasticizer. As time passes, the loss of plasticizer increases and the viscosity of the mix and temperature increases. At about 5 minutes of exposure to continuous mixing, the torque exceeds the maximum safety value of 10,000 mg and severs the safety shear pin, stopping the equipment at a recorded temperature of 114°C. This indicates that starch, with the addition of 5% moisture, was not suitable to be considered efficient in the destructuring and plasticization of dent starch.

Of interest is the assessment of the starch by itself (DMW0). The defined sample of dent starch utilizes in this evaluation contained 10.2% moisture from the manufacturer and is introduced into the 3-piece mix head with no addition of extra moisture. Within the confines of this evaluation, there is no destruction or plasticization of the starch occurring. After six minutes of mixing within the 3-piece mix head, the torque rapidly increases indicating that starch is destructuring or potentially degrading. Within seconds, the torque exceeded the maximum safety value of 10,000 mg, severing the safety shear pin, stopping the equipment with a recorded temperature of 103°C. Figure 4-5 These results indicate that dent starch, containing a minimum of 10.2% moisture from the manufacturing process without any additional moisture, is not efficient in the destructuring of the starch granule nor its plasticization within the 3-piece mix head.
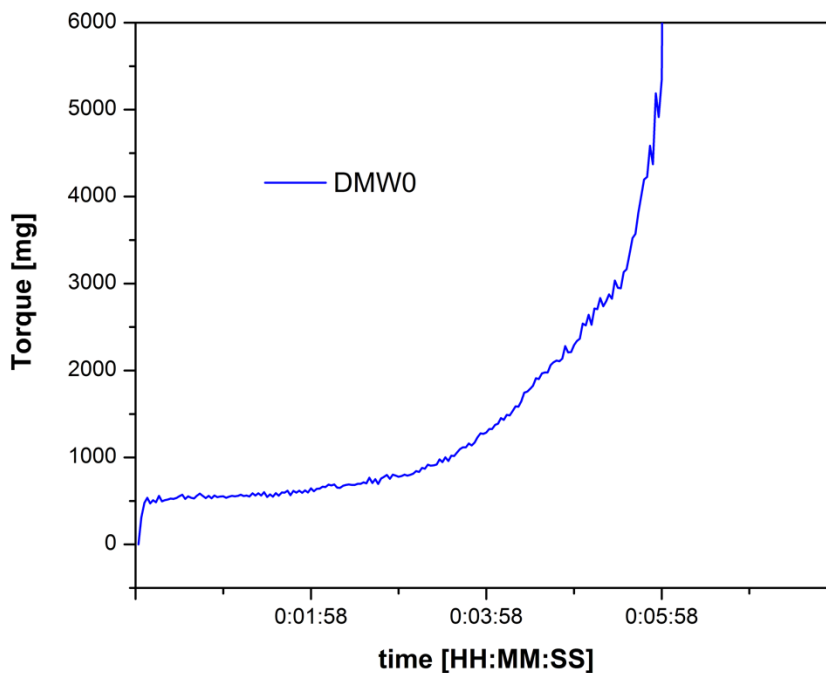
Figure 4-5 Curve of torque versus time for DMWO

From the results seen in Figure 4-1, the addition of 20% moisture seems to suggest effective destruction and plasticization of the starch (DMW20), however not within the confines of the identified time frame. When evaluating the temperature curve for this process in Figure 4-2, it is noted that temperature of the mix is below that of the 3-piece mix head body temperature thereby indicating that the mix is drawing heat from the body and potentially indicating that it is not fully destructured. At three minutes of continuous mixing, the temperature of the mixture finally reaches the temperature of the body of the 3-piece mixer. At that point in time, it is suggested that effective destructure and plasticization of the starch could have occurred. The challenge associated with this time frame is that it exceeds that of the residence time of the twin screw extruder. As such, 20% addition of moisture to starch is not a favourable parameter for consideration.

Polarized light microscopy of dent starch, in Figure 4-6, depicts untreated starch on the left and that of dent starch with 20% moisture addition following 1 minute and 30 seconds of mixing. In both cases, the Maltese cross is present under polarized light confirming that crystallinity still resides within the starch structure, thereby confirming the hypothesis that little or no gelatinization of the starch has occurred.
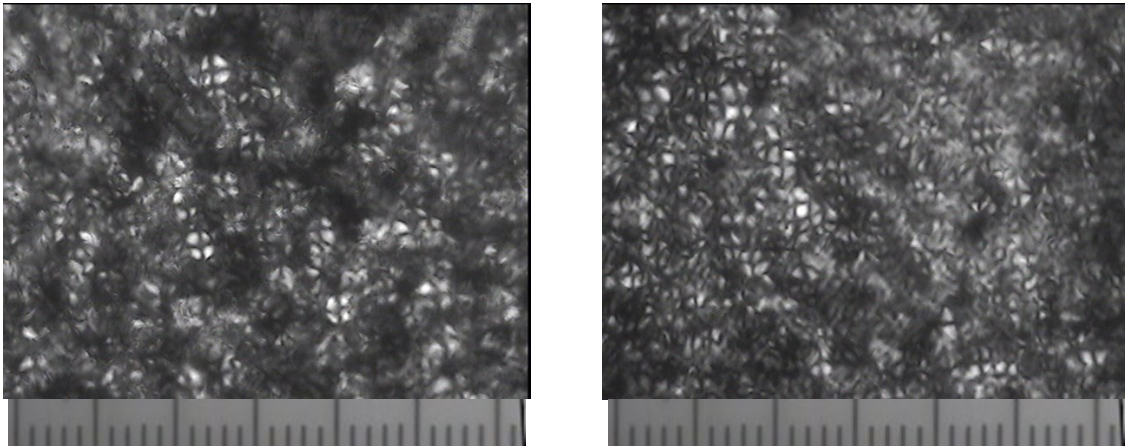
Figure 4-6 Polarized light microscopy photographs of dent starch on the left and that of dent starch with 20% moisture addition following 1 minute and 38 seconds of mixing of the right [Magnification 150x with scale were each mark represents 0.01mm]

Finally, Figure 4-1 suggests that the addition of 10% moisture acts as the most effective level needed to achieve both destruction and plasticization of the starch (DMW10) in a timely fashion. As well, the temperature curve for this process indicated in Figure 4-2, exhibits a minimal temperature increase of the mixture over that of the 3-piece mix head body temperature, thereby indicating effective plasticization of the starch with minimal shearing and additional heat energy buildup. This suggests that 10% moisture addition to dry starch under these conditions would effectively achieve destructuring and plasticization of dent starch.

4.3 The influence of water / glycerol on the destructuring of dent starch

When looking at the destructuring of starch and its subsequent plasticization, Yu & Christie (2005) determined that higher temperatures were required when dealing with higher amylose-based starches. They concluded that starches containing levels of amylose greater than 50% would have gelatinization temperatures in the range 120 – 140°C. Given this understanding and the findings gained from Section 4.2 when exploring the addition of 10% moisture with starch, once the temperature of the mixture rises above 100°C, water tends to evaporate and plasticization of the starch decreases (Figure 4-2 and 4-1). As such, there is the need to explore alternative plasticizers, and/or blends thereof, which offer higher vapour pressures and allow for processing at higher temperatures.

Based on the work of Kaseem 2011, glycerol was identified as the plasticizer of choice to address the high processing temperatures required to destructure starch.

In this evaluation, it was assumed that the starch had a higher affinity for water than it would for glycerol or other plasticizers as stated by Willet 1995. This was confirmed in the evaluation depicted in Figure 4-7. These curves indicate that water is more efficient in destructuring and plasticization of starch than glycerol under similar conditions.

It is to be noted that water is miscible in glycerol. Pure glycerol has a boiling point of 290°C which offers several advantages for higher temperature processing. However, a dilemma occurs with water dilution of glycerol. As the ratio of water to glycerol increases, the blend's boiling point becomes further depressed. Table 4-3 outlines the effect of increasing water percentage on the boiling point of water/glycerol blend. (Miller 1953) Although in the evaluation at 90°C, there is little potential to boil off this plasticizer blend, attention to process temperatures are important to follow when looking at the ability of a water glycerol blend in destructuring and plasticizing starch.

Table 4-3 The effect of water dilution on glycerol's boiling point (Miller 1953)

Glycerol / Water	Ratio	Boiling Point @ 760mm
Wt-%		°C
100 / 0	1:0	290.0
95 / 5	9.5:0.5	164.0
90 / 10	9:1	138.0
80 / 20	4:1	121.0
75/ 25	3:1	116.7
50 / 50	1:1	106.0
25 / 75	1:3	102.3
0 / 100	0:1	100.0

In this section, blends of water and glycerol are evaluated to understand their influence on the destructuring and plasticization of regular dent starch at 90°C.

In Figure 4-7, it is noted that pure glycerol is less efficient than water itself in destructuring and plasticization of starch. It is surmised that some amount of water may be required to achieve destructuring and plasticization of starch within the desired timeframe. Table 4-4 reflects the formulations and blends of water and glycerol that were considered and evaluated, along with the processing parameters for the CWB Intelli-Torque Plasti-Corder® Rheometer with 3-piece mixer/measuring head and Banbury Blades.

Table 4-4 Water / glycerol blends and formulations for determination of their effectiveness to destructure and plasticize starch

Label	Ratio of H_2O:Glycerol	Starch Wt-%	Water Wt-%	Glycerol Wt-%	Screw Speed RPM	Temperature ^oC
DM-W20	1:0	77	23	0	45	90
DM-G20	0:1	77	0	23	45	90
DM-W1:G1	1-1	77	11.5	11.5	45	90
DM-W1:G3	1-3	77	5.7	17.3	45	90
DM-W3:G1	3-1	77	17.3	5.7	45	90
DM-W1:G4	1-4	77	3.6	19.4	45	90
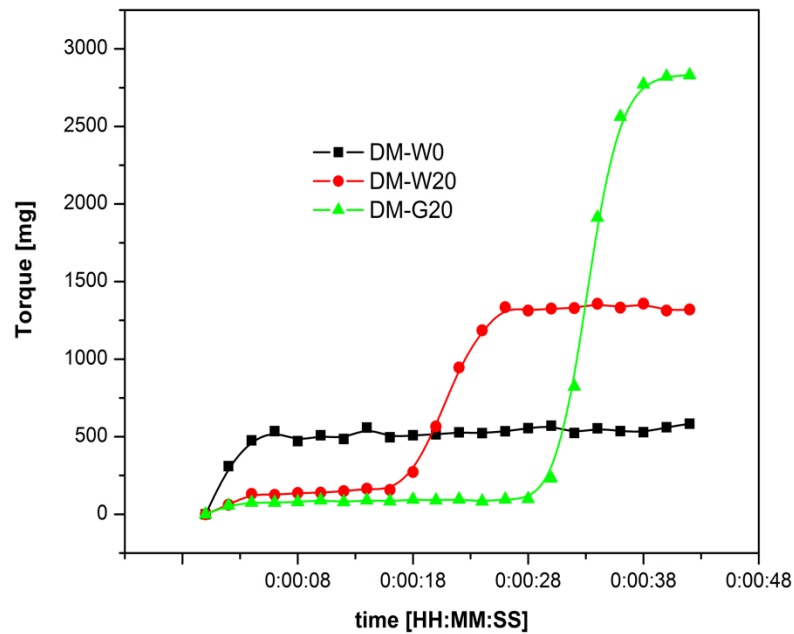
Figure 4-7 Destructuring and plasticization of starch in the presences of water and glycerol

68

Table 4-5 Summary of the effect of glycerol on destructuring starch

	Units	DM-W20	DM-G20	DM-W0
On set	mg	214	99.4	538.10
Max	mg	1334	3986	>10,000
On set	sec	17	28	360
Max	sec	26	56	366

Figure 4-8 depicts the relationship identified between the blends of water and glycerol and their ability to efficiently destructure and plasticize starch. Blends of starch with small amounts of water in glycerol produced significantly faster rates of higher torque than the blends of starch with just glycerol as depicted in Figure 4-8.

From the curves in Figure 4-8 it is noted that the ratio of 1:4 water:glycerol blend was effective in destructuring and plasticizing starch. According to Miller's (1953) finding in Table 4-3, formulation DM-W1:G4 would allow for the highest processing temperature before the plasticizer's boiling point is reached. The formulation DM-W1:G4 was found to be efficient in plasticizing starch with no noticeable increase in mixture temperature over that of the body temperature of 90°C.

Of interest are the results noted from the substitution of a small amount of glycerol with water. Formulation DM-W3:G1 quickly and efficiently destructured and plasticized the starch. However, it lacked the characteristic which would allow for processing at temperatures beyond 102.3°C before evaporating the plasticizer from the compound.

As such, the formulation DM-W1:G4 seems to offer the best compromise for rate of destructured and plasticization of the starch while granting the highest processing temperature before the plasticizer would reach boiling point and evaporate.
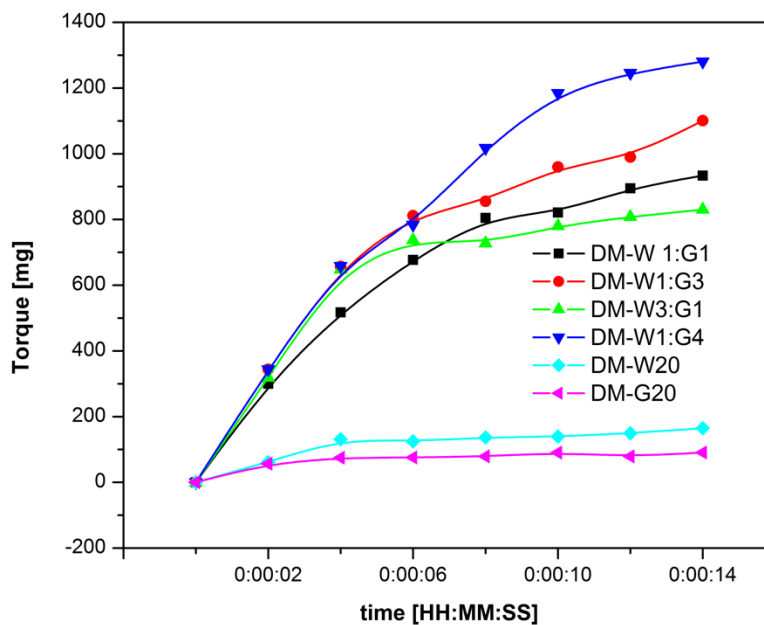
Figure 4-8 Depicts the relationship between ratio of water:glycerol and its ability to destructure and plasticize starch in the initial 14 seconds of mixing.

Table 4-6 Summary of the effects of blends of water and glycerol on destructing starch

Label	Onset mg	Max mg	Onset seconds	Max seconds	Glycerol:Water boiling point °C
DM-W1:G1	0	n/c	0	n/c	106.0
DM-W1:G3	0	1567	0	42	116.7
DM-W3:G1	0	880	0	30	102.3
DM-W1:G4	0	1569	0	42	121.0
DM-W20	156	1334	16	26	100.0
DM-G20	99.4	3986	28	56	290.0
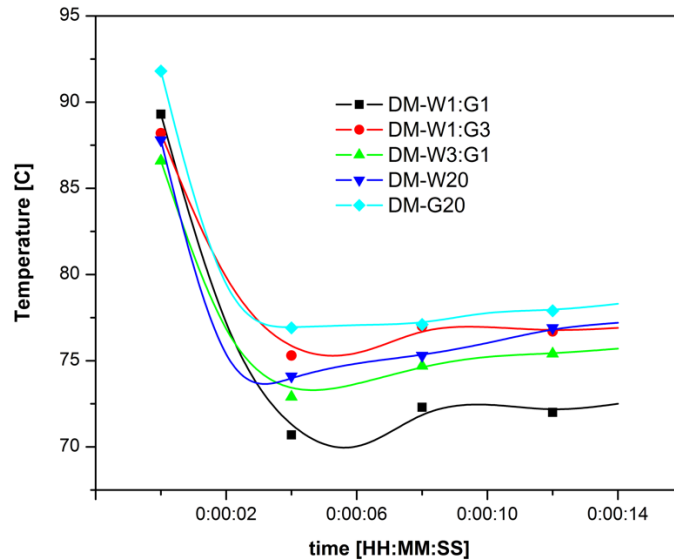
Figure 4-9 Depicts the relationship of torque as a function of time for the various ratios of water:glycerol as outlined in Table 4-4 including those for 20% water and 20% glycerol with starch

4.4 The influence of temperature on the destructuring of starch

Yu & Christie (2005)concluded that shear and heat work together in the extrusion process in order to achieve gelatinization of the starch. In this section, the parameter of temperature was examined by studying torque, material temperature response as a function of times for a mixture under varied temperatures of the CWB.

Table 4-7 outlines the four different temperatures that were evaluated utilizing the same formulation of starch, water and glycerol and the 45 RPM. Figure 4-10 depicts the resulting torque curves and Figure 4-11 the resulting material temperature curves as a function of time for these evaluations over the first twelve seconds.

71

Table 4-7 Evaluation to study the effects of temperature on destructuring starch for Water:Glycerol ratio 1:4 (W1:G4)

Label	Starch – Dent WT-%	Water Wt-%	Glycerol Wt-%	Screw Speed RPM	Temperature ℃
DM-150C	77	3.6	19.4	45	150
DM-160C	77	3.6	19.4	45	160
DM-170C	77	3.6	19.4	45	170
DM-180C	77	3.6	19.4	45	180
DM-90C	77	3.6	19.4	45	90
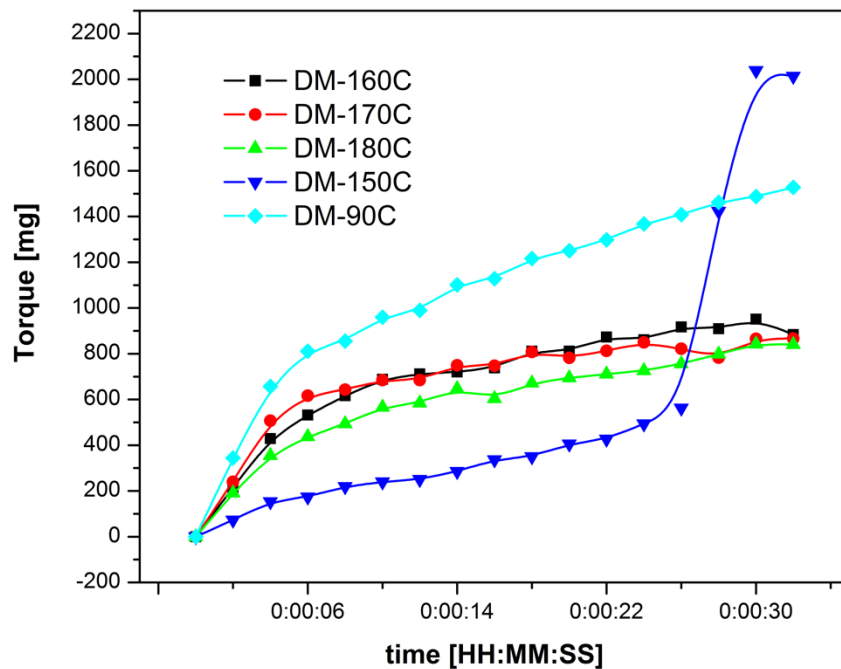
Figure 4-10 Depicts the resulting torque curves as a function of time for various temperatures over the initial 14 seconds of compounding

Table 4-8 Summary of the time frame and maximum torque in achieving starch destructuring

	Onset mg	Max mg	Onset seconds	Max seconds	Max Temperature °C
DM-150C	493	2050	24	31	133.1
DM-160C	0	2537	0	202	137.6
DM-170C	0	2386	0	188	143.0
DM-180C	0	2346	0	162	153.1
DM-90C	0	1569	0	42	86.7
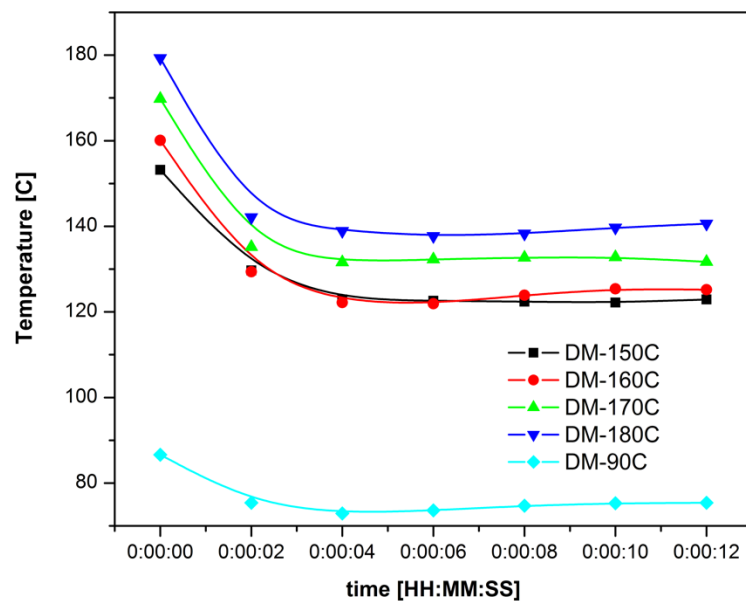
Figure 4-11 Graph of the material temperature curves as a function of time for the temperatures evaluated

The torque curves for temperature of 90, 160, 170 and 180°C demonstrate similar initial behaviour with faster rates for destructuring. It is noted that torque curves for 160 and 170°C, during the first several seconds, seem to almost overlap as depicted in Figure 4-10.

The temperature curves of the compounds, for the first twelve seconds shown in Figure 4-11 ran 25–35°C cooler than the body temperature programmed in each evaluation outlined in Table 4-7. This is an important point to capture. Processing these samples with a CWB Intelli-Torque Plasti-Corder® Rheometer with 3-piece mixer/measuring head and Banbury Blades is a batch process. The total mass of material is quickly charged into the mixer with the weighted chute. The materials rapidly absorb the heat from the mixer's body, thus displaying a drop in the recorded temperature. As time progresses, the continuous heating of the body brings up the temperature of the compound (stock). Additional heating is transferred into the feedstock through the energy imparted through torque and shear to the materials.

The torque curve as a function of time for 160 and 170°C, suggests that these temperatures are effective in achieving the destruction and plasticization of the starch. However, signs of plasticizer evaporation were noted during mixing. In Figure 4-12 the weighted loading ram is seen raised 18mm above its neutral position, resting on the chute. The elevation of the ram suggests the potential of pressure building up in the mixing chamber. When removing the compound, gas bubbles were noted in the polymer melt (Figure 4-13) confirming that evaporation of the plasticizer had occurred. On review of the temperature versus time curves for 170°C trial, the final temperature of the stock was 143°C. According to Miller's (1953) findings, outlined in Table 4-3, the boiling point of the plasticizer had been exceeded.

This insight collected from torque and temperature suggests that the ideal temperature would be closer to 150°C as indicated in Figure 4-15 for torque and Figure 4-16 for temperature to achieve efficiency in destructuring and plasticizing starch.

With extrusion, a continuous process, small quantities of material are being introduced uniformly and constantly into the throat of the extruder. The continuous introduction reduces the early temperature loss between the material and that of the extruder. With the ability to meter material in the extruder, there is the possibility that 150°C may be higher than what is

required for the processing of the starch. This temperature would need to be revisited when finally migrating to an extruder.

Figure 4-12 Photograph depicting the loading chute ram and weight raised above the neutral position displayed at charge.

Figure 4-13 Photograph of the polymer melt with gas bubbles present

4.5 The influence of shear on the destructuring of starch

Yu & Christie (2005) surmised that shear and heat work together in the extrusion process in order to achieve gelatinization of the starch. In this section, the parameter of shear is examined by studying the torque, temperature response as a function of time for a mixture under varying revolutions per minute (RPM) of the Banbary Blades.

Table 4-9 outlines the three different rates of shear that were evaluated utilizing the same formulation of starch, water and glycerol. Figure 4-14 depicts the resulting torque curves and Figure 4-15 the resulting temperature curves as a function of time for these evaluations.
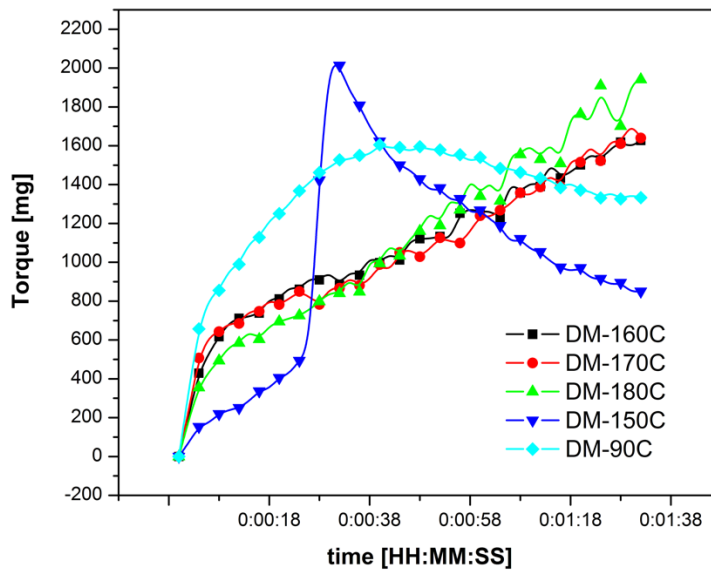
Figure 4-14 Depicts the torque curves as a function of time for the different CWB body temperature
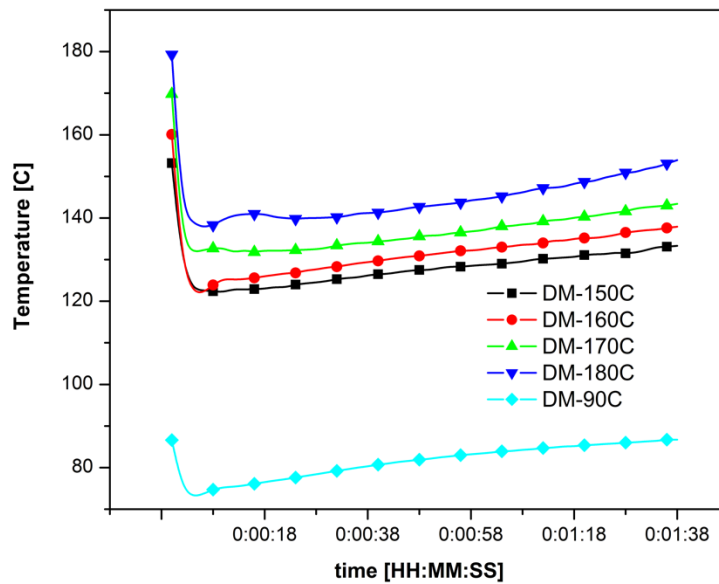
Figure 4-15 Graph of the material temperatures as a function of time for the different CWB body temperature

Table 4-9 The effects of shear on destructuring starch

Label	Starch – Dent Wt-%	Water Wt-%	Glycerol Wt-%	Screw Speed RPM	Temperature ºC
DM-45-150	77	3.6	19.4	45	150
DM-60	77	3.6	19.4	60	150
DM-120	77	3.6	19.4	120	150
DM-45-90	77	3.6	19.4	45	90
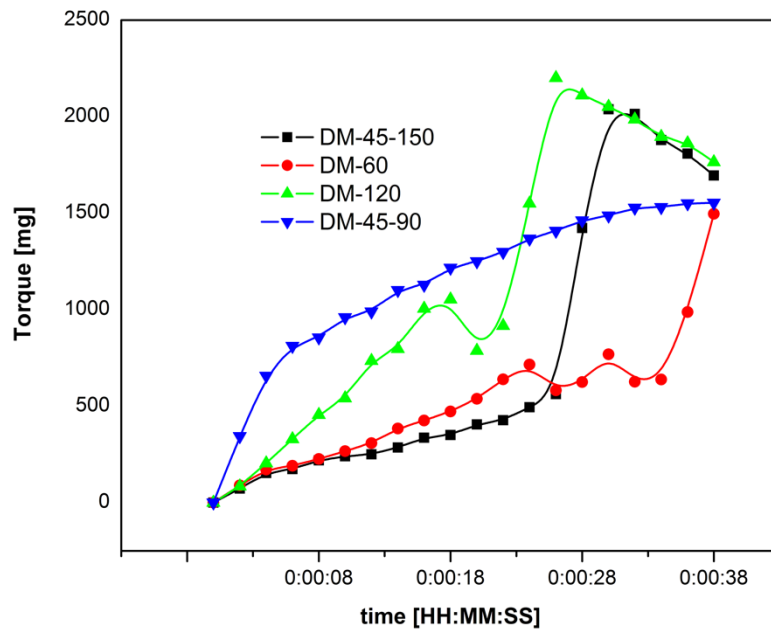
Figure 4-16 Graphs the relationship of shear [torque] as a function of time for the first 38 seconds

Table 4-10 Summary of the torque and time required to achieve destructuring of the starch

Label	Onset mg	Max mg	Onset seconds	Max seconds
DM-45-150	493	2050	24	31
DM-60	638	1604	34	46
DM-120	787	2110	20	28
DM-45-90	0	1587	0	42
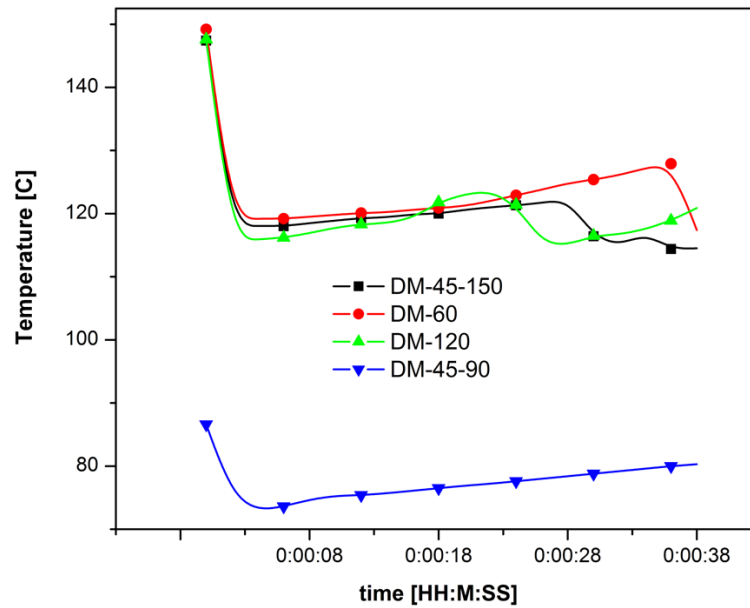
Figure 4-17 Graph of the influence of shear on temperature as a function of time in the first minute and 38 seconds

The application of a higher RPM suggests better efficiency in the destructuring and plasticization of the starch. However, it is noted that by 21 seconds into the mix, DM-120 compound had achieved 121°C, and by a minute and thirty-eight seconds into the mix that temperature had exceeding 145°C. (Figure 4-17) The drop off on the temperature curves in Figure 4-16, seen around 21 seconds, suggests the potential of evaporation of plasticizer and the cooling of the stock. The subsequent increase in temperature would then be the result of low plasticizer present and the net increase in viscosity of the compound. On removal of the compound from the mixing chamber, gas bubbles were found in the stock suggesting that evaporation had occurred.

The compounds of DM-45-150 and DM-60 both indicated similar temperatures below 121°C following 60 seconds of mixing [Figure 4-18] and reached compound temperatures of 128 - 131°C at one minute and thirty-eight seconds into the mix.

DM-45-150 indicated a quicker torque response, suggesting faster destructuring and plasticization of the starch than DM-60.

DM-45-90 saw a quick rise in torque. However, DM-45-90 did not achieve maximum torque until 42 seconds into the mixing. Based on the concept of quick formation of the gel ball, as outlined by Yu & Christie (2005), the destructuring of the starch was not achieved in a reasonable period of time. It was surmised that insufficient heat at 90°C and 45 RPM was present to facilitate destructuring and plasticization of the starch and that significantly more shear and time was required to compensate for lack of heat.

DM-45-150 conditions demonstrated the ability to most effectively destructure and plasticize the starch in a timely manner while not building excessive heat. As such, this defines the optimal condition with 45 RPM shear at 150°C temperature.
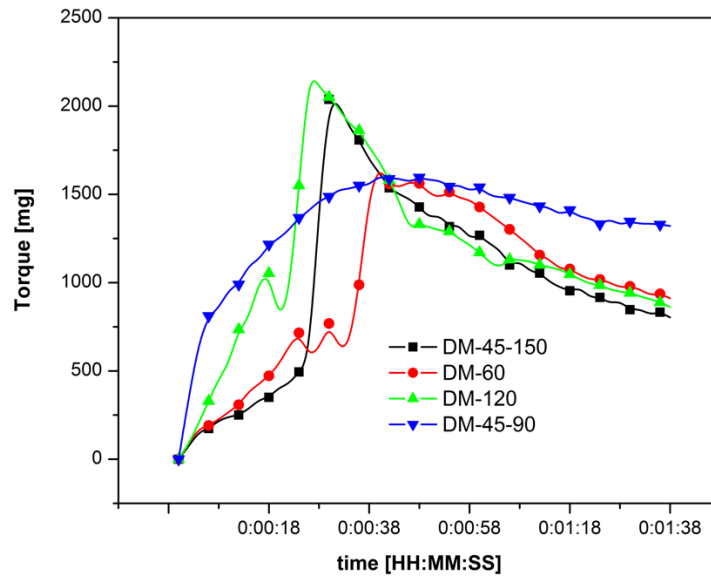
Figure 4-18 Graphs the relationship of shear [torque] as a function of time
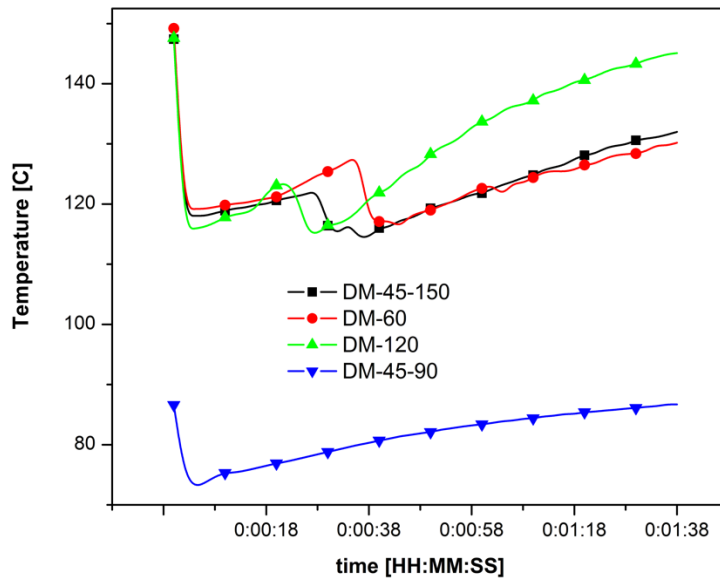
Figure 4-19 Graphs of the relationship of the curves of temperature as a function of time for the compounds defined in Table 4-9

4.6 Summary of the ideal parameters in destructuring and plasticizing starch

In this chapter, the goal was to understand the parameters that would allow for the efficient destructuring and plasticization of the starch in the timeliest fashion. The following parameters were studied:

- Influence of water on the destructuring of dent starch

- Influence of water / glycerol on the destructuring of dent starch

- Influence of shear on the destructuring of dent starch

- Influence of temperature on the destructuring of dent starch

The conclusions reached from these studies are reported and discussed. As a result of this work, the parameters outline in Table 4-11 were established for the formulations and mixing conditions for the materials studied from here forward.

The following conclusions were obtained from the work completed to this point:

- Starch has a preferred affinity towards water, in its ability to quickly destructure the starch granule

- Water can act as an effective plasticizer for starch. Water can reduce the viscosity of the mixture with increased addition. [reducing the interactions between molecules]

- Higher mechanical energy [RPM] is preferential in achieving destructuring of starch granule

- Higher thermal energy [temperature] is preferential in achieving destructuring of starch earlier

- Elevated temperatures [greater than 100ºC] require alternative plasticizer systems are required due to evaporation

- Thermal and mechanical energy employed are limited to the boiling point of the plasticizer in the compound

Glycerol was identified in many literature searches as a suitable plasticizing agent for starch. However, in order to enhance the rate of plasticization, it was determined that some amount of water needs to be present.

Miller's (1953) reviewed the influence which water had on depressing the boiling point of glycerol blends. This information played a significant role in determining appropriate conditions for processing the compounds. (Miller 1953)   Miller determined that the boiling point of the 1:4 glycerol/water blend is 121°C (Table 4-3). Processing compounds at higher temperature would exceed the boiling point of the water / glycerol blend, resulting in the evaporation of the water / glycerol blend from the plasticized starch and the potential for retrogradation of the starch. This suggests that poor aging properties of the thermoplastic starch compound could occur.

Table 4-11 The parameters for compounding and mixing which efficiently allow for the destructure and plasticize starch.

Parameter	Value
Residence time	1 minute, 38 seconds [42mm, 52:1 L/D, Leistritz twin screw extruder]
Minimum plasticizer level	18-25% [including the moisture within the starch]
Minimum moisture level	4-10% [including the moisture within the starch]
Ratio water: glycerol	1:4 [excluding the internal moisture of the starch]
RPM	45 RPM
Temperature	150°C [body temperature]

4.7 The destructuring and plasticization of various starches

In the previous selection, the relationship between several variables and their influence on the rate at which dent starch would be destructured was explored. As a result, parameters were established that define the favourable conditions required to evaluate different materials with the objective to study their similarities and differences within a controlled format.

Subsequently, an assessment of a variety of starches, and their rate of gelatinization was undertaken with standardized conditions. The data was collected for analysis. The ensuing table describes the formulations evaluated.

The objective is to study several commercially available starches (Table 4-12) and understand which starches could offer the fastest destructuring under the parameters defined in Table 4-11. At the same time, to look at the various starches and choose three which offer different characteristics which may impart unique characteristic in the formation of starch co-polyester polymers or alloys.

The starches, listed in Table 4-12, were run in accordance with the conditions defined and analyzed for the speed at which they would be destructured and plasticized. In analysis, it was noted that three fastest destructuring and plasticizing starches where Hylon VII (Hylon), 55310 and 30050. (Figure 4-20) This result was particularly interesting, in that it identified three different types of starch which could offer unique properties to a compound.

Hylon VII starch, derived a genetically modified genus of maize, possesses a high level of amylose within the starch granule. This particular strain exhibited 70:30 amylose: amylopectin ratio. The high amylose starch should offer higher processing stability to the final compound.

The 55310 starch is a chemically oxidized and viscosity reduced grade of industrial starch which offers a broad range of molecular weights. The broad molecular weight may offer ease of processing and produce a good injection molding compound.

83

Table 4-12 Formulation and conditions explored in the destructuring of various starches

Starch	Water Wt-%	Glycerol Wt-%	Screw Speed RPM	Temperature °C
Hylon VII	3.6	19.4	45	150
30050	3.6	19.4	45	150
55310	3.6	19.4	45	150
Novation 1600	3.6	19.4	45	150
055720	3.6	19.4	45	150
Stablebond 055110	3.6	19.4	45	150
Amioca	3.6	19.4	45	150
DM	3.6	19.4	45	150

The 30050 starch is a paper coating starch which has been chemically modified. The modification resulted in a minor substitution of the hydroxyls at C_2 and C_3 with carbonyl and carboxyl groups. This particular starch contains between 0.1 and 0.3% degrees of substitution [DS]. With the DS, this starch was chosen due to its ability to react differently with the peroxides, glycerol and MAH which may offer a compound with more resistance to retrogradation.

Although the Amioca starch showed good potential in the initial screening of the various starches, it was not considered at this time. Amioca starch is a waxy starch with 99% amylopectin. Due to the DS on 30050, it was believed to offer interesting characteristic in reaction with the peroxides and MAH, characteristic which may not have been as easy to achieve with the Amioca starch.
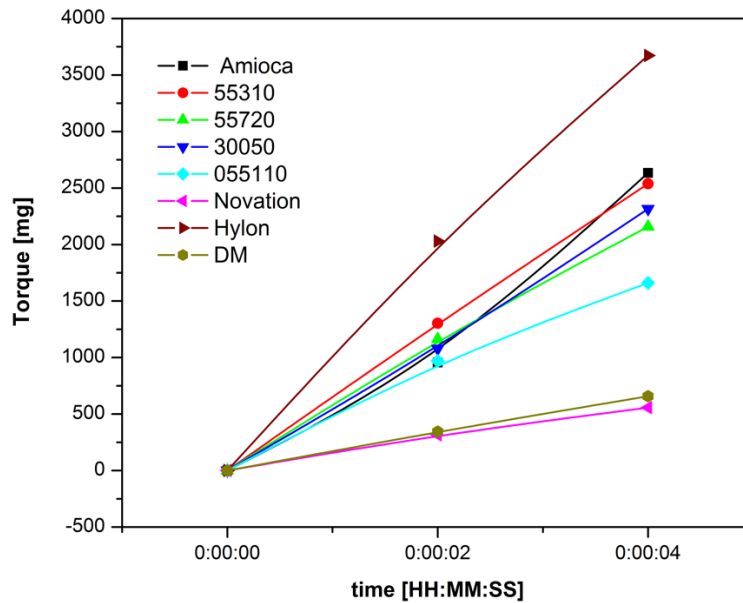
Figure 4-20 Torque curves as a function of time for the destructuring of the starch samples

Table 4-13 Summary of the time and maximum torque required to achieve destructuring of the various starches

Starch	Onset	Max	Onset	Max
	mg	mg	seconds	seconds
Amioca	0	3652	0	8
55310	0	2298	0	6
55720	0	2338	0	16
30050	0	2803	0	16
55110	0	2305	0	18
Novation	0	1079	0	56
Hylon VII	0	3818	0	8
Dent Maize	493	2050	24	31

85
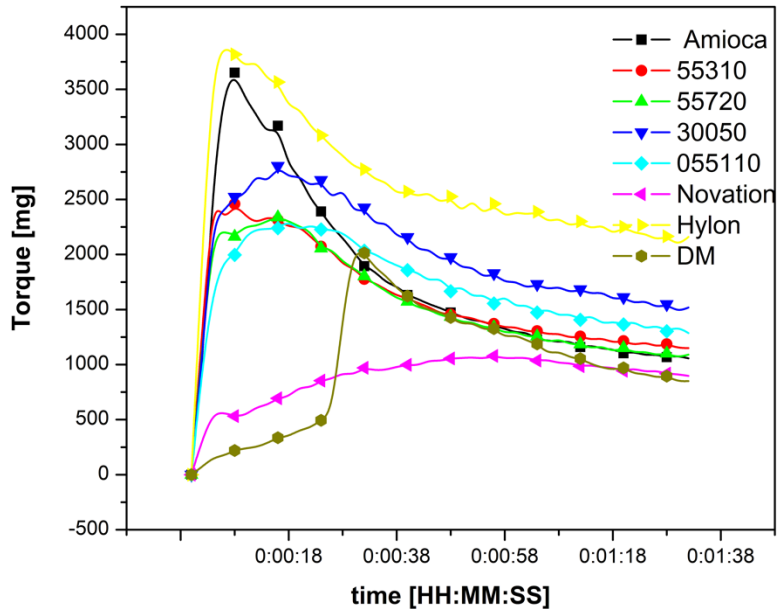
Figure 4-21 Depicts torque as a function of time in the destructuring of various starches

In Figure 4-20, the selection of three starches was made based on the ability of these starches to quickly increase in torque. Kalambur believed that shear in the presence of an appropriate amount of water and heat will facilitate the destructuring of starch. (Kalambur2012) As such, it is concluded that starches which respond quickly with increased torque will destructure faster. Figure 4-21 examines all the starches over the complete time frame. Figure 4-21 confirms the selection of Hylon and 55310 as starches which exhibit their fast ability to effectively destructure and plasticize. As noted in Figure 4-21, starch 30050 is slower than starches 55720 and 55110. The decision to pick 30050 over the other two is because a similar oxidized starch has already been selected. That starch is 55310. The selection of the starch 30050 is due to the presence of carbonyl and carboxy groups resulting from Ingredion chemical modification during production.

4.8 Thermal characteristics of starches (Hylon, 55310, & 30050)

In this section, the thermal characteristic of the starches identified in Section 4.7 were evaluated. Samples were subjected to Thermal Gravimetric Analysis (TGA) and Differential Scanning Calorimetry (DSC) in accordance to their ASTM standards.

4.8.1 TGA analysis of the Dent Maize, Hylon, 30050 and 55310

TGA were conducted on the four starches (Dent Maize, Hylon, 30050 and 55310) and reported in Figure 4-22 and in Table 4-14.

The 55310 starch, having been chemically modified, possessed low viscosity and broader molecular weight, displayed a weight loss curve that reflected higher changes in weight loss at lower temperatures over a larger temperature range. The first derivative of this lost weight curve presented the two peaks. The first at 294ºC, and the second at 374ºC (Table 4-14).

Hylon starch, having 70% amylose and 30% amylopectin, displayed the narrowest (steepest) weight loss curve covering the smallest temperature range. The first derivative of this lost weight curve presented the three peaks. The first at 280ºC, the second at 310ºC, and the third at 500ºC (Table 4-14).

Of particular interest was the loss weight TGA curve for 30050. It indicated relatively higher heat stability over all four starches. Its first derivative of loss weight curve presented three peaks. The first at 283ºC, the second at 317ºC, and the third at 502ºC (Table 4-14). Although 30050 had first derivative peaks with similar values to Hylon, 30050 had a higher weight percentage at 502ºC. (Table 4-14)
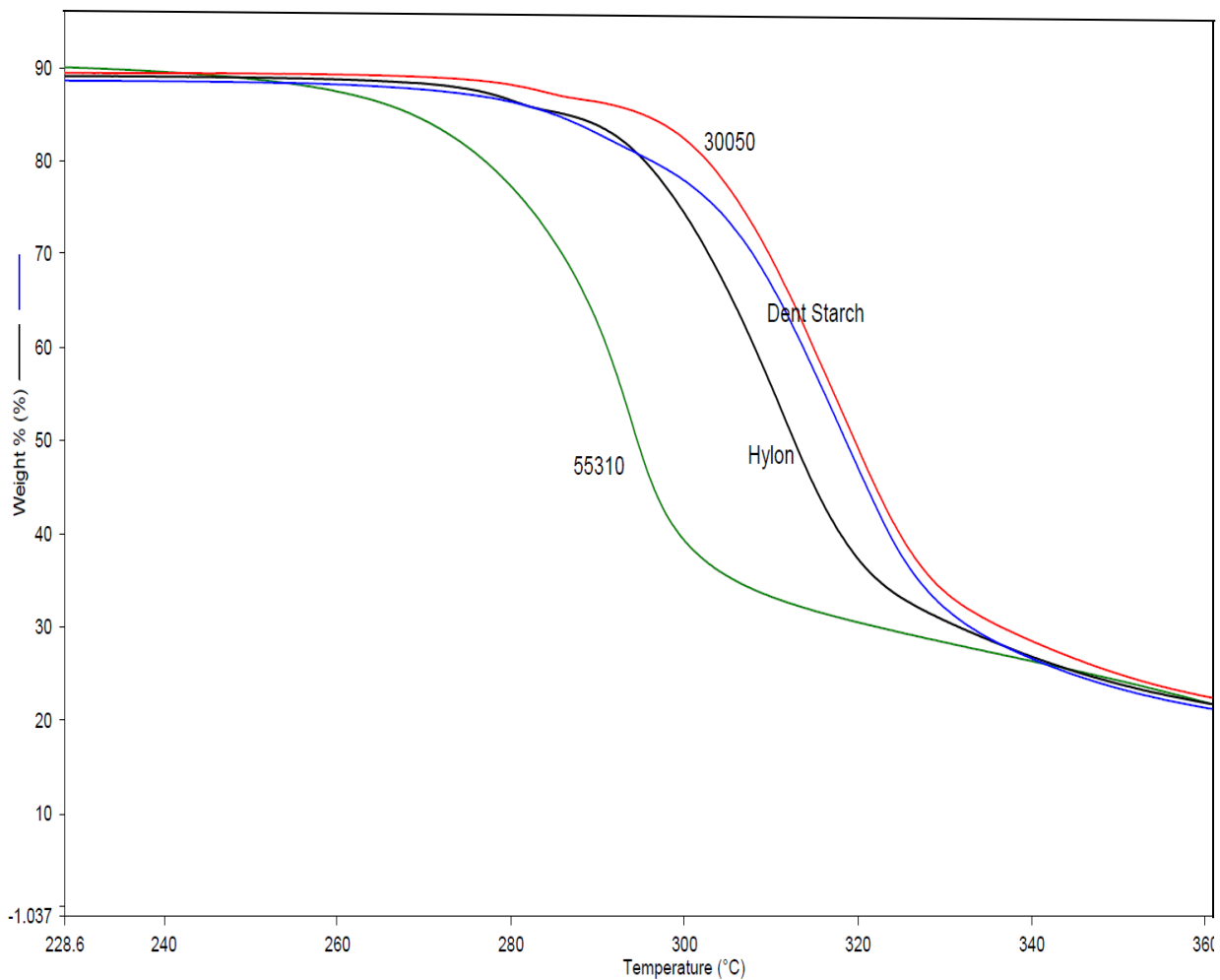
Figure 4-22 TGA curves for the starches 55310,30050, Hylon VII and Dent Maize Starch

4.8.1 DSC Analysis of the Dent Maize, Hylon, 30050 and 55310

Two groups of samples were taken from the four starches. The first group were conditioned at 23°C and 50% relative humidity for 24 hours. While the second set were dried for 4 hours at 104°C. Samples for both groups were weighed out and hermitically sealed in 50 ml pans for DSC analysis.

Table 4-14 Summary of the TGA derivative peaks for the 4 selected starches

Starch	Onset	End	Peak	Wt-%
	ºC	ºC	ºC	
Dent Maize				
volatiles				9.43
	282.55	293.35	**288.97**	5.53
	298.94	331.26	**318.55**	61.40
	487.39	489.11	**488.13**	19.72
Hylon				
volatiles				6.80
	274.17	283.71	**280.01**	2.87
	288.19	324.47	**310.67**	65.17
	444.76	531.11	**500.74**	21.58
30050				
volatiles				7.16
	277.23	287.67	**283.40**	2.22
	294.83	331.37	**317.26**	60.00
	474.10	529.48	**502.61**	27.16
55310				
volatiles				9.261
	283.62	300.17	**293.89**	50.95
	372.25	383.41	**374.15**	37.10

4.8.1.1 DSC analysis of the conditioned starch samples

DSC curves for the normalized 1st heat pass of the conditioned starch samples (Figure 4-23) were analyzed and reported in Table 4-15.

Table 4-15 Summary of the normalized 1st heat pass DSC curves for the four starches

Starch	Onset	End	Peak	ΔH_m
	°C	°C	°C	J/g
Dent Maize				
	90.80	98.39	**69.29**	0.3913
	102.14	103.55	**102.52**	0.1903
	105.22	108.39	**107.51**	0.7052
	108.90	115.06	**113.68**	0.8610
Hylon				
	108.10	113.28	**109.95**	4.3427
30050				
	123.61	125.08	**124.07**	1.0869
	134.60	135.72	**134.94**	6.3878
55310				
	116.69	118.25	**117.15**	1.8196

The DSC curves from the normalized 1st heat pass for the conditioned starch samples concludes that dent maize starch displays a multitude of endothermic peaks which reflect the gelatinization of the starch and the melting of various fat/amylose complexes (Bemiller 2009). The DSC curves for both 55310 and 30050 starches show less melting of fat/amylose complexes and more endothermic peak for gelatinization. This is believed to reflect the chemically modification of both starches.
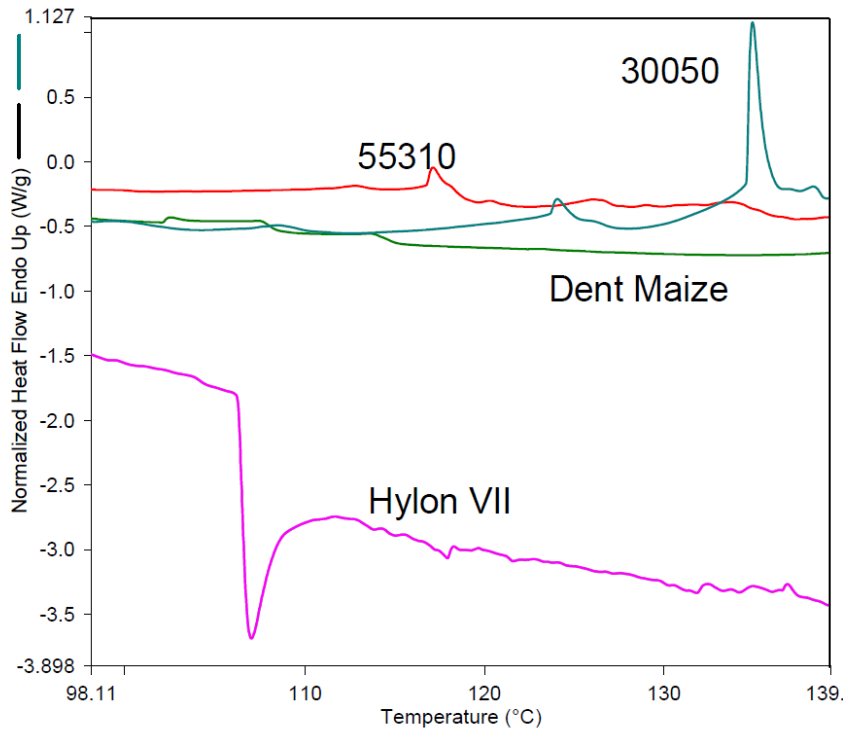
Figure 4-23 DCS curves for the normalized 1st heat pass of the conditioned starch 55310, 30050, Dent Maize and Hylon VII (first heat pass)

The DSC curve for Hylon displays an exothermic step, suggesting a phase transition followed by an endothermic peak for gelatinization. This step transition could not be identified in literature for Hylon VII and seems to be characteristic of this particle lot of starch evaluated.

DSC curves from normalized 2nd heat pass for the conditioned starch samples were analyzed and found not to yield any endothermic peaks, (Figure 4-24) suggesting that all the starches had gelatinized and display amorphous characteristics. (Table 4-16)

On analyzing the 2nd cooling pass for the conditioned starch samples, heats of crystallization were identified (Figure 4-25) and reported in Table 4-17. The presence of peaks occurring in the 2nd cooling pass is believed to be due to syneresis and retrogradation of the starch.

91
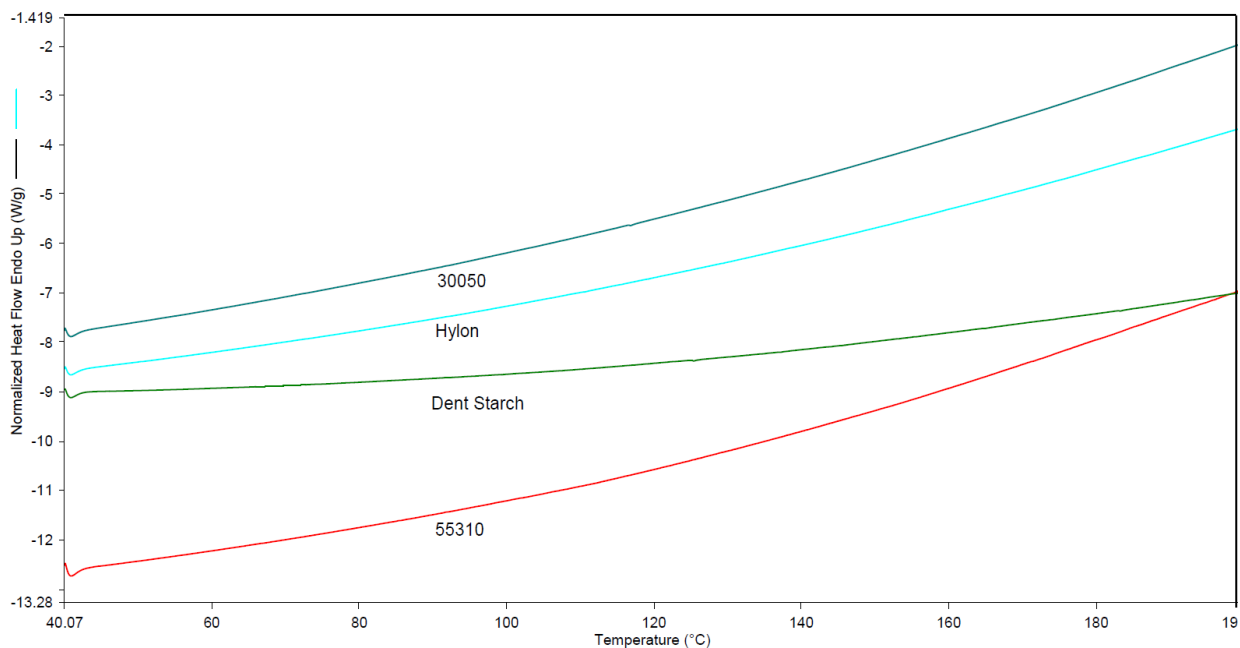
Figure 4-24 DSC 2nd melt cycle curves for the four conditioned starches

To depict all four DSC curves together on the same graph in Figure 4-24, the scale for the Normalized Heat Flow Endothermic legend is too broad to depict the subtleties in the different compound melts.

4.8.1.1 DSC analysis of the dried starch samples

Unlike the DSC curves from normalized 2nd heat pass for the conditioned starch samples in Table 4-16, the DSC curves from normalized 2nd heat pass for the dried starch samples yielded melt peaks which allowed for heat of fusion to be calculated. (Table 4-18) These small peaks suggest that the starches had gone through some form of phase transformation. Due to lack of moisture being present, no gelatinization would be expected to occur. It could be surmised that the minimum signs of crystalline characteristic are from starch degradation.

92

Table 4-16 Summary of the 2nd melt cycle DSC curves on the conditioned starches

Starch	Onset	End	Peak	ΔH_m
	°C	°C	°C	J/g
Dent Maize				
		No peaks were identified		
Hylon				
		No peaks were identified		
30050				
		No peaks were identified		
55310				
		No peaks were identified		

Table 4-17 Summary of the 2nd cooling cycle DSC curves on the conditioned starches

Starch	Onset	End	Peak	ΔH_c
	°C	°C	°C	J/g
Dent Maize	120.99	93.88	**101.12**	-16.58
Hylon	114.36	94.08	**101.57**	-12.30
30050	119.47	63.11	**91.48**	-44.16
55310	119.24	94.53	**94.55**	-5.27
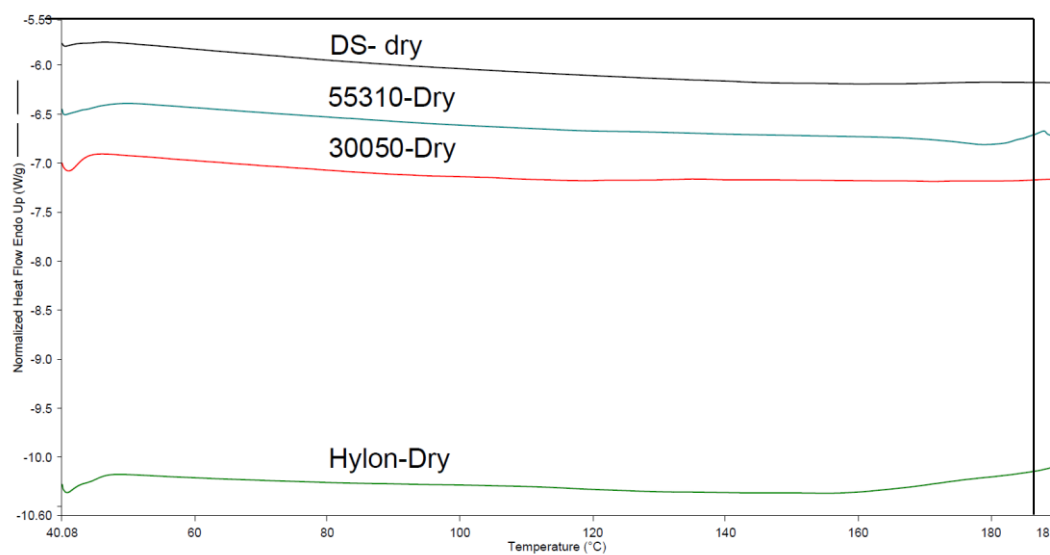
Figure 4-25 Normalized 2nd melt cycle DSC curves on the conditioned starches

On analyzing the 2nd cooling pass for the dried starch samples, heat of crystallization is identified and reported in Table 4-19. It is noted that the ΔH_c in Table 4-17 are significantly higher than those in Table 4-19. This would support the assumption that the starches have degraded in the previous cycle.

Table 4-18 Summary of the 2nd melt cycle DSC curves on the selected starches following drying

Starch	Onset	End	Peak	ΔH_m
	°C	°C	°C	J/g
Dent Maize				
	149.70	154.68	**152.39**	0.15
Hylon				
	104.27	115.19	**109.88**	1.37
	146.87	156.72	**148.21**	0.23
30050				
	99.02	108.23	**103.06**	0.06
	125.85	146.01	**134.74**	0.94
55310				
	132.36	181.67	**165.78**	17.27

Table 4-19 Summary of the 2nd cooling cycle DSC curves on the selected starches following drying

Starch	Onset	End	Peak	ΔH_c
	°C	°C	°C	J/g
Dent Maize				
	113.85	91.06	**97.57**	-0.70
Hylon				
	172.15	158.48	**163.66**	-2.58
	152.07	133.88	**144.94**	-3.44
30050				
	120.45	104.21	**116.70**	-3.00
55310				
	130.99	113.98	**119.74**	-2.33

Chapter 5

Results and Discussions: In situ Plasticization of Starch and Co-blend with Polyesters

5.1 Introduction

The scope of chapter five is to investigate the three starches (Hylon, 30050 and 55310) and the influences which different free radical initiators, maleic anhydride and different polyesters have on the starch - polyester co-blends. Analytical techniques of FTIR, TGA and DSC were conducted on these compounds as well as analyses of the data obtained from the CWB. This information was assembled to paint a picture of the influence of these parameters on starch - polyester compounds.

5.2 The effects of free radical initiators

In Chapter 4, it was determined that the preferred temperature profile for the body of the CWB was 150°C. As such, it brought into question the effectiveness of the peroxide to efficiently dissociate and generate free radicals to promote chemical reactions within the initial seconds of introduction into an extruder, and before exiting one minute and thirty seconds later. This section studies the influence of employing three different free radical initiators with decreasing half-life temperatures. The three starches selected (Hylon, 30050 and 55310) based on their unique properties, were compounded with the free radical initiators and evaluated as per Table 5-1. These starches were conditioned for 24 hours at 23°C and 55% relative humidity before blending and compounding.

Table 5-1 Table of formulations exploring the effects of free radical initiators

Label	Starch	Peroxide Type	Peroxide Wt-%	MAH Wt-%	PBAT Wt-%	Water Wt-%	Glycol Wt-%	Screw Speed RPM	Temperature °C
Hylon-101	Hylon	101	0.1	1.0	58.2	1.5	7.7	45	150
Hylon-Ben	Hylon	Dibenzoyl	0.1	1.0	58.2	1.5	7.7	45	150
Hylon-Lau	Hylon	Dilauroyl	0.1	1.0	58.2	1.5	7.7	45	150
30050-101	30050	101	0.1	1.0	58.2	1.5	7.7	45	150
30050-Ben	30050	Dibenzoyl	0.1	1.0	58.2	1.5	7.7	45	150
30050-Lau	30050	Dilauroyl	0.1	1.0	58.2	1.5	7.7	45	150
55310-101	55310	101	0.1	1.0	58.2	1.5	7.7	45	150
55310-Ben	55310	Dibenzoyl	0.1	1.0	58.2	1.5	7.7	45	150
55310-Lau	55310	Dilauroyl	0.1	1.0	58.2	1.5	7.7	45	150

5.2.1 Hylon starch and the effects of various free radical initiators

In this section, the effects of the three different peroxides were explored using conditioned Hylon starch.

Figure 5-1 illustrates the plots of the torque curves as a function of time for the Hylon compounds described in Table 5-1. In this figure, the Hylon-Lau compound, with the free radical initiator dilauroyl peroxide, displays a rapid response in torque to a maximum of 1559 mg and subsequent decline. The drop in torque indicates the effective plasticization of the starch molecules within the compound following the gelatinization of the starch. The formation of the gel balls, described in the Yu & Christie 2005 paper, suggests that the starch molecules are opening and available for free movement. It is this free movement which accounts for the drop in torque. As the development of the gel balls increase, it creates an environment within the starch molecule to open up and the steric hindrances, hydrogen bonding, van Der Waals forces

and other intermolecular forces are reduced thus producing the opportunity for potential chemical reactions to occur.

The curves for Hylon-Ben and Hylon-101, at nine seconds, start to show the onset of destructuring. Both compounds indicate similar timing to achieve maximum torque before plasticization occurs. Yet, Hylon-Ben exhibits a significantly higher torque value than Hylon-101 at 16 and 17 seconds respectfully.

The maximum torque values recorded for Hylon-Lau and Hylon-101 in the destructuring of the starch were 1559 mg and 1575 mg with Hylon-Ben at 2022 mg. A Summary of the results is found in Table 5-2.
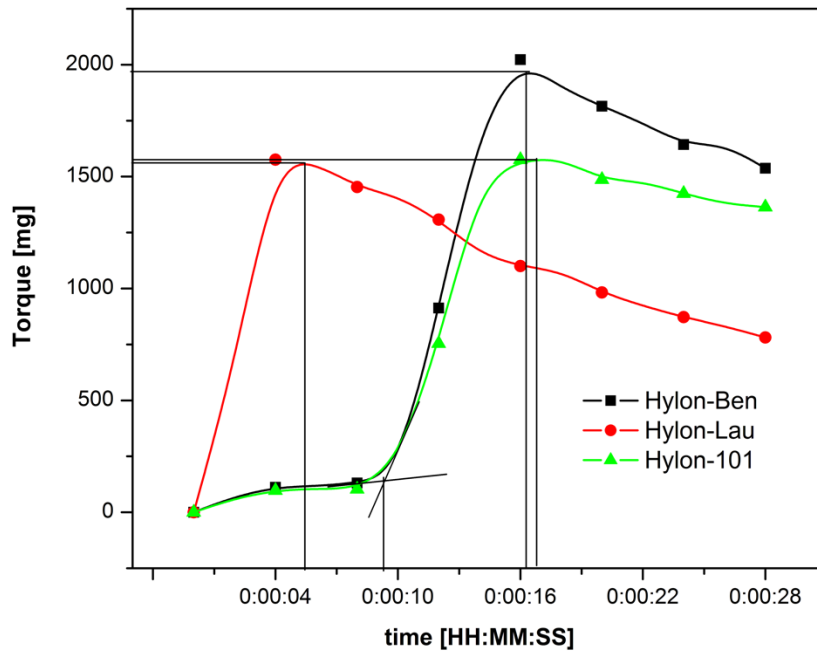
Figure 5-1 The evaluation of torque as a function of time for the various free radical initiators with Hylon starch over the first 28 seconds

Table 5-2 The summary of torque and time for Hylon compounds with various free radical initiators in achieving destructuring

Property	Hylon - 101	Hylon-Ben	Hylon-Lau
Torque	mg	mg	mg
On Set	173	173	0
Max	1575	2022	1559
Time	seconds	seconds	seconds
On Set	9	9	0
Max	17	16	6

Figures 5-2 and 5-4 are of plots of temperature versus time for the Hylon compounds outlined in Table 5-1, although to different time scales. The disruption of the starch granule occurs with the addition of the appropriate amount of thermal and mechanical forces in the presence of the suitable amount of water / plasticizer (Nafchi 2013). For this purpose, it is important to look at the first 15-38 seconds to understand the heat profile and torque required to achieve the free motion of the starch molecules, thereby establishing the potential for a chemical reaction to occur.

In Figure 5-2, the time at which Hylon-Lau's temperature curve is at its lowest corresponds with the time it takes Hylon-Lau torque curve to achieve its maximum torque value as seen in Figure 5-1. This relationship seems to make sense, as until the starch is destructured and the onset of plasticization occurs, all the energy from thermal and mechanical sources are being absorbed by the Hylon-Lau compound. Once the compound has achieved gelatinization and plasticization is occurring, the compound requires less energy to break the lamellae crystalline structure within the amylopectin molecules, thus resulting in an identifiable increase in temperature. The same relationship between torque and temperature as a function of time is seen for Hylon-Ben. However, Hylon-101 displays a delay in obtaining the minimum

temperature. The time to achieve maximum torque does not match up with minimum temperature.
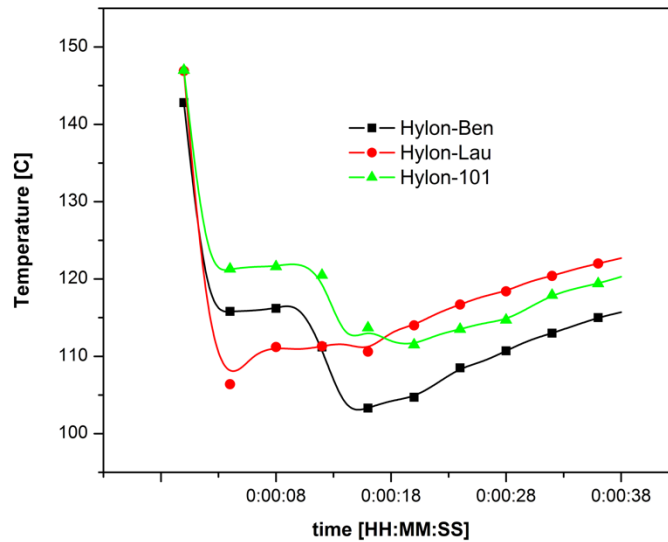
Figure 5-2 The evaluation temperature as a function of time for the various free radical initiators with Hylon starch over the first 38 seconds

In Figure 5-3, it is noted that once the various compounds achieve their maximum torque value, they start to exhibit signs of plasticization with torque decreasing as time progresses. As time approaches one minute, the torque values of the various compound seem to stabilize.

 In compounding thermoplastic starch, it was determined in section 4.6, that the temperature should not exceed 150°C. In Figure 5-4, it is concluded that the three compounds do not exceed that temperature during compounding.
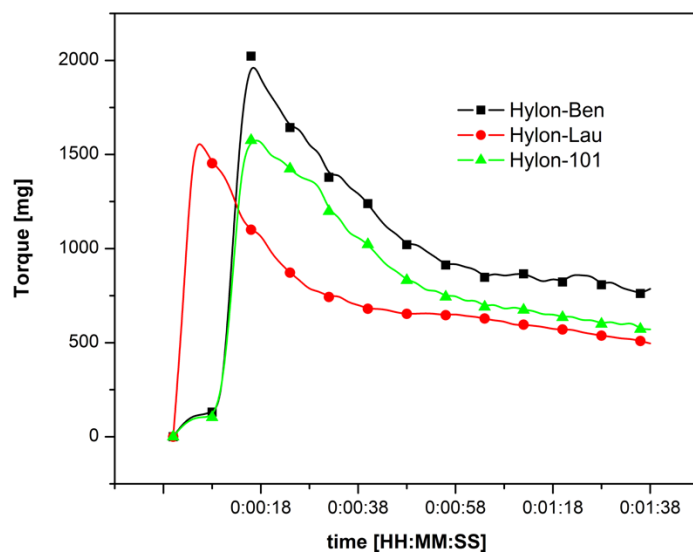
Figure 5-3 The evaluation torque as a function of time for the various free radical initiators with Hylon starch over 1 min. 38 sec.
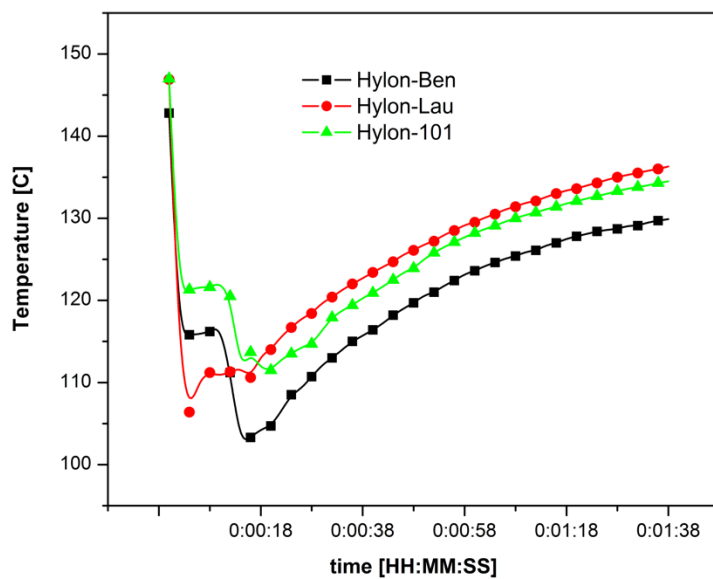
Figure 5-4 The evaluation temperature as a function of time for the various free radical initiators with Hylon starch over 1 min. 38 sec.

TGA analysis was conducted on the individual ingredients and the Hylon compounds outlined in Table 5-1. The objective was to determine if the Hylon compounds displays any signs of change in thermal stability over that of the individual raw materials.

Figure 5-5 displays the derivative of the percentage weight loss curve as a function of temperature with the Hylon compounds outlined in Table 5-1 with Table 5-4 summarizing the data.

In Figure 5-6, higher thermal stability is noted with Hylon-Ben over the temperature range 380-440°C and greater than that of Hylon-101 and Hylon-Lau. Although this is an interesting finding for these compounds, it is to be noted that the thermal decomposition is happening well above the beginning of the thermal degradation of these compounds.

In comparing Tables 5-3 and 5-4, the data suggests that some form of starch molecular interaction or modification occurs within all three compounds. In Table 5-3, the TGA peak for Hylon starch is recorded at 310.67°C and in table 5-4, the peak increased between 321.03 to 326.02°C.

Of interest was Hylon-101 TGA curve, which suggests that the compound may be an add mixture with PBAT with little or no compatibilization occurring between the starch and the PBAT. This conclusion is reached by comparing the peak temperature and the predicted percentage of PBAT between Tables 5-3 and 5-4 and noting minimal change. The results in Table 5-4 for Hylon-Ben suggest increased thermal stability with PBAT. Potentially, a small amount of compatibilization, intermolecular attraction, or chemical modification occurring offer increased thermal stability. As well, the predicted percentage weight of PBAT is noted to be lower than expected by about 9% (Table 5-3). In Table 5-4, two new peaks at 434.6°C and 470.59 are identified which was not expected. These peaks represent 9.8% and 11.4% weight of the overall Hylon-Ben compound, comparatively.

The Hylon-Lau compound displays a loss in thermal stability relative to the other two compounds. Of interest is peak at 409.24ºC. The peak is believed to be from PBAT and represents a temperature shift down from 412.91ºC. This peak reflects 51.8% weight of the overall Hylon-Lau compound, down 5.35% from the predicted value for PBAT in the compound. Other peaks of interest are the two new peaks found at 429.85ºC and 475.51ºC representing 5.1% and 11.4% weight of the overall Hylon-Lau compound, relatively.

Table 5-3 Summary of the TGA derivative peaks for the individual components compounded

Material	OnSet ºC	End ºC	Peak ºC	Wt-%	Formulation Wt-%	Predicted Wt-%
Water			<104	99.9	1.5	1.5
Glycerol 99%	243.26	279.99	**264.72**	99.7	7.8	7.7
Starch	277.23	287.67	**283.40**	2.22	31.5	6.9
Hylon	288.19	324.47	**310.67**	65.17	31.5	18.9
	444.76	531.11	**500.74**	21.58	31.5	8.5
PBAT	379.2	437.58	**412.91**	98.2	58.2	57.15
Peroxide					1.0	
Total					100.0	
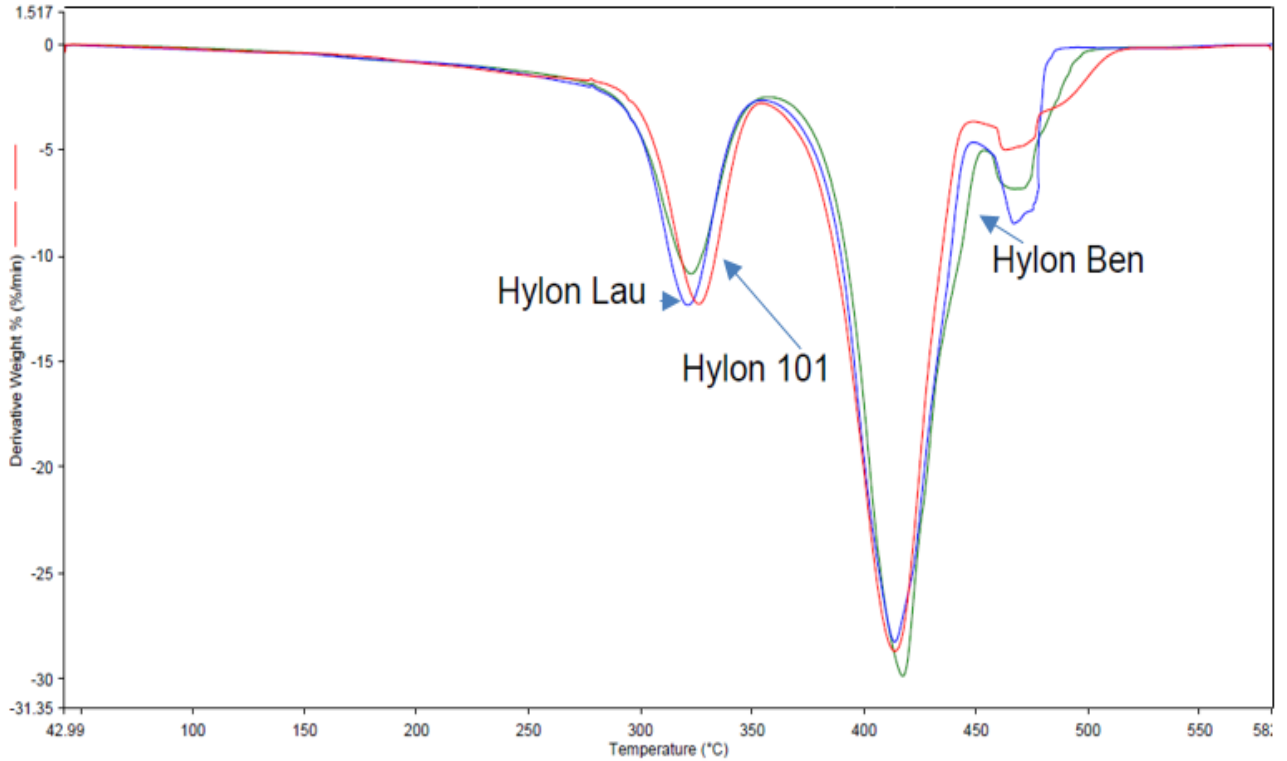
Figure 5-5 Composite of the TGA derivative curves for all three Hylon compounds

Table 5-4 Summary of the TGA derivative peaks for all three Hylon compounds from Table 5-1

Peak Assignment	Hylon-101 °C	Hylon-101 Wt-%	Hylon-Ben °C	Hylon-Ben Wt-%	Hylon-Lau °C	Hylon-Lau Wt-%
<150		7.5		5.2		8.5
1	326.02	23.1	322.94	24.3	321.03	22.9
2	413.40	58.4	414.32	48.5	409.24	51.8
3	467.03	8.1	434.60	9.8	429.85	5.1
4	490.85	2.4	470.59	11.4	475.51	11.4

104
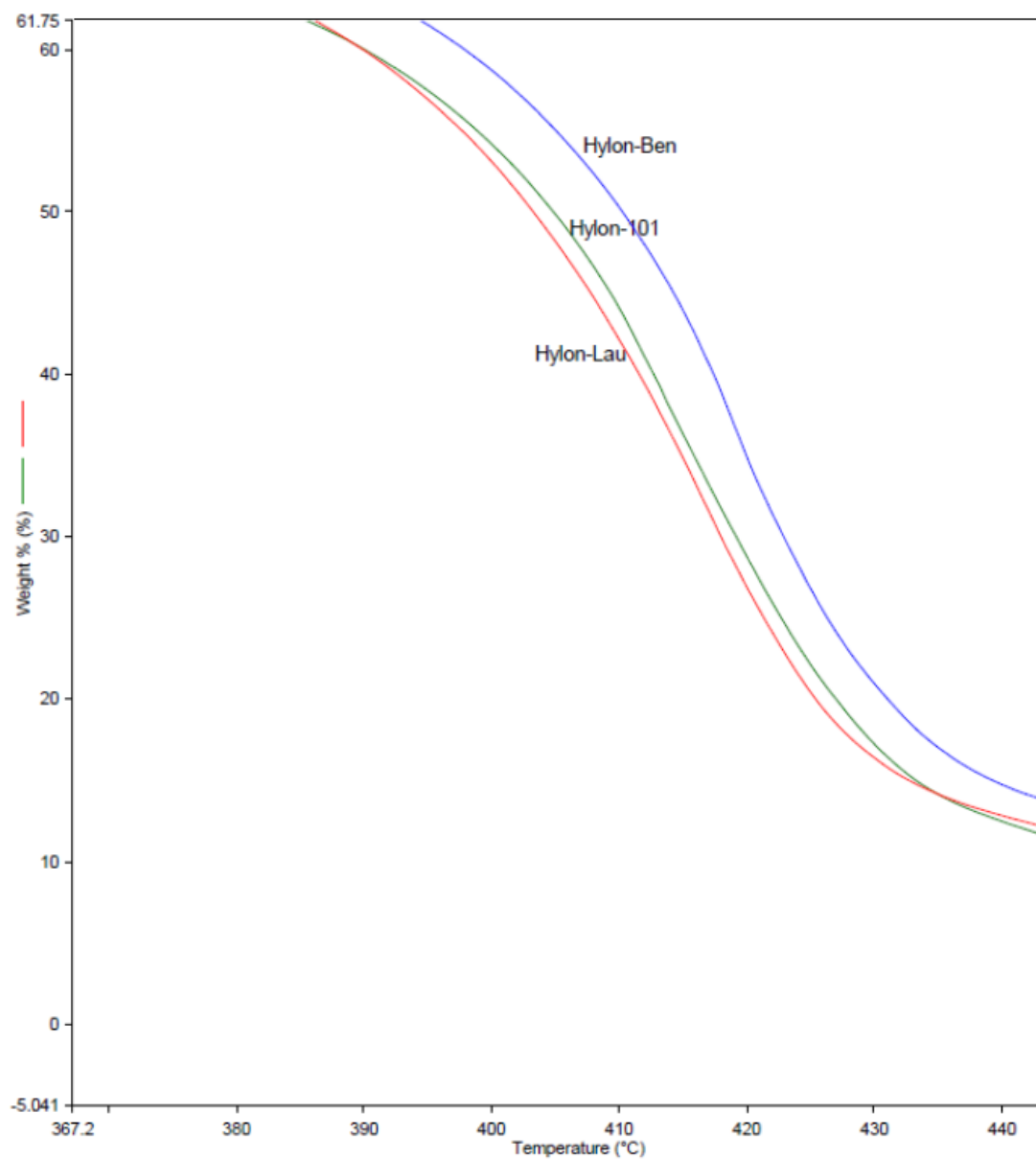
Figure 5-6 Composite of the TGA curves for all three Hylon compounds covering the range of 370ºC – 440ºC

DSC analysis was conducted on the Hylon compounds outlined in Table 5-1. Table 5-5 and Table 5-6 summarize the DSC peaks for 2nd melt cycle and 2nd cooling cycle for the compounds described in Table 5-1.

In Table 5-5, Hylon-Lau presents the lowest enthalpy of melt (ΔH_m) of the three compounds. Overall, all three compounds display a low degree of crystallization and require minimal heat to be absorbed to melt the crystalline regions. The enthalpy of melt (ΔH_m) value is noted to be low and ranging from 0.11 to 1.7 J/g.

In Table 5-6, Hylon-Lau presents the highest enthalpy of crystallization (ΔH_c) of the three compounds. Of interest is the point that all compounds present values for ΔH_c that are greater than the ΔH_m. This phenomenon is also noted with the conditioned Hylon starch sample. It is believed to be a result of plasticizer migration from the sample and subsequent retrogradation of the starch, thereby creating areas of crystallinity within the compound.

Swelling of the DSC pans was noted following the 2nd cycle of heating and cooling. It is believed that the plasticizer evapourated from the sample as a result of exposure to heat during the second heating of the compound, thereby deforming the DSC pan with increased vapour pressure.

To depict all three DSC curves together on the same graph in Figure 5-7, the scale of the Normalized Heat Flow Endothermic legend is too broad to depict the subtleties in the different compound melts. However, the glass transition temperature is visible for each compound and is clearly distinguished at the far left side of each curve. On analysis, both Hylon-Ben and Hylon-101 have the same glass transition temperature of 41.07°C and Hylon-Lau compound is measured at 43.27°C
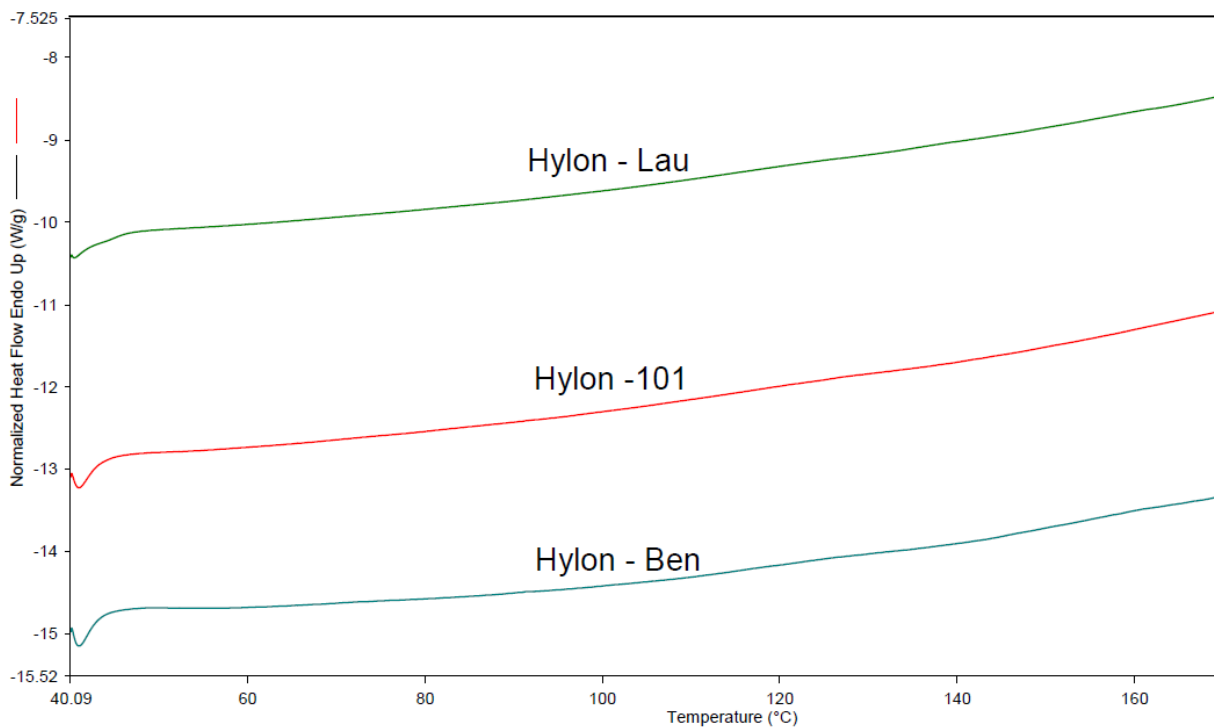
Figure 5-7 Compilation of the normalized DSC curves from the Hylon compounds derived from various free radical initiators

All three samples were analyzed by FTIR with an attenuated total reflectance (ATR) technique.

Figure 5-8 shows the FTIR spectra for all three Hylon compounds. Due to the details in the two regions outlined in Figure 5.8, between 2,500 – 3,450 cm^{-1} and 650 – 1800 cm^{-1}, the spectra were separated into these two areas and zoomed in on with detailed spectra reflected in Figures 5-9 and 5-10 respectfully

Table 5-5 Summary of the DSC melt peaks for the Hylon compounds outlined in Table 5-1 [2nd pass - melt cycle]

Material Peak	On Set °C	End °C	Peak °C	ΔH_m J/g
Hylon				
	No peak			
Hylon-101				
1	117.60	127.64	**126.79**	1.005
Hylon-Ben				
1	119.89	127.92	**126.30**	0.956
2	155.93	162.45	**160.83**	0.821
Hylon-Lau				
1	157.42	162.56	**161.22**	0.11

Table 5-6 Summary of the DSC crystallization peaks for the Hylon compounds outlined in Table 5-1 [2nd pass cooling cycle]

Material Peak	On Set °C	End °C	Peak °C	ΔH_c J/g
Hylon				
	114.36	94.08	**101.57**	-12.30
Hylon-101				
	103.05	80.61	**91.70**	-5.39
Hylon-Ben				
	101.81	82.08	**89.33**	-7.19
Hylon-Lau				
	104.35	79.75	**91.45**	-8.36
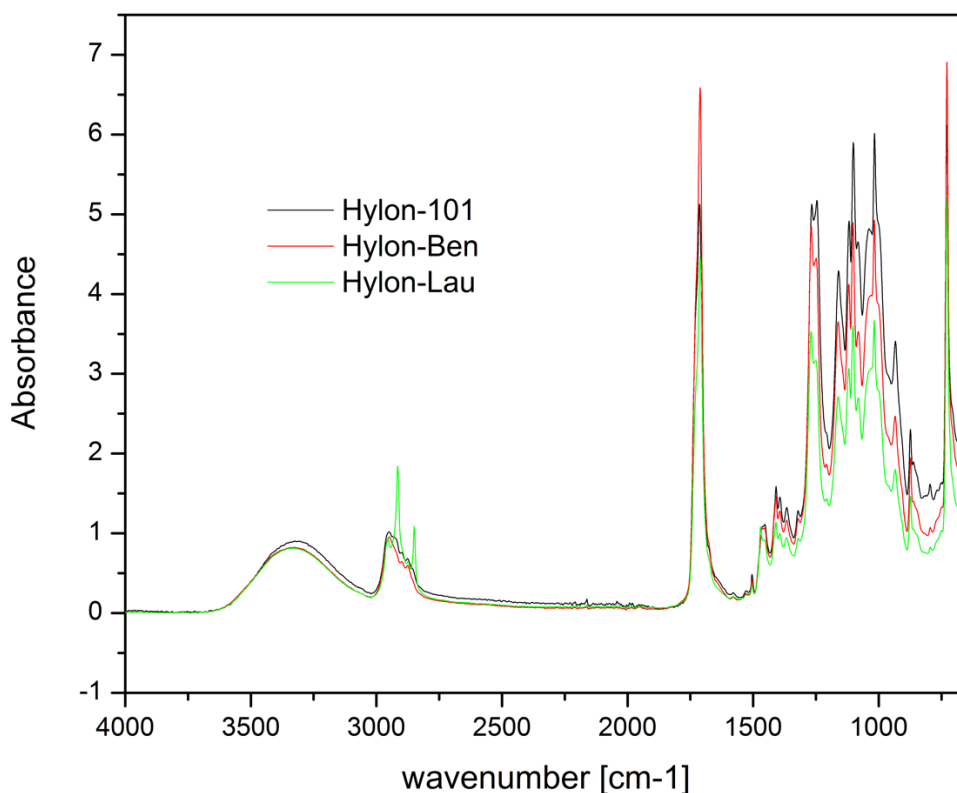
Figure 5-8 FTIR of the three Hylon compounds derived from the various free initiators

The spectra of the three compounds displayed in Figure 5-9 focuses on the wavenumbers between 2,500 and 3,450 cm^{-1}. Of interest are the following areas:

- The peak at 3,330 cm^{-1} arising from the hydroxyl groups (-OH) are seen in both Hylon-Ben and Hylon-Lau compounds. This peak is above the 3,300 cm^{-1} for hydroxyl groups seen in Hylon-101 and that of 3,219 cm^{-1} from the spectra of Hylon starch,

- The two peaks at 2918 cm^{-1} and 2853 cm^{-1}, seen in the spectra of Hylon-Lau, indicate the presence of aliphatic groups arising from grafting. These two peaks are not perceived in any of the spectra for the raw materials including PBAT nor Hylon starch
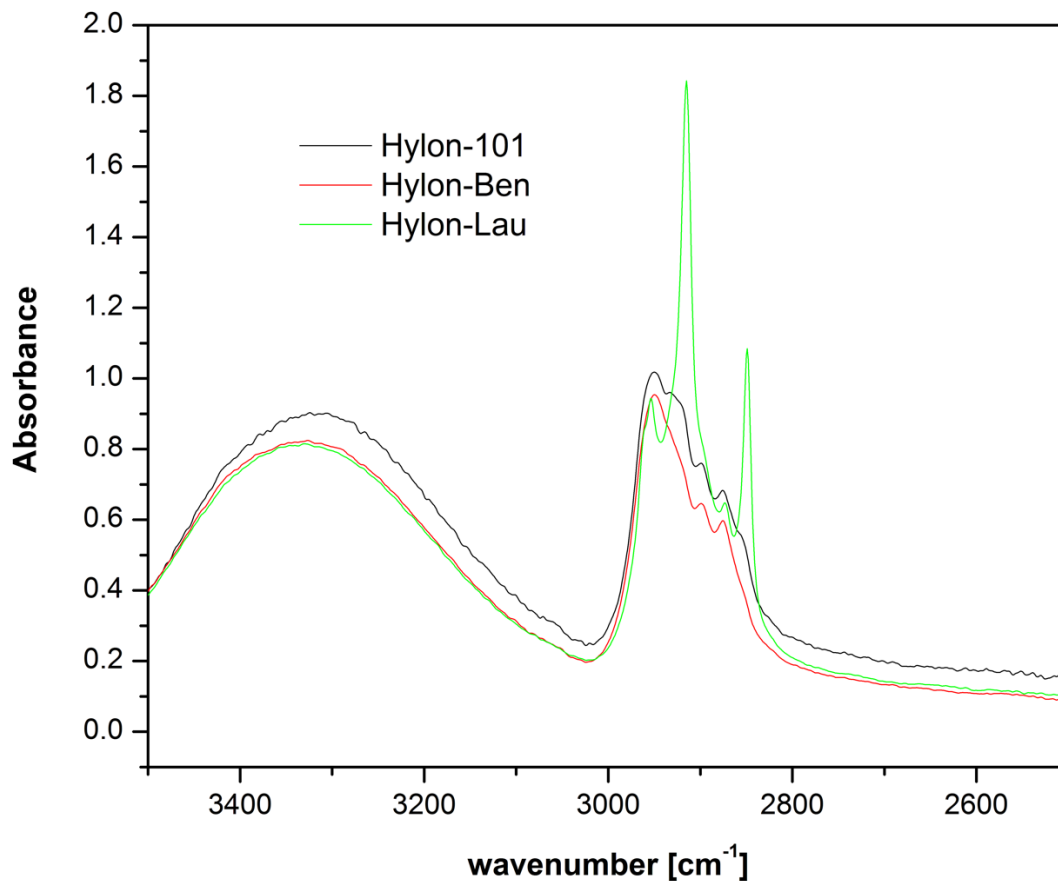
Figure 5-9 Zoom in on Figure 5-11 looking at wavenumbers of 2500 - 3450 cm^{-1}

. The spectra of the three compounds displayed in Figure 5-10 focuses on the wavenumbers between 600 and 1,800 cm^{-1}. The area of interest in these spectra are:

- The peak at 1710 cm^{-1} characteristic of carbonyl groups and suggesting the esterification reaction with maleic anhydride (MAH). Of interest is the increasing intensity of the peak

- from Hylon-Lau to Hylon-101 to Hylon-Ben. It is to be noted that carbonyl peak of 1715 cm^{-1} for PBAT is not present.

- The characteristic peak of 1780 cm^{-1} for the ring anhydride of maleic anhydride (MAH) is absent, thereby suggesting that it has been opened.
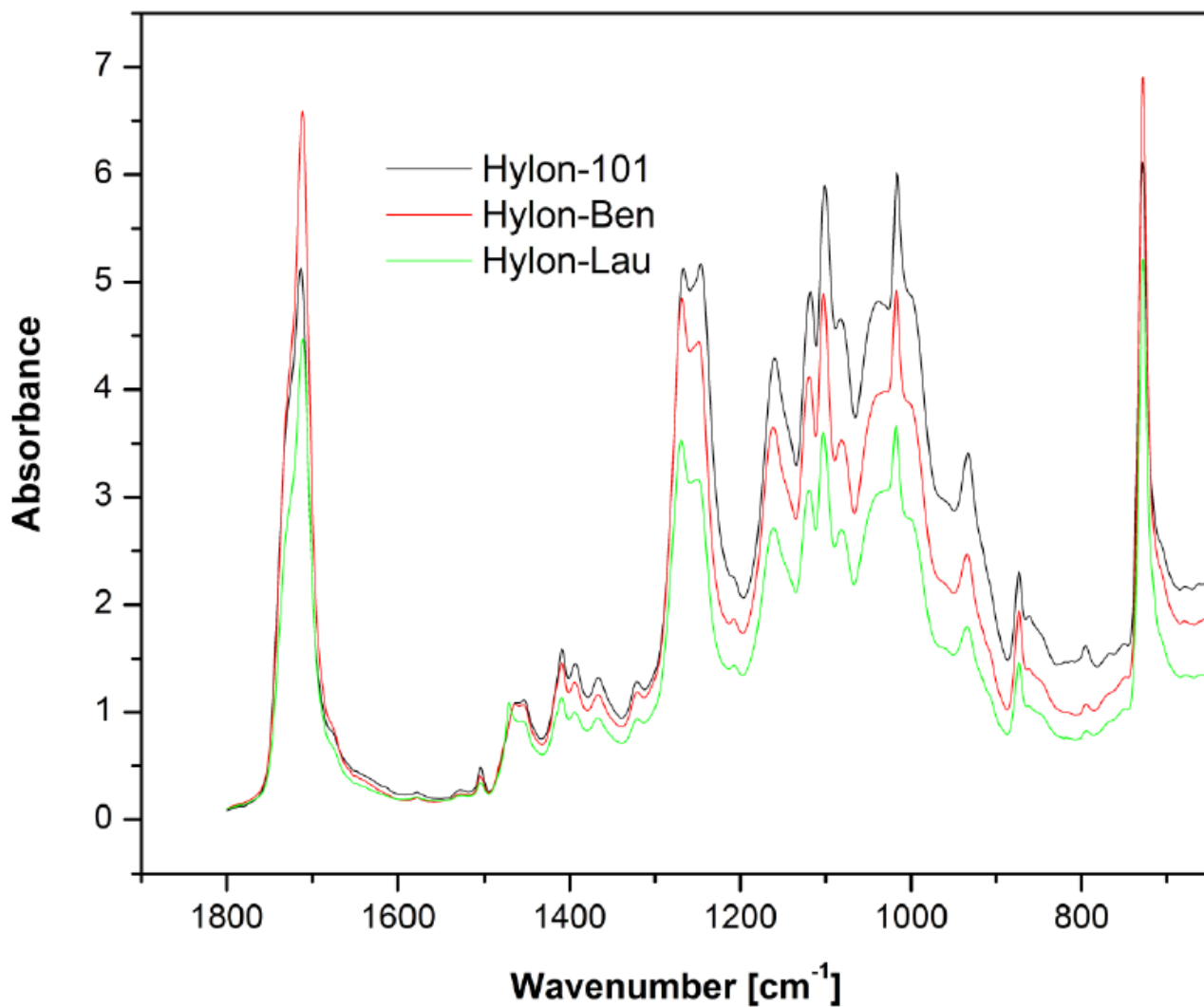
Figure 5-10 Zoom in on Figure 5-11 looking at wavenumbers of 650 - 1800 cm⁻¹

- Characteristic peaks at 1267 cm⁻¹ and 1243 cm⁻¹ represent ester stretches in PBAT. However, the ratio of the intensities between the two peaks is noted to be the same with PBAT and Hylon-101 and different with Hylon-Lau and Hylon-Ben.

5.2.2 30050 starch and the effects of various free radical initiators

In this section, three peroxides were compounded with 30050 starch and the properties evaluated.

Figure 5-11 illustrates the plots of the torque curves as a function of time for the 30050 compounds describe in Table 5-1. In this figure, all compounds display a delay in the onset of starch granular destruction. 30050-101 compound, with the free radical initiator Trigonox 101 peroxide, is the first compound to display a rapid change in torque. Compound 30050-101 achieves a maximum torque peak of 1435 mg and subsequent decline. The drop in torque is in response to the effective plasticization of the starch molecules following the gelatinization of the starch.

The curves for 30050-Lau and 30050-Ben start to show the onset of destructuring shortly after 30050-101. 30050-Lau and 30050-Ben compounds achieve maximum torque at 1841 mg and 1540 mg. However, both 30050-Lau and 30050-Ben exhibit higher torque value than 30050-101.

Summary of torque values for the three 30050 compounds as a function of time is outlined in Table 5-7.

In Figure 5-12, the time at which 30050-101 temperature curve is at its lowest, corresponds with the time it takes 30050-101 torque curve to achieve its maximum torque value in Figure 5-11. This relationship seems to make sense, as until the starch is destructured and the onset of plasticization occurs, all the energy from thermal and mechanical sources are being absorbed by the 30050-101 compound. Once the compound had achieved gelatinization and plasticization is occurring, the compound requires less energy to break the lamellae crystalline structure within the amylopectin molecules, thus resulting in an increase in temperature being identified. The same relationship between torque and temperature as a function of time is seen for 30050-Lau.

However, 30050-Ben displays a delay in obtaining the minimum temperature. The time to achieve maximum torque does not match up with minimum temperature
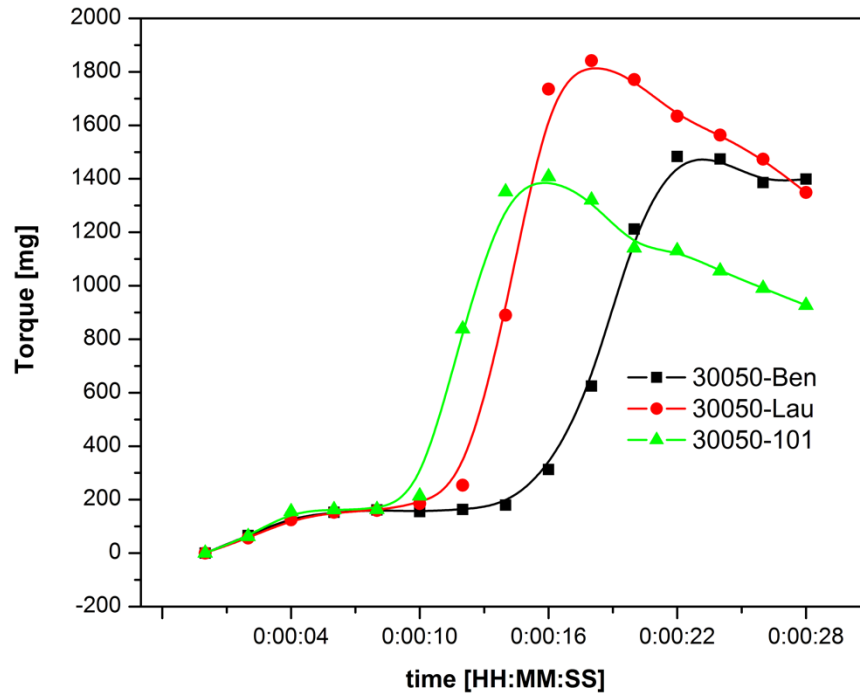
Figure 5-11 Compilation of torque as a function of time curve for the various 30050 compounds over the first 28 seconds

In Figure 5-13, it is noted that once the various compounds achieve their maximum torque value, they start to exhibit signs of plasticization and decreasing torque values as time progresses. As time approaches one minute, the torque values of the various compound seem to stabilize except for 30050-Ben. At one minute, the CWB software notes an increase in the torque of the 30050-Ben compound.

In compounding thermoplastic starch, it was determined in section 4.6, that the temperature should not exceed 150°C. In Figure 5-1, it is concluded that the three compounds do not exceed that temperature during compounding.

Table 5-7 Summary of torque as a function of time for 30050 compounds from Table 5-1

	30050-101	30050-Ben	33050-Lau
Torque	mg	mg	mg
On Set	157	157	157
Max	1435	1540	1841
Time	seconds	seconds	seconds
On Set	9	15	11
Max	15	23	18

Figures 5-12 and 5-14 are plots of temperature versus time for the 30050 compounds outlined in Table 5-1, although to different time scales.
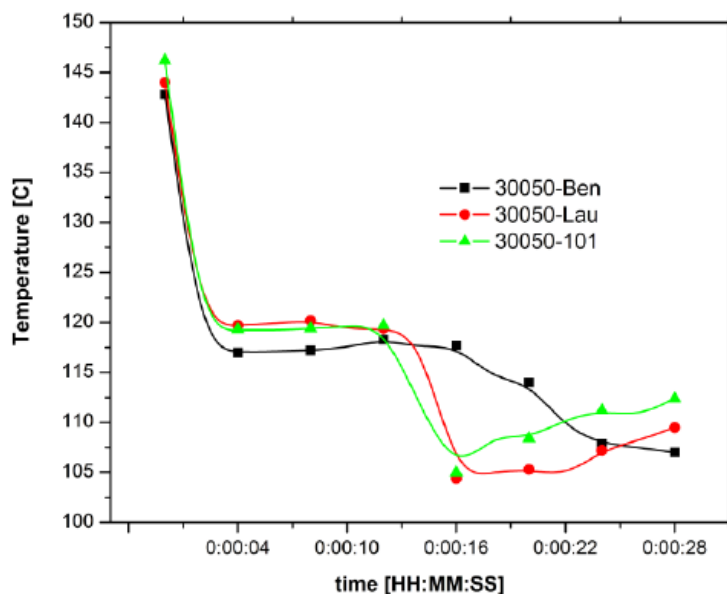
Figure 5-12 Compilation of temperature as a function of time curve for the various 30050 compounds from Table 5-1 for the first 28 seconds

114
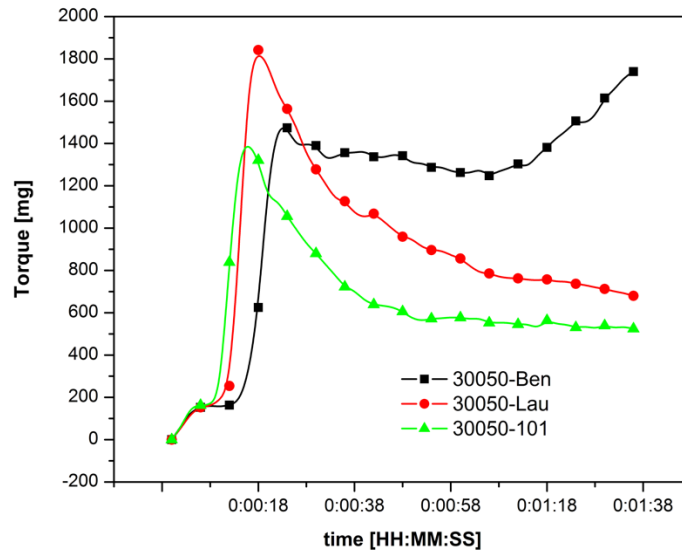
Figure 5-13 Compilation of torque as a function of time curve for the various 30050 compounds from Table 5-1 for the complete cycle
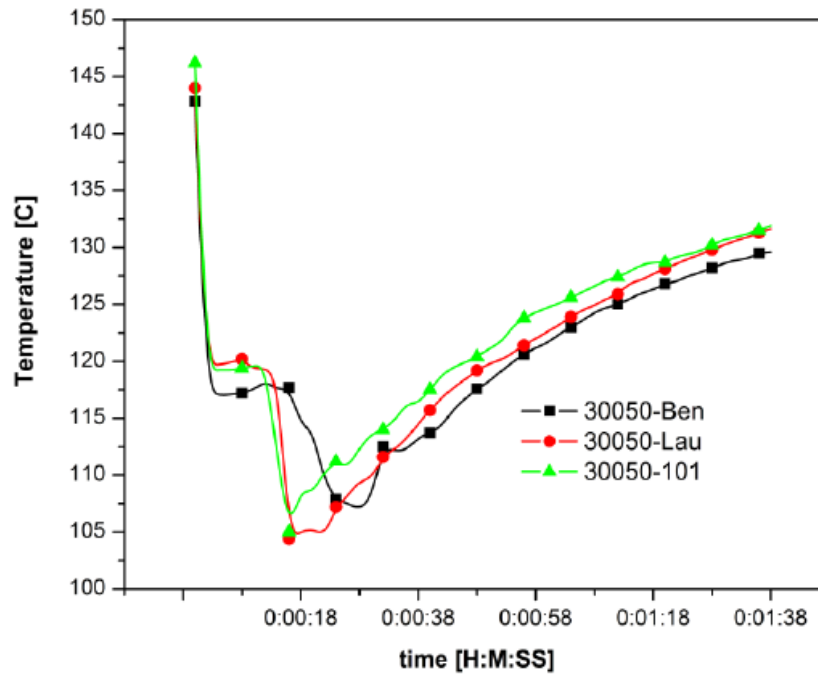
Figure 5-14 Compilation of temperature as a function of time curve for the various 30050 compounds from Table 5-1 for the complete cycle

115
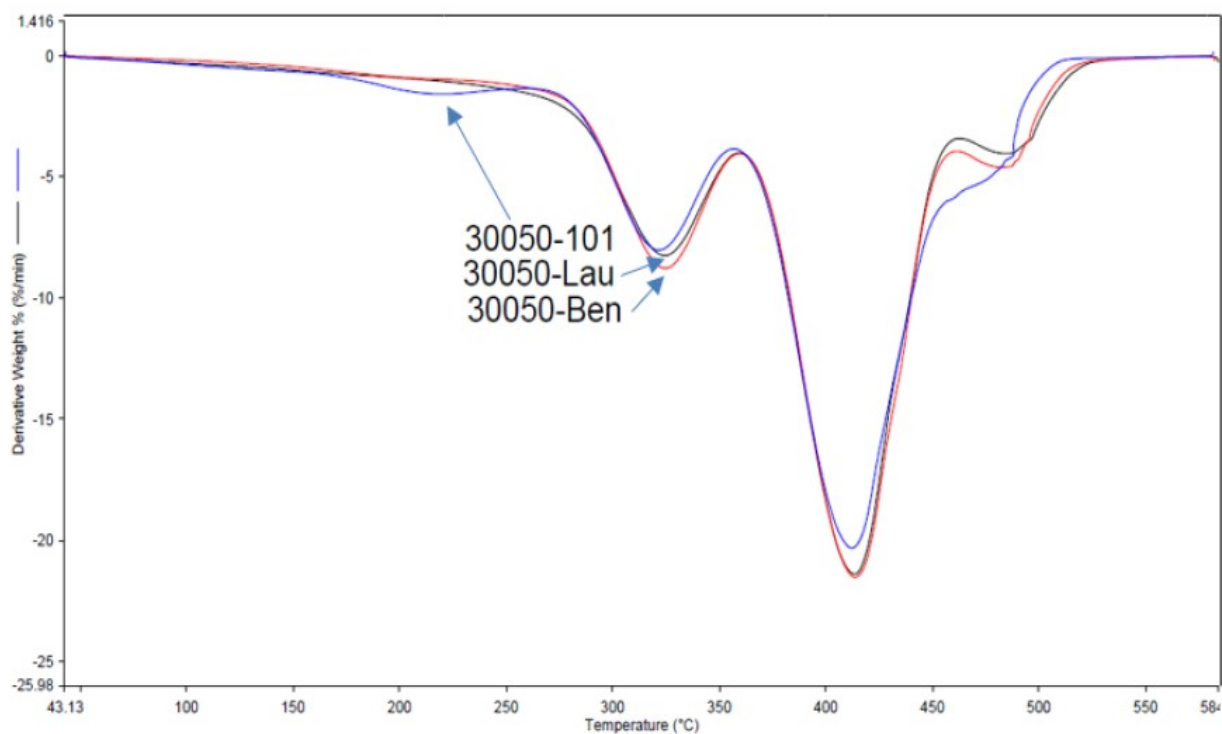
Figure 5-15 Compilation of TGA for the various 30050 compounds from Table 5-1

TGA analysis was conducted on the individual ingredients and the 30050 compounds outlined in Table 5-1. The objective was to determine if the 30050 compounds display any signs of changes in thermal stability over that of the individual raw materials.

Figure 5-15 displays the derivative of the percentage weight loss curve as a function of temperature with the 30050 compounds outlined in Table 5-1, with Table 5-9 summarizing the data.

In Figure 5-16, higher thermal stability is noted with 30050-Lau over the temperature range 160°C - 330°C, and greater than that of 30050-101 and 30050-Ben. Although this is an interesting finding for these compounds, it is to be noted that the thermal decomposition is happening well above the beginning of the thermal degradation of these compounds.

In comparing Tables 5-8 and 5-9, the data suggests that some form of starch molecular interaction or modification occurs within all three compounds. In Table 5-8, the TGA peak for 30050 starch is recorded at 317.26°C and in table 5-9, the peak increases between 321.03 to 323.60°C.

Of interest is 30050-101 TGA curve, with figures suggesting that the compound may be an add mixture with PBAT with little or no compatibilization occurring between the starch and the PBAT. This conclusion is reached by comparing the peak temperature and the predicted percentage of PBAT between Tables 5-8 and 5-9 and noting minimal change. The results in Table 5-9 for 30050-Ben and 33050-Lau suggest slight increased thermal stability with PBAT. This may be due to a small amount of compatibilization, intermolecular attraction or chemical modification occurred which offers increased thermal stability.

Table 5-8 Summary of the TGA peaks for the raw materials

Material	OnSet °C	End °C	Peak °C	Wt-%	Formulation Wt-%	Predicted Wt-%
Water			<104	99.9	1.5	1.5
Glycerol 99%	243.26	279.99	**264.72**	99.7	7.8	7.7
Starch	277.23	287.67	**283.40**	2.22	31.5	6.9
30050	294.83	331.37	**317.26**	60.00	31.5	18.9
	474.10	529.48	**502.61**	27.16	31.5	8.5
PBAT	379.2	437.58	**412.91**	98.2	58.2	57.15
Peroxide					1.0	
Total					100.0	

Table 5-9 Summary of the TGA peaks for various 30050 compounds from Table 5-1

Peak	30050-101		30050-Ben		30050-Lau	
Assignment	ºC	Wt-%	ºC	Wt-%	ºC	Wt-%
<150		1.8		1.0		1.6
1	212.36	7.8	203.48	6.1		
2	321.02	22.1	323.60	23.7	322.92	30.5
3	412.13	55.9	414.74	57.4	414.39	57.9
4	479.93	11.9	481.22	11.3	487.14	9.3
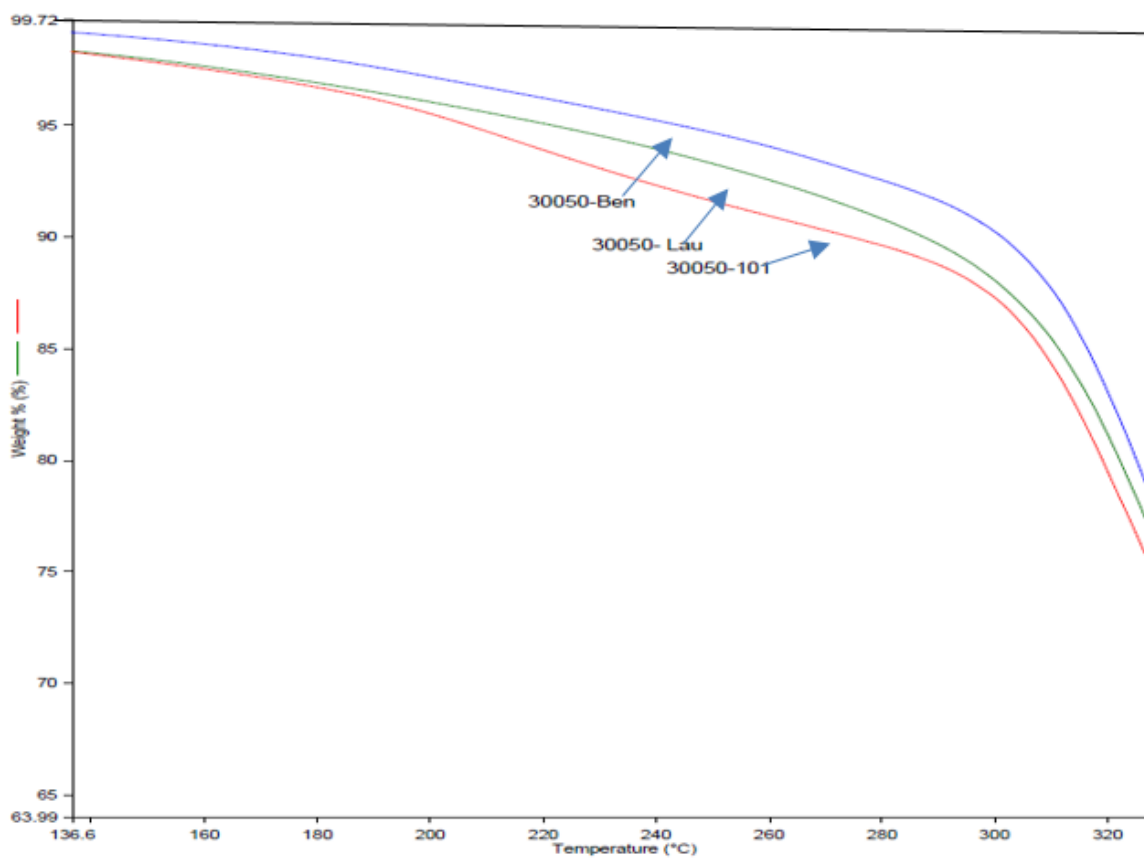
Figure 5-16 Compilation of TGA curve for the various 30050 compounds from Table 5-1 for the temperature range of 136ºC through 320ºC

DSC analysis was conducted on the 30050 compounds outlined in Table 5-1. Tables 5-10 and 5-11 summarize the peaks for 2nd melt cycle, and 2nd cooling cycle of the compounds from Table 5-1, respectively.

In Table 5-10, 30050-101 presents the lowest enthalpy of melt $[\Delta H_m]$ of the three compounds. Overall, all three compounds display a low degree of crystallization and require minimal heat to be absorbed to melt the crystalline regions. The enthalpy of melt ΔH_m value are noted to be low and ranging from 1.20 – 4.43 J/g.

In Table 5-11, 30050 –Lau presents the highest enthalpy of crystallization $[\Delta H_c]$ of the three compounds. Of interest is the point that all compounds present values for ΔH_c that are greater than the ΔH_m. This phenomenon is also noted with the conditioned Hylon starch sample. It is believed to be a result of plasticizer migration from the sample and subsequent retrogradation of the starch, thereby creating areas of crystallinity within the compound.

Swelling of the DSC pans was noted following the 2nd cycle of heating and cooling. It is believed that the plasticizer evapourated from the sample as a result of exposure to heat during the second heating of the compound, thereby deforming the DSC pan with increased vapour pressure.

To depict all three DSC curves together on the same graph in Figure 5-17, the scale of the Normalized Heat Flow Endothermic legend became too broad to depict the subtleties in the different compound melts. However, the glass transition temperature is visible for each compound and is clearly distinguished at the far left side of each curve. On analysis, 30050-Ben has the glass transition temperature of 40.70ºC, 30050-101 at 43.71ºC and 30050-Lau compound is measured at 41.16ºC
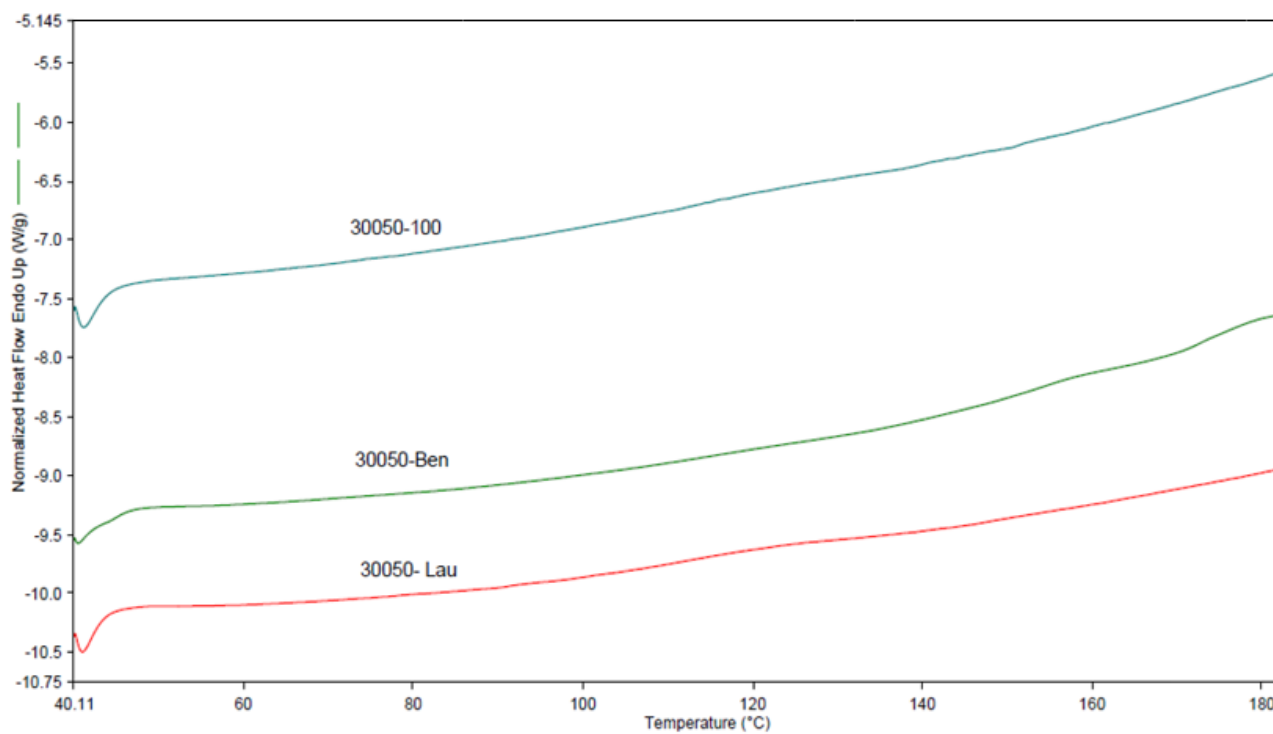
Figure 5-17 Compilation of the DSC curves of 30050 compounds from Table 5-1

Table 5-10 Summary of the DSC melt peaks for 30050 compounds of various free radical initiators outlined in Table 5-1

Material Peak	On Set °C	End °C	Peak °C	ΔH_m J/g
30050-101				
1	113.43	144.69	**119.72**	1.203
30050-Ben				
1	151.13	165.06	**157.62**	1.347
2	171.79	182.53	**178.19**	1.312
30050-Lau				
1	108.88	123.30	**123.06**	4.432

120

Table 5-11 Summary of the DSC cooling peaks for 30050 compounds of various free radical initiators outlined in Table 5-1

Material Peak	On Set °C	End °C	Peak °C	ΔH_c J/g
30050-101				
1	95.24	74.83	**86.42**	-8.08
30050-Ben				
1	102.25	78.71	**89.83**	-11.65
2	158.29	152.25	**156.51**	-7.89
30050-Lau				
1	101.26	81.11	**89.39**	-9.50

All three samples were analyzed by FTIR with an attenuated total reflectance (ATR) technique.

Figure 5-18 shows the FTIR spectra for all three 30050 compounds. Due to the detail in the two regions outlined in Figure 5-18, between $2{,}600 - 3{,}450$ cm^{-1} and $650 - 1800$ cm^{-1}, the spectra were separated into these two areas and zoomed in on with detailed spectra reflected in Figures 5-19 and 5-20, respectfully.

The spectra of the three compounds displayed in Figure 5-19 focuses on the wavenumbers between 2,500 and 3,450 cm^{-1}. Of interest are the following areas:

- The peak at 3,330 cm^{-1} arising from the hydroxyl groups (-OH) is seen in both 30050-101 and 30050-Lau compounds. This peak is above the 3,300 cm^{-1} for hydroxyl groups seen in 30050-Ben and that of 3,224 cm^{-1} from the spectra of 30050 starch.

- The two peaks at 2918 cm^{-1} and 2853 cm^{-1} seen in the spectra of 30050-101 and 30050-Ben indicate the presence of aliphatic groups arising from grafting. These two peaks are not perceived in any of the spectra for the raw materials including PBAT nor 30050 starch.
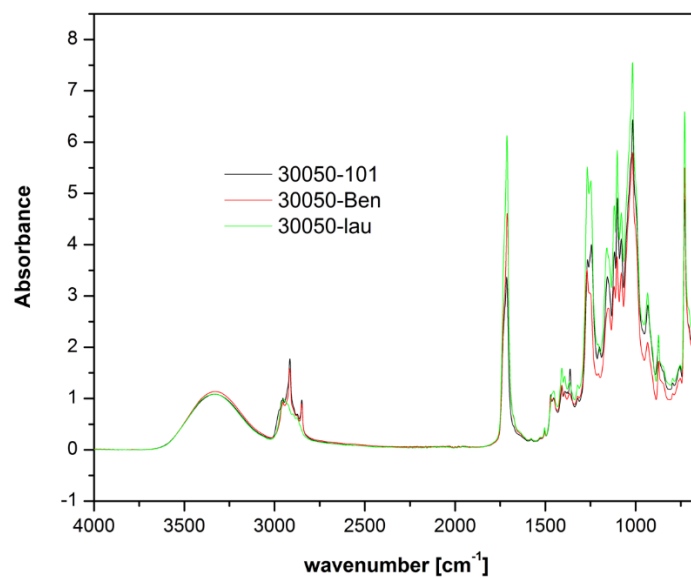
Figure 5-18 FTIR of the three 30050 compounds from Table 5-1
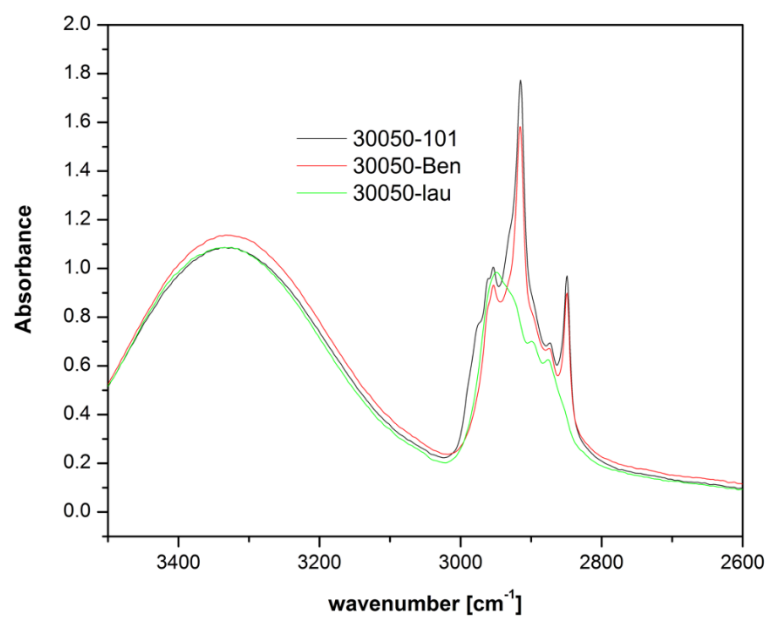
Figure 5-19 FTIR of the three 30050 compounds from Table 5-1 over the wavenumbers of 2600 - 3500 cm^{-1}

122
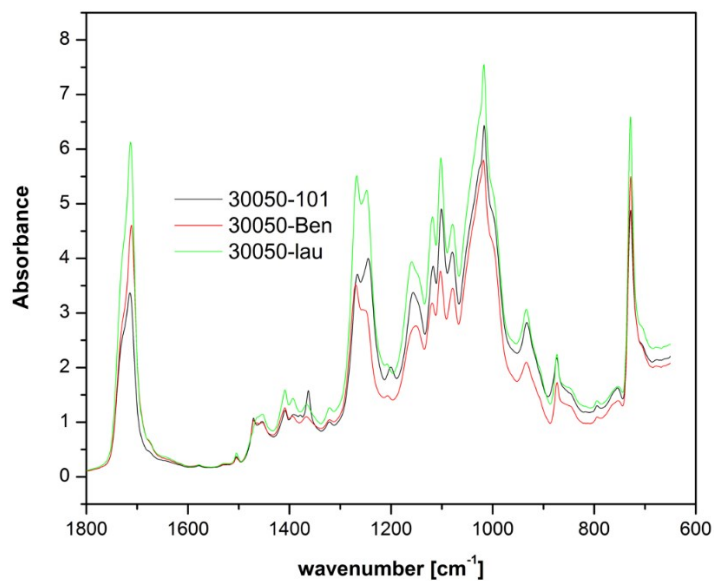
Figure 5-20 FTIR of the three 30050 compounds from Table 5-1 over the wavenumbers of 600 - 1800 cm^{-1}

The spectra of the three compounds displayed in Figure 5-20 focuses on the wavenumbers between 600 and 1,800 cm^{-1}. The area of interest in these spectra are:

- The peak at 1710 cm^{-1} is characteristic of carbonyl groups, suggesting the esterification reaction with maleic anhydride (MAH). Of interest is the increasing intensity of the peak from 30050-101 to 30050-Ben to 30050-Lau. It is noted that carbonyl peak of 1715 cm^{-1} for PBAT has shifted.

- The characteristic peak of 1780 cm^{-1} for the ring anhydride of maleic anhydride (MAH) is absent, thereby suggesting that it has been opened.

- Characteristic peaks at 1267 cm^{-1} and 1243 cm^{-1} represent ester stretches in PBAT with a ratio of intensity which approaches 1:1. However, the ratio of the intensities between the two peaks is noted to be different for all three compounds. 30050-Lau and 30050-Ben have a ratio of 1:>1, and 30050-101 having a ratio of 1>:1.

5.2.3 55310 starch and the effects of various free radical initiators

In this section, the effects of the three different peroxides is explored on conditioned 55310 starch.

Figure 5-21 illustrates the plots of the torque curves as a function of time for the 55310 compounds described in Table 5-1. In this figure, all compounds display a delay in the onset of starch granular destruction. The 55310-101 compound, with the free radical initiator Trigonox 101 peroxide, is the first compound to display a rapid change in torque. Compound 55310-101 achieves a maximum torque peak of 1435 mg and subsequent decline. The drop in torque is in response to the effective plasticization of the starch molecules following the gelatinization of the starch.

The curves for 55310-Lau and 55310-Ben start to show the onset of destructuring shortly after 55310-101. 55310-Lau and 55310-Ben compounds achieve maximum torque at 1209 mg and 1540 mg. However, both 55310-Ben and 55310-101 exhibit higher torque values than 55310-Lau.

Summary of torque values for the three 30050 compounds as a function of time are outlined in Table 5-7

Figures 5-22 and 5-24 are plots of temperature versus time for the 55310 compounds outlined in Table 5-1, although to different time scales.

In Figure 5-22, the time at which 55310-101 temperature curve is at its lowest, corresponds with the time it takes 55310-101 torque curve to achieve its maximum torque value in Figure 5-21. However, both 55310-Lau and 55310-Ben display a time lag in obtaining the minimum temperature after obtaining maximum torque.
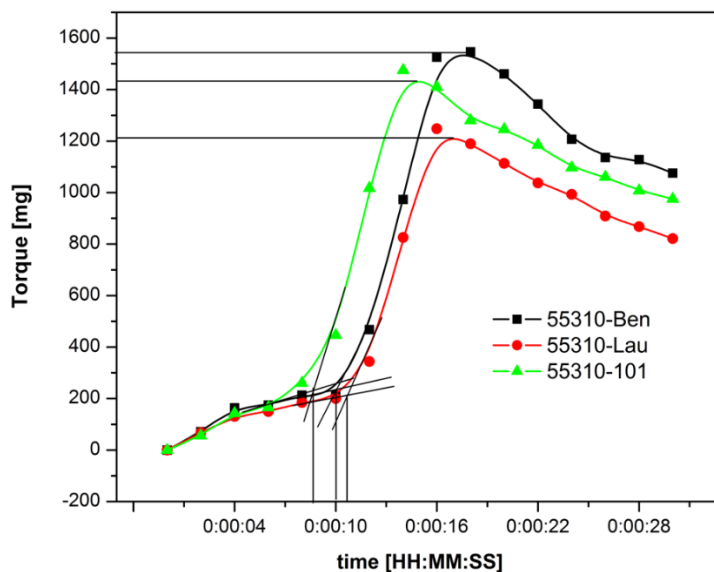
Figure 5-21 Compilation of torque as a function of time curve for the various 55310 compounds for the first 28 seconds

Table 5-12 Summary of torque as a function of time for 55310 compounds from various free radical initiators

	55310-101	55310-Ben	55310-Lau
Torque	mg	mg	mg
On Set	226	211	204
Max	1435	1540	1209
Time	seconds	seconds	seconds
On Set	8	10	11
Max	15	18	18

TGA analysis was conducted on the individual ingredients and the 55310 compounds outlined in Table 5-1. The objective is to determine if the 55310 compounds display any signs of changes in thermal stability over that of the individual raw materials.

Figure 5-25 displays the derivative of the percentage weight loss curve as a function of temperature with the 55310 compounds outlined in Table 5-1, with Table 5-14 summarizing the data.
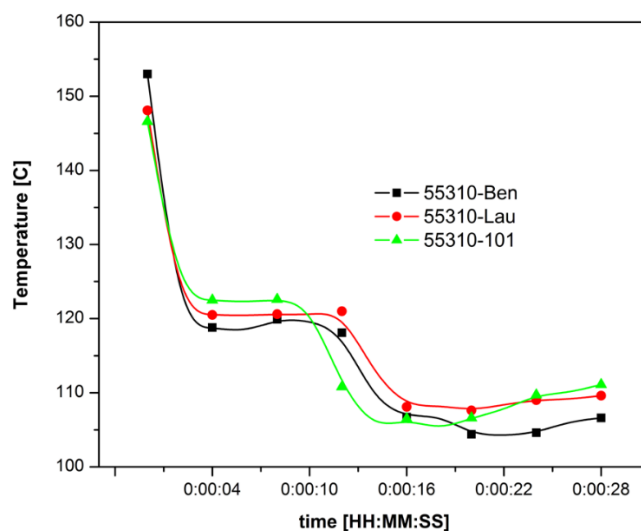
Figure 5-22 Compilation of temperature as a function of time curve for the various 55310 compounds for the first 28 seconds

In Figure 5-25, higher thermal stability is noted with 55310-Ben over the temperature range 380- 440ºC and greater than that of 55310-101 and 55310-Lau. Although this is an interesting finding for these compounds, it is to be noted that the thermal decomposition is happening well above the beginning of the thermal degradation of these compounds.
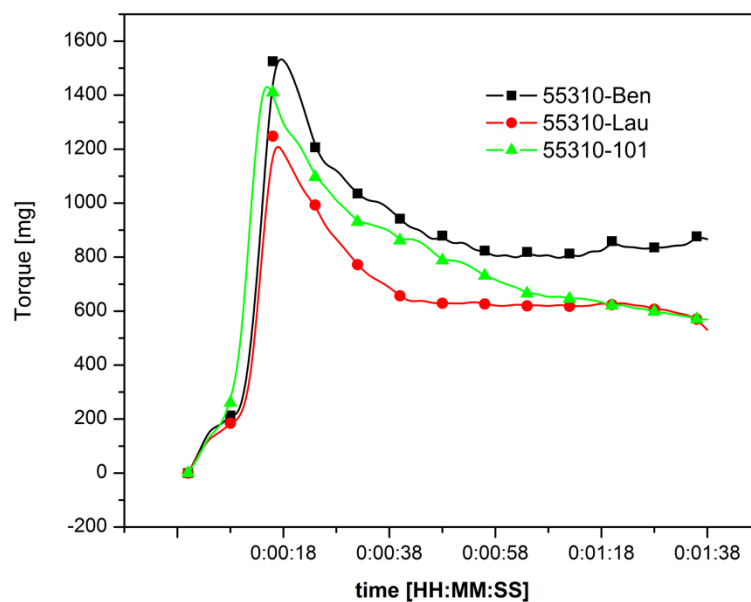
Figure 5-23 Compilation of torque as a function of time curve for the various 55310 compounds for one minute and 38 seconds
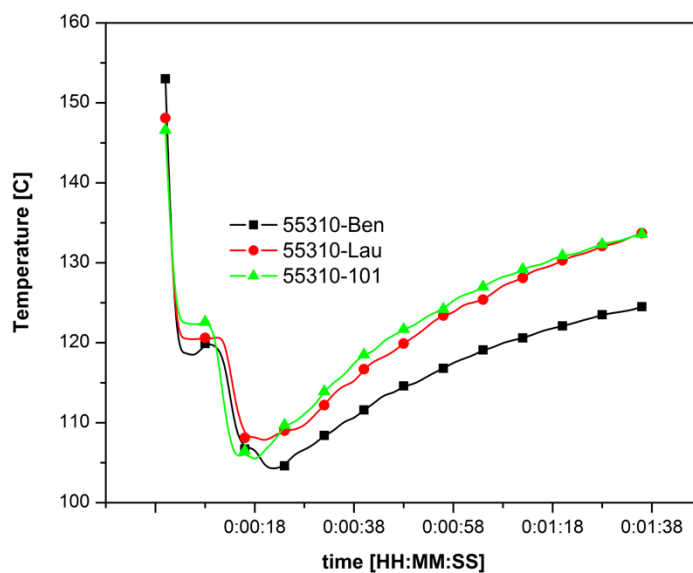
Figure 5-24 Compilation of temperature as a function of time curve for the various 55310 compounds for one minute and 38 seconds

In comparing Tables 5-13 and 5-14, the data suggests that some form of starch molecular interaction or modification has occurred within all three compounds. In Table 5.13, the TGA peak for 55310 starch is recorded at 293.89°C and in Table 5-14 the peak increases between 309.81 °C to 314.54°C.

In Figure 5-25, 55310-Lau TGA curve is lowest thermal decomposition stability of the three 55310 compounds with greater stability being recognized with 55310-101 and 55310-Ben respectively.
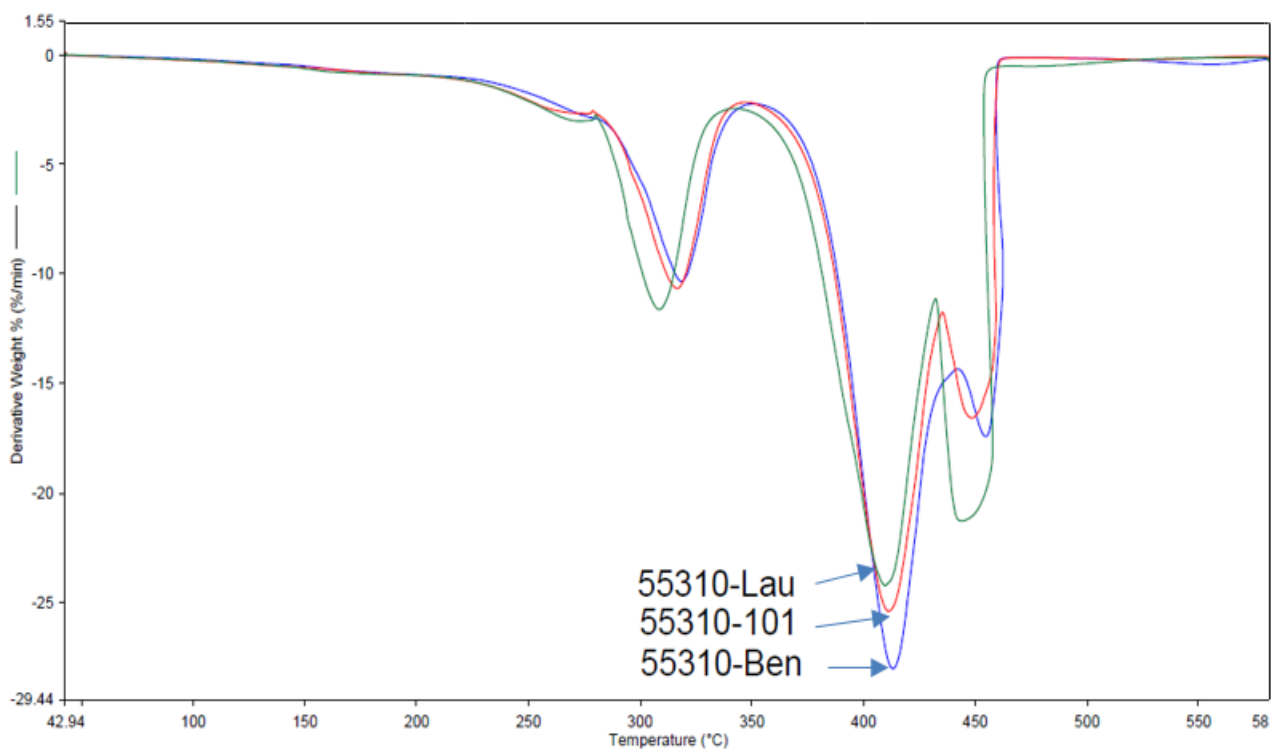
Figure 5-25 Compilation of TGA derivative curves for the various 55310 compounds

Table 5-13 Summary of the TGA derivative curves for the various raw materials

Material	OnSet °C	End °C	Peak °C	Wt-%	Formulation Wt-%	Predicted Wt-%
Water			<104	99.9	1.5	1.5
Glycerol 99%	243.26	279.99	**264.72**	99.7	7.8	7.7
Starch	283.62	300.14	**293.89**	71.68	31.5	22.60
55310	372.25	383.41	**374.15**	16.38	31.5	5.16
PBAT	379.2	437.58	**412.91**	98.2	58.2	57.15
Peroxide					1.0	
Total					100.0	

Table 5-14 Summary of the TGA derivative peaks for 55310 compounds defined in Table 5-1

Peak Assignment	55310-101 °C	Wt%	55310-Ben °C	Wt%	55310-Lau °C	Wt%
<150		1.4		1.4		1.2
1	261.00	5.2	261.00	9.6	269.01	10.1
2	311.95	24.3	314.54	19.8	309.81	19.6
3	410.20	52.4	416.15	53.6	409.15	52.0
4	451.01	15.4	454.26	14.3	446.75	17.5

DSC analysis was conducted on the 55310 compounds outlined in Table 5-1. The summaries of the peaks for 2nd melt cycle and 2nd cooling cycle are presented in Table 5-15 and Table 5-16 respectively.

In Table 5-15, 55310-101 presents the lowest enthalpy of melt $[\Delta H_m]$ of the three compounds. Overall, all three compounds display a low degree of crystallization and require minimal heat to

be absorbed to melt the crystalline regions. The enthalpy of melt ΔH_m value is noted to be low and ranging from $1.71 - 2.33$ J/g.

In Table 5-16, 55310-Ben presents the highest enthalpy of crystallization $[\Delta H_c]$ of the three compounds. Of interest is the point that 55310-Ben and 55310-101 compounds present values for ΔH_c that are greater than the ΔH_m. This phenomenon is also noted with the conditioned 55310 starch sample. It is believed to be a result of plasticizer migration from the sample and subsequent retrogradation of the starch, thereby creating areas of crystallinity within the compound.

Swelling of the DSC pans was noted following the 2nd cycle of heating and cooling. It is believed that the plasticizer evapourated from the sample as a result of exposure to heat during the second heating of the compound, thereby deforming the DSC pan with increased vapour pressure.
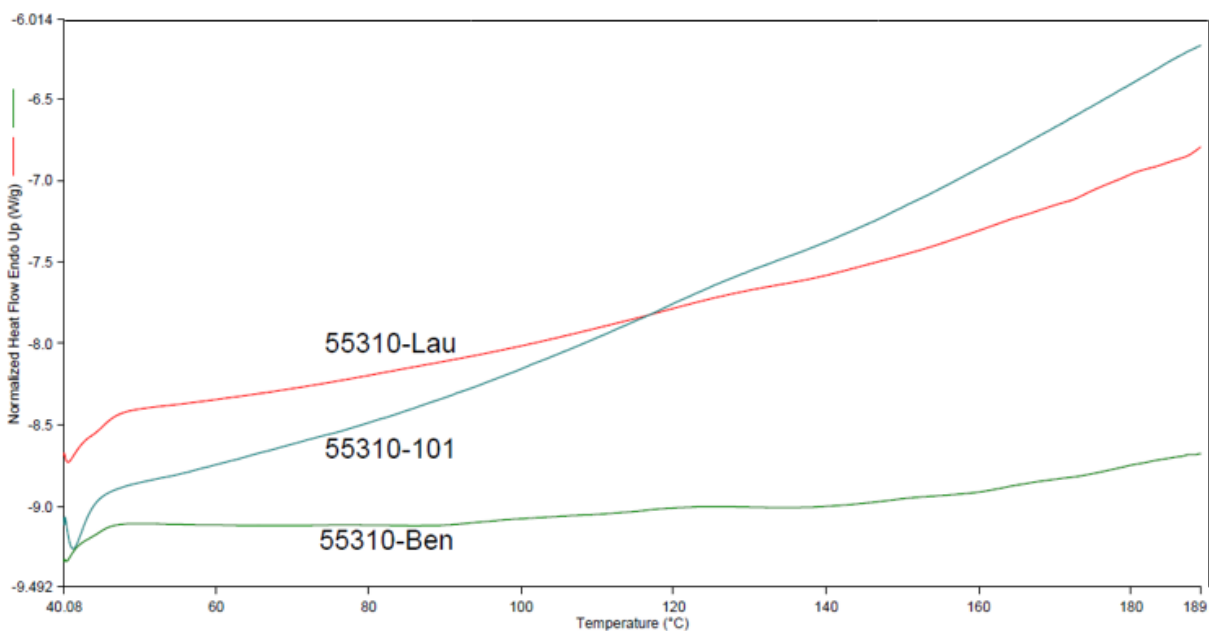
Figure 5-26 Compilation of normalized DSC curve for 55310 compounds defined in Table 5-1

To depict all three DSC curves together on the same graph in Figure 5-26, the scale of the Normalized Heat Flow Endothermic legend became too broad to depict the subtleties in the different compound melts. However, the glass transition temperature is visible for each compound and is clearly distinguished at the far left side of each curve. On analysis, 55310-Ben had the glass transition temperature of 40.70°C, 55310-101 at 43.11°C and 55310-Lau compound is measured at 41.31°C

All three samples were analyzed by FTIR with an attenuated total reflectance (ATR) technique.

Figure 5-27 Shows the FTIR spectra for all three Hylon compounds. Due to the detail in the two regions outlined in Figure 5-27, between 2,600 – 3,450 cm^{-1} and 650 – 1800 cm^{-1}, the spectra were separated into these two areas and zoomed in on with detailed spectra reflected in Figures 5-28 and 5-29 respectfully.

Table 5-15 Summary of the normalized DSC melt peaks for the 55310 compounds

Material Peak	On Set °C	End °C	Peak °C	ΔH_m J/g
55310-101				
1	122.76	126.44	**125.32**	1.709
55310-Ben				
1	92.04	109.33	**98.20**	0.465
2	115.15	133.77	**123.71**	1.364
3	146.45	157.75	**151.35**	0.220
4	161.88	172.17	**167.00**	0.281
55310-Lau				
1	112.11	137.27	**125.53**	1.984

DSC Cool

Table 5-16 Summary of the normalized DSC crystallization peaks for the 55310 compounds

| Material | On Set | End | Peak | ΔH_c |
Peak	°C	°C	°C	J/g
55310-101				
1	96.34	79.89	**88.80**	-6.41
55310-Ben				
1	97.15	78.82	**86.48**	-9.89
2	149.06	134.29	**135.37**	-3.56
55310-Lau				
1	93.88	81.18	**89.78**	-0.86
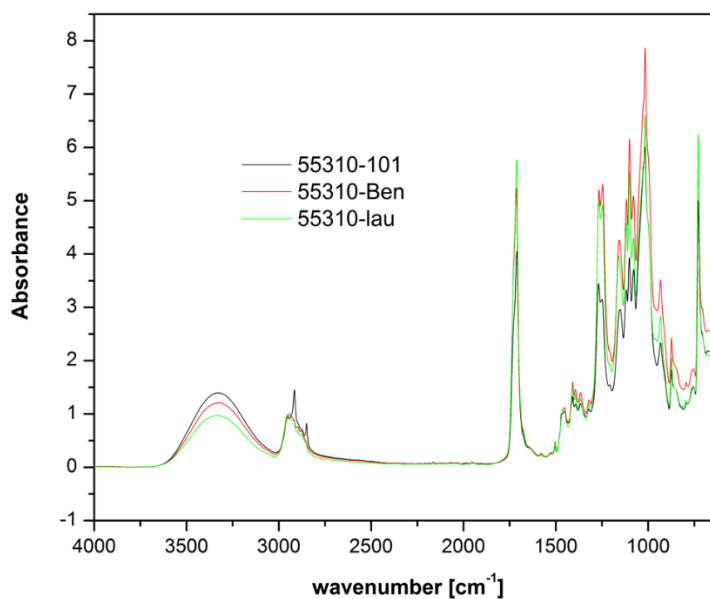
Figure 5-27 Compilation of the FTIR curves for the 55310 compounds
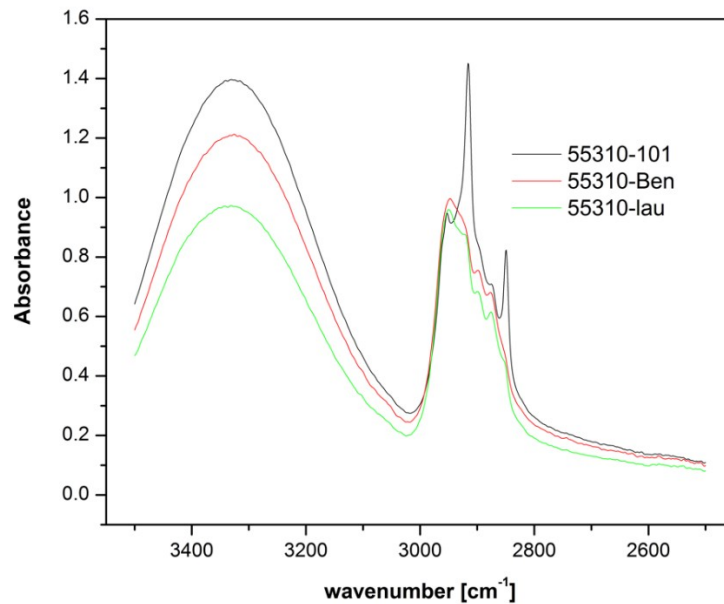
Figure 5-28 Compilation of the FTIR curves for the 55310 compounds from Table 5-1 over the wavenumbers 2500-3450 cm^{-1}

The spectra of the three compounds displayed in Figure 5-28 focuses on the wavenumbers between 2,500 and 3,450 cm^{-1}. Of interest are the following areas:

- The peak at 3,330 cm^{-1} arising from the hydroxyl groups (-OH) is seen in 55310-Lau, 55310-Ben and 55310-101 compounds with increasing intensities.

- The two peaks at 2918 cm^{-1} and 2853 cm^{-1}, seen in the spectra of 55310-101, indicate the presence of aliphatic groups arising from grafting.
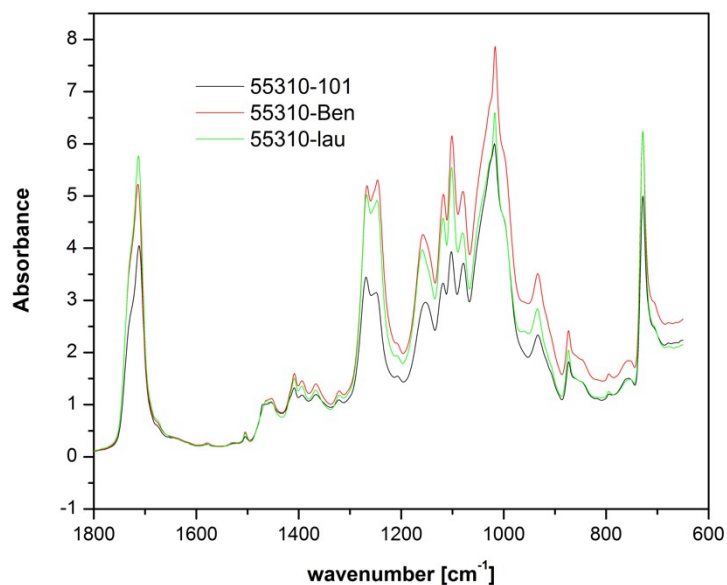
Figure 5-29 Compilation of the FTIR curves for the 55310 compounds from Table 5-1 over the wavenumbers 650-1800 cm^{-1}

The spectra of the three compounds displayed in Figure 5.29 focuses on the wavenumbers between 600 and 1,800 cm^{-1}. The area of interest in these spectra are:

- The peak at 1710 cm^{-1} is characteristic of carbonyl groups and suggests the esterification reaction with maleic anhydride (MAH). Of interest is the increasing intensity of the peak from 55310-101 to 55310-Ben to 55310-Lau. It is to be noted that carbonyl peak of 1715 cm^{-1} for PBAT is not present.

- The characteristic peak of 1780 cm^{-1} for the ring anhydride of maleic anhydride (MAH) is absent, thereby suggesting that it has been opened.

- Characteristic peaks at 1267 cm^{-1} and 1243 cm^{-1} represent ester stretches in PBAT where present with 55310-Lau and 55310-Ben, with both having higher absorbance intensity.

In section 5.2, the question was raised with regards to the selection of free radical initiators and whether certain free radical initiators could dissociate in a timely fashion to allow for chemical reactions to occur within the residence time and body temperature of the CWB at 150°C. The results from the trials conducted are reported in Table 5-17.

From Table 5-17 the following patterns are identified, independent of the starch considered, and for the compounds outlined in Table 5-1. However, it is noted that the type of starch seems to have a predisposition to how it reacts with different free radical initiators. The faster the ability to destructure the starch in the presence of a free radical initiator:

- The more likely that lower torque will be required in the process

- The more likely that the resulting compound will be more amorphous in characteristic

- The more likely that the two peaks at 2918 cm^{-1} and 2853 cm^{-1} will be seen in the FTIR spectra, indicating the presence of aliphatic groups from grafting

- The more likely that a lower amount of carbonyl covalent bonds develop, as seen in the drop in intensity of the peak at 1710 cm^{-1}

Conversely, the following pattern is identified independent of the starch considered with the slower the destruction of the starch granule:

- The more likely that higher torque energy will be required.

- The more likely that higher compound thermal stability can be achieved

- The more likely that more crystallinity residue will reside in the compound

- The more likely additional carbonyl covalent bonds are developed as noted with the increased intensity of FTIR peak at 1710 cm^{-1}, thereby suggesting the potential of greater number of esterification and transesterification bonds occurring.

Table 5-17 Summary of the results in Section 5.2

Starch	Hylon	30050	55310
Amylose : Amylopectin ratio in Starch	70:30	25:75	25:75
Torque / destructuring Increasing rate	101< Ben< Lau	Ben<Lau <101	Ben<Lau <101
Torque / Maximum at destructuring point	Lau<101<Ben	101<Ben<Lau	Lau<101<Ben
TGA / increasing thermal stability	101<Lau<Ben	101 < Lau < Ben	Lau<101<Ben
DSC / Increasing ΔH_m	Lau < 101 < Ben	101 < Ben < Lau	101 < Lau < Ben
DSC / Increasing ΔH_c	101<Ben<Lau	101<Lau<Ben	Lau<101<Ben
FTIR / Additional Peaks 2918 & 2853cm^{-1}	Lau	101 & Ben	101
Increase Intensity @ 1710 cm^{-1}	Lau<101<Ben	101 < Ben < Lau	101 < Ben < Lau

5.3 The effects of increasing the amount of free radical initiators

In section 5.2, dibenzoyl peroxide was identified as being an efficient free radical initiator with various starches at 0.1% addition. In this section, the concept was to look the effects of increasing the amount of free radical initiators by three time (0.3%) and comparing the results found between the two compounds. The formulations in this evaluation are outlined in Table 5-18, with 30050 starch being used in the balance of the recipe.

Table 5-18 Formulations for the evaluation of the effect of increasing of peroxide the compound properties

Label	Peroxide type	Peroxide Wt-%	MAH Wt-%	PBAT Wt-%	Water Wt-%	Glycol Wt-%	Screw Speed RPM	Temperature °C
0.1%	Dibenzoyl	0.1	1.0	58.2	1.5	7.7	45	150°C
0.3%	Dibenzoyl	0.3	1.0	58.2	1.5	7.7	45	150°C

The evaluation of the torque and temperature as a function of time yield similar curves. At 23 seconds into the mix, the maximum torque 1540 mg is obtained, and lowest temperature is reached on both curves for 0.1% and 0.3% peroxide addition.

Looking into the results from TGA, the same level of thermal stability for both compounds (0.1% and 0.3% peroxide) is seen with the different levels of peroxide

The analysis of the DSC curve offers similar results for the two compounds. Both samples were analyzed by FTIR with an attenuated total reflectance (ATR) technique.

Figure 5-31 shows the FTIR spectra for both compounds. Due to the detail in the two regions outlined in Figure 5-31, between $2,600 - 3,450$ cm^{-1} and $650 - 1800$ cm^{-1}, the spectra were separated into these two areas and zoomed in on, with detailed spectra reflected in Figures 5-32 and 5-33 respectfully.

The spectra of the three compounds displayed in Figure 5-32 focuses on the wavenumbers between 2,500 and 3,450 cm^{-1}. Of interest are the following areas:

- The spectra peaks from both samples almost completely overlap each other.

- The peak at 3,300 cm^{-1} arising from the hydroxyl groups (-OH) is seen in both.

- The two peaks at 2918 cm^{-1} and 2853 cm^{-1} seen in the spectra indicate the presence of aliphatic groups arising from grafting. These two peaks are not perceived in any of the spectra for the raw materials including PBAT nor 30050 starch.

137
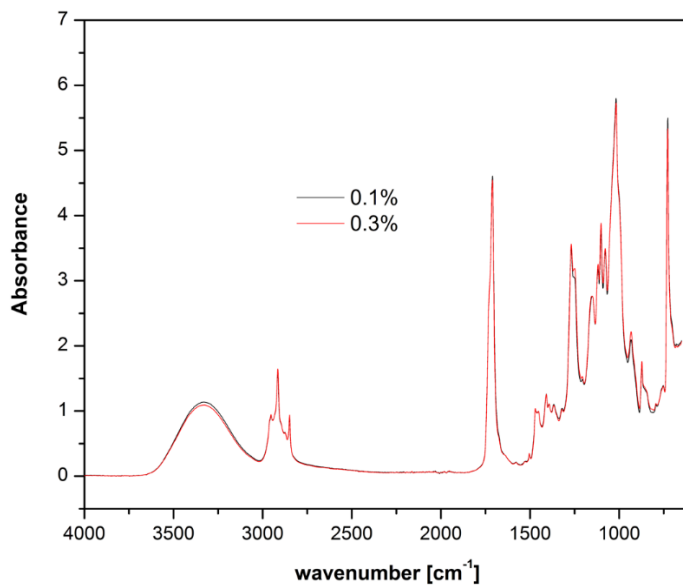
Figure 5-30 FTIR curve on the compound evaluating the effect of increasing of peroxide
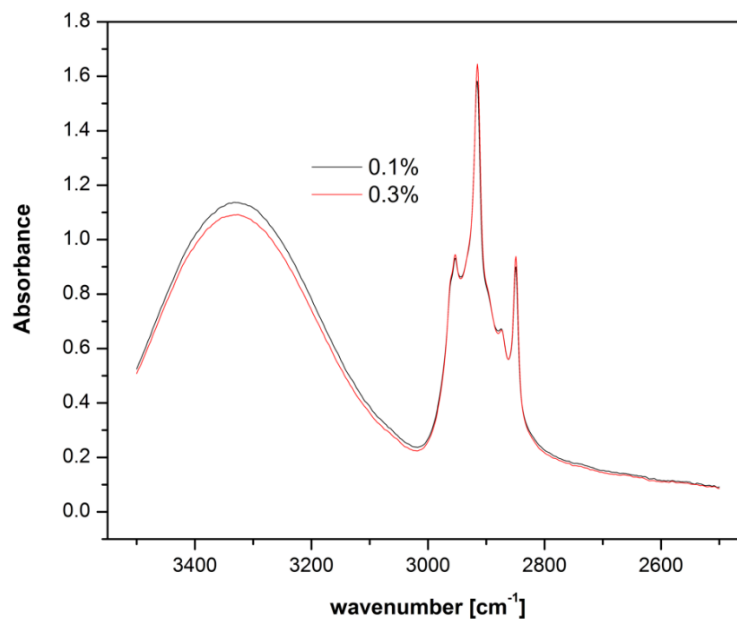
Figure 5-31 FTIR curve on the compound evaluating the effect of increasing of peroxide
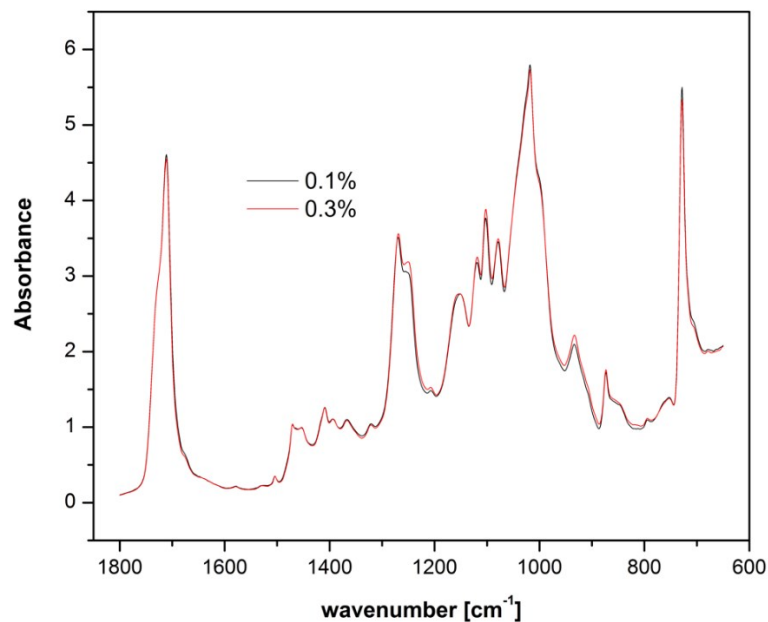
Figure 5-32 FTIR curve on the compound evaluating the effect of increasing of peroxide

The spectra of the two compounds displayed in Figure 5-32 focuses on the wavenumbers between 600 and 1,800 cm^{-1}. The area of interest in these spectra are:

- The peak at 1710 cm^{-1}, characteristic of carbonyl groups, and suggests the esterification reaction with maleic anhydride (MAH). It is to be noted that carbonyl peak of 1715 cm^{-1} for PBAT is not present.

- The characteristic peak of 1780 cm^{-1} for the ring anhydride of maleic anhydride (MAH) is absent, thereby suggesting that it has been opened.

5.4 The influence of increasing the amount of MAH

Maleic Anhydride (MAH) is a well-known building block in polymerization. Its bifunctional nature allows for covalent bonds to be formed. This experimental design examines the starch

139

polyester compound and the impact of increasing the amount of MAH added during compounding. The quantity of MAH added increased by two and three times over the initial amount.

The formulations in this evaluation are outlined in Table 5-19 with 30050 starch being used in the balance of the recipe.

Table 5-19 The Effects of Increasing Maleic Anhydride

Starch	Peroxide type	Peroxide Wt-%	MAH Wt-%	PBAT Wt-%	Water Wt-%	Glycol Wt-%	Screw Speed RPM	Temperature °C
MAH-1X	Lauroyl	0.1	1.0	58.2	1.5	7.7	45	150°C
MAH-2X	Lauroyl	0.1	2.0	58.2	1.5	7.7	45	150°C
MAH-3X	Lauroyl	0.1	3.0	58.2	1.5	7.7	45	150°C

Figure 5-34 illustrates the plots of the torque curves as a function of time for the 30050 compounds describe in Table 5-19. In this figure, all compounds display a delay in the onset of starch granular destruction. MAH-3X compound, with three times the amount of MAH, is the first compound to display a rapid change in torque. Compound MAH-3X achieves a maximum torque peak of 1875.49 mg and subsequent decline. The drop in torque is in response to the effective plasticization of the starch molecules following the gelatinization of the starch.

The curves for MAH-2X and MAH-1X start to show the onset of destructuring shortly after MAH-3X. MAH-2X and MAH-1X compounds achieve maximum torque at 1618.25 mg and 1828.60 mg.

Summary of torque value for the three MAH compounds as a function of time are outlined in Table 5-20.
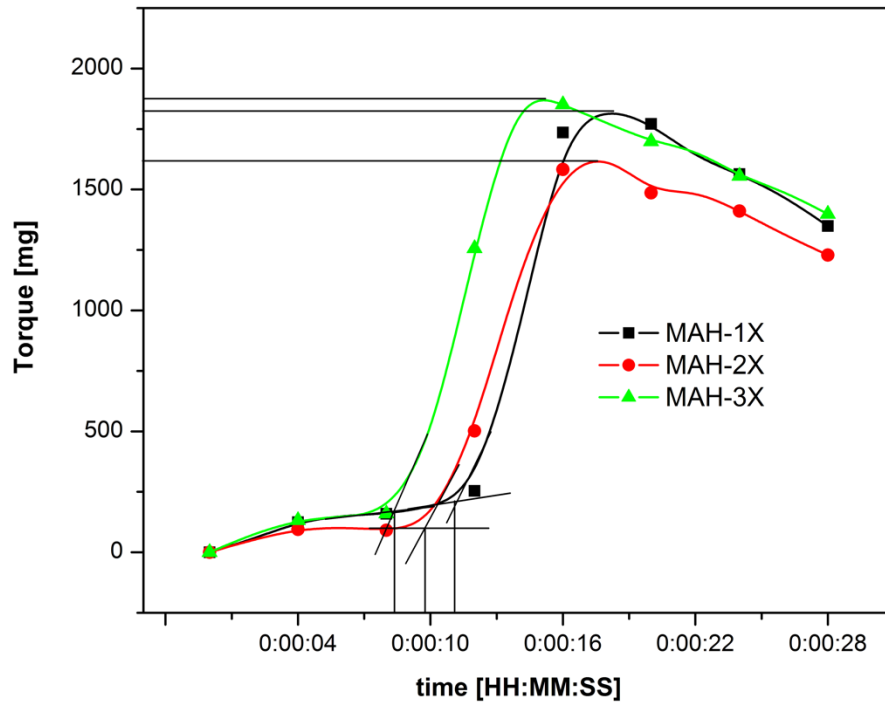
Figure 5-33 Compilation of torque curve as a function of time evaluating the effects of increasing MAH levels.

Table 5-20 Summary of the torque and time values in achieving destructuring of starch

	MAH-1X	MAH-2X	MAH-3X
Torque	mg	mg	mg
On Set	211.91	99.63	169.98
Max	1828.60	1618.25	1875.49
Time	seconds	seconds	seconds
On Set	11	9.5	8
Max	18	17	15
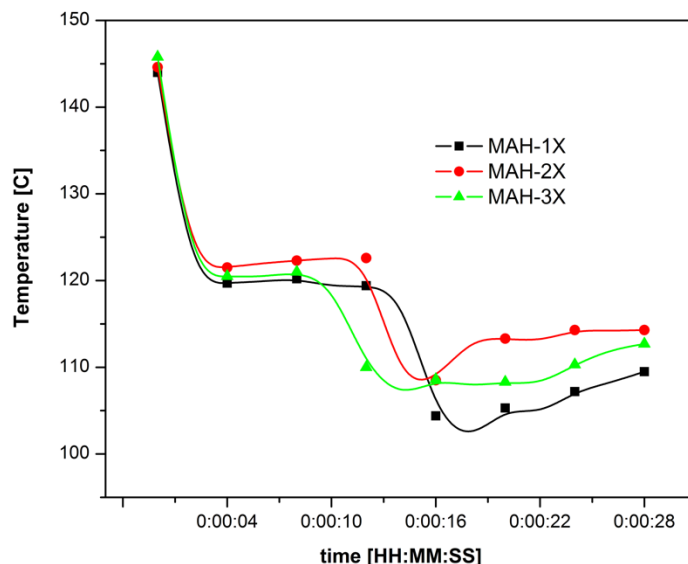
Figure 5-34 Compilation of the temperature as a function of time for the various compounds with increasing levels of MAH over the first 28 seconds of compounding

Figures 5-35 and 5-37 plot temperature versus time for the 30050 compounds outlined in Table 5-19, although to different time scales.

In Figure 5-35, the time at which MAH-3X temperature curve is at its lowest, corresponds with the time it takes MAH-3X torque curve to achieve its maximum torque value as seen in Figure 5-34. This relationship seems to make sense, as until the starch is destructured and the onset of plasticization occurs, all the energy from thermal and mechanical sources is being absorbed by the MAH-3X compound. Once the compound achieves gelatinization and plasticization is occurring, the compound requires less energy to break the lamellae crystalline structure within the amylopectin molecules, thus resulting in an increase in temperature being identified. The same relationship between torque and temperature as a function of time is seen for MAX-2X and MAH-1X.
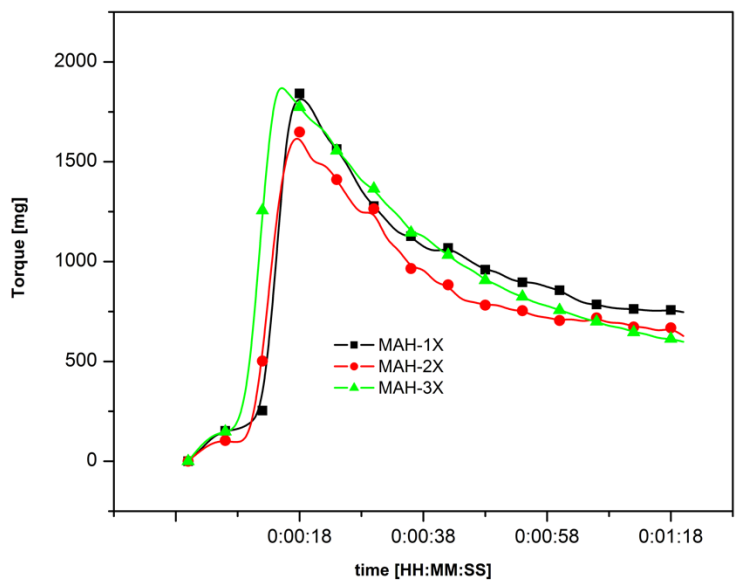
Figure 5-35 Compilation of the torque as a function of time for the various compounds with increasing levels of MAH
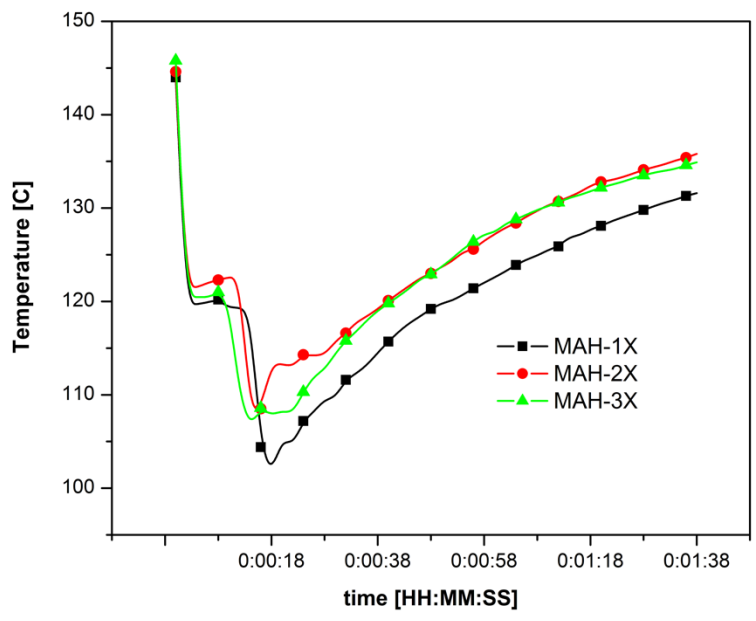
Figure 5-36 Compilation of the temperature as a function of time for the various compounds with increasing levels of MAH

143

In Figure 5-35, it is noted that once the various compounds achieve their maximum torque value, they start to exhibit signs of plasticization and decreasing torque values as time progresses. As time approaches one minute, the torque values of the compounds seem to stabilize

In compounding thermoplastic starch, it was determined in section 4.6, that the temperature should not exceed 150°C. In Figure 5-36, it is concluded that the three compounds do not exceed that temperature during compounding.

TGA analysis was conducted on the individual ingredients and the MAH compounds outlined in Table 5-21. The objective was to determine if the MAH compounds display any signs of changes in thermal stability over that of the individual raw materials.

In comparing Tables 5-21 and 5-22, the data suggests that some form of molecular interaction or modification has occurred within all three compounds. In Figure 5-38, higher thermal degradation temperatures are noted with MAH-1X over the temperature range 350°C - 450°C, than seen with MAH-2X and MAH-3X.

Figure 5-38 displays the derivative of the percentage weight loss curve as a function of temperature with the MAH compounds outlined in Table 5-19, with Table 5-22 summarizing the data.

DSC analysis were conducted on the MAH compounds outlined in Table 5-19. The summaries of the DSC peaks for 2nd melt cycle and 2nd cooling cycle are in Table 5-23 and Table 5-24 respectively.

Table 5-21 TGA derivative peaks for the raw material employed in the various compounds

Material	OnSet °C	End °C	Peak °C	Wt-%	Formulation Wt-%	Predicted Wt-%
Water			<104	99.9	1.5	1.5
Glycerol 99%	243.26	279.99	**264.72**	99.7	7.8	7.7
Starch	277.23	287.67	**283.40**	2.22	31.5	6.9
30050	294.83	331.37	**317.26**	60.00	31.5	18.9
	474.10	529.48	**502.61**	27.16	31.5	8.5
PBAT	379.2	437.58	**412.91**	98.2	58.2	57.15
Peroxide					1.0	
Total					100.0	

Table 5-22 Summary of the TGA derivative peaks for the compounds defined in Table 5-17

Peak Assignment	MAH-1X °C	Wt-%	MAH-2X °C	Wt-%	MAH-3X °C	Wt-%
<150		1.53		11.44		10.76
1	322.92	30.5	306.60	21.73	306.78	22.34
2	414.39	57.88	411.51	60.36	399.25	50.84
3	484.17	9.26	478.80	5.69	425.57	14.35

In Table 5-23, MAH-3X presents the lowest enthalpy of melt $[\Delta H_m]$ of the three compounds. Overall, all three compounds display a low degree of crystallization and require minimal heat to be absorbed to melt the crystalline regions. The enthalpy of melt ΔH_m values are noted to be low and ranging from 1.28 – 4.43 J/g.

145
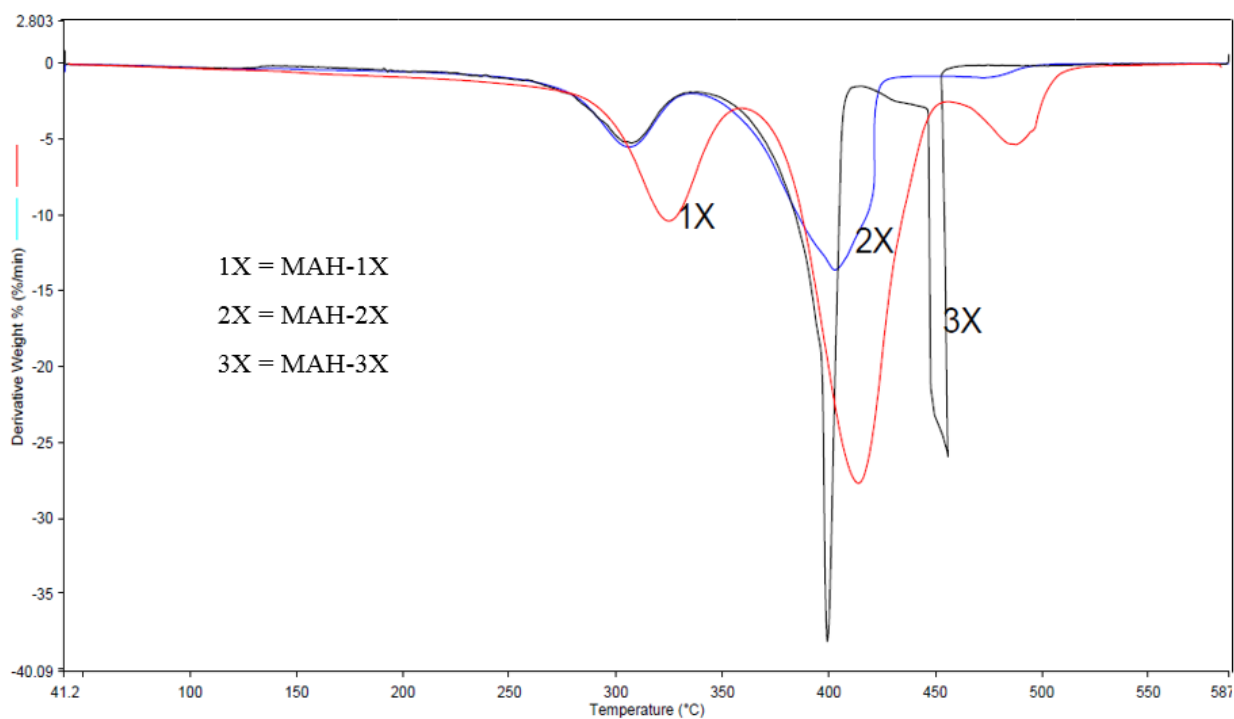
Figure 5-37 Compilations of the TGA derivative curves for the compounds defined in Table 5-17

In Table 5-24, MAH-1X presents the highest enthalpy of crystallization [ΔH_c] of the three compounds. It is noted that as the level of MAH increases, the measurement for ΔH_c decreases along with ΔH_m for the same compound.

To depict all three DSC curves together on the same graph in Figure 5-26, the scale of the Normalized Heat Flow Endothermic legend became too broad to depict the subtleties in the different compound melts. However, the glass transition temperature is visible for each compound and is clearly distinguished at the far left side of each curve. On analysis, MAH-1X had the glass transition temperature of 40.70°C, MAH-2X at 43.11°C and MAH-3X compound is measured at 41.31°C.
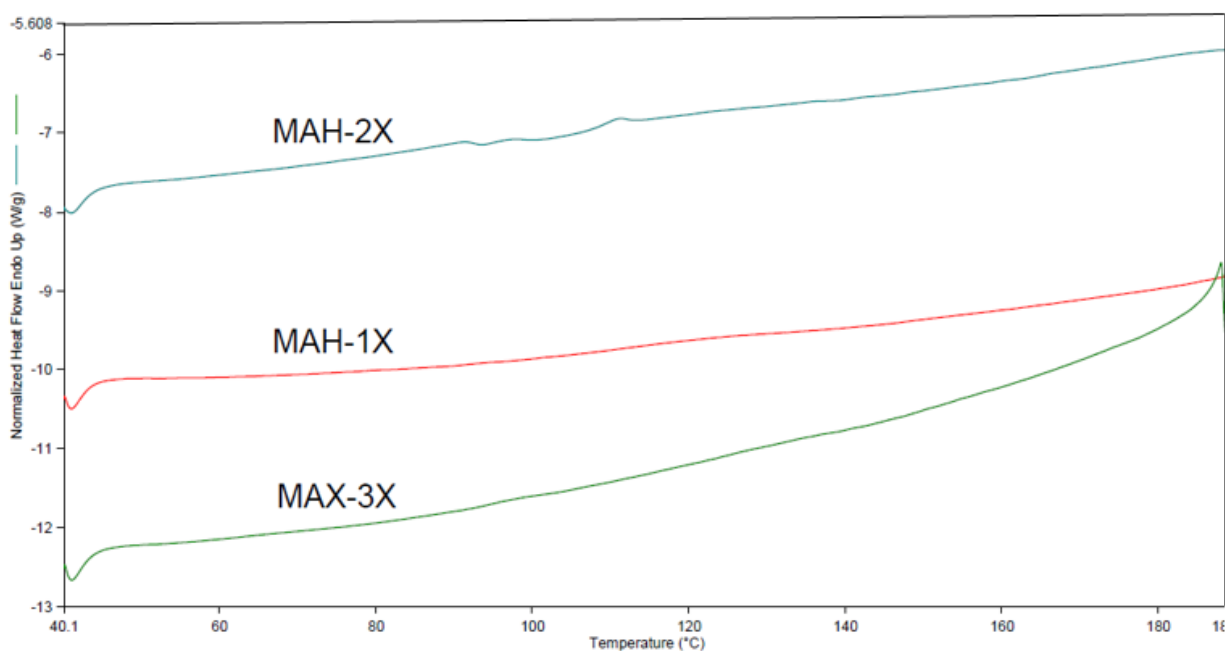
Figure 5-38 Compilations of the normalized DSC curves for the compounds defined in Table 5-19

Table 5-23 Summary of the normalized DSC melt curves for the compounds defined in Table 5-19

Material Peak	On Set °C	End °C	Peak °C	ΔH_m J/g
MAH-1X				
1	108.88	123.30	**123.06**	4.432
MAH-2X				
1	84.52	93.24	**91.02**	1.607
2	94.08	100.34	**97.00**	0.720
3	107.28	114.86	**110.82**	1.977
MAH-3X				
1	95.17	96.76	**96.18**	0.197
2	124.46	134.14	**133.76**	1.0864

147

Table 5-24 Summary of the normalized DSC crystallization curves for the compounds defined in Table 5-19

Material	On Set	End	Peak	ΔH_c
Peak	°C	°C	°C	J/g
MAH-1X				
	101.26	81.11	**89.39**	-9.50
MAH-2X				
	93.03	78.53	**87.53**	-0.60
MAH-3X				
	82.04	74.59	**78.71**	-0.39

All three samples were analyzed by FTIR with an attenuated total reflectance (ATR) technique.

Figure 5-40 shows the FTIR spectra for all three MAH compounds. Due to the detail in the two regions outlined in Figure 5-40, between 2,600 – 3,450 cm^{-1} and 650 – 1800 cm^{-1}, the spectra were separated into these two areas and zoomed in on with detailed spectra as reflected in Figures 5-41 and 5-42 respectively.

The spectra of the three compounds displayed in Figure 5-41 focuses on the wavenumbers between 2,500 and 3,450 cm^{-1}. Of interest are the following areas:

- The peak at 3,300 cm^{-1} arising from the hydroxyl groups (-OH) is seen for all three compounds. It is noted that the intensity of this peak increases as the amount of MAH increases.

- The two peaks at 2918 cm^{-1} and 2853 cm^{-1}, seen in the spectra of MAH-2X and MAX-3X, indicate the presence of aliphatic groups arising from grafting. These two peaks are not perceived in any of the spectra for the raw materials, including PBAT and 30050 starch

148
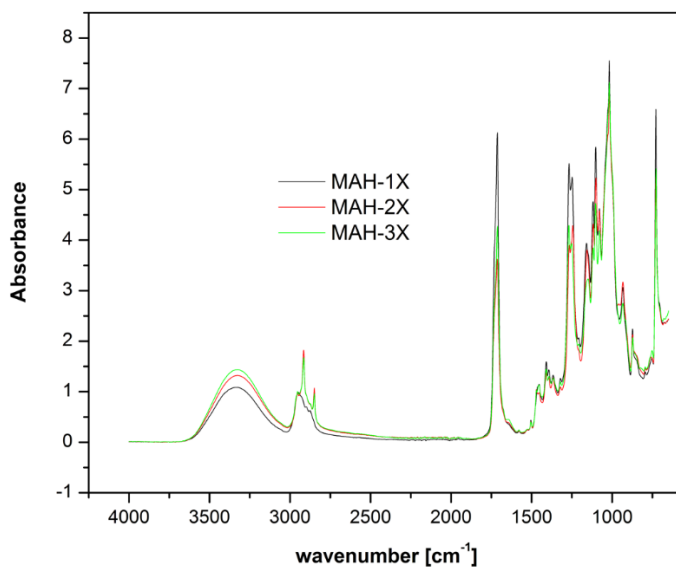
Figure 5-39 Compilation for the FTIR curves for the compounds define in Table 5-19
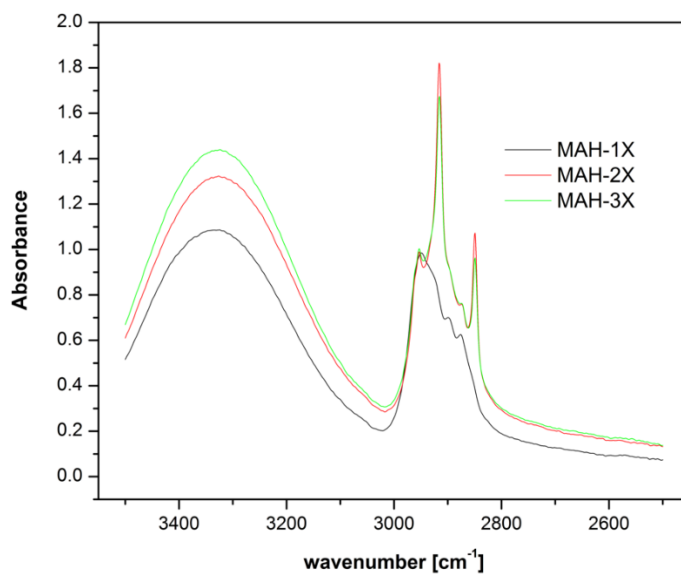
Figure 5-40 FTIR spectra for MAH effect on starch over the wavenumber between 2500-3500 cm^{-1}

149
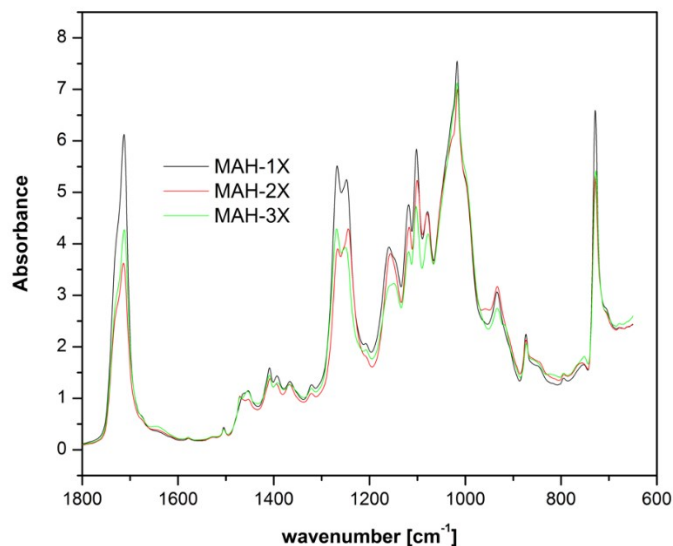
Figure 5-41 FTIR spectra for MAH effect on starch over the wavenumber between 650-1800 cm^{-1}

The spectra of the three compounds displayed in Figure 5-42 focuses on the wavenumbers between 600 and 1,800 cm^{-1}. The area of interest in these spectra are:

- The peak at 1710 cm^{-1} is characteristic of carbonyl groups. It is noted that this peak decreases in intensity as the amount of MAH increases.

- The characteristic peak of 1780 cm^{-1} for the ring anhydride of maleic anhydride (MAH) is not seen, thereby suggesting that it has been opened.

5.5 The effect of the starch's initial moisture on the compound synthesized

In the Wolff's patent (2013), it is suggested that drying the starch is important in achieving the desired results. In section 5.5, starch samples were dried to various levels of moisture as outlined in Table 5-26 and compounded in accordance with the formulations outlined in Table 5-25. The compounds were evaluated with the analytical techniques of FTIR, TGA and DSC in

combination with the data of torque and temperature versus time obtained from the CWB during compounding. This information was assembled to shed some light on the influence of starch moisture and the formation of starch co-polyester polymers.

Table 5-25 Formulation developed to evaluate the effects of pre-drying starch before compounding

Starch	Dried hours	Peroxide Wt-%	MAH Wt-%	PBAT Wt-%	Water Wt-%	Glycol Wt-%	Temperature °C	Scew Speed RPM
Hylon VII	0	0.1	1.0	58.2	1.5	7.7	150	45
Hylon VII	3	0.1	1.0	58.2	1.5	7.7	150	45
Hylon VII	5	0.1	1.0	58.2	1.5	7.7	150	45
30050	0	0.1	1.0	58.2	1.5	7.7	150	45
30050	3	0.1	1.0	58.2	1.5	7.7	150	45
30050	5	0.1	1.0	58.2	1.5	7.7	150	45
55310	5	0.1	1.0	58.2	1.5	7.7	150	45

Table 5-26 Moisture levels of the starch following a period of drying

Label	Starch	Dried hours	Moisture level Wt-%	Peroxide
Hylon -7%	Hylon	0	7.8	Dilauroyl
Hylon -1.6%	Hylon	3	1.6	Dilauroyl
Hylon -0.7%	Hylon	5	0.7	Dilauroyl
30050 -8%	30050	0	8.02	Dilauroyl
30050 -3%	30050	3	3.0	Dilauroyl
30050- 0.7%	30050	5	0.7	Dilauroyl
55310-0.7%	55310	5	0.7	Dilauroyl

5.5.1 Compounds of dried Hylon VII starch with various moisture levels

In section 5.2.1 Hylon starch was studied with various free radical initiators. In that study, Hylon-Lau displayed the quickest ability to destructure and plasticize. This study looks at the effects of moisture on the ability of the Hylon starch at various levels of moisture before compounding, to destructure and plasticize, then reviews the analytical data collected from the TGA, DSC, FTIR and from torque and temperature versus time figures obtained from the CWB during compounding.

Figure 5-42 illustrates the plots of the torque curves as a function of time for the various levels of dried Hylon compounds describe in Table 5-25. In this figure, the compounds display a delay in the onset of starch granular destruction as the moisture level of the Hylon starch drops. Hylon-7% compound is the first compound to display a rapid change in torque. Compound Hylon-7% achieves a maximum torque peak of 1,275.6 mg and subsequent decline. The drop in torque is in response to the effective plasticization of the starch molecules following the gelatinization of the starch.

Hylon-7% is the same compound as Hylon-Lau evaluated earlier. In section 5.2.1, Hylon-Lau was found to be the quickest and most effective achieve in the destructure and plasticize the starch.

The curves for Hylon-1.6% and Hylon-0.7% start to show the onset of destructuring shortly after Hylon-7%. Hylon-1.6% and Hylon-0.7% compounds achieve maximum torque at 2,466.7 mg and 2,347.2 mg. The summary of torque value for the three Hylon compounds as a function of time is outlined in Table 5-27.
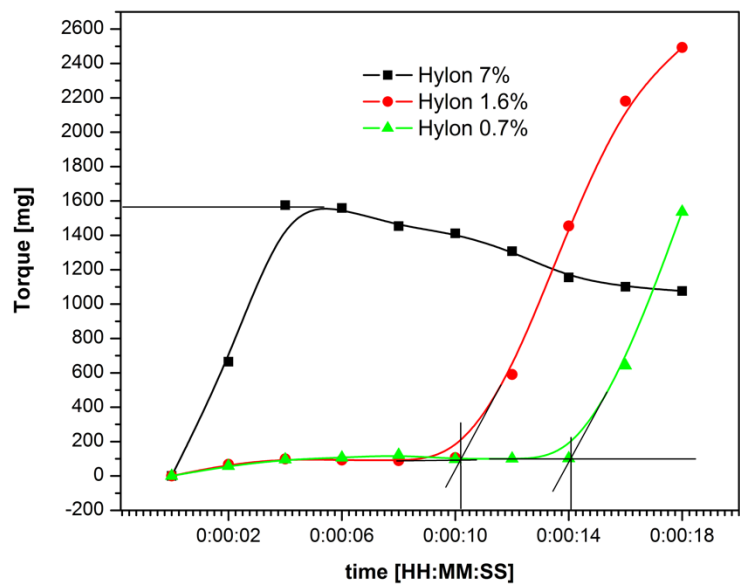
Figure 5-42 The effect of drying Hylon starch on destructuring through the measurement of torque as a function of time over the first 18 seconds

Table 5-27 Summary of the torque and time in achieving destructuring of dried Hylon starch

	7%	1.6%	0.7%
Torque	mg	mg	mg
On Set	0	97	102
Max	1275.6	2466.7	2347.2
Time	seconds	seconds	seconds
On Set	0	10	14
Max	6	21	26
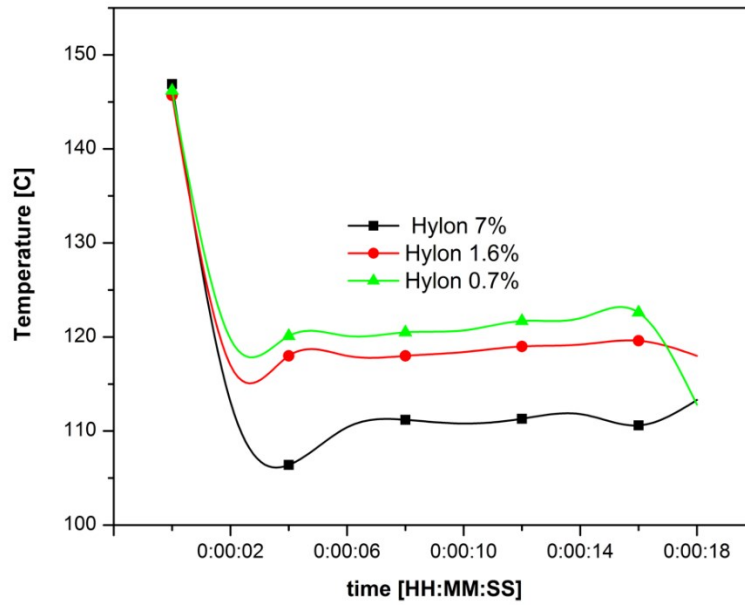
Figure 5-43 Compilation of the temperature as a function of time curves evaluating the destructuring of starch over the first 18 seconds
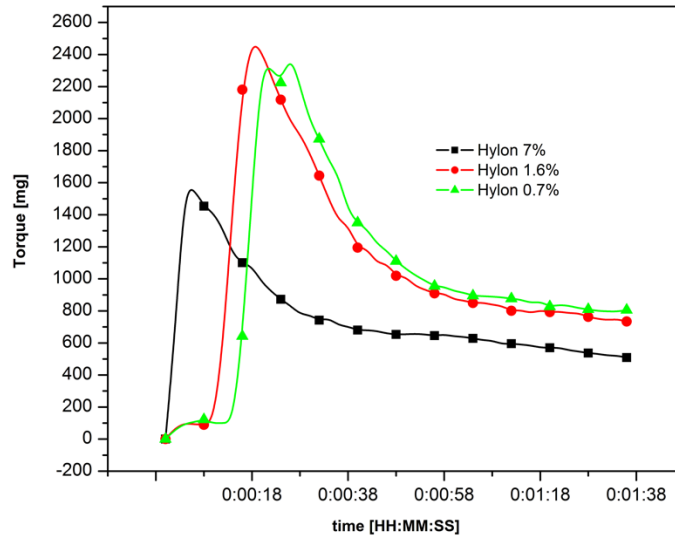
Figure 5-44 Compilation of torque as a function of time curves evaluating the destructuring of starch

154

In Figure 5-44, it is noted that once the compounds achieve their maximum torque value, they start to exhibit signs of plasticization with torque decreasing as time progresses. As time approaches one minute, the torque values of the various compounds seem to stabilize.

In compounding thermoplastic starch, it was determined in section 4.6, that the temperature should not exceed 150°C. In Figure 5-45, it is concluded that the three compounds do not exceed that temperature during compounding.
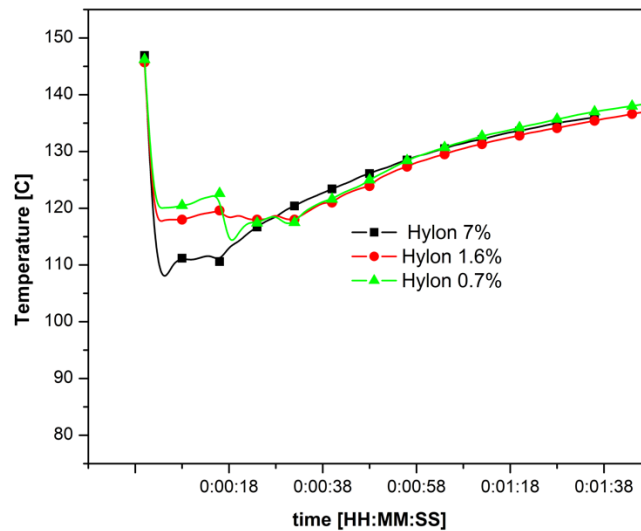
Figure 5-45 Compilation of temperature as a function of time curves evaluating the destructuring of starch

TGA analysis was conducted on the individual ingredients and the Hylon compounds outlined in Table 5-25. The objective is to determine if the Hylon compounds display any changes in thermal stability as a result of reducing the amount of moisture in Hylon starch from its native level.

Figure 5-46 displays the derivative of the percentage weight loss curve as a function of temperature with the Hylon compounds outlined in Table 5-25 with Table 5-29 summarizing the data.

Figure 5-46 notes a higher level of thermal stability with Hylon-7% over the temperature range 350- 440°C, and greater than that of Hylon-1.6% and Hylon-0.7%. In comparing Tables 5-28 and 5-29, the data suggests that, as the amount of moisture in Hylon starch is reduced from its native level of 7%, the thermal stability correspondingly decreases as well.

DSC analysis was conducted on the Hylon compounds outlined in Table 5-25. Table 5-30 and Table 5-31 summarize the peaks for 2nd melt cycle and 2nd cooling cycle, respectively

In Table 5-30, Hylon-7% presents the lowest enthalpy of melt $[\Delta H_m]$ of the three compounds. Overall, all three compounds display a low degree of crystallization and require minimal heat absorption to melt the crystalline regions. The enthalpy of melt ΔH_m values are noted to be low and ranging from 0.11 to 1.1 J/g.

In Table 5-31, Hylon-0.7% presents the highest enthalpy of crystallization $[\Delta H_c]$ of the three compounds. Of interest is the point that all compounds present values for ΔH_c that are greater than the ΔH_m. This phenomenon is also noted with the conditioned Hylon starch sample. It is believed to be a result of plasticizer migration from the sample and subsequent retrogradation of the starch, thereby creating areas of crystallinity within the compound.

Swelling of the DSC pans was noted following the 2nd cycle of heating and cooling. It is believed that the plasticizer evapourated from the sample as a result of exposure to heat during the second heating of the compound, thereby deforming the DSC pan with increased vapour pressure.

Table 5-28 Summary of TGA peaks of the raw materials

Material	OnSet ºC	End ºC	Peak ºC	Wt-%	Formulation Wt-%	Predicted Wt-%
Water			<104	99.9	1.5	1.5
Glycerol 99%	243.26	279.99	**264.72**	99.7	7.8	7.7
Starch	277.23	287.67	**283.40**	2.22	31.5	6.9
Hylon VII	294.83	331.37	**317.26**	60.00	31.5	18.9
	474.10	529.48	**502.61**	27.16	31.5	8.5
PBAT	379.2	437.58	**412.91**	98.2	58.2	57.15
Peroxide					1.0	
Total					100.0	

Table 5-29 Summary of the TGA peaks for the evaluation of the effects of drying Hylon starch

Peak Assignment	Hylon – 7% ºC	Wt-%	Hylon – 1.6% ºC	Wt-%	Hylon – 0.7% ºC	Wt-%
<150		8.5		0.42		7.52
1					269.01	1.35
2	321.03	22.9	308.72	25.48	308.87	21.66
3	409.24	51.8	396.44	14.10	397.75	39.69
4	429.85	5.1	412.24	44.13	407.71	17.28
5	475.51	11.4	456.92	10.58	472.64	11.86
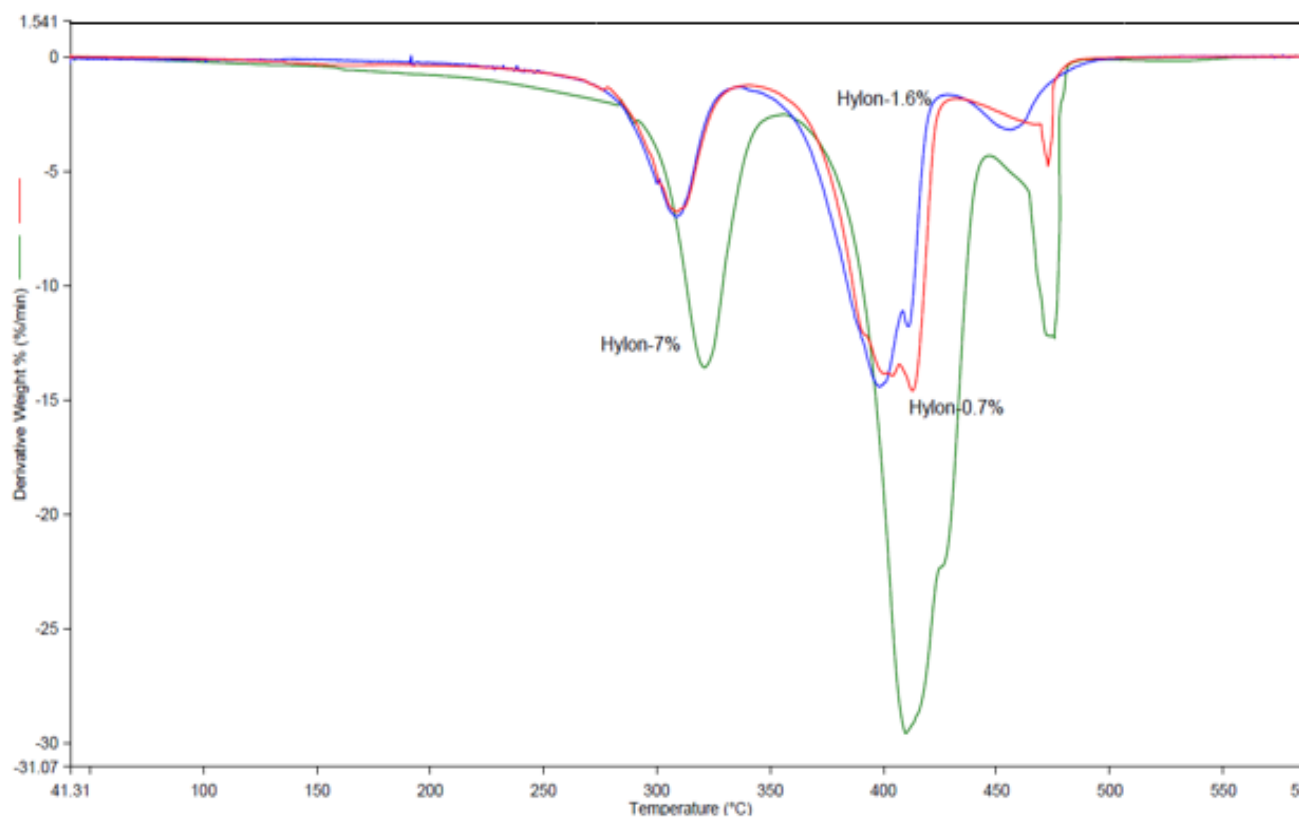
Figure 5-46 The TGA derivative curves for the evaluation of the effects of drying Hylon starch

Table 5-30 Summary of the DSC melt peaks for the evaluation of the effects of drying Hylon starch

Material	On Set	End	Peak	ΔH$_m$
	°C	°C	°C	J/g
Hylon-7%				
[Hylon-Lau]	157.42	162.56	**161.22**	0.11
Hylon – 1.6%				
1	123.43	128.39	**126.68**	1.092
2	152.31	154.63	**153.74**	0.05
Hylon – 0.7%				
1	111.68	135.43	**121.55**	1.08

Table 5-31 Summary of the DSC crystallization peaks for the evaluation of the effects of drying Hylon starch

Material	On Set	End	Peak	ΔH_c
Peak	°C	°C	°C	J/g
Hylon – 7%				
	104.35	79.75	**91.45**	-8.36
Hylon – 1.6%				
	105.82	79.71	**91.73**	-9.45
Hylon – 0.7%				
	96.36	78.28	**89.42**	-2.58

All three samples were analyzed by FTIR with an attenuated total reflectance (ATR) technique.

Figure 5-47 shows the FTIR spectra for all three Hylon compounds. Due to the detail in the two regions outlined in Figure 5-47, between 2,600 – 3,450 cm^{-1} and 650 – 1800 cm^{-1}, the spectra is separated into these two areas and zoomed in on with detailed spectra reflected in Figures 5-48 and 5-49 respectively.

The spectra of the three compounds displayed in Figure 5-48 focuses on the wavenumbers between 2,500 and 3,450 cm^{-1}. Of interest are the following areas:

- The peak at 3,330 cm^{-1} arising from the hydroxyl groups (-OH) is seen in all spectra of Hylon-7%, Hylon 1.6% and Hylon-0.7% compounds.

- The two peaks at 2918 cm^{-1} and 2853 cm^{-1} are seen in the spectra of Hylon-7% and Hylon-1.6% indicating the presence of aliphatic groups arising from grafting. However, these peaks exhibited very lower intensity with Hylon-0.7% compound.
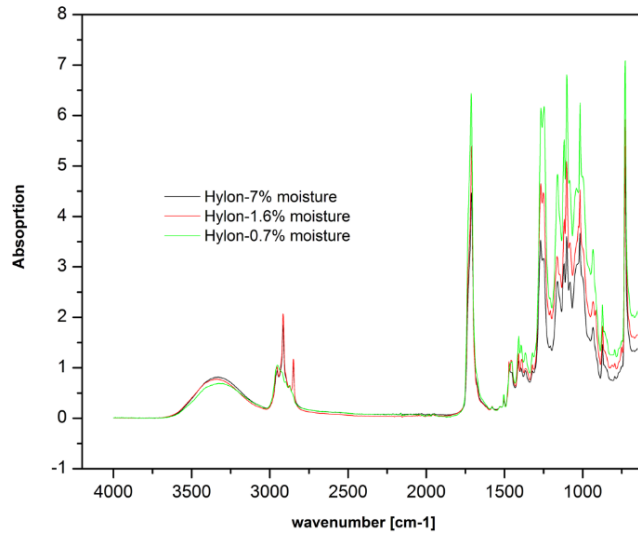
Figure 5-47 FTIR spectra for the evaluation of the effects of drying Hylon starch
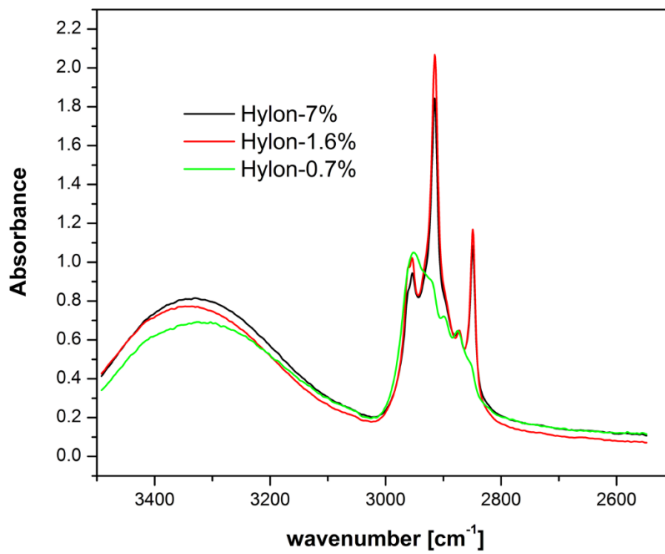
Figure 5-48 FTIR spectra for the evaluation of the effects of drying Hylon starch over the wavenumbers 2500 – 3500 cm^{-1}
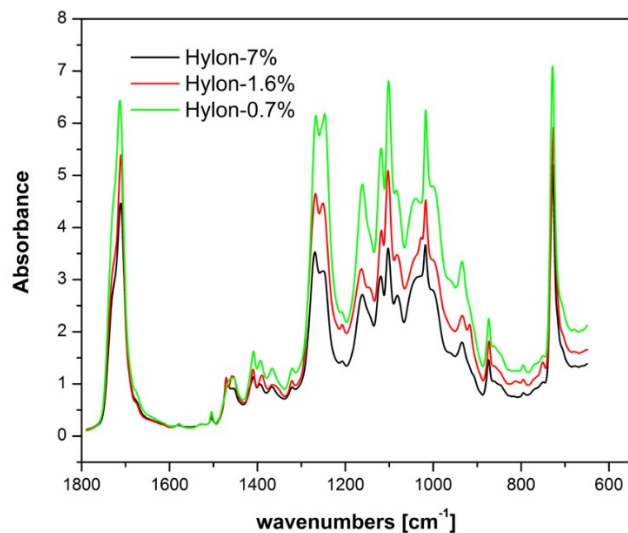
Figure 5-49 FTIR spectra for the evaluation of the effects of drying Hylon starch over the wavenumbers 650 – 1800 cm^{-1}

The spectra of the three compounds displayed in Figure 5-49 focuses on the wavenumbers between 600 and 1,800 cm^{-1}. The area of interest in these spectra are:

- The peak at 1710 cm^{-1}, characteristic of carbonyl groups, suggests the esterification reaction with maleic anhydride (MAH) and or glycerol. Of interest is the increasing intensity of the peak from Hylon-7% to Hylon-1.6% to Hylon-0.7%. It is noted that carbonyl peak of 1715 cm^{-1} for PBAT shift down to 1710 cm^{-1}.

- The characteristic peak of 1780 cm^{-1} for the ring anhydride of maleic anhydride (MAH) is absent, thereby suggesting that the MAH was opened with the possibility of forming esters and or transesterification.

- Characteristic peaks at 1267 cm^{-1} and 1243 cm^{-1} represent ester stretches in PBAT. However, the ratio of the intensities between the two peaks is noted to be the same with PBAT and Hylon-0.7% and different with Hylon-7% and Hylon-1.6%.

161

5.5.2 Reaction compounding with dried Starch 30050 of various moisture levels

In section 5.2.2, 30050 was studied with various free radical initiators. In that study, 30050-Lau displayed the ability to destructure and plasticize. This study looks at the effects of 30050 starch at various levels of moisture, before compounding, in destructure and plasticization of those compounds. The analytical data was collected from the TGA, DSC, FTIR and the torque and temperature versus time curves from the CWB for further analysis and review.

Figure 5-50 illustrates the plots of the torque curves as a function of time for the various level of dried 30050 compounds described in Table 5-25 and 5-26. In this figure, the compounds display a delay in the onset of starch granular destruction as the moisture level of the 30050 starch drops. 30050-3% compound is the first compound to display a rapid change in torque. Compound 30050-3% achieves a maximum torque peak of 2,075 mg and subsequent decline. The drop in torque is in response to the effective plasticization of the starch molecules following the gelatinization of the starch.

The curves for 30050-8 and 30050-0.7% start to show the onset of destructuring shortly after Hylon-3%. The 30050-8% and 30050-0.7% compounds achieve maximum torque at 1,842 mg and 2,591 mg. A summary of torque values for the three 30050 compounds as a function of time is outlined in Table 5-32.

Figures 5-51 and 5-53 are plots of temperature versus time for the 30050 compounds outlined in Table 5-25 although to different time scales.

In Figure 5-51, the time at which 30050-3% temperature curve is at its lowest corresponds with the time it takes 30050-3% torque curve to achieve its maximum torque value in Figure 5-52. This relationship seems to make sense, as until the starch is destructured and the onset plasticization occurs, all the energy from thermal and mechanical sources is being absorbed by

162

the 30050-3% compound. The same relationship between torque and temperature as a function of time is seen for 30050-8% and 30050-0.7%.
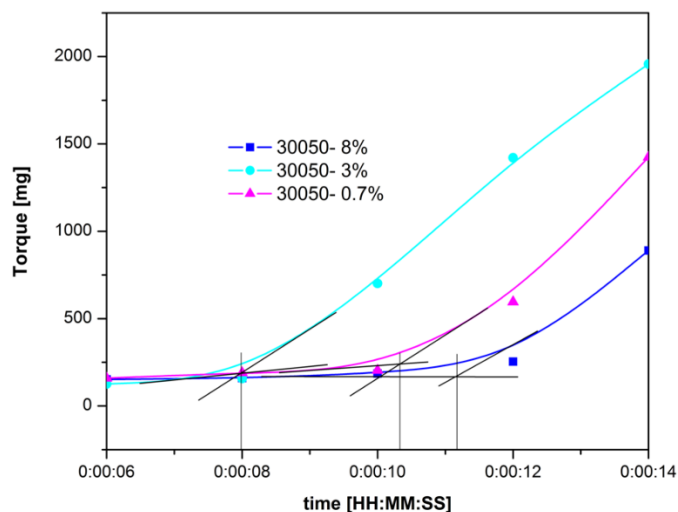
Figure 5-50 Torque as a function of time for the effects of drying 30050 starch on compounds over the first 14 seconds

Table 5-32 Summary of the torque and time values, at the point of destructuring, for 30050 starch compounds

	30050-8%	30050-3.0%	30050-0.7%
Torque	mg	mg	mg
On Set	165	165	155
Max	1842	2075	2591
Time	seconds	seconds	seconds
On Set	11.2	8	10.4
Max	18	16	18
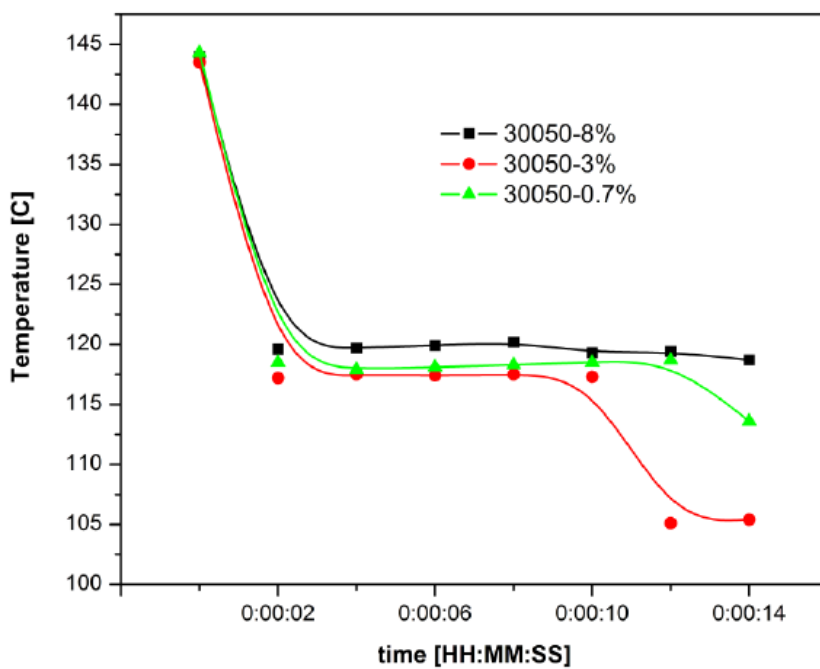
Figure 5-51 Temperature as a function of time for the effects of drying 30050 starch on compounds over the first 14 seconds
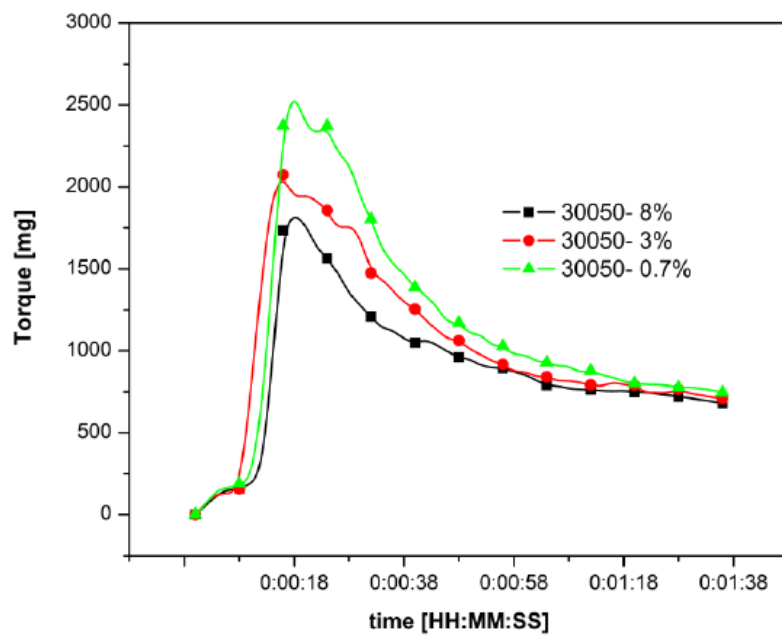
Figure 5-52 Torque as a function of time for the effects of drying 30050 starch on compounds
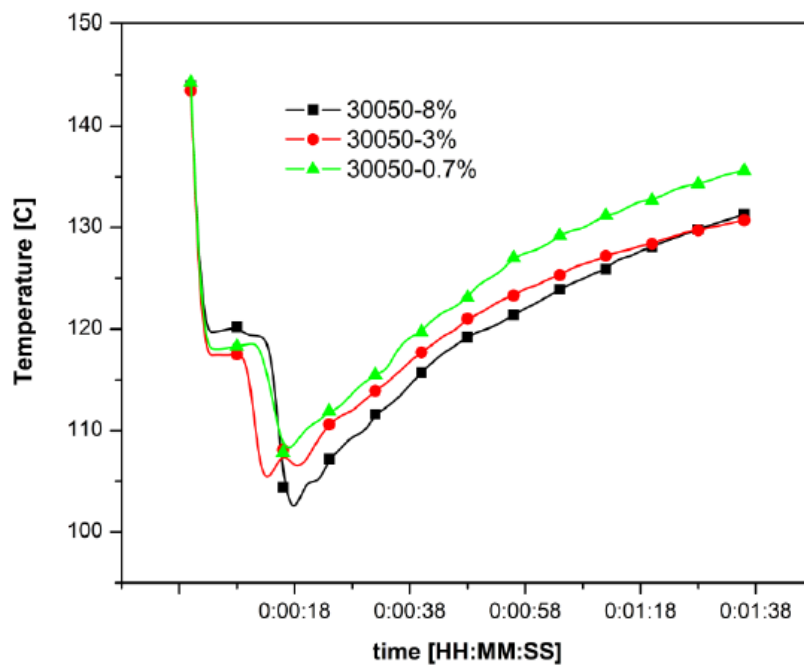
Figure 5-53 Temperature as a function of time for the effects of drying 30050 starch on compounds

TGA analysis was conducted on the individual ingredients and the 30050 compounds outlined in Table 5-25. The objective was to determine if the 30050 compounds display any sign of changes in thermal stability as the level of moisture in the starch changed.

Figure 5-54 displays the derivative of the percentage weight loss curve as a function of temperature with the 30050 compounds outlined in Table 5-25, with Table 5-33 summarizing the data.

In Figure 5-55, highest thermal stability is noted with 30050-8% over the temperature range 380- 440°C, and greater than that of 30050-3% and 30050-0.7%. Figure 5-54 and Table 5-34 suggest that the thermal stability of the 30050 compounds outlined in Table 5-25 diminishes as the amount of initial moisture in the starch decreases.

Table 5-33 Summary of the TGA peaks for the raw materials

Material	OnSet ºC	End ºC	Peak ºC	Wt-%	Formulation Wt-%	Predicted Wt-%
Water			<104	99.9	1.5	1.5
Glycerol 99%	243.26	279.99	**264.72**	99.7	7.8	7.7
Starch	277.23	287.67	**283.40**	2.22	31.5	6.9
30050	294.83	331.37	**317.26**	60.00	31.5	18.9
	474.10	529.48	**502.61**	27.16	31.5	8.5
PBAT	379.2	437.58	**412.91**	98.2	58.2	57.15
Peroxide					1.0	
Total					100.0	

Table 5-34 Summary of the TGA peaks for 30050 compounds with various levels of drying

Peak Assignment	30050-8% ºC	Wt-%	30050-3% ºC	Wt-%	30050-0.7% ºC	Wt-%
<150		1.5		1.8		6.7
1	322.92	30.5	307.20	24.7	306.63	26.3
2			407.62	45.1	391.37	42.9
3	414.39	57.9	417.20	10.1	410.52	17.1
4	487.14	9.26	466.28	11.4	453.96	5.5

DSC analysis was conducted on the 30050 compounds outlined in Table 5-25. Table 5-35 and 5-36 summarizes the peaks for 2nd melt cycle and 2nd cooling cycle for the compounds outlined in Table 5-25.
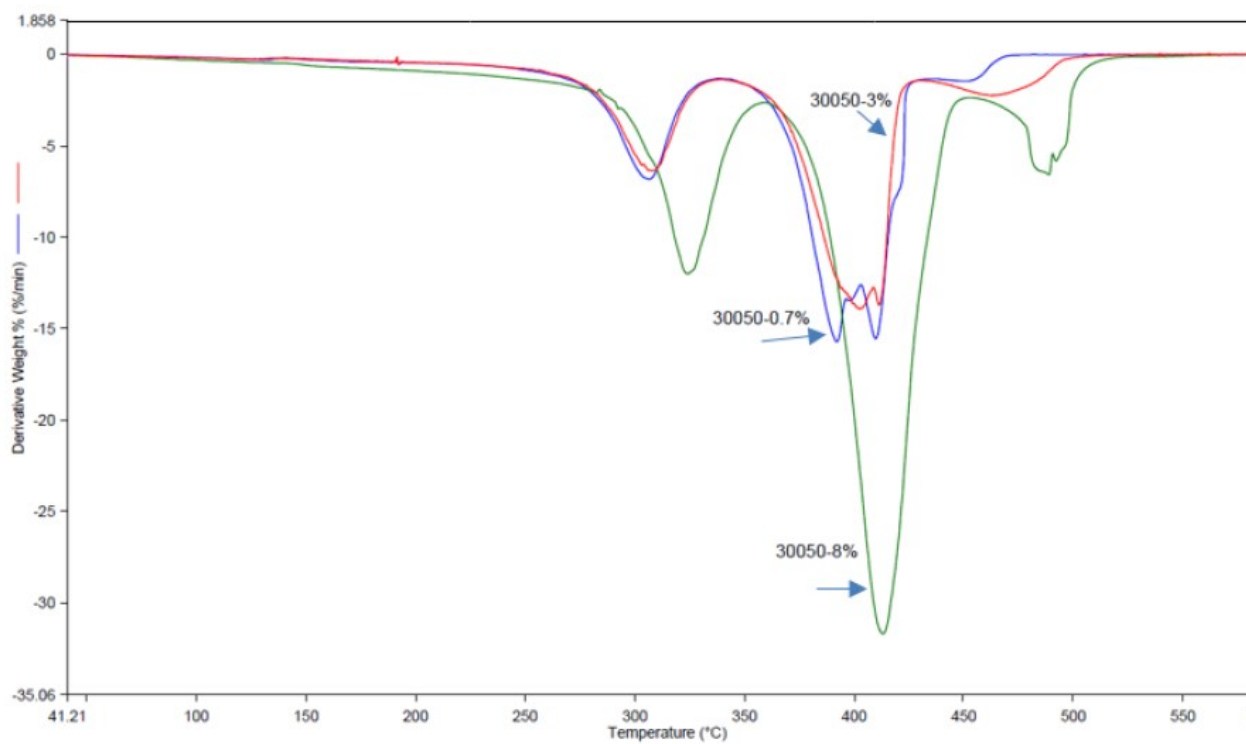
Figure 5-54 Compilation of the TGA derivative curves for 30050 compounds outlined in table 5-24

In Table 5-35, 30050-3% presents the lowest enthalpy of melt $[\Delta H_m]$ of the three compounds. Overall, all three compounds display a low degree of crystallization and require minimal heat to be absorbed to melt the crystalline regions. The enthalpy of melt ΔH_m values are noted to be low and ranging from $1.00 - 5.31$ J/g.

In Table 5-36, 30050-3% presents the highest enthalpy of crystallization $[\Delta H_c]$ of the three compounds. Of interest is that all three compounds possess values for ΔH_c that are greater than the ΔH_m. This phenomenon is also noted before and is believed to be a result of plasticizer migration from the sample and subsequent retrogradation of the starch, thereby creating areas of crystallinity within the compound.
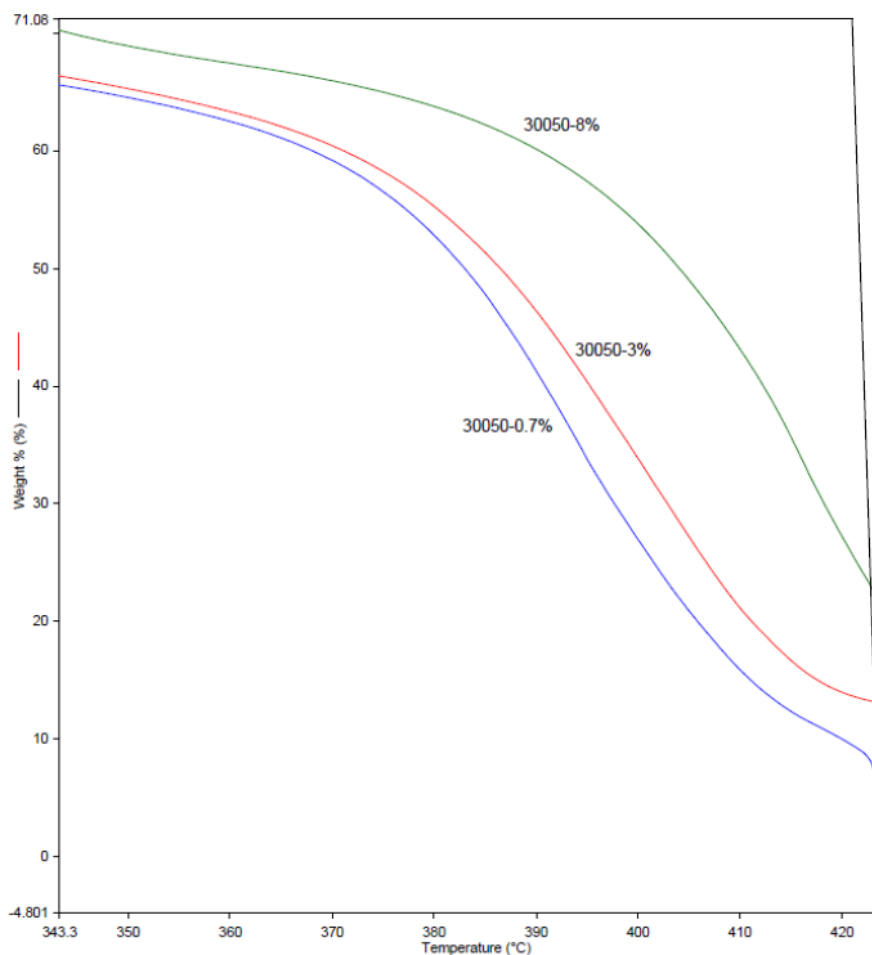
Figure 5-55 Compilation of the TGA curves for the temperature range of 343 - 420ºC

Swelling of the DSC pans was noted following the 2nd cycle of heating and cooling. It is believed that the plasticizer evapourated from the sample as a result of exposure to heat during the second heating of the compound. The plasticizer, when heated, goes through a phase transition and forms gas. As the heat increases, the gas expands within the sealed pan resulting in the deformation the DSC pan.

All three samples were analyzed by FTIR with an attenuated total reflectance (ATR) technique.

Table 5-35 DSC peaks from the melt curves of the 30050 compounds defined in Table 5-25

Material	On Set	End	Peak	ΔH_m
Peak	ºC	ºC	ºC	J/g
30050-8%				
1	108.88	123.30	**123.06**	4.43
30050-3%				
1	124.28	128.23	**126.65**	1.00
30050-0.7%				
1	62.73	66.69	**63.71**	0.37
2	118.17	128.07	**122.93**	0.63
3	136.09	137.32	**136.41**	4.31

Table 5-36 DSC crystallization peaks from the cooling curves of the 30050 compounds defined in Table 5-25

Material	On Set	End	Peak	ΔH_c
Peak	ºC	ºC	ºC	J/g
30050-8%				
	101.26	81.11	**89.39**	-9.50
30050-3%				
1	105.82	78.62	**91.78**	-11.37
30050-0.7%				
2	102.99	79.94	**91.55**	-9.78

Figure 5-56 shows the FTIR spectra for all three 30050 compounds. Due to the detail in the two regions outlined in Figure 5-56, between 2,600 – 3,450 cm^{-1} and 650 – 1800 cm^{-1}, the spectra are separated into these two areas and zoomed in on with detailed spectra reflected in Figures 5-57 and 5-58 respectively.
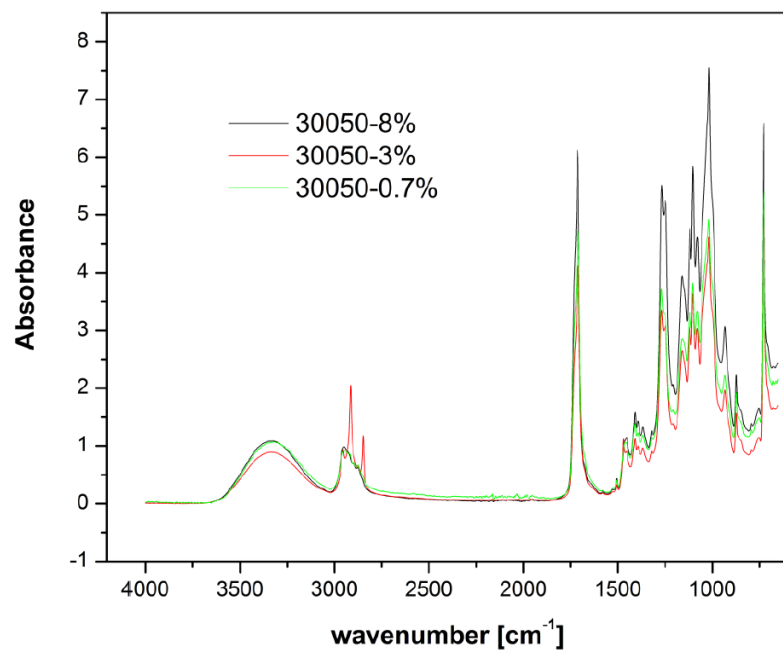
Figure 5-56 FTIR spectra for the 30050 compounds with differing levels of moisture
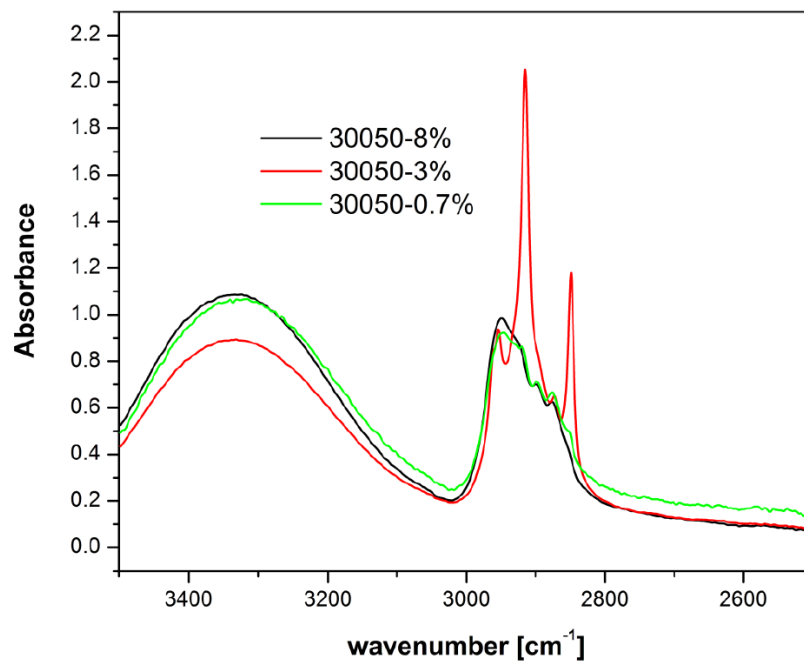
Figure 5-57 FTIR spectra for the 30050 compounds for 2500-3500 cm^{-1}

The spectra of the three compounds displayed in Figure 5-49 focuses on the wavenumbers between 2,500 and 3,450 cm^{-1}. Of interest are the following areas:

- The peak at 3,330 cm^{-1} arising from the hydroxyl groups (-OH) is seen in all spectra of 30050-8%, 30050-3% and 30050-0.7% compounds.

- The two peaks at 2928 cm^{-1} and 2886 cm^{-1}, are seen in the spectra of 30050-0.7% and 30050-8%, and are due to the formation of inter and intramolecular bonding of hydroxyl groups between starch and glycerol.

- The two peaks at 2918 cm^{-1} and 2853 cm^{-1} are seen in the spectra of 30050-3% indicating the presence of aliphatic groups arising from grafting.
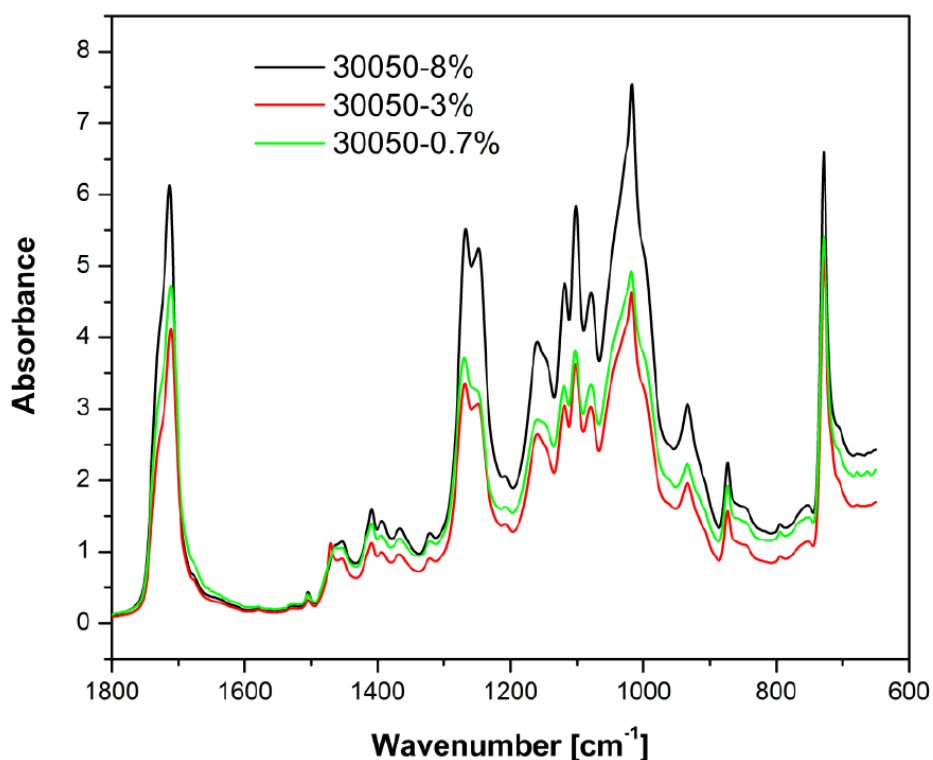
Figure 5-58 FTIR spectra for the 30050 compounds for 650-1800 cm^{-1}

The spectra of the three compounds displayed in Figure 5-50 focuses on the wavenumbers between 600 and 1,800 cm^{-1}. The area of interest in these spectra are:

- The peak at 1710 cm^{-1} is characteristic of carbonyl groups. Of interest is the increasing intensity of the peak from Hylon-3% to Hylon-0.7% to Hylon-8%.

- The characteristic peak of 1780 cm^{-1} for the ring anhydride of maleic anhydride (MAH) is absent, thereby suggesting that it has been opened.

- Characteristic peaks at 1267 cm^{-1} and 1243 cm^{-1} represent ester stretches in PBAT. However, the intensities of two peaks change with the level of moisture initially in the starch.

5.6 The ability to offline dry and master batch the starch for further synthesis

The data collected in section 5.5 suggests that mechanisms can be driven in favour of an alternative by changing the level of moisture in the starch before compounding. In section 5.6, it is assumed that drying the starch is required. As such, for processing it is assumed that once the starch is dried, it can be fully blended before compounding. The question then arises, "what is the influence on the final compound from fully blending the raw materials together (master batch) then allowing it to sit for a period of time before compounding?" Is there a window of time which master batched materials can offer the best results?

The 55310 starch sample was dried for 5 hours and analyzed for moisture content. Four samples of 55310 starch were drawn, blended with all the other ingredients outlined in Table 5-37 and placed in a labeled zip locked bag. These mixtures were left standing for a predetermined time before compounding, as defined in Table 5-37. At time zero (0), bag one was immediately compounded. Then at two hours, five hours and 24 hours corresponding to the compound label.

Figure 5-59 illustrates the plots of the torque curves as a function of time for the 55310 compounds describe in Table 5-37. In this figure, the compound t=5 immediately responds with a fast rate of granular destruction while the other three compounds display a delay in the onset of starch granular destruction. Starch 55310 compounds t=0 and t=2 seem to respond at the

same time, while t=24 is the slowest to reflect the onset of destruction. The torque values and

the time frames are recorded in Table 5-38

Table 5-37 Formulation for evaluating the ability to process drying off line, master batch the materials and allow them to stand before processing

Label	Time	Peroxide	MAH	PBAT	Water	Glycol	Temperature	Screw Speed
	hours	Wt-%	Wt-%	Wt-%	Wt-%	Wt-%	ºC	RPM
t=0	0	0.1	1.0	58.2	1.5	7.7	150	45
t=2	2	0.1	1.0	58.2	1.5	7.7	150	45
t=5	5	0.1	1.0	58.2	1.5	7.7	150	45
t=24	24	0.1	1.0	58.2	1.5	7.7	150	45
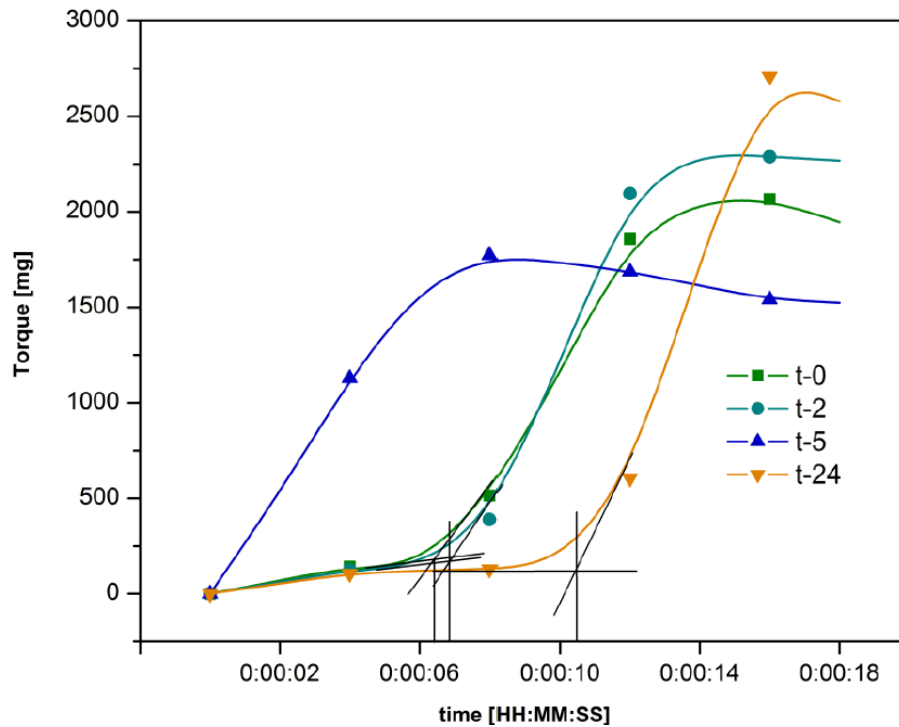
Figure 5-59 Torque as a function of time evaluation of the ability to master batch the raw materials and allowing them to sit for a period of time before processing over the first 18 seconds of compounding

173

Figures 5-60 and 5-62 are plots of temperature versus time for the 55310 compounds outlined in Table 5-37, although to different time scales.

Figure 5-60 does not reflect the similar relationship noted be the peak torque value and the lowest temperature. In all cases there seems to be a delay, where the temperature seems to lag the torque curve.

Table 5-38 Summary of the torque and time required to destructure the starch in the master batched compounds defined in Table 5-37

Label	t=0	t=2	t=5	t=24
Torque	mg	mg	mg	mg
On Set	172	184	0	118
Max	2066	2310	1773	2645
Time	seconds	seconds	seconds	seconds
On Set	6.4	7.3	0	11.2
Max	16.1	15.2	8	17.2

In Figure 5-61, it is noted that once the various compounds achieved their maximum torque value, they started to exhibit signs of plasticization with torque decreasing as time progresses. As time approaches one minute, the torque values of the various compound seem to stabilize.

In compounding thermoplastic starch, it was determined in section 4.6, that the temperature should not exceed 150°C. In Figure 5-62, it is concluded that the four compounds do not exceed that temperature during compounding
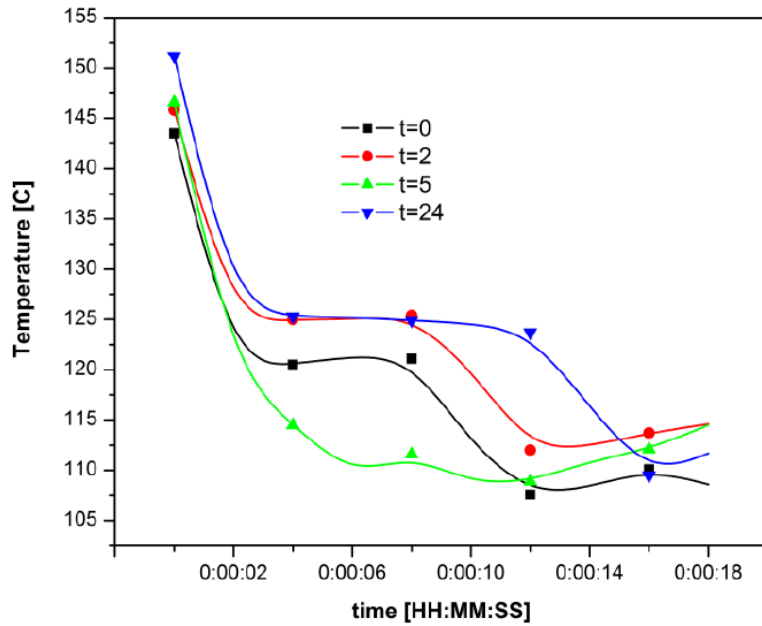
Figure 5-60 Temperature as a function of time evaluation of the ability to master batch the raw materials and allowing them to sit for a period of time before processing over the first 18 seconds of compounding
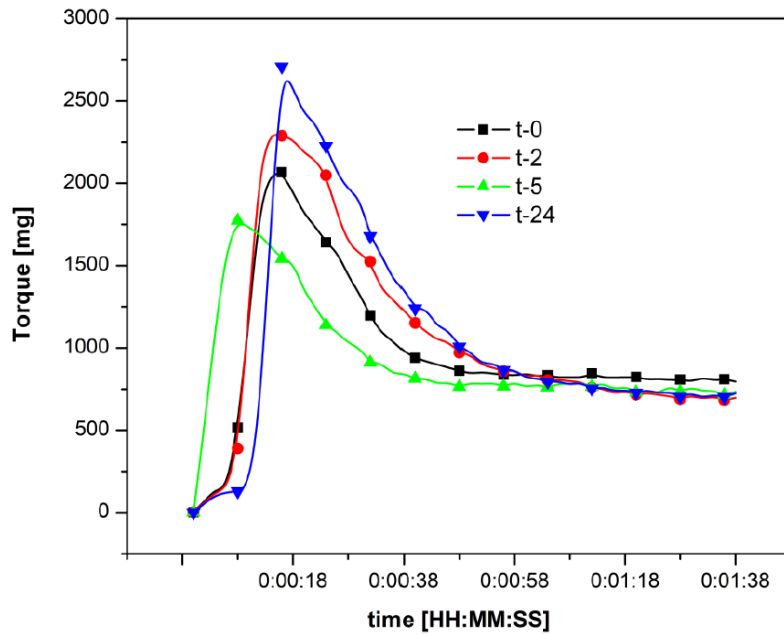
Figure 5-61 Torque as a function of time evaluation of the ability to master batch the raw materials and allowing them to sit for a period before processing

175

TGA analysis was conducted on the individual ingredients and the 55310 master batched compounds outlined in Table 5-37. The objective was to determine if the 55310 master batches displayed any signs of changes in thermal stability as the level of moisture in the starch was changed.
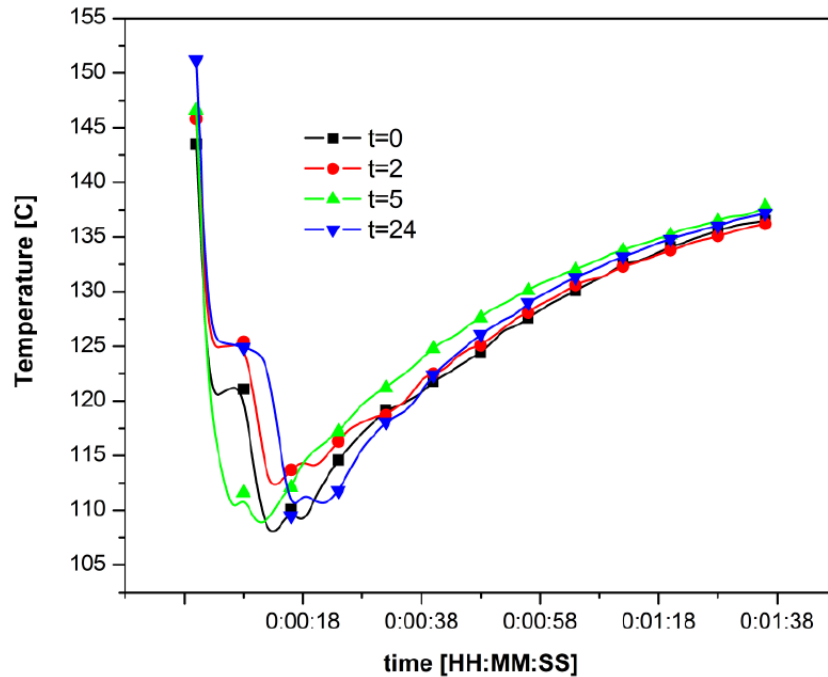
Figure 5-62 Torque as a function of time evaluation of the ability to master batch the raw materials and allowing them to sit for a period of time before processing

Figure 5-63 displays the derivative of the percentage weight loss curve as a function of temperature with the 30050 compounds outlined in Table 5-37, with Table 5-40 summarizing the data.

In Figure 5-63, highest thermal stability is noted with master batch t=5 over the temperature range 380- 440°C and greater than t=0, t=2 and t=24. Figure 5-63 and Table 5-34 suggest that the thermal stability of the 55310 compounds outlined in Table 5-37 obtain the greatest thermal stability at t=5 hours, and that thermal stability marginally drop off earlier or 19 hours later.

Table 5-39 TGA of the raw material used in the compounds defined in Table 5-37

Material	OnSet °C	End °C	Peak °C	Wt-%	Formulation Wt-%	Predicted Wt-%
Water			<104	99.9	1.5	1.5
Glycerol 99%	243.26	279.99	**264.72**	99.7	7.8	7.8
Starch	283.62	300.14	**293.89**	71.68	31.5	22.60
55310	372.25	383.41	**374.15**	16.38	31.5	5.16
PBAT	379.2	437.58	**412.91**	98.2	58.2	57.15
Peroxide					1.0	
Total					100.0	

Table 5-40 TGA of the raw material used in the compounds defined in Table 5-37

Peak Assignment	t=0 °C	t=0 Wt-%	t=2 °C	t=2 Wt-%	t=5 °C	t=5 Wt-%	t=24 °C	t=24 Wt-%
<150		5.50		3.65		5.37		5.14
1	264.35	6.56	263.13	7.80	264.72	6.02	266.00	4.14
2	317.55	22.14	316.81	20.81	318.44	22.08	314.72	21.95
3	417.32	58.20	414.94	60.17	419.84	58.66	415.44	52.99

DSC analysis was conducted on the 55310 master batched compounds outlined in Table 5-37. The summaries of the peaks for 2nd melt cycle and cooling cycle are in Table 5-41, and Table 5-42, respectively.

In Table 5-41, 55310 master batch compound t=0 presents the lowest enthalpy of melt (ΔH_m) of the four compounds. Overall, all four compounds display a low degree of crystallization and require minimal heat to be absorbed to melt the crystalline regions. The enthalpy of melt ΔH_m value were noted to be low and ranging from 0.44 – 3.34 J/g.
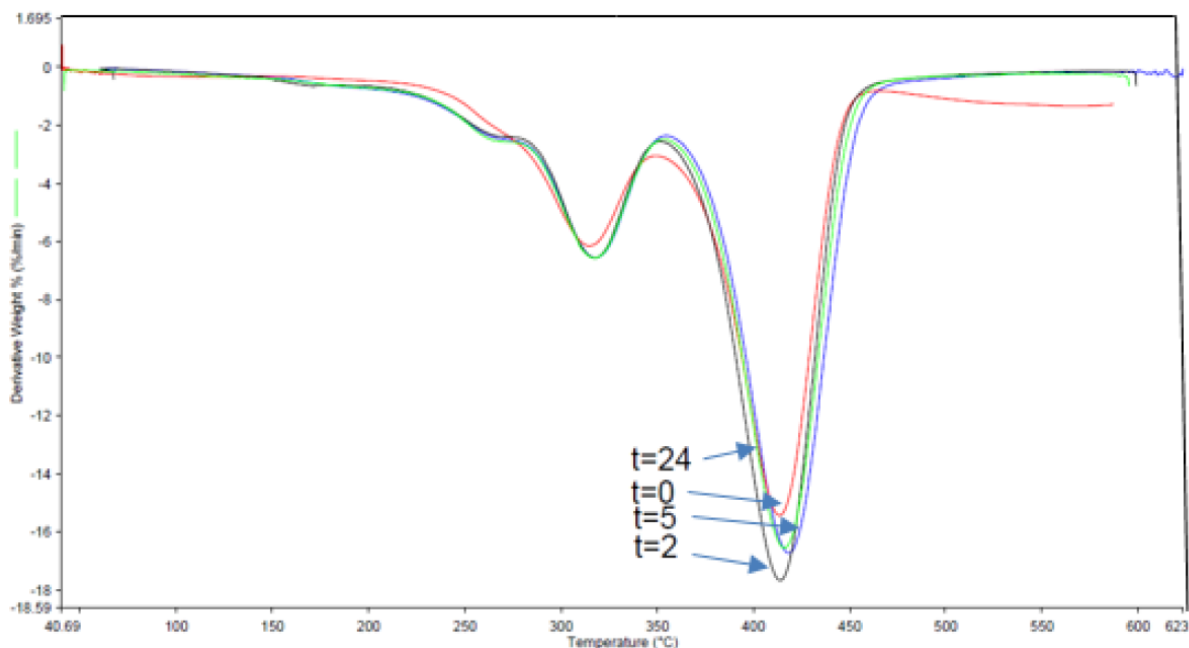
Figure 5-63 Compilation of the derivative curves for the TGAs of the master batched compounds

In Table 5-42, 55310 master batch compound t=5 presents the highest enthalpy of crystallization (ΔH_c) of the four compounds. Of interest is that all four compounds possess values for ΔH_c that are greater than the ΔH_m. This phenomenon was noted before and believed to be a result of plasticizer migration from the sample and subsequent retrogradation of the starch, thereby creating areas of crystallinity within the compound.

Swelling of the DSC pans was noted following the 2nd cycle of heating and cooling.

All four samples were analyzed by FTIR with an attenuated total reflectance (ATR) technique.

178
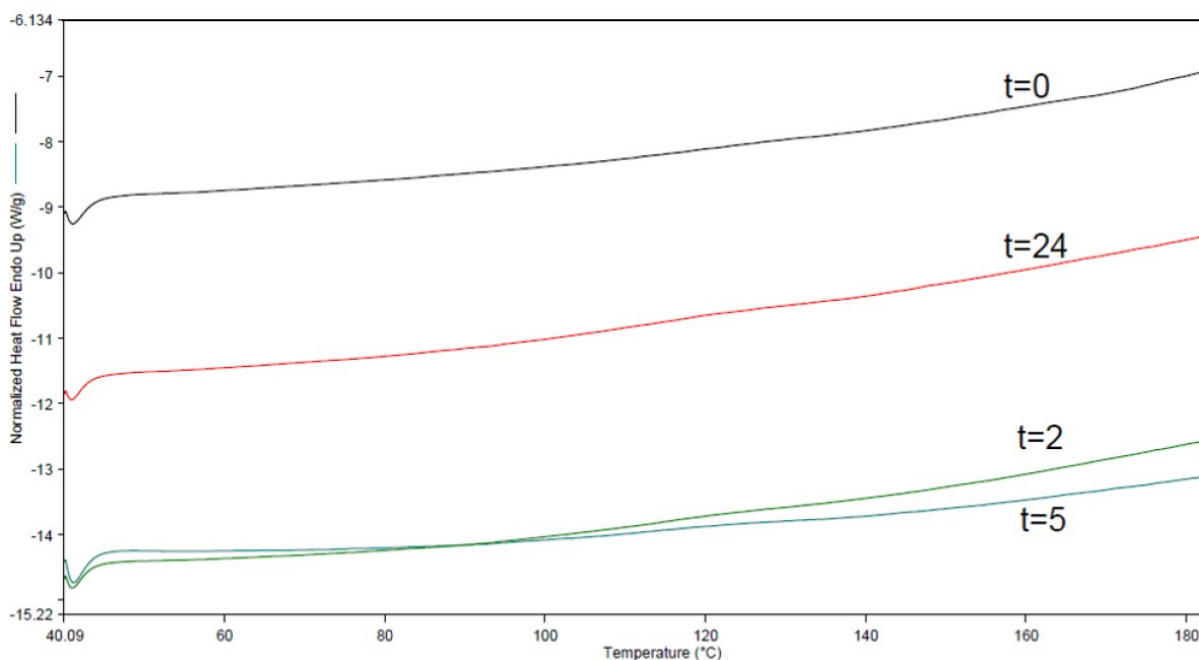
Figure 5-64 Compilation of the normalized DSC curves for master batched compounds

Table 5-41 Summary of the DSC peaks for the master batched compounds

Material Peak	On Set °C	End °C	Peak °C	ΔH_m J/g
t=0				
	111.74	128.02	**127.45**	0.44
t=2				
	115.07	127.30	**121.94**	1.66
t=5				
	114.76	126.61	**122.91**	2.24
t=24				
	114.35	125.93	**120.05**	3.34

Figure 5-65 shows the FTIR spectra for all four 55310 master batched compounds. Due to the detail in the two regions outlined in Figure 5-65, between 2,600 – 3,450 cm^{-1} and 650 – 1800 cm^{-1}, the spectra were separated into these two areas and zoomed in on with detailed spectra reflected in Figures 5-66 and 5-67 respectively.

179

Table 5-42 Summary of the DSC peaks for the master batched compounds

Material Peak	On Set °C	End °C	Peak °C	ΔH_c J/g
t=0				
	94.03	78.56	**86.02**	-6.25
t=2				
	95.73	79.06	**86.76**	-8.57
t=5				
	95.81	78.46	**86.60**	-9.35
t=24				
	90.55	77.07	**85.21**	-2.76

The spectra of the four compounds displayed in Figure 5-66 focuses on the wavenumbers between 2,500 and 3,500 cm^{-1}. Of interest are the following areas:

- The peak at 3,330 cm^{-1}, arising from the hydroxyl groups (-OH) is seen in all spectra of 55310 master batched compounds. The intensity of the peak seems to be somewhat aligned and increasing with time. The only anomaly exists with t=2.

- The two peaks at 2928 cm^{-1} and 2886 cm^{-1}, seen in the spectra of t=0, t=5, and t=24, are due to the formation of inter and intramolecular bonding of hydroxyl groups between starch and glycerol. The peak intensity increases over time.

- The two peaks at 2918 cm^{-1} and 2853 cm^{-1} seen in the spectra of 55310 master batch t=2, indicate the presence of aliphatic groups arising from grafting.
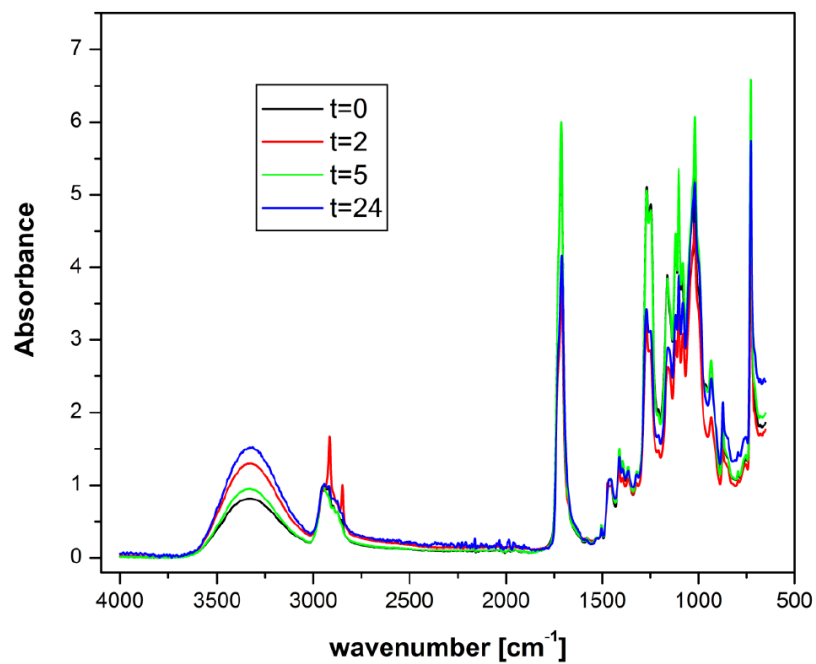
Figure 5-65 FTIR spectra for the master batched compounds
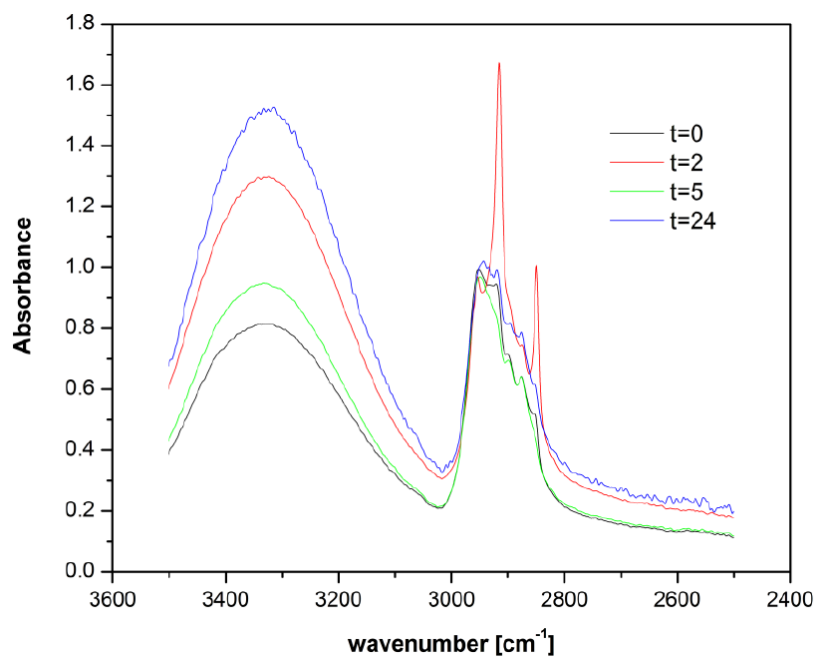
Figure 5-66 FTIR spectra for the master batched compounds for the wavenumbers of 2500-3500 cm^{-1}

The spectra of the four compounds displayed in Figure 5-67 focuses on the wavenumbers between 600 and 1,800 cm⁻¹. The area of interest in these spectra ae:

- The peak at 1710 cm⁻¹ is characteristic of carbonyl groups. Of interest is the increasing intensity of the peak as the master batch sat. The 55310 master batch t=5 didn't follow the relationship and noted a significant increase in carbonyl functional groups.

- The characteristic peak of 1780 cm⁻¹ for the ring anhydride of maleic anhydride (MAH) is absent, thereby suggesting that it has been opened.

Characteristic peaks at 1267 cm-1 and 1243 cm-1 represent ester stretches in PBAT. The intensities of these two peaks seem to follow the same relationship noted above at 1710 cm-1 . The intensity of the peak increases as the master batch sat longer before compounding. However, 55310 master batch t=5 didn't follow that relationship.
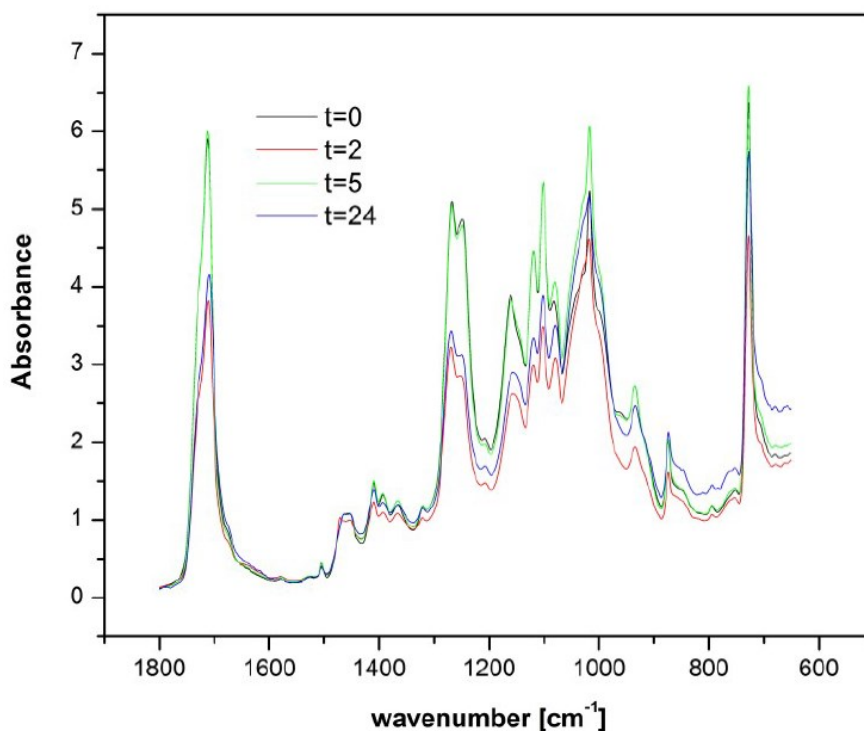
Figure 5-67 FTIR spectra for the master batched compounds for the wavenumbers of 650-1800 cm⁻¹

5.7 Investigation of various polyesters in the co-blending

In this section, the intension was to evaluate the two main biodegradable polyester resins, PLA and PBAT, under the same conditions and compound formulation, and in the same process, studying the physical / chemical properties which developed. The compound's formulations, outlined in Table 5-43, employed dilauroyl peroxide as a free radical initiator.

Table 5-43 Starch co-polyesters with PBAT & PLA

Label		Peroxide	MAH	Hylon	Water	Glycol	Temperature	RPM
	%	%	%	%	%	%	°C	revolutions
PBAT-St	58.2	0.1	1.0	31.5	1.5	7.7	150	45
PLA-St	58.2	0.1	1.0	31.5	1.5	7.7	150	45

The torque versus time graph, in Figure 5-68, suggests that starch is effectively destructured and plasticized for the PBAT-St compound as reflected in the maximum torque peak at 1540 mg and six seconds, and follows with the subsequent decay of the curve.

Although a peak is seen at 750 mg and 16 seconds for PLA-St compound of the torque versus time curve (Figure 5-68), the PLA-St curve continues to increase afterwards. In Figure 5-70 the evaluation is run over a wider time frame, the PLA-St curve is seen to achieve maximum torque at 2527 mg and 100 second. This period of 105 seconds is beyond the compounding time frame established. This could suggest that neither the starch nor PLA-St had achieved destructuring, or melt phase, respectively, in the initial evaluation depicted in Figure 5-68, suggesting that the probability for covalent bonding between the PLA-St and modified starch would be low during the first 90 seconds of compounding.

In Chivac 2007 paper, the ΔH_m for PBAT at 100% crystallinity is identified at 114 J/g, and Khoo's 2016 paper defines ΔH_m for PLA at 100% crystallinity as 93.6 J/g.
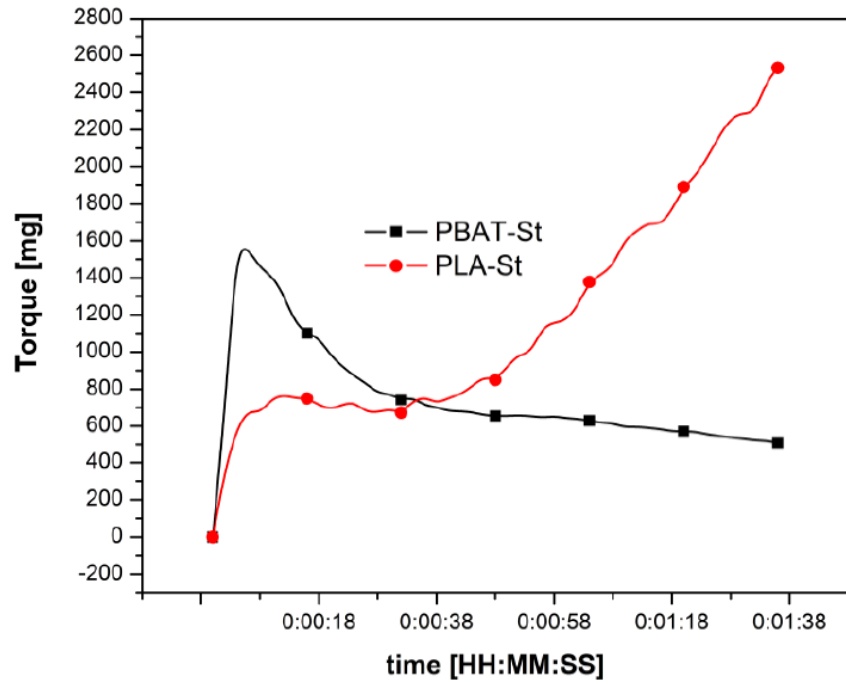
Figure 5-68 Torque as a function of time for the two starch copolyester compounds
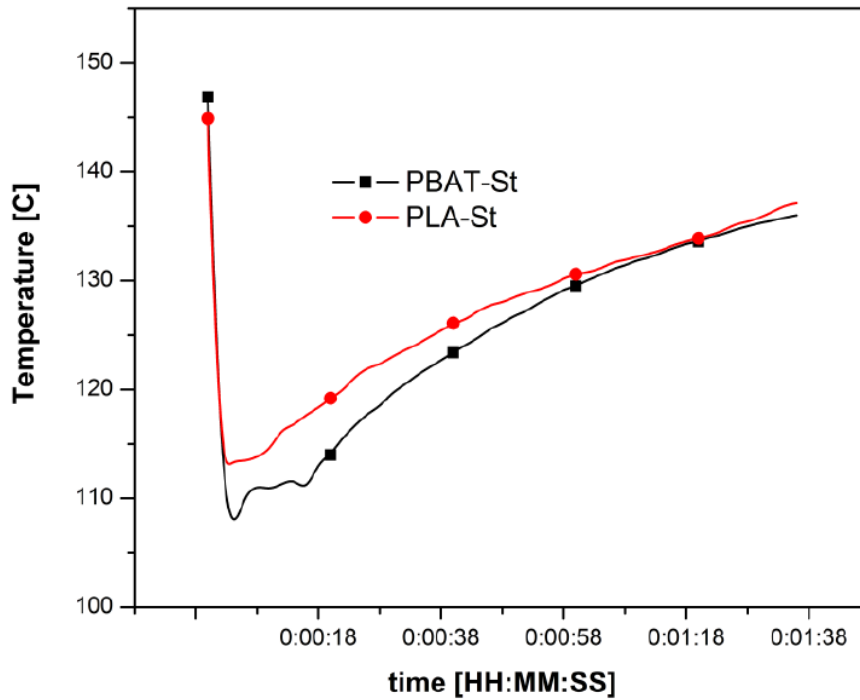
Figure 5-69 Temperature as a function of time for the two starch copolyester compounds

184
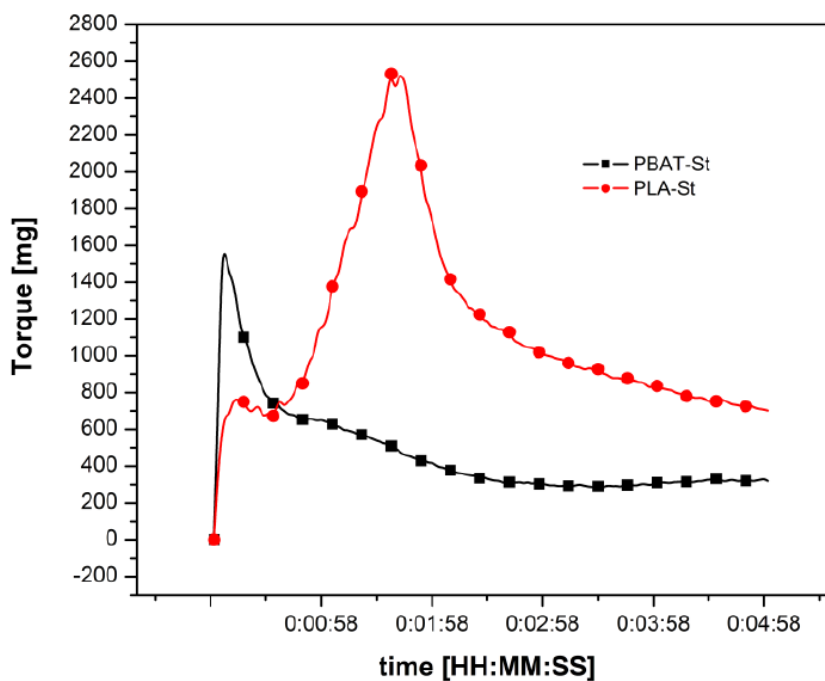
Figure 5-70 Torque as a function of time for the two starch copolyester compounds over a great compounding window.

Based on the assumption that the starch is believed to have been destructured and plasticized in both compounds, then it is assumed that ΔH_m is a reflection of the crystallinity resulting from the polyester resin fraction of the compound. In Table 5-44, the values of ΔH_m are determined for the DSC curves and interpreted with Pyris software for the two compounds. This enthalpy of fusion for the starch – PBAT compound concludes that the degree of crystallization is less than one percent or presents amorphous characteristics. The PLA-St compound presents a significantly higher enthalpy of fusion, thereby suggesting a 49.5% degree of crystallinity within the PLA-St compound.

The degree of crystallinity (χ_c) is noted to be the higher within PLA-St copolymer than any of the PBAT compounds in this paper. The high level of PLA-St crystallinity is believed to be a result of the compounding conditions. It is suggesting that these conditions were not effective in creating a melt of the PLA early enough. As a result, chemical modified of starch occurred

first. This suggests that the PLA Starch compound is more of an add mixture with limited, or no, modification of the PLA.

In Table 5-45, Starch-PBAT compound presents the higher enthalpy of crystallization [ΔH_c] of the two compounds. Of interest is that Starch-PBAT compound possesses values for ΔH_c that are greater than the ΔH_m. This phenomenon is also noted before and is believed to be a result of plasticizer migration from the sample and subsequent retrogradation of the starch, thereby creating areas of crystallinity within the compound

The DSC pans for both PLA-St and PBAT-St are noted to have swollen following the 2nd cycle of heating and cooling suggesting that a vapour had been released from the compound.

Table 5-44 DSC melt peaks for the polyester copolymers outlined in Table 5-43

Label Peak	On Set °C	End °C	Peak °C	ΔH_m J/g
PBAT-St				
1	116.13	135.26	**131.80**	0.411
2	157.42	162.56	**161.22**	0.11
PLA-St				
1	83.46	104.35	**95.96**	17.09
2	137.34	144.14	**141.06**	4.62
3	145.43	152.53	**145.43**	5.24

Table 5-45 DSC cooling peaks for the polyester copolymers outlined in Table 5-43

Label Peak	On Set °C	End °C	Peak °C	ΔH_c J/g
PBAT-St				
	104.35	79.75	**91.45**	-8.36
PLA-St				
	130.68	105.07	**105.74**	-6.58
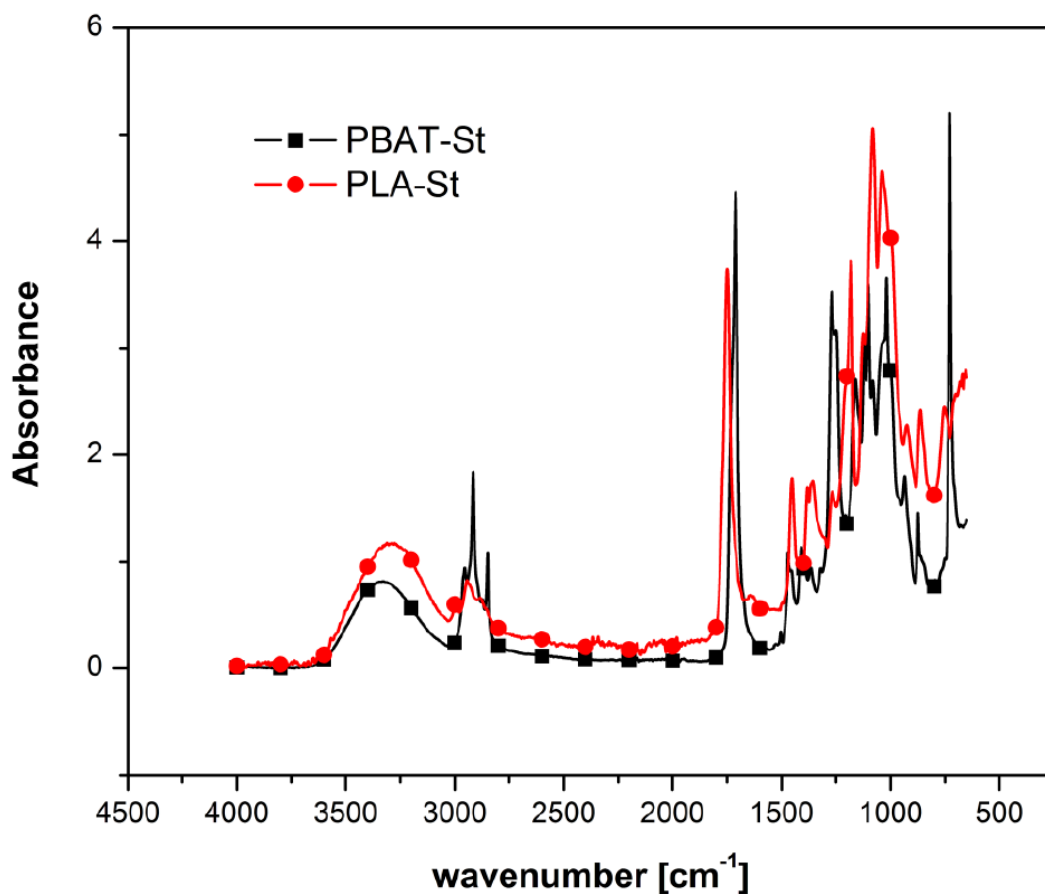
Figure 5-71 FTIR spectra of the copolymers of PBAT and PLA

The spectra of the two polyester compounds with starch are displayed in Figure 5-71. On review of these spectra, there is evidence of maleic and glycerol interactions with both the polyester and the starch. The following are comments highlighting those peaks:

- The peak at 3,330 cm^{-1} arising from the hydroxyl groups (-OH) from the starch and glycerol is seen in spectra of both PLA-St and PBAT-St compounds. This peak is absent in PLA and PBAT polymers by themselves.

- The two peaks at 2918 cm^{-1} and 2853 cm^{-1} are seen in the spectra of PBAT-St indicating the presence of aliphatic groups arising from grafting.

- Absorbance peaks at 1850 cm^{-1} and 1854 cm^{-1} are seen in the PLA-St curve. It represents the antisymmetric and asymmetric C-O stretching of the MAH, forming succinic anhydride.

- The characteristic peak of 1780 cm^{-1} for the ring anhydride of maleic anhydride (MAH) is absent in the PBAT-St curve, thereby suggesting that it has been opened.

- The peak at 1748 cm^{-1} is characteristic of carbonyl groups from δ lactone C=O bond and other ester formations.

- The peak at 1710 cm^{-1} is characteristic of carbonyl groups. The peak is existing in the PBAT-St compound.

- The characteristic peak of 1640 cm^{-1} associated with δ (O-H) bend for water in starch is not observed in either PLA-St or PBAT-St compound spectrum. This suggests plasticization with glycerol and the displacement of the water within the starch.

- Characteristic peaks at 1267 cm^{-1} and 1243 cm^{-1} represent ester stretches in PBAT-St.

5.8 Mechanism

In Chapter 2.6, several different reaction mechanisms were suggested, and some of them were found within this study. The potential of maleation, etherification, esterification and transesterification of starches with various polyesters were discussed. The mechanisms suggested by Stagner 2011, Raquez 2006 / 2008, Narayan 2009, Moad 2011, Hablot 2012, Kalambur 2012 and Nabar 2005 were outlined to create a baseline to evaluate the samples generated with hopes of proposing mechanism(s) for the reactions.

These potential reactions and modification of starches and polyesters were identified in their writings and are simplified into five categories. These categories cover the breadth of the experimentation covered in this thesis:

- Maleated Poly(butylene adipate-co-terephthalate) PBAT in the presence of peroxide

- Maleated Polylactic Acid (PLA) in the presence of peroxide

- Maleated Starch

- Starch hydrolysis followed by its subsequent maleation

- Starch ether formation with glycerol

The maleation of Poly(butylene adipate-co-terephthalate) (PBAT) in the presence of peroxide was studied in Nabar's 2005 paper. Nabar suggested a mechanism for the maleation of PBAT with the subsequent reduction in molecular weight through the β scission of the PBAT as outlined in Figure 2-25. Nabar noted that maleation of the PBAT would occur with the assistance of a free radical initiator and the temperature of $185 \, ^{\circ}\mathrm{C}$ within a twin screw extruder. In Nabar's experiments, Trigonox 101 was employed as the free radical initiator to achieve the grafting of MAH to PBAT. Nabar concluded that maleation of the PBAT had occurred with the presence of two new carbonyl peaks being observed with the FTIR at 1861 and 1787 cm^{-1}.

In the experiments conducted in this paper, neither peak at 1861 nor 1787 cm^{-1} were observed in the FTIR spectral analysis of the compounds developed. This suggests that maleation of the PBAT, as described by Nabar, did not occur in this work.

Starch maleation described in the Jean-Marie Raquez (2008) and Elodie Hablot (2013) work was achieved through reaction extrusion. In their work, they noted that they could maleate starch, and as well, esterify glycerol with starch and achieve transesterification of glycerol with starch-polymer graft copolymers. Raquez and Hablot's work defines five reaction mechanisms which can occur during reactive extrusion and formation of modified thermoplastic starch.

1. Maleation of starch by means of a condensation reaction between the hydroxyl group at C_6 in the starch and opened MAH, thereby forming an ester covalent bond at C_6, and releasing water

2. Hydrolysis of starch in the presence of maleated starch and an excess of water

3. Hydrolysis and ether formation between glycerol and the C_1 hydroxyl group of starch

4. Transesterification of MAH grafted starch to the C_6 of glycerylated starch

5. Transesterification of MAH grafted starch to the C_1 of glycerylated starch

Raquez (2008) and Hablot (2013) were able to qualify the occurrence of maleation of starch and other reactions through the presence of FTIR peaks developing, or disappearing, depending on what mechanism was taking place. The following are specific FTIR peak that they had identified, defined in Table 2.2 and embellished here:

- 3200-3400 cm^{-1} for O-H stretching resulting for change in O-H in starch and the glycerol

- 2940 cm^{-1} for C-H stretching from heterocyclic ring hydrogen

- 2890 cm^{-1} for C-H stretching from glycerol

- 1780 cm^{-1} for the ring anhydride of maleic anhydride (MAH)

- 1710-1715 cm^{-1} for C=O stretching from carbonyl and carboxyl bonds and characteristic of PBAT. As well, from the maleation of the starch and or PBAT in the development of esters, transesterification and cross linking

- 1640-1690 cm^{-1} for δ (O-H) bending of water – derived from the free water residing in the starch granule

- 1440 cm^{-1} for CH2- bending peak

- 1400 cm^{-1} for CH2- bending peak

- 1200-1275 cm^{-1} for C-O stretching of alkyl aryl ethers (PBAT)

- 1163-1210 cm^{-1} for C-O bond stretches esters – carboxyl formation from maleation

- 1160 and 770 cm^{-1} for C-O bond stretches ether formation from glycerylated

- 1025-1060 cm^{-1} for -O-H primary hydroxyl groups stretch

- 1040-1050 cm^{-1} for -CO-O-CO anhydride stretching

- 770 cm^{-1} for C-O bond stretches ethers potential from condensation reaction between two (-OH) hydroxyl groups forming an ether
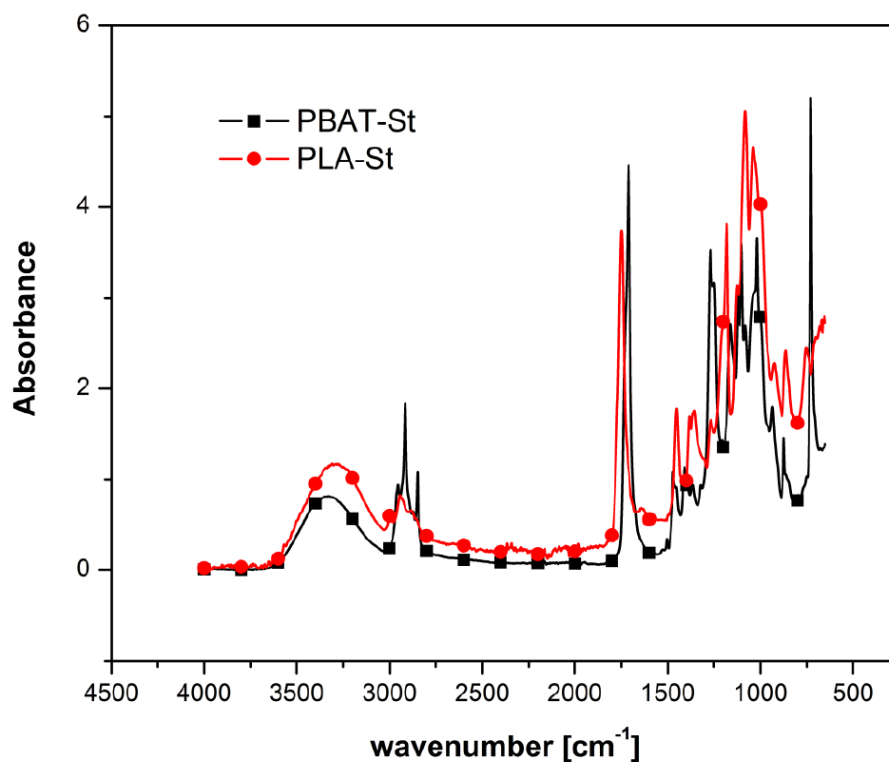
Figure 5-72 FTIR spectra of PBAT, Starch-Hylon VII, and compounds Hylon-Lau and Hylon-Ben from section 5.2.1

Within this paper, two different FTIR spectra signatures were identified as occurring. It seemed peculiar that only a limited number of similar spectra were found, given that several compounds derived from different starches and peroxides with PBAT were evaluated.

For the point of discussion, the spectra of Hylon-Lau and Hylon-Ben were identified as representing the two different FTIR spectra and were reviewed to discern if potential mechanisms could be identified.

Figure 5-72 depicts the FTIR spectra of the raw materials starch Hylon VII and PBAT in the compounding of Hylon-Lau and Hylon-Ben as outlined in section 5.2.1. Several of peaks described by Hablot exist in both spectra of Hylon-Lau and Hylon-Ben indicating the maleation of starch.

Figure 5-72 contains the spectra for Hylon VII starch, PBAT and that of the two compounds, however there is too much spectra congestion which makes it difficult to identify key peaks of interest. As such, Figure 5-73 and 5-74 were created to focus on the individual spectra of Hylon-Ben and Hylon-Lau in comparison with the raw materials over the wavenumbers between 2600-3200 cm^{-1}.

Figure 5-73 FTIR spectra of raw materials and Hylon-Ben compounds obtained from compounding

In Figure 5-73, the spectra for Hylon-Ben is very similar to Hablot's spectra for maleated starch. Key peaks of interest exist on the spectra at 2938 cm^{-1} C-H stretching from heterocyclic

ring hydrogen, 2912 cm^{-1} C-H stretching from an alkane, and 2890 cm^{-1} for C-H stretching from glycerol.
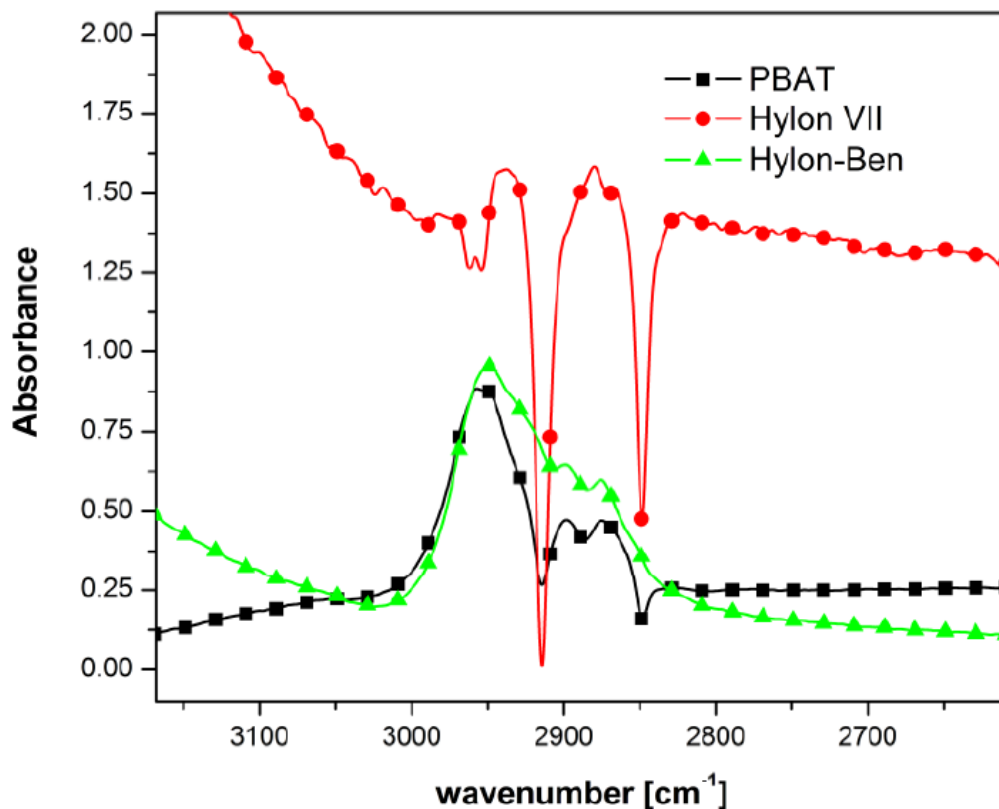
Figure 5-74 FTIR spectra of raw materials and Hylon-Lau compounds obtained from compounding

In Figure 5-74, the spectra for Hylon-Lau is similar to Hablot's spectra for maleated starch. However, key peaks of interest exist on Hylon-Lau spectra at 2949 cm^{-1} C-H stretching from heterocyclic ring hydrogen, 2917 cm^{-1} C-H stretching from CH_3 glycerol , 2874 cm^{-1} for C-H stretching from the CH_2 of glycerol, and 2850 cm^{-1} C-H stretching from an alkane. However, the intensity of the peaks at 2917 cm^{-1} is significantly higher, and the presence of 2850 cm^{-1} peak is new altogether. The difference between the Figures 5-73 and 5-74 suggest that alkane groups are added into the Hylon-Lau copolymer structure.

In Figure 5-72 there exists the spectra for Hylon VII starch, PBAT and that of the two compounds, however, here too there is too much congestion which makes it difficult to identify key peaks of interest. As such, Figure 5-75 and 5-76 were created to focus on the individual spectra of Hylon-Ben and Hylon-Lau in comparison with the raw materials over the wavenumbers between 800-1950 cm^{-1}.
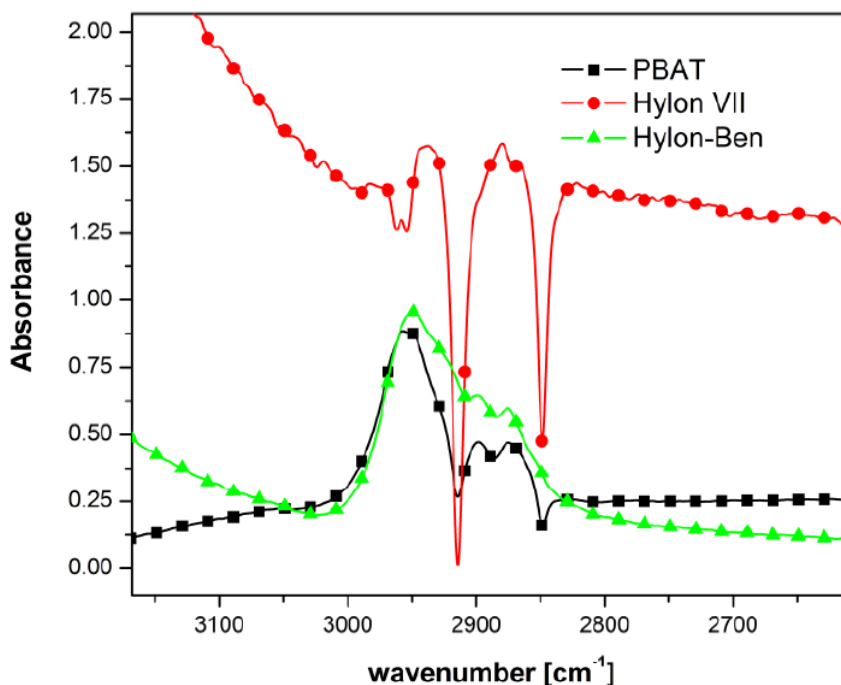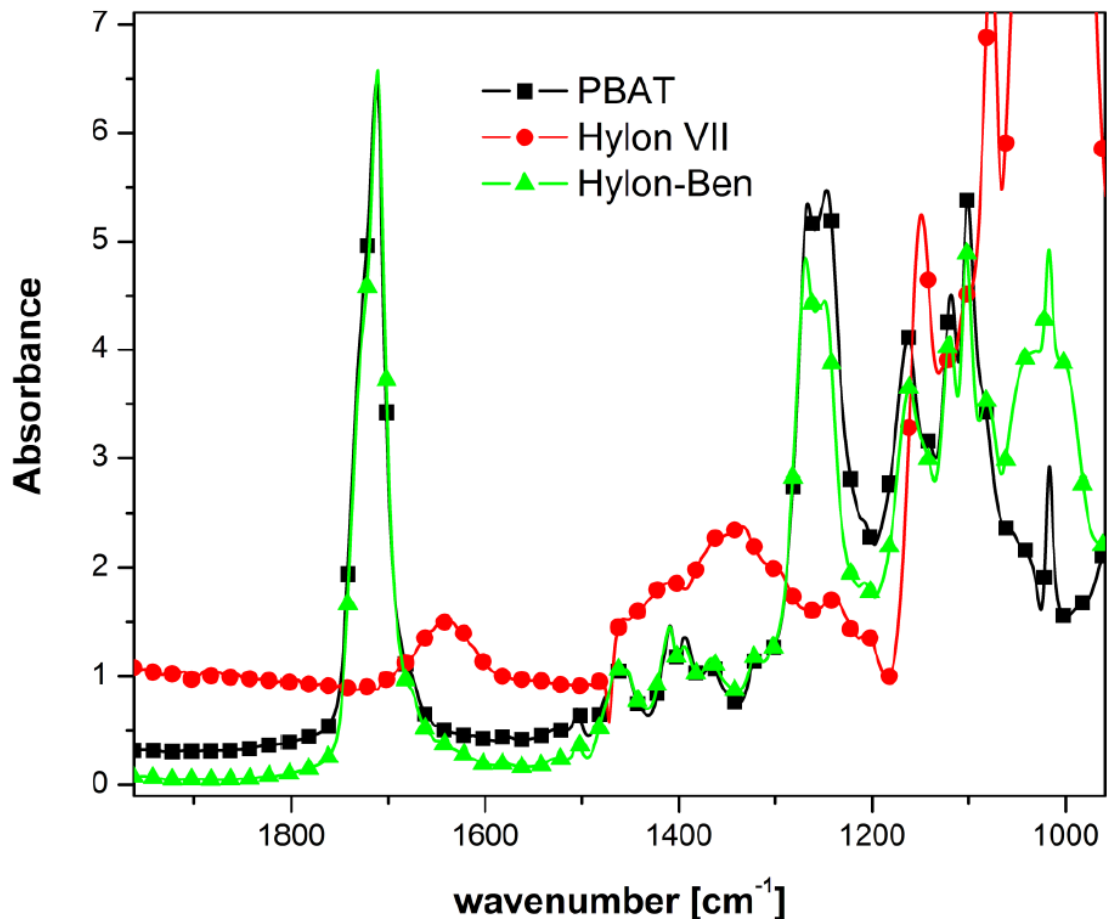

Figure 5-75 FTIR spectra of raw materials and Hylon-Ben compounds over the wavenumbers 800 – 1950 cm^{-1}

In Figure 5-75, the spectra of the Hylon-Ben compound focus on the wavenumbers between 800 and 1,950 cm^{-1}. The area of interest in these spectra are:

- The peak at 1712 cm^{-1} is characteristic of carboxyl groups and suggests the reaction with maleic anhydride (MAH) implying that esterification and or transesterification had occurred.

- A peak at 1640 cm^{-1} for δ (O-H) bending of water, derived from the free water residing in the starch granule, is noted in Hylon VII starch FTIR spectra, disappears in the spectra of the Hylon-Ben compound.

- The characteristic peak of 1780 cm^{-1} for the ring anhydride of maleic anhydride (MAH) is absent, thereby suggesting that it has been opened.

- Characteristic peaks at 1267 cm^{-1} and 1243 cm^{-1} represent ester stretches in PBAT. However, the ratio of the intensities between the two peaks is different between PBAT resin and Hylon-Ben compound. This suggests the possibility that some portion of the PBAT may have been scissored. This explains the reduction in intensity of the spectra at wavenumbers 1267 and 1243 cm^{-1}.

- The characteristic peak of 1780 cm^{-1} for the ring anhydride of maleic anhydride (MAH) is absent, thereby suggesting that it has been opened

- Characteristic peaks at 1267 cm^{-1} and 1243 cm^{-1} represent ester stretches in PBAT. However, the ratio of the intensities between the two peaks is different between PBAT resin and Hylon-Lau compound. This suggests that the PBAT may have been scissored at some the ester sights in the PBAT structure. A similar phenomenon was described in Nibar's paper with regards to β scissoring of ester groups following maleation of PBAT. However, the typical FTIR peaks which Nibar had identified are not present.

Based on the information obtained from the FTIR spectra of the compounds in this paper, and the discussion on these two compound spectra in reference to the raw materials, it is believed that two groups of mechanisms were prevalent
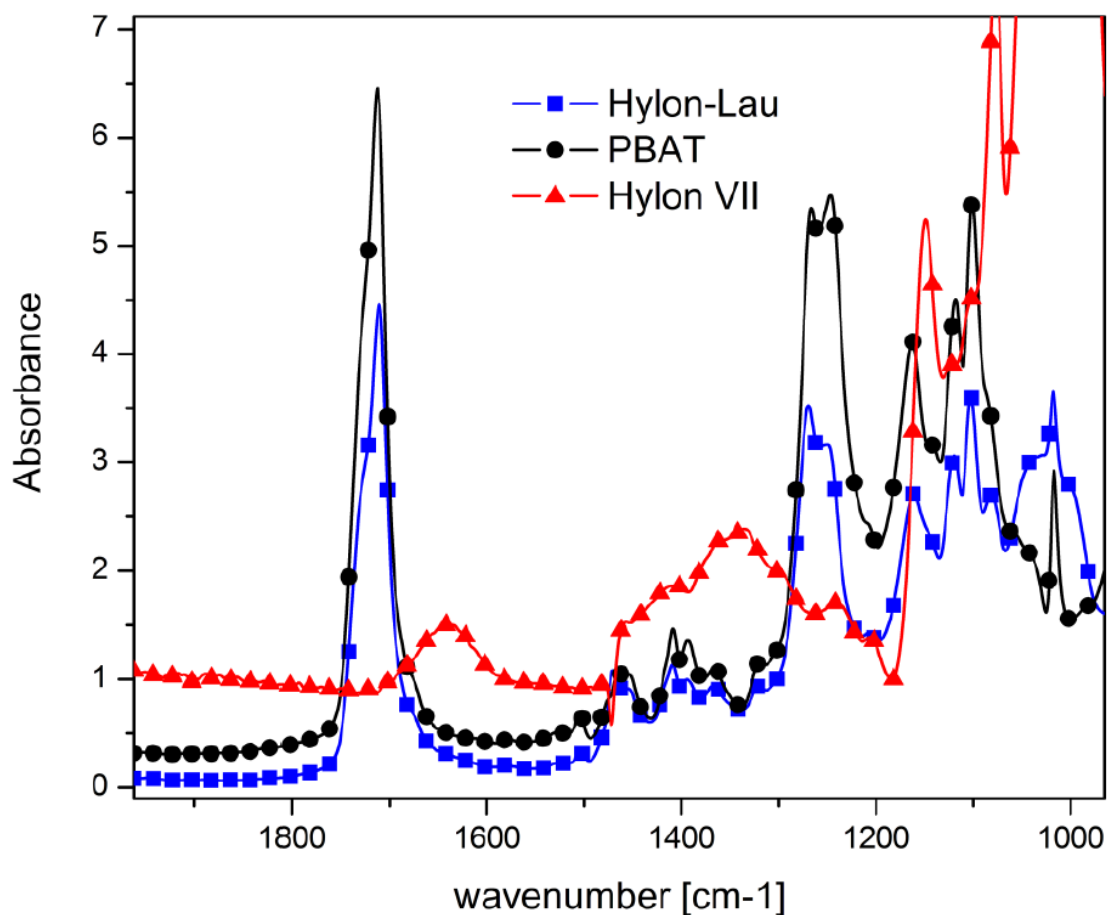
Figure 5-76 FTIR spectra of raw materials and Hylon-Lau compounds over the wavenumbers 800 – 1950 cm^{-1}

As Hablot and Raquez outlined in their papers, the spectra of Hylon-Ben reflect the maleation of the starch including the glycerylate of starch forming esters and transesterification.

However, the spectra of Hylon-Lau offers unique peaks not identified by Hablot and Raquez in their compounds of starch – PBAT copolymer. The Hylon-Lau spectra presents unique peaks at 2917 cm^{-1} C-H stretching from CH$_3$ glycerol , 2874 cm^{-1} for C-H stretching from the CH$_2$ of glycerol, and 2850 cm^{-1} C-H stretching from an alkane.

As well, the spectra of Hylon-Lau reflect the loss in intensity at several other peaks. This suggests a lower incidence of specific bonds occurring. These are reflected at 1712 cm^{-1}, 1267

196

cm^{-1} and 1243 cm^{-1}. The peak at 1712 cm^{-1} is characteristic of carboxyl groups and suggests the reaction with maleic anhydride (MAH) implying that esterification and or transesterification has occurred. However, the intensity of the curve is reduced for the Hylon-Lau. This suggests a decrease in carboxyl ester bonds in the compound.

The characteristic peaks of 1267 cm^{-1} and 1243 cm^{-1} represent ester stretches in PBAT. However, the ratio of the intensities between the two peaks were different between PBAT resin and Hylon-Lau compound. One explanation for this phenomenon was described in Nibar's paper with regards to β scissoring of ester groups following maleation of PBAT. However, the lack of peaks described by Nibar suggests the possibility of other reactions occurring which involve the β scissoring of ester groups in the PBAT.

It is believed that the mechanisms proposed by Raquez and Hablot cover much of the work conducted in this paper. However, additional analysis with other tools is required to understand why there was a loss in ester, and what mechanism may be contributing towards that.

Chapter 6

Conclusion and Recommendation

6.1 Contributions and Summary

At the onset, the objective of this research was to understand starch and the conditions which are required for its physical and chemical modification, examine the influence of different type of starches, taking into consideration the various sources and ratios of amylose / amylopectin. The initial focus was to be on the gelatinization of the starch granule and then progress to an understanding of the influences that grafting agents, free radical initiators, and polyester resins have on the synthesized polymer.

The first study was to understand the parameters that would allow for the efficient destructuring and plasticization of the starch in the timeliest fashion. The following parameters were studied:

- Influence of water on the destructuring of dent starch

- Influence of water / glycerol on the destructuring of dent starch

- Influence of shear on the destructuring of dent starch

- Influence of temperature on the destructuring of dent starch

The following conclusions were obtained regarding the parameters required to destructure and gelatinize starch granules.

- Starch has a preferred affinity towards water, specifically its ability to quickly destructure the starch granule.

- Water can act as an effective plasticizer for starch. Water can reduce the viscosity of the mixture with increased addition (reducing the interactions between molecules).

- Higher mechanical energy (RPM) is preferential in achieving destructuring of starch granule.

- Higher thermal energy (temperature) is preferential in achieving destructuring of starch.

- Elevated temperatures (greater than 100°C) require alternative plasticizer systems due to evaporation.

- Blends of alternative plasticizer with limited amounts of water enhance the ability of the mixture to quickly destructure and plasticize the starch.

- Thermal and mechanical energy employed are limited to the boiling point of the plasticizer in the compound.

The second study was to select three starches, from the collection of starches studied, and evaluate their properties. Hylon VII, 30050 and 55310 starches were chosen from the collection, and used for evaluation throughout the balance of the paper. They represented the three starches which would quickly destructure and plasticize. These starches also represented starches with different ratios of amylose to amylopectin and modification.

The third study dealt with the selection of the desired free radical initiator, and the question of whether certain free radical initiators could dissociate in a timely fashion to allow for chemical reactions to occur within the residence time and body temperature of the CWB at 150°C. The choice of free radical initiator is dependent on the ratio of amylose to amylopectin. Quicker free radical initiators seem to favour high amylose grades of starch, while slower free radical initiators favour higher amylopectin grades of starch.

The influence of free radical initiators on the rate of destructure and plasticization of the compound was examined. Hylon starch with 70:30 amylose to amylopectin ratio favoured the use of dilauroyl peroxide. The 30050 and 55310 starches, with a 25:75 amylose to amylopectin ratio, favoured Trigonox 101. In this study, it was noted that two very distinct mechanisms

199

presented themselves. The choice of peroxide with the amylose to amylopectin ratio allowed for one mechanism to prevail over the other. Table 6.1 offers some insight into the relationship which was seen between starch and peroxide.

Table 6-1 Summary of the free radical initiators on the compound generated

Starch	Hylon	30050	55310
Amylose : Amylopectin ratio in Starch	70:30	25:75	25:75
Torque / destructuring Increasing in rate	101< Ben< Lau	Ben<Lau <101	Ben<Lau <101
Torque / Maximum at destructuring point	Lau<101<Ben	101<Ben<Lau	Lau<101<Ben
TGA / increasing thermal stability	101<Lau<Ben	101 < Lau < Ben	Lau<101<Ben
DSC / Increasing ΔH_m	Lau < 101 < Ben	101 < Ben < Lau	101 < Lau < Ben
DSC / Increasing ΔH_c	101<Ben<Lau	101<Lau<Ben	Lau<101<Ben
FTIR / Additional Peaks 2918 & 2853cm^{-1}	Lau	101 & Ben	101
Increase Intensity @ 1710 cm^{-1}	Lau<101<Ben	101 < Ben < Lau	101 < Ben < Lau

Study four looked at the influence of increasing the level of peroxide from 0.1 – 0.3% in the compound. Changing the level of peroxide seemed to have little or no effect on the resulting compound. However, work done by Raquez and Hablot suggested that employing levels greater than 0.5% had an impact on the mechanism and species generated.

Study five investigated the effect of increasing the ingredient MAH from one percent to two and three times that level, in the compound. Changes in the level of MAH had a dramatic effect on the resulting compound and gave rise to a change in the predominate reaction mechanism.

Study six looked at the influence of initial starch moisture and its effect on destructure, plasticization and resulting physical-chemical properties. It was noted that lowering the initial moisture content before compounding changed the predominate reaction mechanism expected.

Study seven looked at blending the dry starch with the other raw materials into a master batch and allowing it to sit for a period of time before compounding. The question posed by the study was: "is there a window of time for which the master batch blend is good and able to obtain the desired results?" It was concluded from this study that, if looking for the predominate reaction mechanism to occur, one must blend the materials together and allow the mixture to sit for five hours, or more, before compounding. It was seen that blended material, which sat for two hours before compounding, resulted in a change in the reaction mechanism.

6.2 Main Conclusions

The reaction mechanisms offered by Raquez and Hablot were seen in the studies conducted. By adjusting the parameters as outlined below, the ability to drive the mechanisms in one direction or another exists. The following relationships played a role in achieving the desired reaction mechanisms:

- The starch must efficiently destructure and plasticize to form the gel balls in order for the starch molecules to open up and be available for modification.

- Effective achievement of gelatinization is obtained with a limited amount of water and plasticizer blend in the presence of energy (heat, shear) over a period of time.

- The desire reaction is predicated on the relationship between peroxide and the amylose to amylopectin ratio.

- The addition of excess peroxide is of little value to the developing the final compound.

- The addition of excess MAH influences the reaction mechanism.

- Drying starch has an influence on the reaction mechanism desired.

6.3 Recommendations

This paper offers a firm foundation to build upon. There is still more to learn from this work. The following is recommended as the next steps in this research:

- Additional analysis be conducted on the samples developed

- The compounds be taken to a twin screw reaction extrusion

- Application development be explored

Looking at the additional analysis to be conducted, it is suggestion that the following be explored:

- Look at preforming dynamic mechanical analysis on the sample and explore the glass transition temperature T_g over the two different mechanisms.

- Look at the physical properties of tensile and elongation analysis and how they change between the two different mechanisms.

- Explore the compound viscosities between the two different mechanisms.

- Consider running proton and C_{13} NMR on the compounds. This information will shed more light on the final structures synthesis and allow for more refined mechanisms to be predicted.

- Explore the morphology of the compounds developed through the SEM and XRD studies to validate the destructurization and plasticization of the starch.

Expand the research into reactive extrusion on a twin screw extruder and look at what other variables present themselves. The following is suggested:

- Sequencing of the same raw materials in their introduction to the extruder

- The physical-chemical analysis of the compounds created

When compounds of interest are developed, look at the potential applications in which the material could be used. Explore the materials processing ability to blow film, injection mold, sheet extrude and vacuum form.

These are but a few of thoughts and recommendations to explore in continuing the concepts explored in this thesis. More concepts and opportunities will present themselves as further studies are pursued.

Bibliography

Altskär A, Andersson R, Boldizar A, Koch K, Stading M, Rigdahl M, Thunwall M (2008) Some effects of processing on the molecular structure and morphology of thermoplastic starch. Carbohydrate Polymers 71:591-597

Anastas P, Zimmerman J (2003) Through the 12 principles green engineering. Environmental Science & Technology March: 95-101

Arreola D, Robledo-Oritz J, Moscoso F, Arellano M, Rodrigue D, Gonzalex-Nunez R. (2011) Film processability and properties of polycaprolactone/thermoplastic starch blends. Journal of Applied Polymer Science 123: 179-190

Ashogbon A, Akintayo E (2012) Morphological, functional and pasting properties of starches separated from rice cultivars grown in Nigeria. International Food Research Journal 19(2): 665-671

Abbès B, Ayad R, Prudhomme J, Onteniente J. (1998) Numerical simulation of thermoplastic wheat starch injection molding process. Polymer Engineering and Science, Volume 38, 12: 2029-2038

Ayadi F, Dole P (2011) Stoichiometric interpretation of thermoplastic starch water absorption and relation to mechanical behavior. Carbohydrate Polymers 84: 872-880

Babu R, O'Connor, K, Seeram, R. (2013) Current progress on bio-based polymers and their future trends. Progress in Biomaterials, 2:8: 1-16

Beach E, Weeks B, Stern R, Anastas P. (2103) Plastics additives and green chemistry. Pure Applied. Chemistry., Volume 85, 8: 1611-1624

Bemiller J, Whistler R. (2009), Starch: Chemistry and Technology, 3rd edition, Academic Press ISBN:978-0-12-746275-2

Bennett S, Pearson P. (2009) From petrochemical complexes to biorefineries? The past and prospective co-evolution of liquid fuels and chemicals production in the UK. Chemical Engineering Research and Design 87: 1120-1139

Bertolini A. (2010) Starches: Characterization, Properties and Applications, CRC Press, ISBN: 978-1-4200-8023-0

Boons F, Montalvo C, Quist J, Wagner M. (2013). Sustainable innovation, business models and economic performance: an overview. Journal of Cleaner Production 45: 1-8

Bozell J (2008) Feedstocks for the future—biorefinery production of chemicals from renewable carbon. Clean, 36(8): 641-647

Brandelero, R, Grossmann, M, Yamashita, F. (2012) Films of starch and poly(butylene adipate co-terephthalate) added of soybean oil (SO) and Tween 80. Carbohydrate Polymers 90: 1452-1460

BRIDGE 2020 Vision Strategy Paper (2012) Accelerating innovation and market uptake of biobased products. A public-private partnership on biobased industries. Bridge 2020 Biobased and Renewable Industries for Development and Growth in Europe.

Chabrat E, Abdillahi H, Rouilly A, Rigal L. (2012) Influence of citric acid and water on thermoplastic wheat flour/poly(lactic acid) blends. I: Thermal, mechanical and morphological properties. Industrial Crops and Products 37: 238-246

Chandra R, Rustgi R (1998) Biodegradable polymers. Progress in Polymer. Science, 23: 1273-1335

Chaudhary A, Miller M, Torley P, Sopade P, Halley P. (2008) Amylose content and chemical modification effects on the extrusion of thermoplastic starch from maize. Carbohydrate Polymers 74: 9007-913

Chaudhary A, Torley P, Halley P, McCaffery N, Chaudhary D. (2009) Amylose content and chemical modification effects on thermoplastic starch from maize – Processing and characterization using conventional polymer equipment. Carbohydrate Polymers 78: 917-925

Demirgöz D, Elvira C, Mano J, Cunha A, Piskin E, Reis, R. (2000) Chemical modification of starch based biodegradable polymeric blends: effects on water uptake, degradation behaviour and mechanical properties. Polymer Degradation and Stability 70: 161-170

Ekabutr P, Lerdwijitjarud W, Sittattrakul A. (2013) Glycerol and esterified Products of palmitic acid as a mixed plasticizer for thermoplastic tapioca starch. Polymer Engineering and Science 2013: 134-145

Escamilla G, Canche-Canche M, Duarte-Aranda S, Cacres-Farfin M, Borges-Argaez R. (2011) Mechanical properties and biodegradation of thermoplastic starches obtained from grafted starches with acrylics. Carbohydrate Polymers 86 (2011): 1501-1508

European Commission (2012) Innovating for sustainable growth: A Bioeconomy for Europe. Communication from the Commission to the European Parliament, The Council, the European Economic and Social Committee and the Committee of the Regions, Brussels, 13.2.2012 COM(012) 60 final: 1-9

Ferrarezi, M, Taipina, M, Escobar da Silva, L, Goncalves, M . (2013) Poly(ethylene glycol) as a compatibilizer for poly(lactic acid)/ thermoplastic starch blends. Journal Polymer Environment 21: 151-159

García N, Ribba L, Dufresne A, Aranguren M, Goyanes S. (2011) Effect of glycerol on the morphology of nanocomposites made from thermoplastic starch and starch nanocrystals. Carbohydrate Polymers 84: 203-210

Gironès J, Lopez J, Mutje P, Carvalho A, Curvelo A, Vilaseca F. (2012) Natural fiber-reinforced thermoplastic starch composites obtained by melt processing. Composites Science and Technology 72: 858-863

Gonzalez F, Ramsay B, Favis B. (2004) Rheological and thermal properties of thermoplastic starch with high glycerol content. Carbohydrate Polymers 58: 139-147

Graeme Moad, (2011) Chemical modification of starch by reactive extrusion, Progress in Polymer Science 36 pp 218-237

Gu G, Xia Y, Lin C, Meng Y, Zhou Q. (2013) Experimental study on characterizing damage behavior of thermoplastics. Materials and Design 44: 199-207

Hablot E, Dewasthale Zhao Y, Zhiguan Y, Shi X, Graiver D, Narayan R. (2013) Reactive extrusion of glycerylated starch and starch-polyster graft copolymers. European Polymer Journal 49: 873-881

Hassan M, Yee L, Yee P, Ariffin H, Raha A, Shirai Y, Sudesh K. (2013) Sustainable production of polyhydroxyalkanoates from renewable oil-palm biomass. Biomass and Bioenergy 50: 1-9

Hejri Z, Seifkordi A, Ahmadpour A, Zabarjad S, Maskooki A. (2013) Biodegradable starch/poly (vinyl alcohol) film reinforced with titanium dioxide nanoparticles. International Journal of Minerals, Metallurgy and Materials, Volume 20, 10: 1001-1011

Henrist D, Remon J (1999) Influence of the process parameters on the characteristics of starch based hot stage extrudates. International Journal of Pharmaceutics 189: 7-17

Hietala M, Mathew A, Oksman K. (2013) Bionanocoposites of thermoplastic starch and cellulose nanofibres manufactured using twin-screw extrusion. European Polymer Journal 49: 950-956

Huneault M, Li H (2007) Morphology and properties of compatibilized polylactide /thermoplastic starch blends. Polymer 48: 270-280

Imre B, Pukánsky B (2013) Compatibilization in bio-based and biodegradable polymer blends. European Polymer Journal 49: 1215-1233

Jenkins P, Donald A (1995) The influence of amylose on starch granule structure. Internal Journal. Biological Macromolecules. Volume 17, 6: 315-321

Kaewtatip K, Tanrattanakul V (2012) Structure and properties of pregelatinize cassava starch/ kaolin composites. Materials and Design 37: 423-428

Kaewtatip K, Thongmee J (2013) Effect of kraft lignin and esterified lignin on the properties of thermoplastic starch. Materials and Design 49: 701-704

Kalambur, S. (2012) Modification of Biodegradable Polymer through Reactive Extrusion-II, Starch-Based Material and Nanocomposites, Chemistry, Processing and Applications, Ahmed J, Tiwari B, Imam S, Rao M. editors CRC Press, ISBN: 978-1-4398-5116-6

Kalanbut S, Rizvi S. (2006) An overview of starch-based plastics blends from reactive extrusion. Journal Plastic Film and Sheeting, 22: 39-58

Kale G, Kijchavengkul Auras R, Rubino M, Selke S, Sign S. (2007) Compostability of Bioplastic Packaging Materials: An Overview. Macromolecular Bioscience 7: 255-277

Kaseem M, Hamad K, Deri F. (2012) Thermoplastic starch blends: a review of recent works. Polymer Science, Series A. Volume 54, 2: 165-176

Kaseem M, Hamad K, Deri F. (2012) Rheological and mechanical properties of polypropylene / thermoplastic starch blend. Polymer Bulletin 68: 1079-1091

Lescher P, Jayaraman K, Bhattacharyya D. (2012) Characterization of water-free thermoplastic starch blends for manufacturing processes. Materials Science and Engineering A 532: 178-189

Li X, Zhu J, Li L, Huang C, Chen L. (2013) Plasticization effect of triacetin on structure and properties of starch ester film. Carbohydrate Polymers 94: 874-881

Lindeboom N, Chang P, Tyler R. (2004) Analytical, biochemical and physiochemical aspects of starch granule size, with emphasis on small granule starches: a review. Starch 56: 89-99

Liu H, Xie F, Yu L, Chen L, Li L. (2009) Thermal processing of starch-based polymers. Progress in Polymer Science 34: 1348-1368

López O, Zaritzky E, Grossmann V, Garcia M. (2013) Acetylated and native corn starch blend films produced by blown extrusion. Journal of Food Engineering 116: 286-297

Luo X, Li J, Lin X. (2012) Effect of gelatinization and additives on morphology and thermal behavior of corn starch/PVA blend films. Carbohydrate Polymers 90: 1595-1600

Bastioli C, (2008) Biopolymers present new market opportunities for additives in packaging. Plastics Additives & Compounding Magazine, May/June: 22-25

Mbey J, Hoppe S, Thomas F. (2012) Cassava starch-kaolinite composite film. Effect of clay content and clay modification on film properties. Carbohydrate Polymers 88: 213-222

Miller C.S., Dalton N.N. Physical Properties of Glycerol and Its Solutions, American Chemical Society Monograph 117, 1953

Mirabel A, Scholz L, Carus M. Editors (2013) Market study: Bio-based Polymers in the World, Capacities, production and applications: status quo and trends towards 2020. Nova Institute

Moad G (2011) Chemical modification of starch by reactive extrusion. Progress in Polymer Science 36: 218-37

Nafchi A, Moradpour M, Saeidi M, Alias A. (2013) Thermoplastic starches: Properties, challenges, and prospects, Starch, 65: 61-72

Niazi M, Zijlistra M, Broekhuis A. (2013) Spray drying thermoplastic starch formulations: need for processing aids and plasticizers? European Polymer Journal 49: 1861-1870

Olivato J, Grossmann M, Bilick A, Yamashita F. (2012) Effect of organic acids as additives on the performance of thermoplastic starch/polyester blown films. Carbohydrate Polymers 90: 159-164

Ottenhof M, Farhat I (2004) Starch Retrogradation. Plant Biotechnology Part 5, Biotechnology and Genetic Engineering Reviews, 21: 215-228

Phua Y.J., Chow W.S., Mohd Ishak Z.A. (2013) Reactive processing of maleic anhydride-grafted poly(butylene succinate) and the compatibilizing effect on poly(butylene succinate) nanocomposites, Polymer Letters Vol. 7, 4: 340-354

Raphael I, Yang A (2013) Plastics production from biomass: assessing feedstock requirement. Biomass Conversion and Biorefinery 3: 319-326

Raquez Nabar Y, Dubois P, and Narayan R, (2008) Maleated thermoplastic starch by reactive extrusion, Carbohydrate Polymers 74: 159–169

Shen L, Haufe J, Patel M. (2009) Product overview and market projection of emerging bio-based plastics. Commissioned by European Polysaccharide Network of Excellence and European Bioplastics June 2009.

Shen, L (2011) PhD Thesis Bio-based and recycled polymers for cleaner production: an assessment of plastics and fibres. Group of Science, Technology and Society, Copernicus Institute, Faculty of Science, Utrecht University, Netherlands

Shin B, Jang S, Kim B. (2011) Thermal, morphological, and mechanical properties of biobased and biodegradable blends of poly(lactic acid) and chemically modified thermoplastic starch. Polymer Engineering and Science 826-834

Sichina W. (2000) DSC as problem solving tool: Measurement of percentage crystallinity of thermoplastics, Thermal Analysis Application Note Perkin Elmer Instruments, PETech-40

da Silva M, Ascheri D, Galdeano M , Carvalho C. (2014) Characterization of cassava starch processed in an internal mixer. Polimeros, 23: 725- 732

Stepto, R (2000) Thermoplastic starch. Macromolecules Symposia. 152: 73-82

Stepto, R (2003) The processing of starch as a thermoplastic. Macromolecules Symposia. 201: 203-212

Thunwall M, Boldizar, A, Rigdahl, M, Kuthanova, V. (2006) On the stress-strain behavior of thermoplastic starch melts. International Journal of Polymer Anal. Charact. 11: 419-428

Thunwall, M, Boldizar A, Rigdahl M, Kuthanova V. (2008) Film blowing of thermoplastic starch. Carbohydrate Polymers 71: 583-590

Van Soest J, Bezemer R, Wit D, Vliegenhart F. (1996) Influence of glycerol on the melting of potato starch. Industrial Crops and Products 5: 1-9

Van Soest J, Vliegenthart J. (1996) The influence of starch molecular mass on the properties of extruded thermoplastic starch. Polymer, Volume 37, 16: 3543-3552

Van Soest, Vliegenthart, J. (1997) Crystallinity in starch plastics: consequences for material properties. Tibtech, 15: 208-215

Widmann G (2001) Interpreting TGA Curves, Technical Information Bulletin, Metter Toledo Switzerland UserCom 1/2001

Widmann, G. 2001 Determination of polymer crystallinity with DSC measurements, Technical Information Bulletin Metter Toledo Switzerland UserCom 11/2001

Willett J, Jasberg B, Swanson C. (1995) Rheology of thermoplastic starch: effects of temperature, moisture content, and additives on melt viscosity. Polymer Engineering and Science, January 1995, Volume 35, Number 2: 202-210

Xie S, Liu Q, Cui S. (2005) Starch modifications and applications. Food carbohydrates: chemistry, physical properties and applications, Cui S editor, Taylor and Francis Publishers ISBN 978-0-8493-1574-9   362-411

Xie F, Yu L, Su B, Liu P, Wang J, Liu H, Chen L. (2009) Rheological properties of starches with different amylose/amylopectin ratios. Journal of Cereal Science 49: 371-377

Xie F, Halley P, Averous L. (2012) Rheology to understand and optimize processability, structures and properties of starch polymeric materials. Progress in Polymer Science 37: 595-623

Yan Q, Hou H, Dong H. (2012) Effects of extrusion and glycerol content on properties of oxidized and acetylated corn starch-based films. Carbohydrate Polymers 87: 707-712

Yang Z (2013) PhD Thesis, Biobased products from starch using extrusion processing and chemical modifications. Department of Chemical Engineering, Michigan State University.

Yu L, Christie G, (2005) Microstructure and mechanical properties of orientated thermoplastic starches. Journal of Materials Science 40: 111-116

Zhang C, Su, X. (2013) Thermal, mechanical and rheological properties of polylactide toughened by expoxidized natural rubber. Materials and Design 45: 198-205

Zhang Q, Yu Z, Xie X, Naito, K, Kagawa, Y. (2007) Preparation and crystalline morphology of biodegradable starch/clay nanocomposites. Polymer 48: 7193-7200

Zheng P, Chang P, Yu J, Ma X. (2009) Formamide and 2-hydroxy-N-[2-(2-hydroxy-propionylamino)-ethyl] propionamide (HPEP) as a mixed plasticizer for thermoplastic starch. Carbohydrate Polymers 78: 296-301

Zuo Yingfeng, (2013) Synthesis and characterization of maleic anhydride esterified corn starch by the dry method, International Journal of Biological Macromolecules 62: 241-247
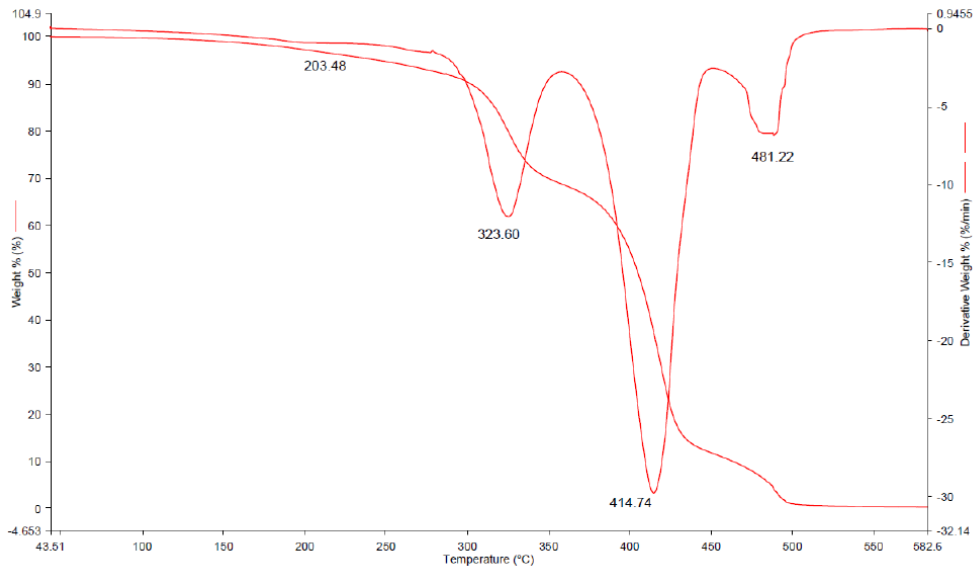
Zhou X, Baik B, Wang R, Lim S. (2010) Retrogradation of waxy and normal corn starch gels by temperature cycling. Journal of Cereal Science 51: 57-65
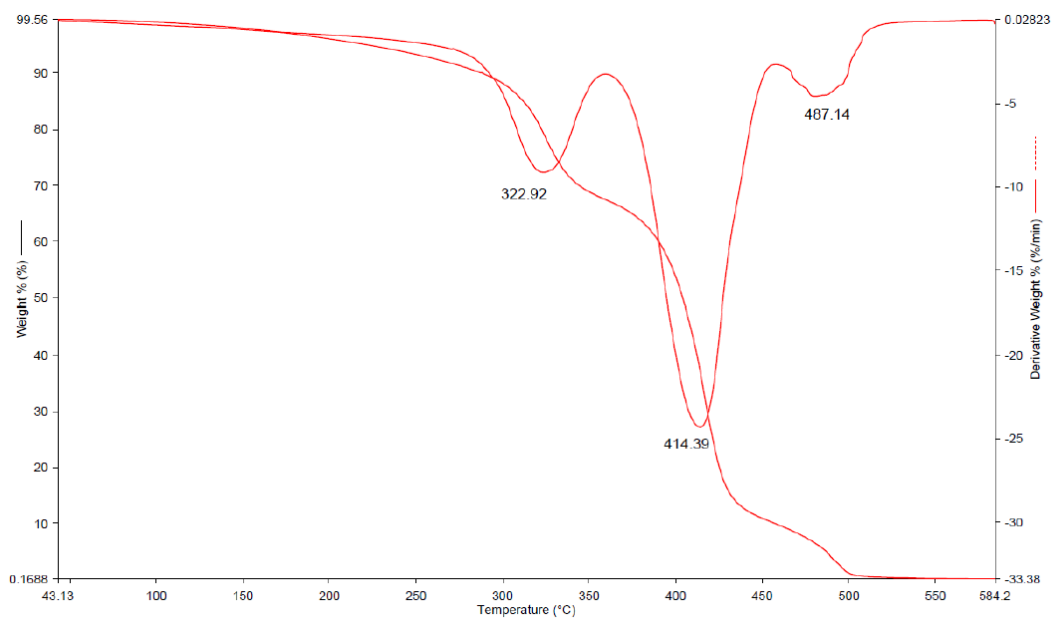
Appendix

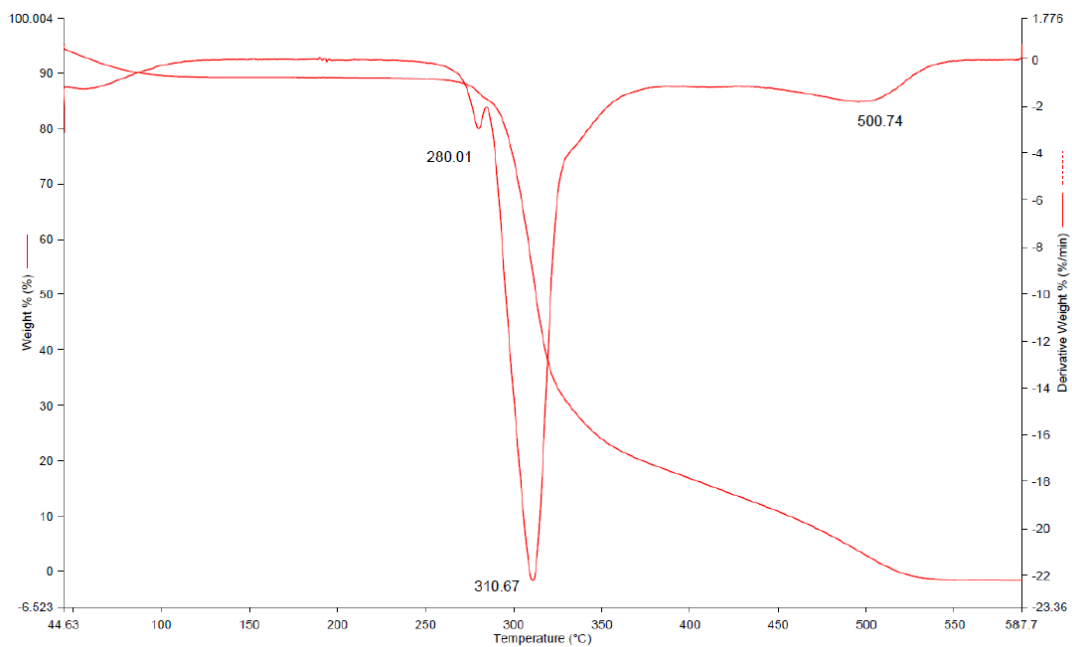**Appendix 1 TGA Analysis of starch 30050 with peroxide 101, glycerol and PBAT**
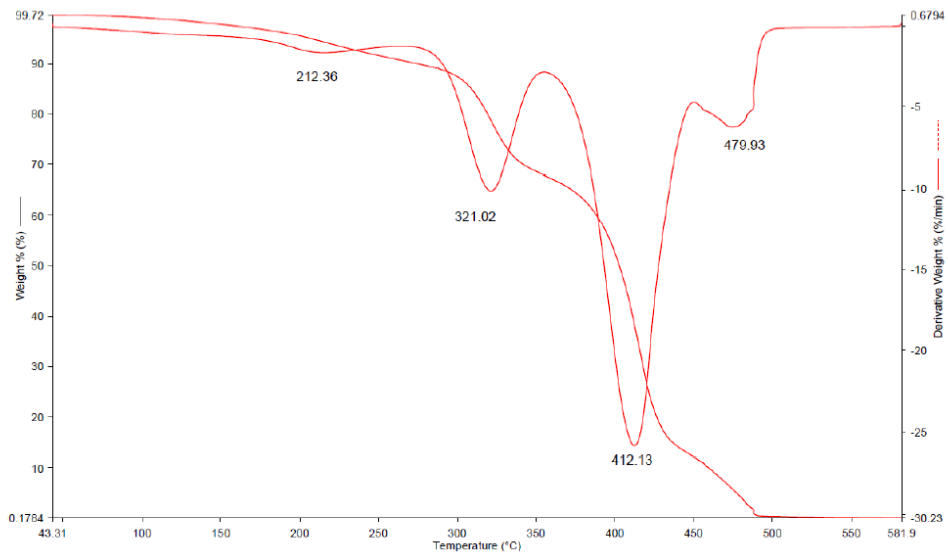
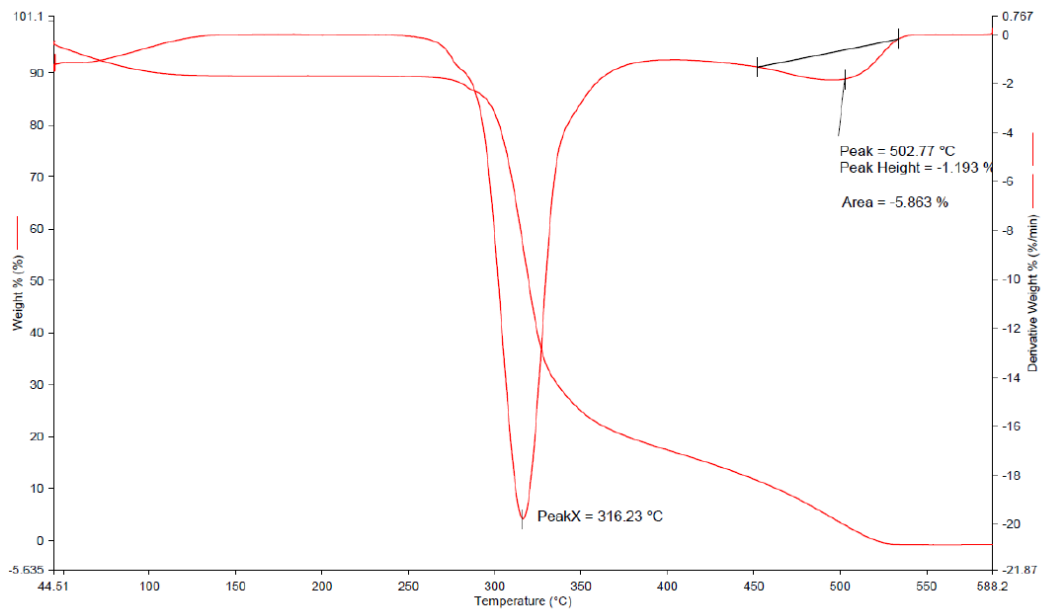**Appendix 2 TGA Analysis of starch 30050 with dibenzoyl peroxide, glycerol and PBAT**

Appendix 3 TGA Analysis of starch 30050 with dilauroyl peroxide, glycerol and PBAT

Appendix 4 TGA Analysis of starch Hylon

Appendix 5 TGA Analysis of starch 30050
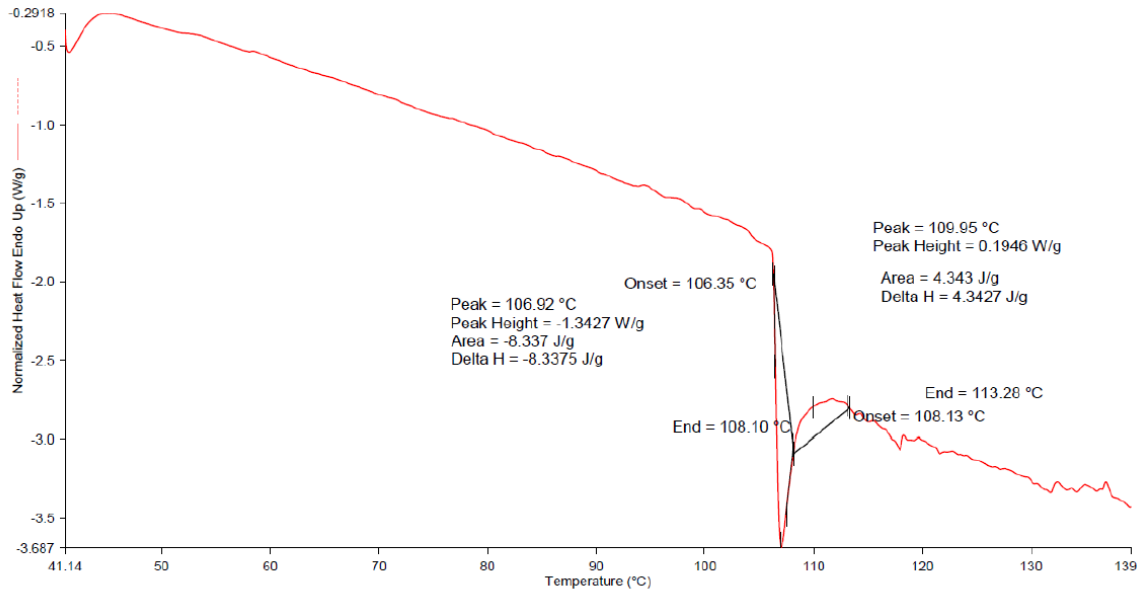

Appendix 6 TGA Analysis of starch 55310
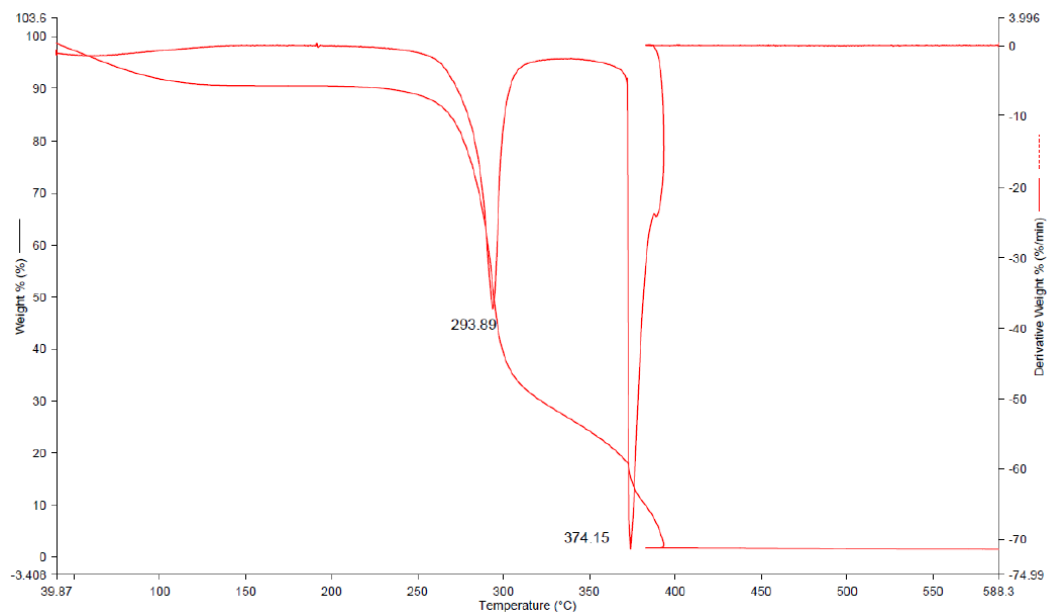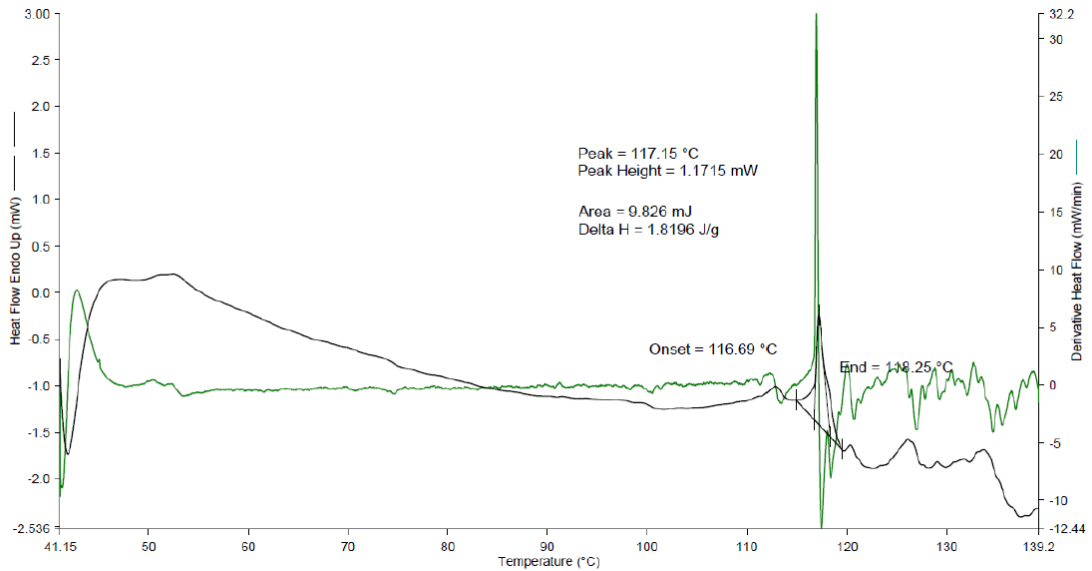
Appendix 7 TGA Analysis of dent maize starch
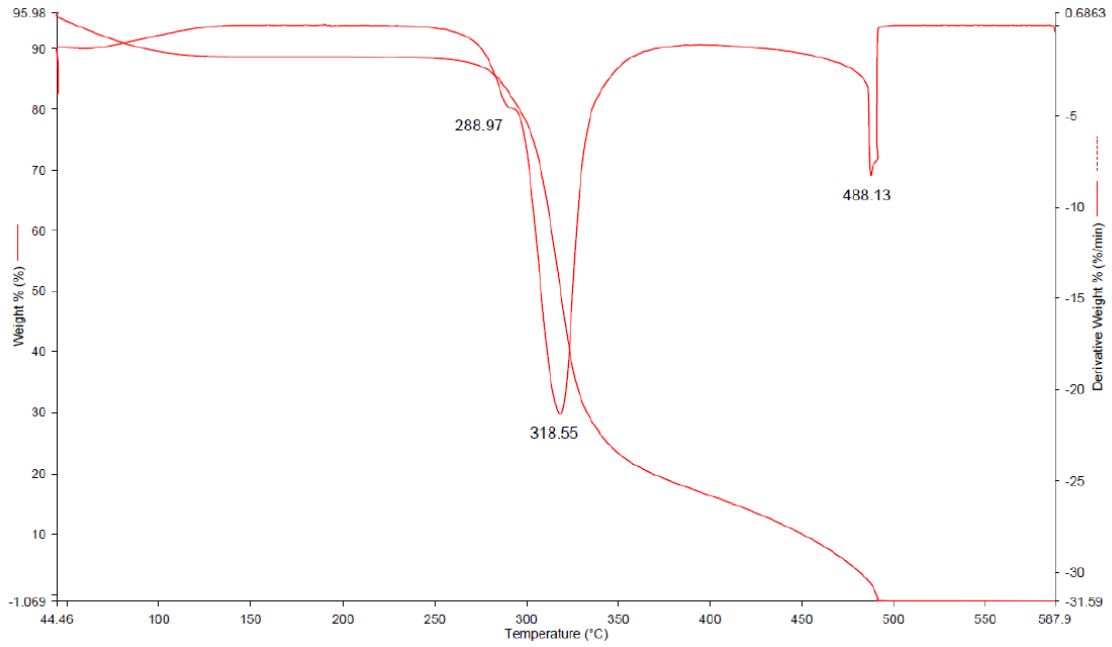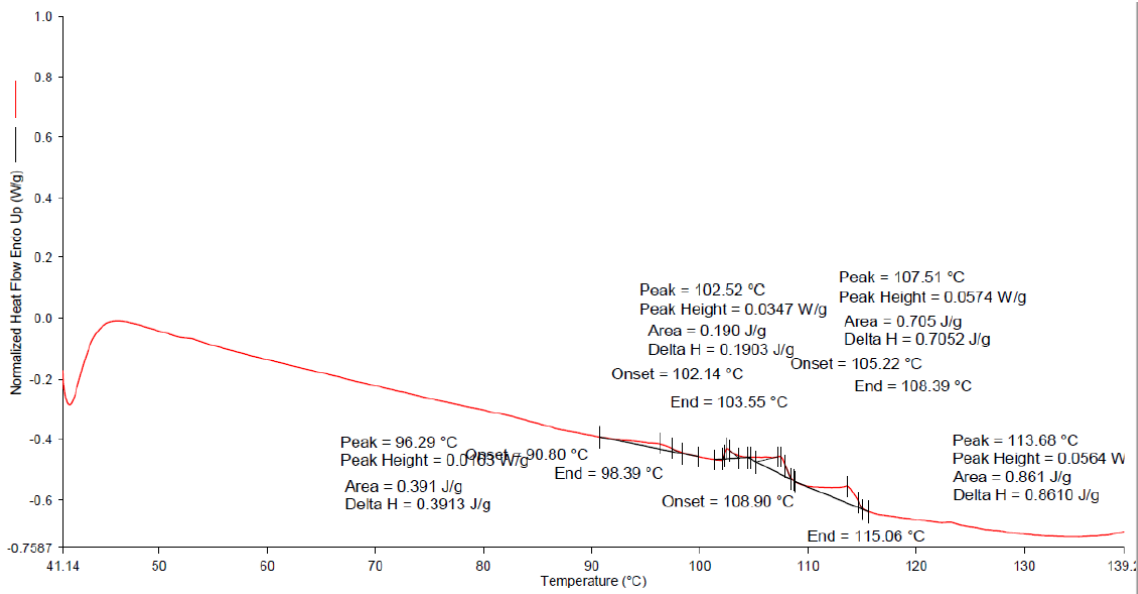

Appendix 8 DSC Analysis (1st heat pass) of 30050
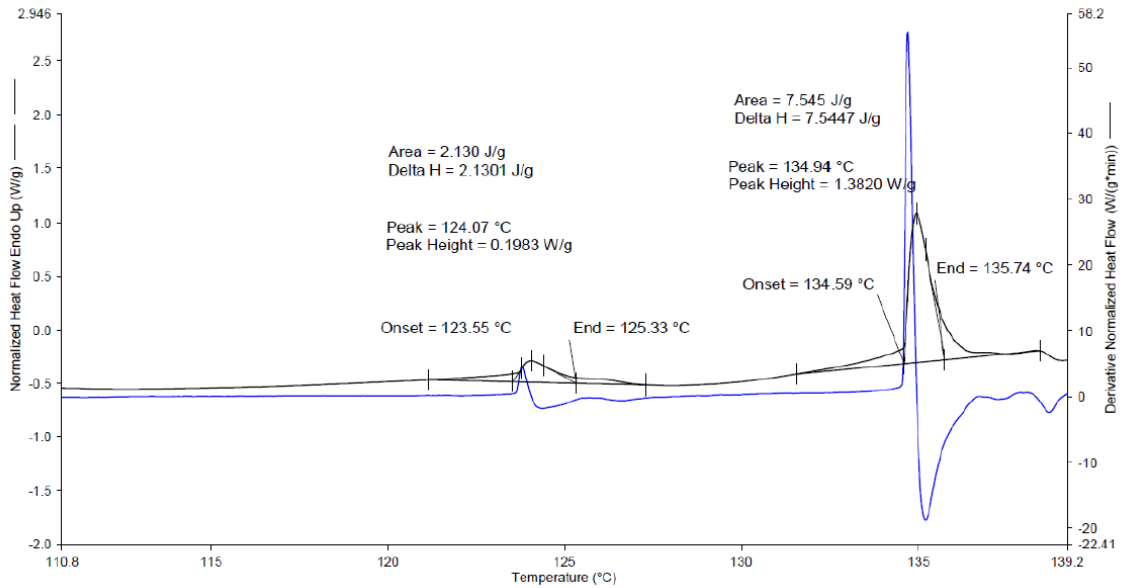
Appendix 9 DSC Analysis (1st heat pass) of Hylon
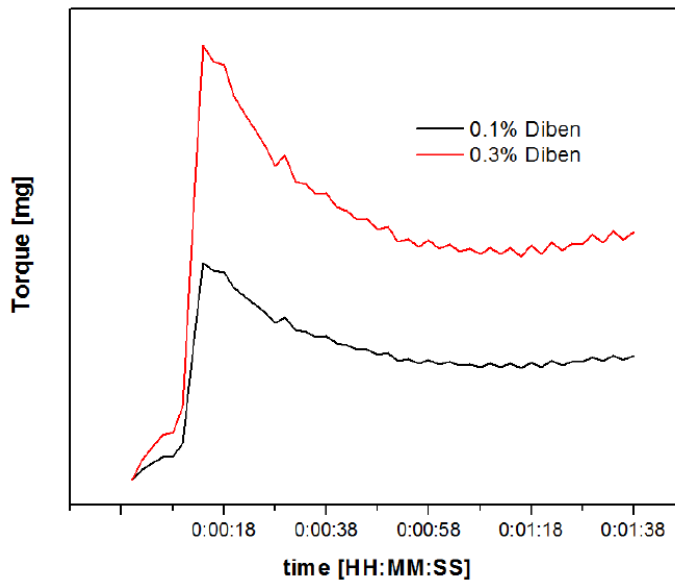

Appendix 10 DSC Analysis (1st heat pass) of 55310

**Appendix 11 DSC Analysis (1st heat pass) of dent maize starch**

Appendix 12 CWB Torque curves as a function of time for various levels of peroxide in compounding

The torque curves for both the 0.1% and 0.3% dibenzoyl peroxide lay on top of each other. As such, they have been stacked to show that they are identical. Otherwise you would not be able to distinguish

Appendix 13 CWB Temperature curves as a function of time for various levels of peroxide in compounding
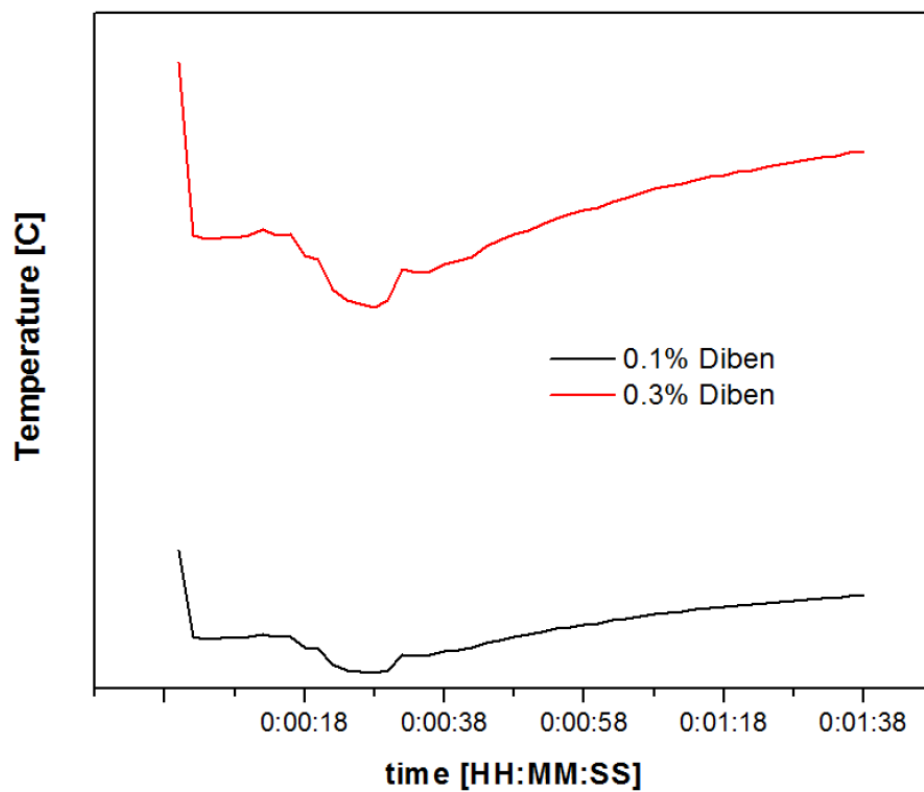
The temperature curves for both the 0.1% and 0.3% dibenzoyl peroxide lay on top of each other. As such, they have been stacked to show that they are identical. Otherwise you would not be able to distinguish